Contribution to the study of passive control by nonlinear interactions in mechanics and acoustics

Alireza Ture Savadkoohi

Ecole Centrale de Lyon et Université Claude Bernard Lyon 1
LTDS UMR CNRS 5513

pour obtenir le titre de

Habilitation à diriger des recherches
Spécialité : MÉCANIQUE

Présentée et soutenue par

Alireza TURE SAVADKOOHI

Contribution à l'étude du contrôle passif par interactions non linéaires en mécanique et acoustique

soutenue le 12/11/2019

Jury :

Rapporteurs :	Bruno COCHELIN	-	ECM, LMA
	Emmanuel FOLTÊTE	-	Univ Franche-Comté, FEMTO-ST
	Gaëtan KERSCHEN	-	Univ Liège, S3L
Examinateurs :	Éric JACQUELIN	-	Claude Bernard Lyon 1, LBMC
	Anne TANGUY	-	INSA Lyon, LaMCoS
	Fabrice THOUVEREZ	-	ECL, LTDS
Invités :	Manuel COLLET	-	CNRS, LTDS
	Claude-Henri LAMARQUE	-	ENTPE, LTDS

Statement by author

This report has been submitted in fulfillment of requirements for the highest degree in French higher educational system, namely "Habilitation à Diriger des Recherches" (HdR), at the École Centrale de Lyon and the Université Claude Bernard Lyon 1.
During the literature review, references of figures which are taken from others works, are cited in the body of the text and also in their captions. All figures which are my own works and are published in journals, conferences and thesis of my supervised students, are cited directly in the body of the text without repetition of citations in the captions of figures.

Contents

CHAPTER 1

Introduction

Contents

1.1 An overview of structural controller systems

Evolutions of the structural systems with respect to the time and also induced time depended forces on them seek for necessary design tools for providing an appropriate and desirable structural behaviours during their life time which leads to comfort and safety of the users of these systems. One of the important design criterion for such structures is the control. The control process can be carried out via some modifications on main structural systems, eg. rigidities, masses, dampings or shapes and/or by inducing active/passive counter forces [Housner et al., 1997]. The aim of this report is to control/localize vibratory energies of structures via passive control systems. In following sections, after introducing some types of control systems, a review about passive control solutions is carried out.

1.1.1 Active control

An active control systems is composed of sensors and actuators that modify the response of the host structure to applied forces. In fact, an external source powers control actuator(s) that apply forces to the structure in prescribed manners. These forces can be endowed to add and/or to dissipate energies in structural systems. In active feedback control systems, the received signals by actuators are functions of the response of the main structure captures by physical sensors. This control system requires a power supply for assuring the operationally of actuators which provide control forces on the main structure [Housner et al., 1997, Chu et al., 2005, Korkmaz, 2011].

1.1.2 Passive control

The passive control process is carried out by localization and/or transformation of the vibratory energy to special structural elements and/or to other coupled oscillators [Mead, 1999]. This control

system does not need any external power source for its activation. In this case control forces are functions of the response of the main structure.

1.1.3 Hybrid control

The hybrid control system exploits combined properties of active and passive control systems [Chu et al., 2005]. For example, vibration control of cables combining distributed passive solution by shape wrapped memory alloy wires with an open loop actuator [Faravelli et al., 2010].

1.1.4 Semi-active control

The semi-active control system globally are a class of active vibration control systems. They only require external energy of smaller order of magnitude than normal active control systems to change system parameters, such as damping and stiffness [Liu et al., 2005, Liu et al., 2008].

1.1.5 Semi-passive control

Semi-passive systems globally are a class of passive vibration control systems, mainly endow adaptability properties of some multi-physics materials/systems such as electgromechanical ones in general and as an example shunted piezoelectric ceramics. These systems are used as sensors and as actuators in structural vibration control systems and create strong coupling between mechanical and electrical fields [Moheimani and Fleming, 2006]. The system presents change(s) in some of its mechanical/physical properties against modification of the parameters of electronic circuit connected to the electrodes. The adaptability properties of such systems provides interesting tools for the purpose of control where electromechanical parameters of such systems are modified according to the vibratory behaviours of main systems. These systems need a very small of energy for commanding/fitting the parameters of the electromechanical systems to characteristics of the vibration such as frequency [Guyomar and Badel, 2006, Guyomar et al., 2007, Mohammadi, 2008].

1.2 Passive system protectors

Passive system protectors change the behaviour of main system against induced vibration via localization, dissipation [Housner et al., 1997] and/or isolation [Ibrahim, 2008]. The concept of the vibration isolation is divided into two main categories [de Silva, 2005]: either the source of vibration is kept in isolation from other systems (force), see Fig. 1.1, or the main system is protected from the vibration (displacement) induced via its coupling with the source, as presented in Fig. 1.2. The controller systems can be partitioned in two parts: the first type of controlling logic deals with exploiting linear and/or nonlinear characteristics of some coupled oscillators for triggering vibration of main systems (see Fig. 1.3) [Frahm, 1911, Roberson, 1952] while the second category which is depicted in Fig. 1.4 uses the nonlinear capacities of some of elements of the main structures, eg. hysteresis behavior of semi-rigid joints, or another added devices such as viscous dampers [Braconi et al., 2008a, Braconi et al., 2008b, Dorka et al., 2005]. These devices can be divided into two large families, namely velocity-dependent devices and displacement-dependent devices.

1.2.1 Velocity dependent devices

In what it follows, we discuss about two types of velocity-dependent dampers

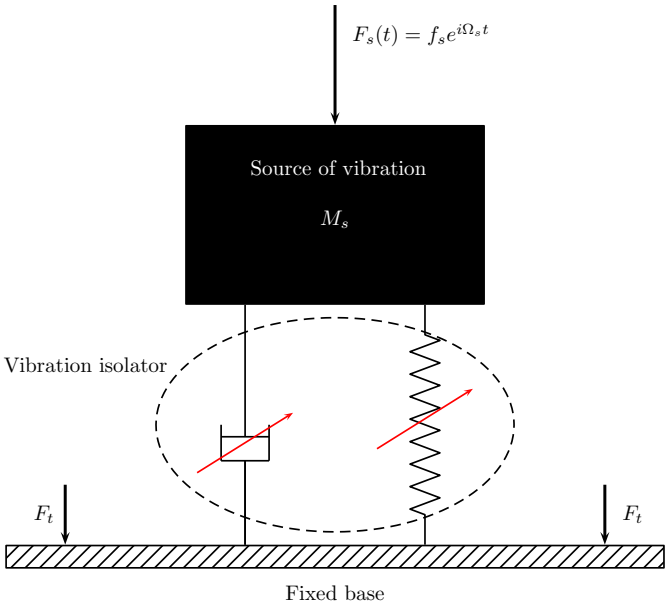

Figure 1.1: Isolation of the source of vibration M_s from other systems [de Silva, 2005].

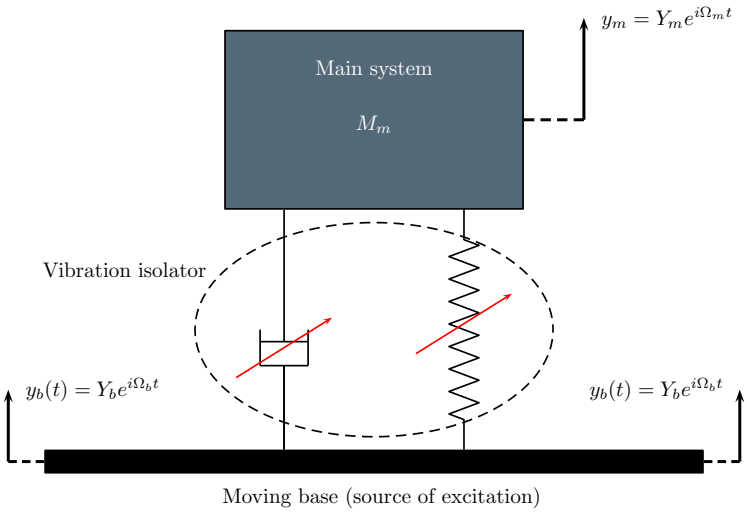

Figure 1.2: Isolation of the main system M_m from transmitted displacements via its coupling to the source (e.g. $y_b(t) = Y_b e^{i\Omega_b t}$) [de Silva, 2005].

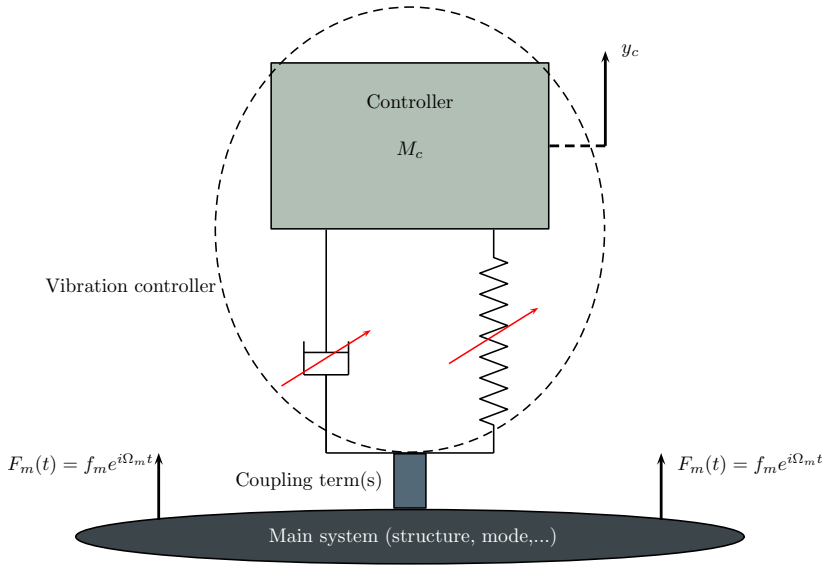

Figure 1.3: The passive control process via exploiting linear/nonlinear capacities of other coupled oscillators [de Silva, 2005].

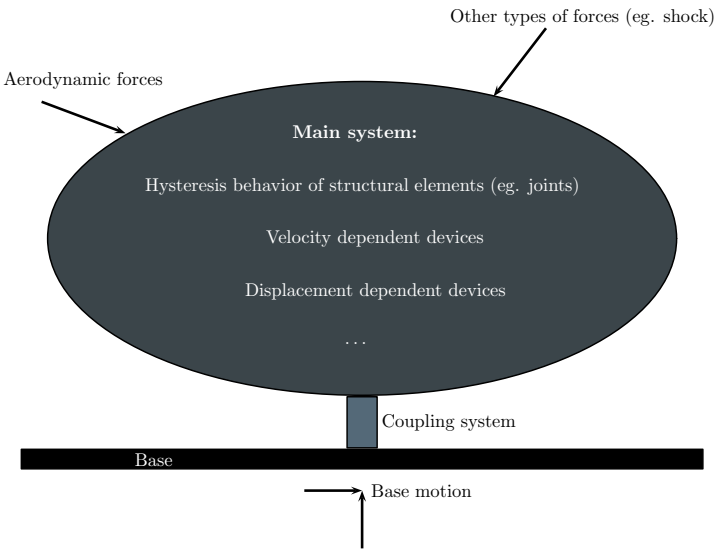

Figure 1.4: The localization of induced vibratory energy via exploiting the nonlinear capacities of some of elements (internal or external).

1.2.1.1 Fluid viscous dampers

Fluid viscus dampers are those which exploit the restoring force of the fluid forced to flow through an orifice and/or valve mechanism. An example of the constitutive law of such systems is as it follows:

$$F = C\dot{x}^{\alpha} \tag{1.1}$$

where x and C stand for displacement, respectively while the exponent α controls the type of the nonlinearity of constitutive law, eg. $\alpha = 0.15$ [FIP Industrial, 2016]. Figure 1.5 presents an example of such devices which is developed and fabricated by FIP Industrial while two example of their applications are represented in Fig. 1.6.

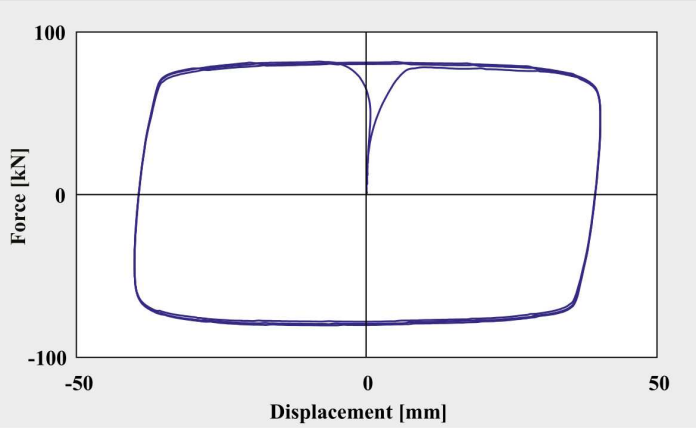

Figure 1.5: Hysteresis behaviours of the fluid viscus damper developed by FIP Industrial [FIP Industrial, 2016].

(a) (b)

Figure 1.6: Fluid viscus dampers [FIP Industrial, 2016]: a) Tests at FIP Industrial laboratory on a fluid viscous dampers at Rion-Antirion Bridge, Greece. ; b) Fluid viscous dampers installed in the tuned mass damper at the skyscraper Taipei 101, Taiwan.

1.2.1.2 Fluid spring dampers

Governing constitutive law of fluid spring dampers is summarized as it follows:

$$F = F_0 + Kx + C\dot{x}^{\alpha} \tag{1.2}$$

In this case the restoring force F depends on both velocity, via damping i.e. C, and displacement, via stiffness i.e., K. An example of hysteresis behaviour of such devices which is developed by FIP Industrial [FIP Industrial, 2016] is given in Fig. 1.7 while applications of such devices on structures are provided in Fig. 1.8.

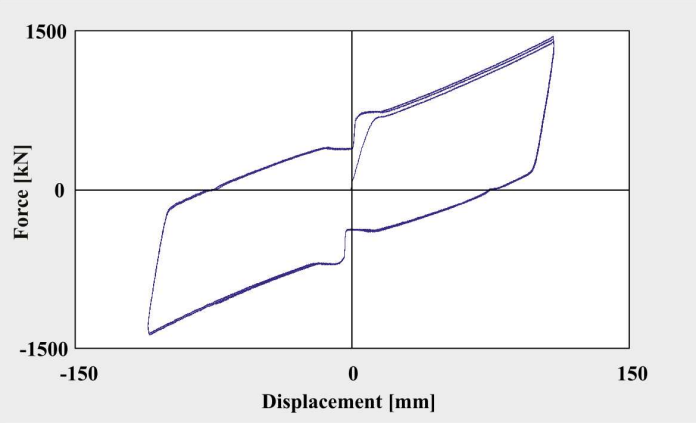

Figure 1.7: Hysteretic cycles of a spring fluid viscous damper without pre-load force, developed by FIP Industrial [FIP Industrial, 2016].

1.2.2 Displacement dependent devices

These dissipative systems are divided in two categories as nonlinear and linear absorbers. Some example of nonlinear displacement dependent devices are steel hysteretic dampers, shape memory

(a) (b)

Figure 1.8: Fluid spring dampers [FIP Industrial, 2016]: a) Spring fluid viscous dampers for the Badia Nuova flyover on highway A1; b) Fluid viscous dampers installed in Rio Higuamo Bridge, Dominican Republic.

alloy devices, buffer, etc while we can name elastomeric visco-elastic dampers as linear displacement dependent dampers.

1.2.2.1 Steel hysteretic dampers

Steel hysteretic dampers endow the elasto-plastic capacities of appropriately shaped elements in term of hysteresis response, designed to ensure a stable cyclic behaviour. Crescent-shaped and peg-shaped elements are the most used for bridges which can be combined with shock transmitters, while buckling-restrained axial dampers (BRAD®) are the most used as dissipative bracing in buildings [FIP Industrial, 2016]. An example of the constitutive law for such dampers is provided in Fig. 1.9 while two real applications of such system are presented in Fig. 1.10.

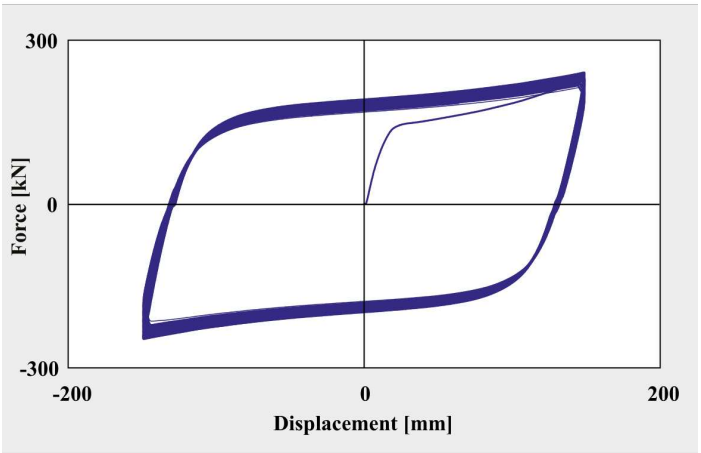

Figure 1.9: Experimental hysteresis cycles of a hysteretic damper with crescent-shaped elements, developed by FIP Industrial [FIP Industrial, 2016].

(a) (b)

Figure 1.10: Steel hysteretic dampers [FIP Industrial, 2016]: a) A damper consisting of double tapered peg elements and shock transmitters (Jamuna Bridge, Bangladesh); b) BRAD® dampers installed at the Cappuccini school of Ramacca, Italy.

1.2.2.2 Shape memory alloy devices

Shape-memory alloys present strongly nonlinear thermo-mechanical response associated with stress- or temperature-induced transformations of their crystalline structure [McNaney et al., 2003]. They are axial restraining devices that exploit the superelastic properties of shape memory alloys. These materials can recover plastic strain by suitable thermal cycles [Casciati et al., 1998]. The force-displacement curve, characterized by one or more plateaux (sections where force remains nearly constant while displacement increases), allows the devices to limit the maximum force transferred to the structure which they are connected to. They are also characterized by a significant re-centring capacity [FIP Industrial, 2016]. A typical experimental force-displacement curve of such systems is depicted in Fig. 1.11 and two examples of such systems in vibration control of masonry walls and systems are illustrated in Fig. 1.12.

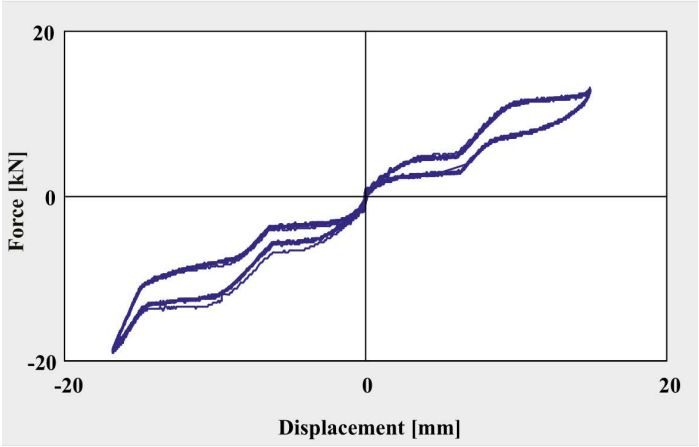

Figure 1.11: Experimental force-displacement curve of a shape-memory alloy device, developed by FIP Industrial [FIP Industrial, 2016].

(a) (b)

Figure 1.12: Shape-memory alloy devices [FIP Industrial, 2016]: a) Vibrating table tests on masonry walls with shape-memory devices used as horizontal tie rods; b) Devices installed at the San Francesco Basilica in Assisi, Italy.

1.2.2.3 Elastic devices (buffers)

Buffers are anti-lifting axial devices consisting of a set of elastomeric disc encased between steel plates. Steel plates are connected to the anchoring end via a particular arangements of a set of bars which permit the the discs to operate under compression, despite the direction of displacement, eg. shear. These devices are mainly implemented in bridges next to an abutment and/or between adjacent decks, over the joints [FIP Industrial, 2016]. A typical force-displacement curve of such devices is given in Fig. 1.13. Figure 1.14a shows the implemented elastic devices in the Rosario-Victoria link, Argentina. The connection between Rosario and Victoria is composed of several bridges, viaducts and earth-filled sections: The main structure is a cable-stayed bridge spanning 610 m with 1.1 km and 2.4 km long access ramps (see Fig. 1.15). There are 12 additional viaducts in the so-called Islas Z area, comprising more than 8 km in length, as well as 48 km of embankments to complete the total 60 km link. One of the design criterion was control of longitudinal hammering effects between adjacent bridge decks under seismic conditions. As a result, the total of 181 buffers was used. In detail: 106 units were endowed for the 12 viaducts in Islas Z area as well as 21 units for the Western approach bridge and 54 units for the Eastern access [FIP Industrial, 2016]. As a second example, these systems has been also implemented in the Somplago flyover, Italy, which is illustrated in Fig. 1.14b.

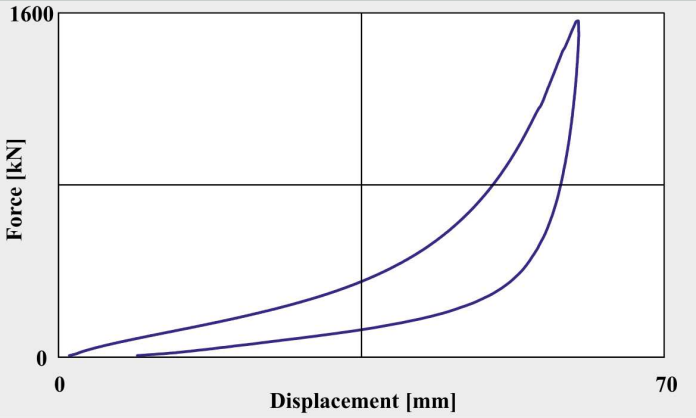

Figure 1.13: Experimental force-displacement curve of a buffer, developed by FIP Industrial [FIP Industrial, 2016].

1.2.2.4 Elastomeric viscoelastic dampers

Elastomeric viscoelastic dampers are in the category of linear displacement dependent devices, as it is depicted in Fig. 1.16. They are composed of one or several layers of high damping elastomeric mixture, characterized by equivalent viscous damping $15\% - 20\%$ and shear deformation of 100%. These devices connect the relative moving parts of structures. They are mainly used in bracing systems in buildings; the layers of elastomer can be arranged both on the vertical and horizontal plane (see Fig. 1.17) [FIP Industrial, 2016].

(a) (b)

Figure 1.14: Elastic devices [FIP Industrial, 2016]: a) Devices installed along the "Conexion Rosario-Victoria", Argentina; b) devices installed in the Somplago flyover, Italy: the first seismically isolated European bridge (1974-1976).

Figure 1.15: Rosario-Victoria motorway bridge, Argentina [Flores, 2007].

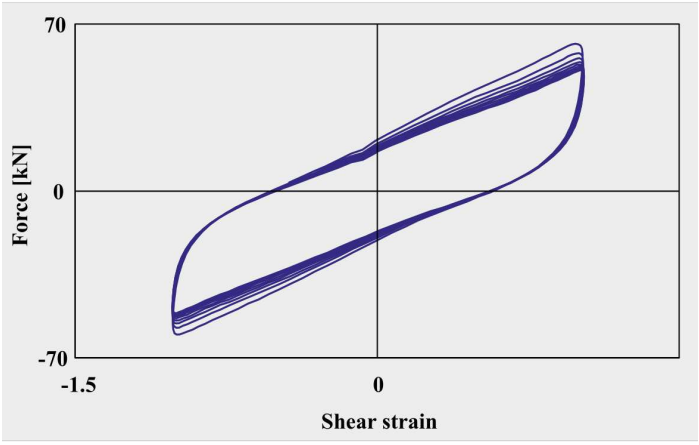

Figure 1.16: Experimental force-displacement curve of an elastomeric viscoelastic damper, developed by FIP Industrial [FIP Industrial, 2016].

(a) (b)

Figure 1.17: Elastomeric viscoelastic dampers [FIP Industrial, 2016]: a) Vibrating table tests on a concrete frame with Elastomeric viscoelastic dampers on top of a reverse V bracing; b) An elastomeric viscoelastic damper installed at the Gentile-Fermi school of Fabriano, Italy.

1.3 Aims and scopes of the report

The goal is to localize induced time depended forces on: i) structures by exploiting their own capacities, and/or ii) other coupled oscillators. Passive control of systems is divided in two main categories namely, linear and nonlinear controls. The most famous linear passive control soloutions is the Frahm device that is known as Tuned Mass Damper (TMD) [Frahm, 1911]. Here, a secondary linear oscillator, a TMD, is coupled to the main structure for destroying its resonance. Main drawbacks of such systems are: they are heavy and they modify the frequency of the main structure. Moreover, they are operational for narrow frequency bands. Nonlinear passive control process of systems exploits nonlinear potential of soul structural systems and/or coupled oscillators [Ibrahim, 2008]. Using the potential of soul structural systems for the aim of passive control consists of exploiting their nonlinear behavior(s) during time depended efforts. In this case induced external energy is dissipated via hysteresis responses of structural elements, such as joints, in the form of stress-strain and generalised force-generalised displacement [Bursi et al., 2004a, Braconi et al., 2008a, Braconi et al., 2008b]. Other types of nonlinear passive control systems consist of exploiting nonlinear (or non-smooth) behaviours of coupled oscillators for cancellation of vibrations of main structures [Gendelman, 2001, Gendelman and Vakakis, 2000, Tirelli and Anthoine, 2013]. Passive control systems have wide variety of applications including in acoustics [Cochelin et al., 2006], aerospace [Gendelman et al., 2010], civil and mechanical engineering [Vaurigaud et al., 2011a, Lamarque et al., 2011].

This report collects a summary of my own research contributions and works about nonlinear passive control of structural systems during my Ph.D. studentships (one chapter of my thesis) at the "Department of Mechanical and Structural Engineering" of the University of Trento in Italy (2004-2008), my postdoctoral period at the "LGM FRE CNRS 3237" and "LTDS UMR CNRS 5513" laboratories of the ENTPE in France (2008-2012) and finally as a faculty member and a researcher at the "LTDS UMR CNRS 5513" of ENTPE in France (2012-2019). Organization of the report as it follows:

Passive control of structures by endowing their own nonlinear behaviours and responses is described in Chapter 2. Experimental test results on the prototype structure, its identification process and damage quantifications are explained at the same chapter. A detailed literature review about passive control and vibratory energy localizations by using nonlinear systems is collected in Chapter 3. The targeted energy transfer [Aubry et al., 2001, Kopidakis et al., 2001] between main primary systems and other nonlinear oscillators is discussed in Chapter 4. The chapter starts with a general method-

ology for treatment of coupled oscillators during a 1:1 resonance and furnishes several studied cases in mechanical/structural engineering domains by using explained methodologies. Chapter 5 treats the targeted energy transfer in acoustics. The behaviours of a Helmholtz resonator (as an absorber) in nonlinear regimes are investigated in detail. Then, this resonator is coupled to an acoustical mode for the aim of passive noise control via using pure acoustical systems. Finally, the paper is concluded in Chapter 6 and several ideas as perspectives for my future works are provided.

CHAPTER 2

Localization of sever cyclic loads on semi-rigid joints of a steel-concrete moment-resisting structure

Contents

2.1 Introduction

Novel seismic design of steel and steel-concrete composite structures houses semi-rigid beam-to-column and base joints with inelastic behaviours. During seismic and cyclic excitations, semi-rigid composite steel-concrete moment-resisting frame structures can be designed to develop a ductile and hysteresis responses localised in components of beam-to-column joints and column bases, including flexural yielding of beam end plates, shear yielding of column web panel zones and yielding of anchors. So, global beam hinging mechanisms for seismic resistance can be obtained at a reduced cost as the force demand in joints and columns is governed by the expected capacity of the ductile connection components rather than by the beam flexural capacity. As a result, detection and evaluation of the actual damage owing to earthquakes in these structures becomes different to that in structures with rigid joints. The work described in this chapter is a part of my PhD thesis [Ture Savadkoohi, 2008] in the framework of an European projects, "ECOLEADER HPR-CT-1999-00059" [Bursi et al., 2004a] where a series of vibration experiments followed the application of pseudo-dynamic (PsD) [Bursi and Wagg, 2008] and quasi-static cyclic loadings on a semi-continuous moment resisting (MR) structure. The specimen was constructed and tested at the European Laboratory for Structural Assessment (ELSA) of the Joint Research Centre (JRC) in Ispra, and consisted of a full-scale two-storey two-bay frame with concrete slab dimensions in plan of 12.8×7.4 m^2, and 7.0 m in height. The testing programme included a sequence of PsD tests, simulating earthquakes with peak ground acceleration (pga) scaled up to the collapse onset limit

state (COLS), followed by a final cyclic test. The evaluation of damage due to seismic loading can be preformed by means of damage detection techniques that rely on Finite Element (FE) structural models and on the observations that structural frequencies decrease owing to damage while damping ratios increase. The initial FE model of a structural system is often a rough representation of its characteristics due to simplifications; for instance modelling the actual behaviour of semi-rigid joints can be a challenging task. Meanwhile, experimental data provide valuable information of how the structure behaves with regard to the initial FE model. As a result, the FE model can be improved in an FE model updating procedure that belongs to the class of inverse problems in classical mechanics [Friswell and Mottershead, 1995]. Model updating methods can be classified as sensitivity or direct methods [Friswell and Mottershead, 1995]. Sensitivity-type methods rely on a parametric FE model of the structure and the minimization of some penalty function based on the error between measured and predicted data. Direct updating methods are based on changes to complete mass and/or stiffness matrices. Structural model updating can rely on different data types: i) data from dynamic tests and ii) data retrieved from static or quasi-static tests. Dynamic-based identification techniques are more mature and therefore the corresponding literature is quite extensive [Ewins, 2000, Kerschen et al., 2006, Heller et al., 2009, Laxalde and Thouverez, 2009, Hot et al., 2012, Ouisse and Foltête, 2015, Samagassi et al., 2015, Samagassi et al., 2019]. With regard to the damage evaluation of structural joints, Wong et al. [Wong et al., 1995], Koh et al. [Koh et al., 2003], Wu and Li [Wu and Li, 2006], Pal et al [Pal et al., 2017] and Döhler et al. [Döhler et al., 2018] among others, identified damages in joints. These studies were successful in joint identification, although only simple beam-to-column joint models in the elastic range were considered. These studies highlight that the damage detection of semi-rigid joints experiencing severe inelastic damage, and more generally of composite structures characterized by low masses, low damping and complex geometry, remains largely unexplored. Three separate vibration test series were performed on the MR steel-concrete composite test structure: first, on the intact, undamaged structure; second, after attaining the life safe limit state; and finally, after that the structure had suffered severe cyclic loadings [Bursi et al., 2004a, Bursi et al., 2004b]. The structure was subjected to both sinusoidal and impulsive excitation and its response was recorded via three different configurations of accelerometers: one arrangement for the overall or global structural response and two sets for the analysis of interior and exterior joints, respectively. Since the structure was in a laboratory, the damage imposed was known and the bare structure could always be inspected.

2.2 Description of the structure and test programme

2.2.1 The test structure

The prototype two-storey structure shown in Fig. 2.1 was selected to have representative dimensions, member sizes and connection details in order to study the seismic behaviour of steel-concrete composite structural systems. The structure includes five identical two-bay moment-resisting frames with different span dimensions. The test structure was a two-storey, two-bay building specimen 7m high with plan dimensions from centre to centre of two exterior columns equal to 6.0 m $\times 12.0$ m; dimensions of composite slabs were slightly greater. The model was constructed with three moment resisting frames shown in Fig. 2.2, with unequal spans of 5 and 7 meters, respectively. Steel-concrete composite beams were formed by IPE300 steel profiles connected by full shear connection studs to a 15 cm thick concrete slab, cast on profiled sheeting. HEB260 and HEB280 partially-encased steel-concrete composite columns were used and high-ductile partial-strength composite beam-to-column joints were designed to provide plastic joint rotations of 35 mrad associated with a residual strength of at least 80% of their maximum value under earthquake loading [CEN. Eurocode 8, 2005]. In the transverse direction, secondary beams

were pinned and connected to column webs; and as illustrated in Fig. 2.3, two concentrically braced frames were designed to prevent any lateral instability. Each concrete slab was extended along the longitudinal and transverse directions of the exterior beam-to-column joints in order to provide additional resistance to hogging bending moments and to achieve the effective width of longitudinal composite beams. Figure 2.4 shows the general view of the test structure. Braconi et al. [Braconi et al., 2008a, Braconi et al., 2008b] provide more detailed information about the design and performance of the test structure.

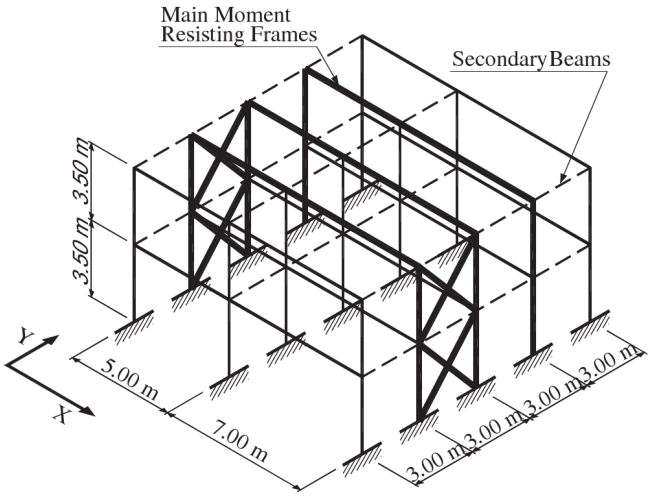

Figure 2.1: The scheme of the MR test structure.

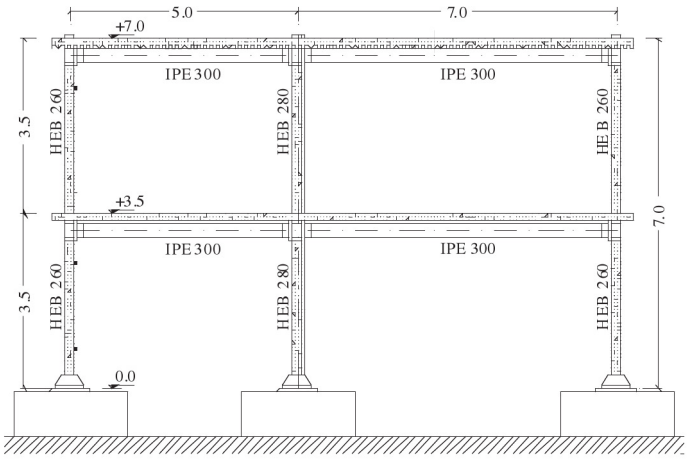

Figure 2.2: Side view of the test structure.

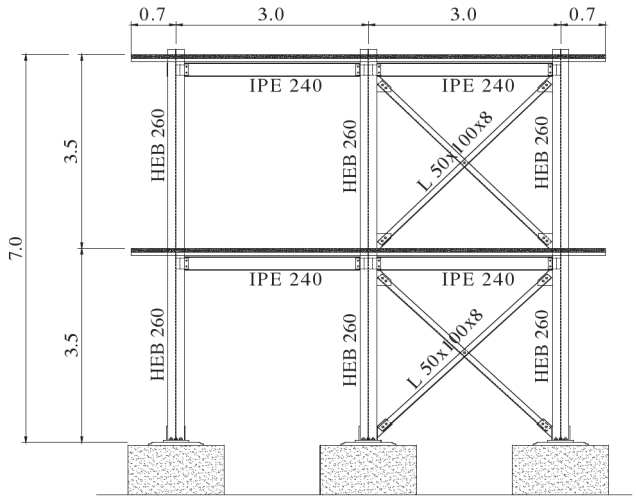

Figure 2.3: End view of the test structure.

Figure 2.4: Overall view of the test structure.

Table 2.1: Test programme and performance objectives.

Test	Vibration test	PsD test-pga (g)	Performance objective
I	Phase I		Identification at the undamaged state
1		0.1	Pseudo-elastic state
2		0.25	Serviceability limit state
3		1.4	Life safe limit state (LSLS)
II	Phase II		Identification at the LSLS
4		1.8	Collapse onset limit state (COLS)
5		Cyclic	Maximum top displacement to $300mm$
III	Phase III		Identification beyond the COLS

2.2.2 Test programme

The performance of the benchmark structure was investigated at four different pga levels during the PsD tests. The test levels were: 0.1g in order to characterize the pseudo-elastic state; 0.25g for the Serviceability Limit State (SLS); 1.4g for the Life Safe Limit State (LSLS); and 1.8g for the Collapse Onset Limit State (COLS). A final cyclic test beyond the COLS was also performed. Table 2.1 summarizes the test programme, with relevant objectives.

2.2.3 Dynamic tests, instrumentation and modal extraction

Forced vibration tests were performed in the three phases reported in Table 2.1[Bursi et al., 2004a]. They read as stepped sinusoidal tests (SST) and shock hammer Tests (SHT), performed by means of an electro-dynamic shaker ELECTRO-SEIS 400 with 33.79kg of total mobile mass and an instrumented sledge-hammer PCB 086D50 with a total mass of 10.77kg, respectively. Figure 2.5 shows the locations of the excitation forces. Three different accelerometer configurations were employed in each test. To acquire accelerations corresponding to the six global degrees of freedom (dof) of the structure, i.e. four translational and two torsional modes, a total of six accelerometers were applied to the structure as illustrated in Fig.2.5. In addition, local configurations, labelled B and C in Figs. 2.6a and 2.6b, were used to characterize the local dynamic behaviour of interior and exterior beam-to-column joints, respectively. To this end, accelerometers were applied to the column flanges with horizontal axes to acquire the web panel angular accelerations, shown in Figs. 2.7a and 2.7b, respectively. Translational and rotational accelerations were acquired on instrumented sections of both beams and columns, by arranging pairs of accelerometers above and below member axes. To improve the rotation measurements, accelerometers were well separated. With the same set-up, some kinematic components of some base joint rotations were also monitored, as shown in Figs. 2.6a and 2.6b. The six lowest natural frequencies of the structure, corresponding to translational and torsional modes, were evaluated by the dynamic tests. Modes were well separated and modal data were extracted by the circle-fit modal analysis technique [Ewins, 2000]. The resulting modal data are presented in Table 2.2 and the progressive reduction of the natural frequencies with damage, with an associated increase in the damping coefficients, is evident [Molinari et al., 2009, Ture Savadkoohi et al., 2011b]. Due to the fact that low energy dynamic tests were performed by means of the aforementioned exciters, the level of noise of the accelerometers may have introduced uncertainties in the damping ratios associated with higher modes. This trend can be noted in the torsional first mode, i.e. Mode 3 in Table 2.2, and with the flexural and torsional second modes, i.e. Modes 4-6. The results are coherent with values identified by other identification techniques [Chellini et al., 2008].

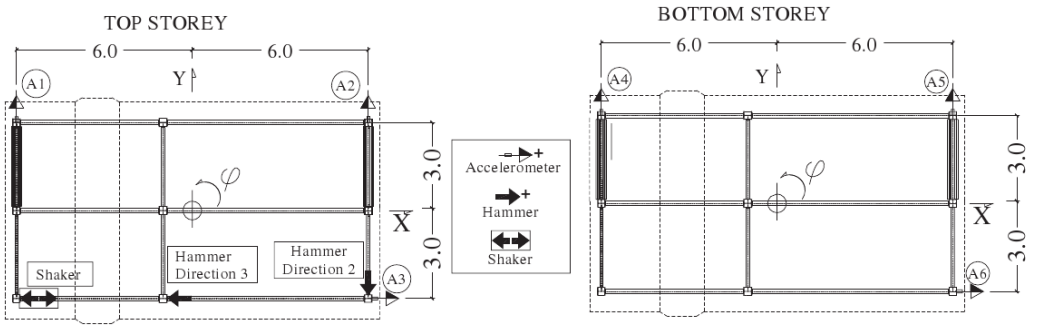

Figure 2.5: Location of the excitation devices, global configuration A of the accelerometers and location of sensors on top and bottom storeys.

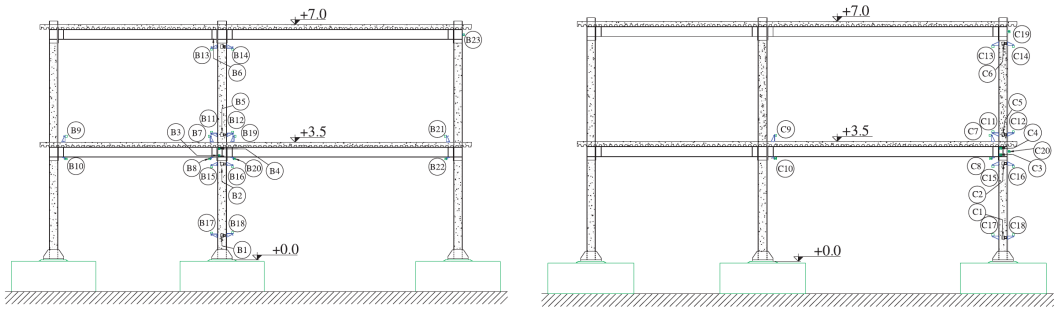

(a) (b)

Figure 2.6: Local configurations of accelerometers: a) interior frame; b) exterior frame.

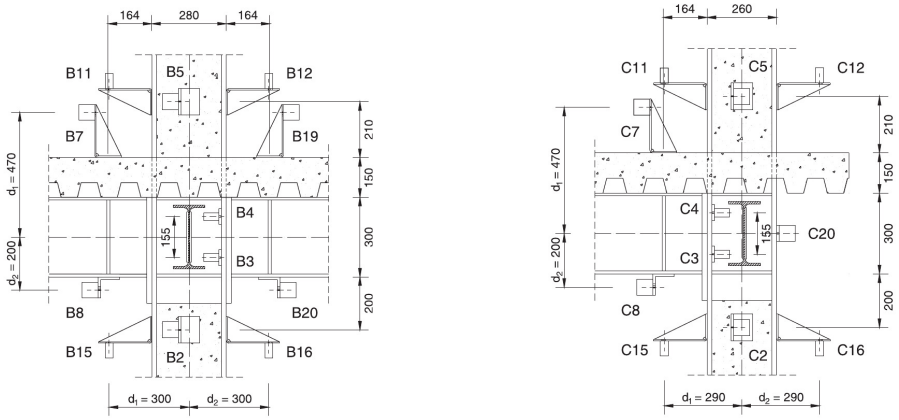

(a) (b)

Figure 2.7: Local configurations of accelerometers: a) interior beam-to-column joint; b) exterior beam-to-column joint.

Table 2.2: Experimental natural frequencies and damping coefficients extracted from both SST and SHT tests.

	Phase I		Phase II		Phase III	
Mode	Frequency (Hz)	Damping (%)	Frequency (Hz)	Damping (%)	Frequency (Hz)	Damping (%)
1	3.36	0.57	2.38	1.27	1.95	1.44
2	5.09	0.66	4.44	0.83	4.15	0.96
3	6.92	0.70	6.24	0.67	5.70	0.68
4	10.94	0.69	8.95	0.61	8.18	0.90
5	16.48	0.49	13.95	0.30	13.72	0.59
6	22.52	0.76	19.97	0.54	19.05	0.44

2.2.4 Cyclic test profile and instrumentation

The sinusoidal displacement profile shown in Fig. 2.8, characterized by stepwise increasing amplitudes, was applied at the top storey through two actuators, whilst the actuators at the bottom storey were controlled to keep the bottom/top storey reaction force ratio equal to 0.97 for the whole test. That ratio was determined from examining the first mode shape of the structure after the COLS. The corresponding bottom storey displacement is illustrated in Fig. 2.8 and is also characterized by a displacement increment of 50mm between cycles of increasing amplitude, with two equal cycles, up to a maximum of 300mm at the top storey. Two frames of the structure, shown in Fig. 2.9, are referred to as the exterior (A) and interior (B) frames, and were instrumented by means of strain gauges (SG), inclinometers (Inc) and transducers (Tr). Typical sensor lay-outs of an interior joint as well as column base joints are illustrated in Figs. 2.10a and 2.10b, respectively. All measurements obtained from inclinometers and storey displacements and forces are used for cyclic model updating, described in next section.

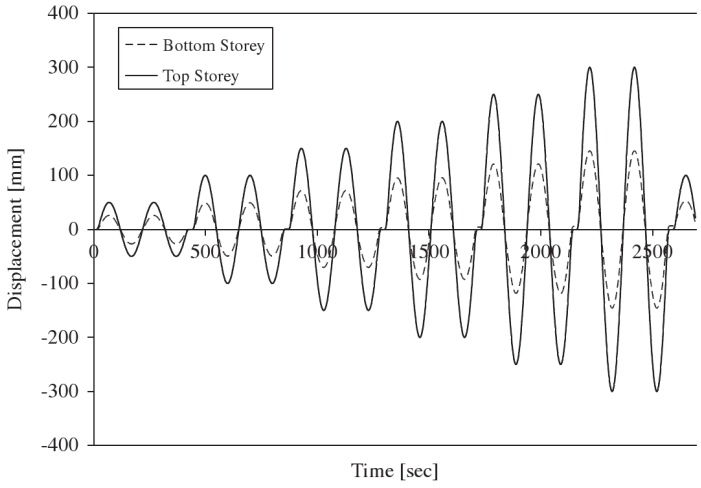

Figure 2.8: Displacement profile during the cyclic test.

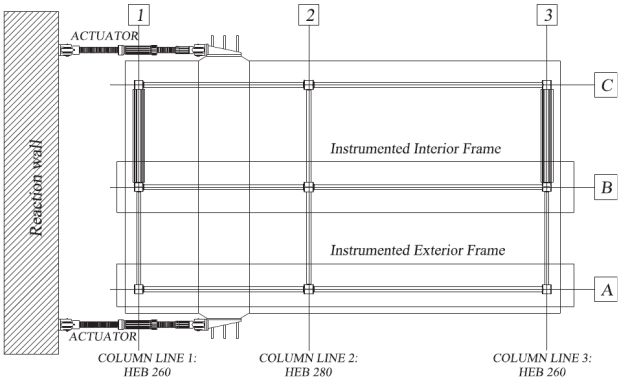

Figure 2.9: Test structure and instrumented frames during cyclic test.

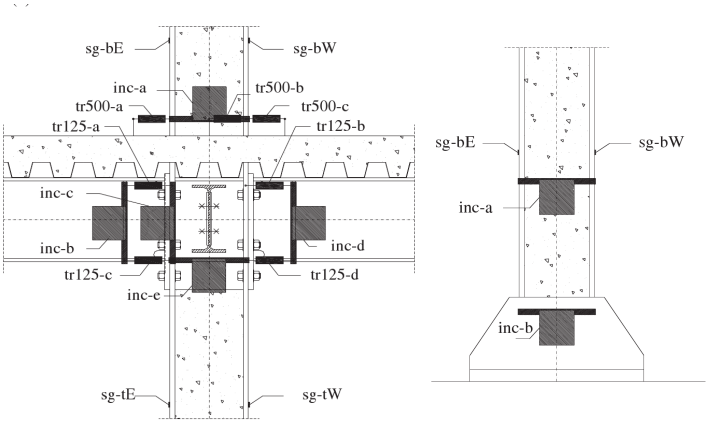

(a) (b)

Figure 2.10: Examples of instrumented joints: a) interior joints (2-B) at the bottom storey; b) base joint (2-B).

2.3 Identification and damage evaluation under cyclic loadings

2.3.1 Optimization procedure

A FE-based model updating leads to an optimisation process where discrepancies between numerically and experimentally traced data are minimised by adjusting some unknown model parameters. The objective function, $F(\mathbf{p})$, is the L_2-norm of the errors between the vectors of numerical and experimental data, and is minimized by seeking optimal parameter values through an inverse modelling process. A local minimizer, $\mathbf{p}^*$, is sought in a least squares problem,

$$F(\mathbf{p}) = \frac{1}{2}\Delta(\mathbf{p})^T\Delta(\mathbf{p}) \tag{2.1}$$

Normally, optimization algorithms [Bonnans et al., 2006] are iterative. The process starts with an initial guess of the optimal values of the variables and proceeds by generating a sequence of improved estimates until a solution is reached. The strategy used to move from one iteration to the next distinguishes one algorithm from another. Two well known methods are the steepest descent (SD) and the trust region (TR) methods. The SD method is a line search technique in the opposite direction to the gradient of $F(\mathbf{p})$, i.e. $\mathbf{h}_{SD} = -\nabla F_t(\mathbf{p})$, at the t^{th} iteration, and where the step length is chosen in various ways. TR methods generate steps via using a quadratic model of $F(\mathbf{p})$. They define a region around the current iterate within which they trust the model to be an adequate representation of $F(\mathbf{p})$. The step is then selected to minimize this approximate model in the trust region, and the direction and length of the step are determined simultaneously. If a step is not acceptable, the size of the region is reduced and a new minimizer is found. In general, the step direction alters whenever the size of the trust region is changed.
The Powell's Dog Leg (DL) technique [Powell, 1970, Madsen et al., 2004] belongs to the category of TR methods, but is a hybrid technique based on a combination of the Gauss-Newton (GN) and SD methods. A major problem with the DL method is the mechanism used to switch between two methods when it is appropriate. Depending on the solution at the previous step, the DL method constructs a trust region where the radius changes automatically depending on whether the step is far or close to a minimum. Let $\mathbf{p}_t$ and $\mathbf{h}_t$ be the current estimate of the parameter vector and the parameter increment at the t^{th} iteration, respectively. Then, there are two candidates for the step to be taken from the current position $\mathbf{p}_t$, given by steepest descent, $\aleph\mathbf{h}_{SD}$ (where $\aleph$ is determined by a line search), and Gauss-Newton, $\mathbf{h}_{GN}$. The strategy to choose the DL step size ensures that $\|\mathbf{h}_{DL}\| \leq R_{RT}$, where R_{RT} is the radius of the TR. This radius is adjusted at each iteration depending on the quality of the second order Taylor series approximating the penalty function [Madsen et al., 2004]. There are two main stopping criteria for the algorithm:

- the gradient $\nabla F(\mathbf{p})$ approaches zero, or

$$\| \nabla F(\mathbf{p})\|_\infty \leq \wp_1 \tag{2.2}$$

  where $\| \nabla F(\mathbf{p})\|$ is the infinite norm of $F(\mathbf{p})$ and $\wp_1$ is a very small positive number.

- the change in the parameters is small, or

$$\| \mathbf{p}_{t+1} - \mathbf{p}_t\| \leq \wp_2(\wp_2 + \| \mathbf{p}_t\|) \tag{2.3}$$

  where $\wp_2$ is also a very small positive number. This stopping criterion modulates the relative step size from $\wp_2$ when $\| \mathbf{p}_t\|$ is large to $\wp_2^2$ when $\| \mathbf{p}_t\|$ is close to zero.

2.3.2 Two-dimensional FE model of the structure

A two-dimensional (2D) FE model of the interior frame with 168 degrees of freedom was endowed for model updating of the system under cyclic loads. This model was considered appropriate because: i) the three main MR frames were identical; ii) cyclic tests were performed only in one direction; iii) the level of the static loading was very high. Beams and columns were modelled by means of the beam element formulation provided by the IDARC 2D software [IDARC2D, 2002]. Figure 2.11 shows the model of the beam-to-column joints while the column base joints were represented with springs and rigid links. The model was implemented in Mathematica® [Wolfram Research, Inc., 2007]. Figure 2.12 summarises the 2D FE model of the frame accompanied with joint numberings.

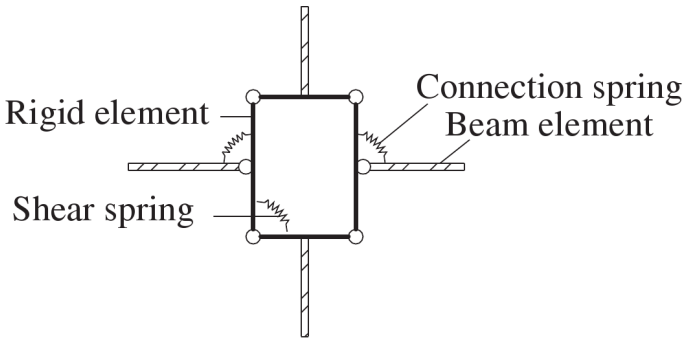

Figure 2.11: Semi-rigid beam-to-column joint model.

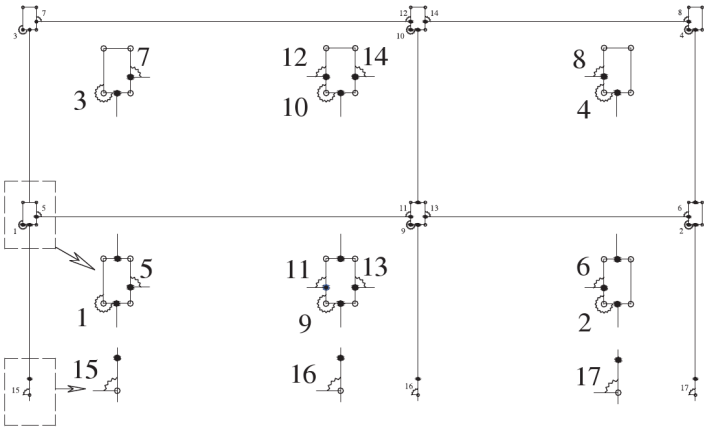

Figure 2.12: Employed 2D FE model of the interior frame for model updating under cyclic loading.

2.3.3 Model updating methodology under cyclic loading

Thirty-two data sets were acquired from the instrumentation during the cyclic test, including rotations of joint components, external forces and storey displacements. The model updating procedure for the structure under cyclic loading was based on the minimization of $F(\mathbf{p})$ represented in Eq. 2.1, where $\Delta(\mathbf{p})$ stands for residuals of experimental and analytical above mentioned quantities.

Twenty-five parameters are exploited to define the mechanical properties of different elements of the FE model as it follows:

$$K^{\text{element}} = p_j K_0^{\text{element}} \qquad j = 1, 2, \dots 25 \tag{2.4}$$

K_0^{element} defines the initial set of the stiffness corresponding to each parameter. Assigned parameters are listed as it follows: i) three parameters for the rotational stiffness of each base joints; ii) six parameters for the rotational stiffness of each shear panel; iii) eight parameters for the rotational stiffness of each connection; iv) four parameters for the flexural rigidity of each beam, long and short span at the top and bottom storeys; v) four parameters for the flexural rigidity of columns, one parameter to the flexural rigidity of both lateral columns and one parameter to the middle column, at each storey. As a result, $\Delta_t(\mathbf{p})$ at each iteration t reads:

$$\Delta_t(\mathbf{p}) = \mathbf{U}_{Xt} - \mathbf{U}_{Nt} \tag{2.5}$$

$\mathbf{U}_{Xt}$ and $\mathbf{U}_{At}$ are experimentally and numerically collected vectors (rotations and displacements), respectively. Equation 2.5 can be represented as:

$$\Delta_t(\mathbf{p}) = \mathbf{U}_{Xt} - \mathbf{K}_t^{-1}(\mathbf{p})\mathbf{L}_t \tag{2.6}$$

where $\mathbf{K}_t$ and $\mathbf{L}_t$ are the secant stiffness matrix and the external force vector imposed by the actuators, respectively. The corresponding Jacobian, $\mathbf{J}_t$, reads

$$\mathbf{J}_t = -\frac{\partial\left(\mathbf{K}_t^{-1}(\mathbf{p})\mathbf{L}_t\right)}{\partial \mathbf{p}} = \mathbf{K}_t^{-1}(\mathbf{p})\frac{\partial \mathbf{K}_t(\mathbf{p})}{\partial \mathbf{p}}\mathbf{K}_t^{-1}(\mathbf{p})\mathbf{L}_t \tag{2.7}$$

The DL optimization technique was employed using an initial radius $R_{TR}^0 = 1$ and $\wp_1 = \wp_2 = 10^{-6}$ in Eqs. 2.2 and 2.3. In order to bypass numerical instabilities due to nonlinear behaviours of the structure, especially when the secant stiffness becomes singular, as shown in Fig. 2.13a for a single parameter, a novel method was conceived. The technique is based on the transformation of origin coordinates of all time series at each half cycle to their absolute maximum value and updating the structure half cycle by half cycle, as shown in Fig. 2.13b [Ture Savadkoohi, 2008, Ture Savadkoohi et al., 2011b]. So, after updating the FE model in the very first half cycle, all of the measured data were transformed to their own absolute maximum values in all of the other half cycles. Hence the FE was updated in each virtual half cycle, and then the identified results were transformed to their original values using identified data from the previous half cycle. The implemented technique is fast as there is no need to exploit complex algorithms for tracing loading/unloading segments of response curves. Figures 2.14a and 2.14b summarise identified curves and corresponding experimental results, showing good agreements between both types of curves. So, the hysteresis behaviour of joint components of a statically indeterminate structure can be identified by cyclic model updating. Some of these relationships are shown in Fig. 2.15 (see Fig. 2.12 for numberings). It can be seen that the joint components exhibited a complex seismic performance complying with the requirements of Eurocode 8 for high ductility class MR frames [CEN. Eurocode 8, 2005].

2.3.4 Damage evaluations of the structure under cyclic loadings

After tracing the hysteresis behaviours of structural joints, their damage can be evaluated. The low-cycle fatigue energy-based model proposed by Chai et al. [Chai et al., 1995] is employed to quantify structural damage. The model uses a damage index, D_i, base on both displacement and energy, reads as:

$$D_i = \frac{\Delta_m}{\Delta_{um}} + \frac{\beta^*(E_h - E_{hm})}{V_y \Delta_{um}} \tag{2.8}$$

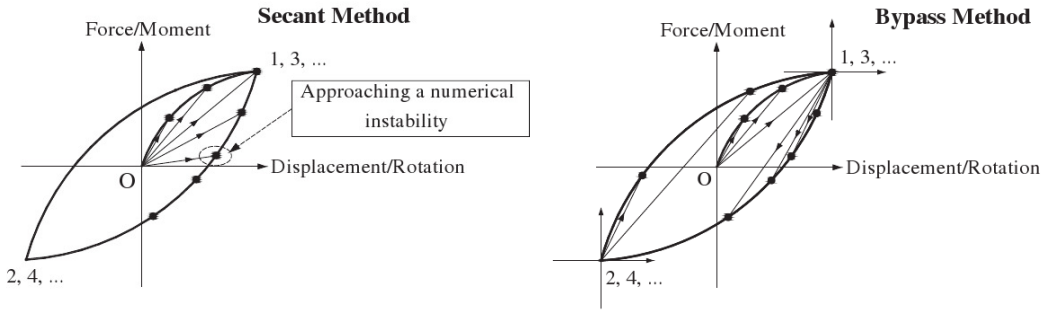

(a) (b)

Figure 2.13: Model updating procedure under cyclic loading for a single parameter: a) typical case involving numerical instabilities; b) the transformation of origin coordinates in the bypass method.

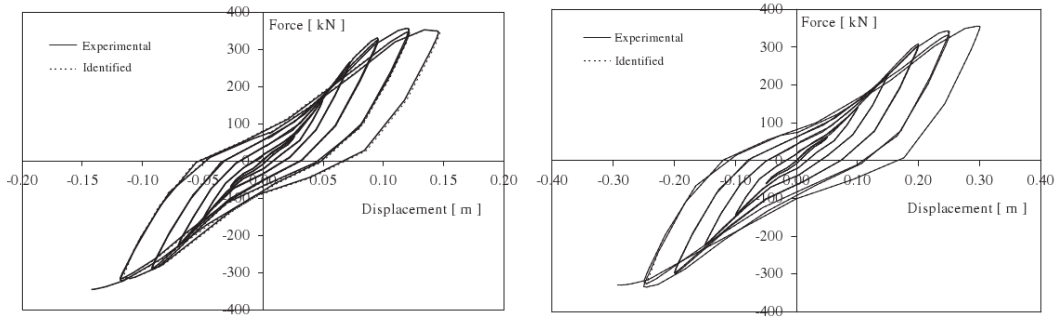

(a) (b)

Figure 2.14: Comparison of updated and experimental force vs. displacement: a) bottom storey; b) top storey.

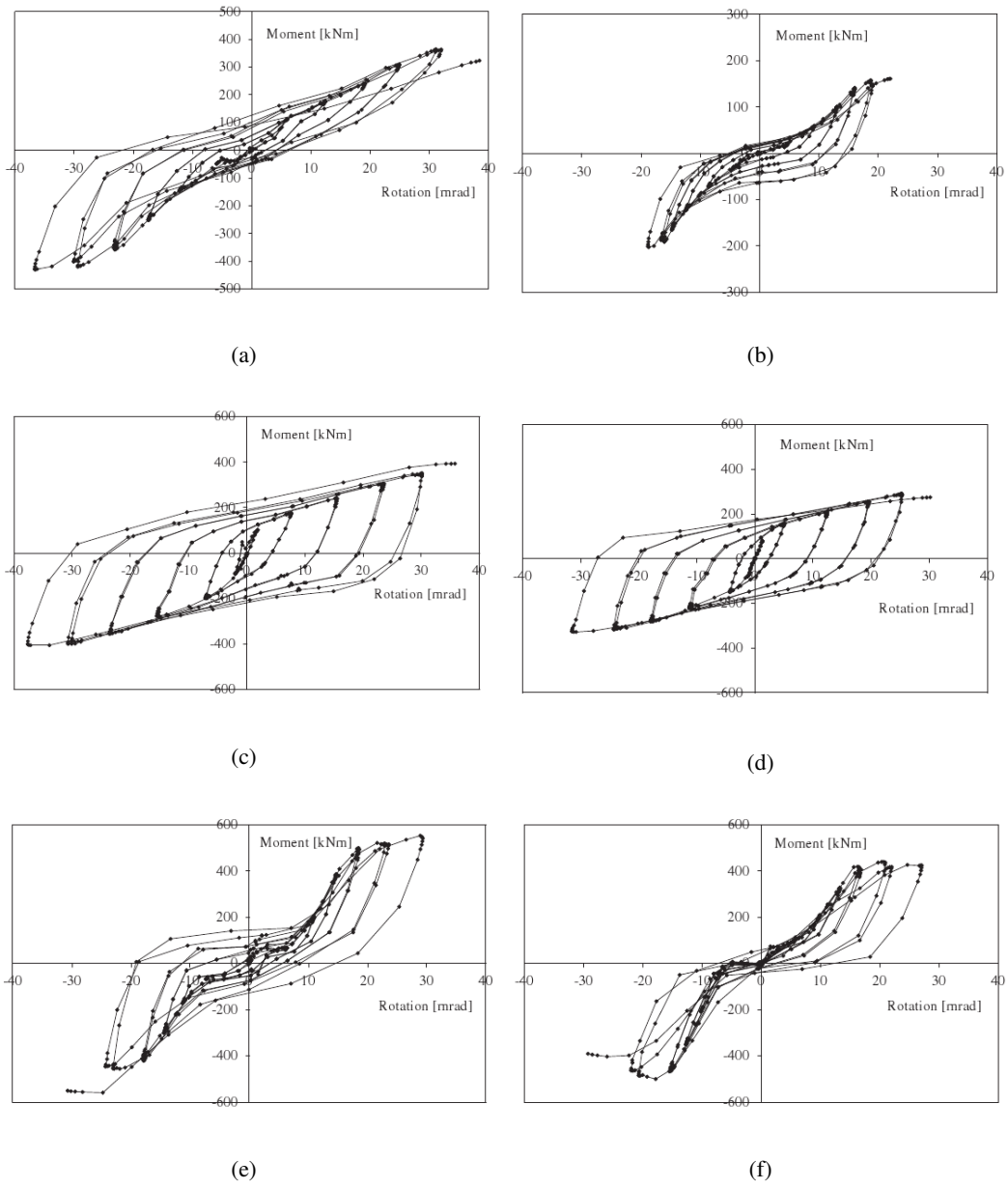

Figure 2.15: Identified joint components under cyclic loading-see Fig. 2.12 for elements numberings: a) connection spring n°5; b) connection spring n°8; c) shear panel spring n°9; d) shear panel spring n°10; e) column base joint spring n°16; f) column base joint spring n°17.

Table 2.3: Damage indices D_i of joint components using the model after Chai et al [Chai et al., 1995]. Components numbers are taken from Figs. 2.12 and 2.15.

Spring no.	3	4	6	7	8	15	16	17
D_i	0.34	0.90	0.89	0.96	0.78	0.55	0.63	0.48

where Δ_m is the maximum response displacement; Δ_{um} is the maximum displacement under monotonic loading; E_h is the plastic strain energy dissipated by the component; E_{hm} is the plastic strain energy dissipated by the components under monotonic loading. V_y is the yield strength of the component and β^* is the strength deterioration parameter that characterizes the damage contribution owing to cumulative plastic strain energy. Typical damage index values represent:

- $D_i \leq 0.4$: minor damage
- $0.4 \leq D_i \leq 1$: irreparable damage
- $D_i \geq 1$: component collapse

The parameter β^* can be obtained by calibrating the model against experimental data assuming that $D_i = 1$ corresponding to component collapse. As a results, from Eq. 2.8, one gets:

$$\frac{E_h}{V_y \Delta_{um}} = \frac{1}{\beta^*}\left(1 - \frac{\Delta_m}{\Delta_{um}}\right) + \frac{E_{hm}}{V_y \Delta_{um}} \tag{2.9}$$

This defines a damage limit domain that relates the normalized plastic strain capacity of the component to the maximum [Chai et al., 1995]. The slop of the line is $-\frac{1}{\beta^*}$. The plastic strain energy E_h is estimated using the procedure given by Chai et al. [Chai et al., 1995]. The lack of sufficient experimental results on the substructures means that β^* cannot be evaluated for each component, and hence monotonic and cyclic simulations of the 2D FE model by means of the IDARC 2D software [IDARC2D, 2002] are performed. As a result, estimates of $\frac{E_h}{V_y \Delta_{um}}$ and $\frac{\Delta_m}{\Delta_{um}}$ are defined for joint components with the corresponding best plots for each damage limit domain. The highest evaluated value of β^* is related to the base joints and is $\beta^* = 0.21$. This clearly indicates the high capacity of the base joints in absorbing and dissipating cyclic energy through end plates and anchor yielding. The D_i values of some of joint components are gathered in Table 2.3 [Ture Savadkoohi et al., 2011b]. The values of D_i generally higher than 0.4, explains both the design objectives and the severity of cyclic loads.

CHAPTER 3

Vibratory energy control by coupled nonlinear oscillators

Contents

3.1 A review of nonlinear passive control

One of well known and widely applied solutions for controlling vibratory energies of main structural systems is using linear capacities of coupled oscillators which are known as Frahm devices [Frahm, 1911] or TMD [Den Hartog, 1956, Sun et al., 1995]. This kind of devises, if tuned well, are capable of controlling the targeted mode of the system considerably. However, they suffer from some drawbacks which are listed here: practically their (modal) mass is big; they are tuned and operational for a narrow frequency band and they create new resonances for the overall system; they are designed for controlling particular solutions of forced systems while controlling their transient responses rest unsolved. It has been proved that by exploiting nonlinear capacities of coupled oscillators some interesting phenomena can be occurred which they do not exist in linear systems [Roberson, 1952].

The nonlinear oscillations due to nonlinear properties of systems have been in the centre of attentions of researches and under developments since (at least) the early 20$^{\text{th}}$ century, which studied theoretically (eg. see [Duffing, 1918, Den Hartog, 1933, Rauscher, 1936]) and experimentally (eg. [Ludeke, 1946]). Some of these developments aimed at endowing nonlinear properties of oscillators for passive vibratory control. Roberson [Roberson, 1952] considered the system which is depicted in Fig. 3.1 with following characteristics: a linear damped oscillator with the mass M_1 under sinusoidal excitations of constant amplitude as $F(t) = f_m \sin(\omega t)$, is attached to a dynamic absorber with the mass M_2 by means of a spring whose restoring forcing function, i.e. $\bar{\mathcal{H}}$, is sum of a linear and a cubic terms. Overall system equations read as:

$$\begin{cases} M_1\ddot{x}_1 + C\dot{x}_1 + Kx_1 + \bar{\mathcal{H}}(x_1 - x_2) = f_m \sin(\omega t) \\ \\ M_2\ddot{x}_2 + \bar{\mathcal{H}}(x_2 - x_1) = 0 \end{cases} \tag{3.1}$$

If one scales the system with respect to the dimensionless time $\omega t = \tau$ and defines $y_1 = x_1 \dfrac{k_1}{M_1} = x_1\omega_1^2$, $y_2 = (x_2 - x_1)\omega_1^2$, $\Omega = \dfrac{\omega}{\omega_1}$ and $\mu = \dfrac{M_2}{M_1}$, then following scaled form of the Eq. 3.1 can be obtained:

$$\begin{cases} \Omega^2\ddot{y}_1 + 2c\Omega\dot{y}_1 + y_1 - \mu\lambda^2 y_2 - \nu y_2^3 = \sin(\tau) \\ \\ \mu\Omega^2(\ddot{y}_1 + \ddot{y}_2) + \mu\lambda^2 y_2 + \nu y_2^3 = 0 \end{cases} \tag{3.2}$$

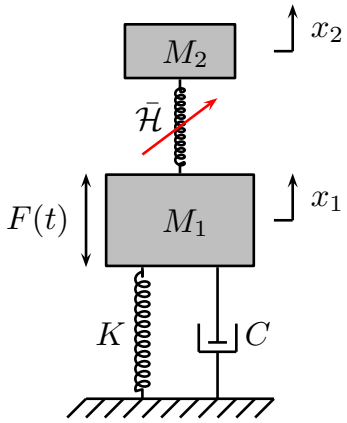

Figure 3.1: Considered system by Roberson [Roberson, 1952]: an oscillating main mass (M_1) is coupled to a nonlinear dynamic absorber (M_2).

where

$$\mathcal{H}(y_2) = \mu\lambda^2 y_2 + \nu y_2^3 \tag{3.3}$$

stands for the scaled nonlinear cubic restoring forcing function of the dynamic absorber. The algebraic sign of the cubic part of the function $\mathcal{H}$ can be positive or negative. The fact that linear vibration absorber can act as a vibration amplifier for some frequency intervals apart from the design value, was the motivation for the development of the Roberson [Roberson, 1952]. Let us name the finite value of Ω where the amplitude of the main oscillator, a_1, become zero as "cross-over" point denoted as Ω_x. Moreover, an interval of Ω^2-values around Ω_x^2 for which $\mid a_1 \mid \leqq 1$ is called as "suppression band" for the unit amplitude. The work of Roberson followed by an optimization criterion: the expected working frequency and maximum permitted response amplitudes are known ($a_1 = 1$). The goal is to place working frequency within the suppression band with the restriction that the absorber vibration amplitude not to be too large, defined as "forbidden region" (specially for a system with negative nonlinear part). Roberson designed a nonlinear absorber by imposing above mentioned criterion and restriction which is depicted in Fig. 3.2. Moreover, they showed that the suppression band for a system with nonlinear absorber is wider compared to corresponding linear one which it can be seen in Fig. 3.3. Later on Caughey [Caughey, 1954] performed a detailed investigation on the stability of stationary regimes of such systems. The same as "absorber" systems which are categorized globally into linear and nonlinear ones, the vibration isolators can be linear or nonlinear. The main structure (to be protected) is mounted on a flexible support. The stiffness of the support is tuned so that the natural frequency of the suspension stays far below the excitation frequency ranges. As a result, the effectiveness of the suspension as a vibration isolator will increase via lowering its natural frequency. Typical linear vibration isolators are not suitable for cancelling low frequency vibrations where in addition to stationary regime, the danger of shock excitations exists. The linear isolators to be capable of suppressing low frequency vibrations demand soft springs and so present excessive large displacements. To overcome these inconveniences, Tobias [Tobias, 1959] used symmetrical nonlinear springs which were able to support the "static weight" of the vertical systems (i.e. the effect of the gravity) to be isolated in the form of a preload. Their proposed isolator units for low frequency isolation incorporated "sine springs" (and a coil spring)

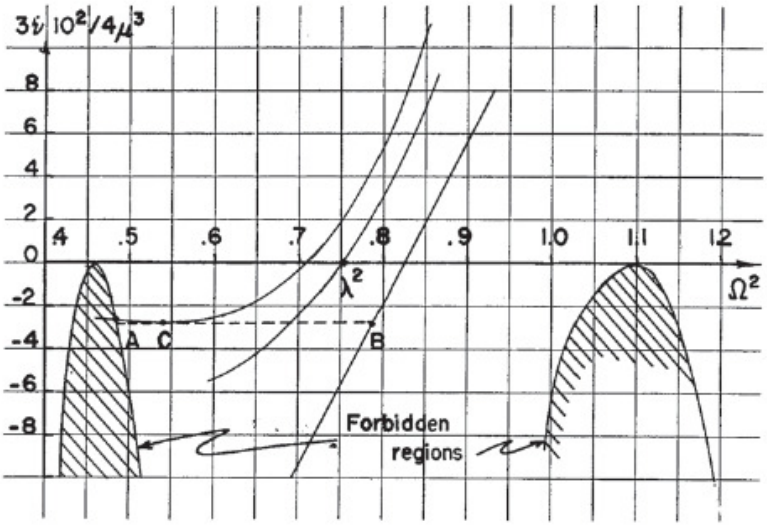

Figure 3.2: Cross-over curve (middle curve), boundaries of the suppression (left and right hand side curves) and forbidden regions for $\lambda^2 = 0.75$ and $\mu = 0.1$[Roberson, 1952].

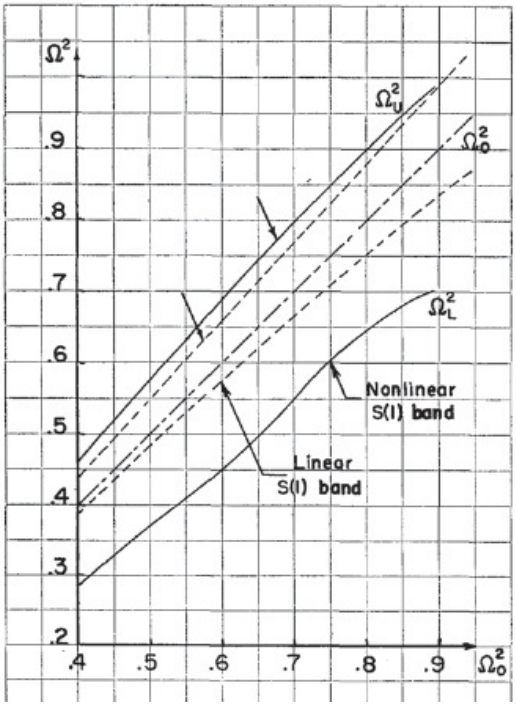

Figure 3.3: Comparison of the suppression band for optimum nonlinear absorber and the corresponding linear absorber [Roberson, 1952].

for vertical vibrations and “leaf springs" for horizontal vibrations.
Following the work of the Roberson [Roberson, 1952] for nonlinear vibration absorbers, there have been quite a lot of studies which consider systems of coupled nonlinear oscillators where one of them can be used for controlling the rest. Henry and Tobias [Henry and Tobias, 1959, Henry and Tobias, 1961] considered a general class of two dof nonlinear systems which is depicted in Fig. 3.4, showing their intention of exploiting nonlinear properties of coupled oscillators for control and isolation. The governing system equations have been reduced to the form of single mode motions via eliminating some coupling terms. They carried out stability analyses by perturbing a periodic motion of the system, which includes only first harmonic, reaching to the well-known Mathieu equation [Roseau, 1987]. They concluded that a mode initially at rest in a free nonlinear system may be parametrically excited via vibration in another mode and may become unstable. In this case modes of the system are coupled which prevents the occurrence of single-mode excitation, the motion which is typical characteristic of linear systems. Their studies have been completed via analysing the effects of damping on the stability of modes.
The free oscillations of a two-dof quasilinear conservative systems studied by Gilchrist [Gilchrist, 1961]. If x_1 and x_2 stand for normal coordinates, then the kinetic (T) and potential (V) energies of a conservative, linear two-dof system read as:

$$\begin{aligned} 2T &= T_1\dot{x}_1^2 + T_2\dot{x}_2^2 \\ 2V &= V_1x_1^2 + V_2x_2^2 \end{aligned} \tag{3.4}$$

The V is evaluated from the equilibrium position $x_1 = x_2 = 0$ which should be stable for the system under study. So, V_1 and V_2 are positive constants (the same as T_1 and T_2). If the system under consideration possesses quasilinear energy functions, then the dominant linear parts of energies are transferred to normal coordinates so that T and V may are written as:

$$\begin{aligned} 2T &= T_1\dot{x}_1^2 + T_2\dot{x}_2^2 + \varepsilon f_T(x_1, x_2, \dot{x}_1, \dot{x}_2) \\ 2V &= V_1x_1^2 + V_2x_2^2 + \varepsilon f_V(x_1, x_2) \end{aligned} \tag{3.5}$$

where ε is a positive and small parameter and f_T and f_V are analytic functions of velocities and displacements. Finally, governing system equations for considered conservative systems, i.e.

$$V + T = \text{constant} \tag{3.6}$$

may written as:

$$\begin{aligned} \ddot{x}_1 + k_1^2x_1 &= \varepsilon f_1(x_1, x_2, \dot{x}_1, \dot{x}_2) \\ \ddot{x}_2 + k_2^2x_2 &= \varepsilon f_2(x_1, x_2, \dot{x}_1, \dot{x}_2) \end{aligned} \tag{3.7}$$

with $k_j^2 = \dfrac{V_j}{T_j}$, $j = 1, 2$. Gilchrist [Gilchrist, 1961] treated in a pedagogic manner described class of two-dof conservative quasilinear systems of Eq. 3.7 via using asymptotic form of solution as described by Bogoliubov and Mitropolski [Bogoliubov and Mitropolsky, 1961] for systems with slowly varying phases and amplitudes. They studied “resonance” and “non resonance” cases. Resonance occurs when linear frequencies of the system 3.7 read:

$$\frac{k_1}{k_2} \approx \frac{q_2}{q_1} \tag{3.8}$$

with q_1 and q_2 are small mutually-prime integers. Let us distinguish two different cases:

- Resonances case, i.e. Eq. 3.8, is valid. In this case a frequency ω can be chosen in such a way that:

$$k_j^2 = (\frac{\omega}{q_j})^2 + \varepsilon\Delta_j \qquad j = 1, 2 \tag{3.9}$$

where Δ_j are de-tuning parameters. Equation 3.7 can be reorganised as:

$$\ddot{x}_j + (\frac{\omega}{q_j})^2 x_1 = \varepsilon \left(f_j \left(x_1, x_2, \dot{x}_1, \dot{x}_2 \right) - \Delta_j x_j \right) \qquad j = 1, 2 \tag{3.10}$$

To treat the system 3.10, Gilchrist [Gilchrist, 1961] sought its solution in the following form [Bogoliubov and Mitropolsky, 1961]:

$$x_j = a_j \cos(\frac{\omega}{q_j} t + \theta_j) + \varepsilon u_j^{(1)}(a_1, a_2, \theta_1, \theta_2, t) + \varepsilon^2 u_j^{(2)}(a_1, a_2, \theta_1, \theta_2, t) + \dots \tag{3.11}$$

with $j = 1, 2$ and $\varepsilon u_j^{(r)}$, $r = 1, 2, \dots$, are periodic functions in θ_1 and θ_2 while a_j and θ_j are variables evaluated from:

$$\begin{aligned} \frac{\mathrm{d}a_j}{\mathrm{d}t} &= \varepsilon A_j^{(1)}(a_1, a_2, \theta_1, \theta_2, t) + \varepsilon^2 A_j^{(2)}(a_1, a_2, \theta_1, \theta_2, t) + \dots \\ \frac{\mathrm{d}\theta_j}{\mathrm{d}t} &= \varepsilon B_j^{(1)}(a_1, a_2, \theta_1, \theta_2, t) + \varepsilon^2 B_j^{(2)}(a_1, a_2, \theta_1, \theta_2, t) + \dots \end{aligned} \tag{3.12}$$

$A_j^{(r)}$ and $B_j^{(r)}$, $r = 1, 2, \dots$, are periodic with $\dfrac{2\pi}{\omega}$ in θ_1 and θ_2. If one sets $\varepsilon = 0$ in the Eq. 3.7, then the described system solutions in Eq. 3.11 yield to:

$$x_j = a_j \cos(\frac{\omega}{q_j} t + \theta_j) \tag{3.13}$$

with a_j and θ_j being constant, i.e.

$$\frac{\mathrm{d}a_j}{\mathrm{d}t} = \frac{\mathrm{d}\theta_j}{\mathrm{d}t} = 0 \tag{3.14}$$

It is seen that, if $\varepsilon = 0$, then defined solutions in Eqs. 3.11, 3.12 are reduced to the system 3.13 and 3.14. To evaluate functions $u_j^{(r)}$, $A_j^{(r)}$, $B_j^{(2)}$ (when $\varepsilon \neq 0$), Eqs. 3.11 and 3.12 are injected in each equation of the system 3.10 and terms of the same order of ε are equated and are solved successively. Meanwhile, terms f_j in Eq. 3.10 can also be extended in the form of series. Then, at each order of the ε obtained ordinary differential equations should be solved by imposing solvability conditions such as removing secular terms.

- Non-resonance case, i.e. $\dfrac{k_1}{k_2}$ is far from $\dfrac{q_2}{q_1}$. The solution of 3.9 is taken as [Gilchrist, 1961]:

$$x_j = a_j \cos(\psi_j) + \varepsilon u_j^{(1)}(a_1, a_2, \psi_1, \psi_2) + \varepsilon^2 u_j^{(2)}(a_1, a_2, \psi_1, \psi_2) + \dots, \qquad j = 1, 2 \tag{3.15}$$

with ψ_j being the full phase and

$$\begin{aligned} \frac{\mathrm{d}a_j}{\mathrm{d}t} &= \varepsilon A_j^{(1)} + \varepsilon^2 A_j^{(2)} + \dots \\ \frac{\mathrm{d}\psi_j}{\mathrm{d}t} &= k_j + \varepsilon B_j^{(1)} + \varepsilon^2 B_j^{(2)} + \dots \end{aligned} \tag{3.16}$$

These expressions should be injected to Eq. 3.7 and terms with different orders of ε should be equated.

Free vibrations of a undamped pendulum type vibration absorber, see Fig. 3.5, studied by Sevin [Sevin, 1961] and Struble and Heinbockel [Struble and Heinbockel, 1963]; it consists of a simple flexible beam suspended at both ends from a gravity pendulum. The Rayleigh-Ritz method

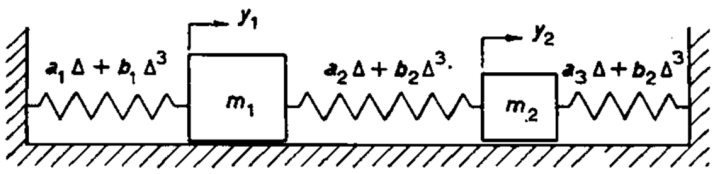

(a)

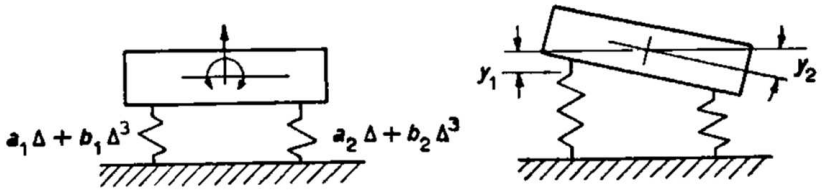

(b)

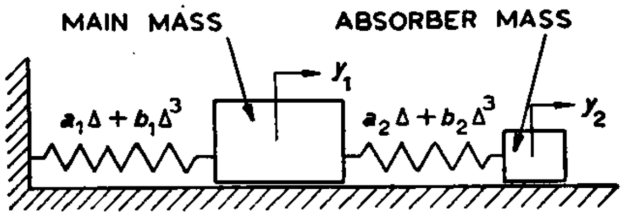

(c)

Figure 3.4: Studied nonlinear systems by Henry and Tobias [Henry and Tobias, 1959, Henry and Tobias, 1961]: Δ stands for spring deflection; a) General two dof system with symmetrical nonlinear springs; b) Vibration isolating suspension; c) Vibration absorber.

[Temple, 1928], was endowed for deriving system equations. For this, the deflection of the beam, i.e. $y(x,t)$ imposed to take following form:

$$y(x,t) = \sum_{n=1}^{N} a_n(t) \sin\left(\frac{n\pi x}{L_0}\right) \tag{3.17}$$

Governing system equations read as [Struble and Heinbockel, 1963]:

$$\begin{aligned} &\ddot{\theta} + \frac{\beta^2}{\Omega}\sin(\Omega\bar{\theta}) = \frac{1}{\Omega}\sin(\Omega\bar{\theta})\sum_{n=1}^{N}\ddot{\bar{a}}_{2n-1} \\ &\ddot{\bar{a}}_n + n^4\bar{a}_n = \frac{1-(-1)^n}{2n^2}\left(\frac{1}{\Omega}\ddot{\bar{\theta}}\sin(\Omega\bar{\theta}) + (\dot{\bar{\theta}})^2\cos(\Omega\bar{\theta})\right) \quad \text{with} \quad n = 1,2,\ldots \end{aligned} \tag{3.18}$$

If we set EI and m as beam modulus and its mass per unit length, g as gravitational acceleration, then the nondimensional variables of Eq. 3.18 read as: $\Omega^2 = \frac{\pi^2}{8}$, $\bar{\theta} = \frac{\theta}{\Omega}$, $\tau = \frac{L_0^2}{\pi^2}\sqrt{\frac{m}{EI}}$, $\bar{t} = \frac{t}{\tau}$,

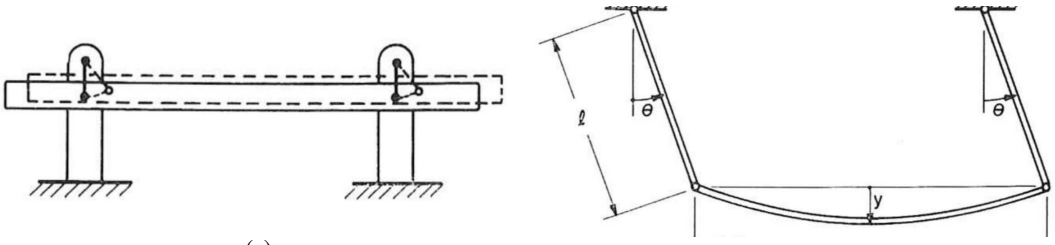

(a) (b)

Figure 3.5: Pendulum-type vibration absorber studied by Sevin [Sevin, 1961] and Struble and Heinbockel [Struble and Heinbockel, 1963]: a) The real system: a platform suspended on hangers; b) Idealized beam-pendulum system: a flexible beam simply supported at either end by hangers.

$\beta^2 = \dfrac{g\tau^2}{l}$, $a_{2n} = \bar{a}_{2n}$ and $a_{2n-1} = \dfrac{(2n-1)\pi l}{2}\bar{a}_{2n-1}$ with $n = 1, 2, \ldots$.
Sevin [Sevin, 1961] imposed small rotations assumptions on the behaviours of pendulums. It detail: two nonlinear coupled equations have been derived whose periodic solutions, based on the development as [Sevin, 1961],

$$\bar{\theta}(t) = \bar{\theta}_0 \cos(\beta \bar{t}) \tag{3.19}$$

are either stable or unstable depending on the initial conditions and also the ratio of the simple pendulum frequency to the frequency of the beam. The unstable mode causes a complete energy transfer which takes place periodically between two modes. A special internal resonance ("instability" according to Sevin [Sevin, 1961]) occurs when the beam frequency is about twice that of simple pendulum. Struble and Heinbockel [Struble and Heinbockel, 1963] sought solutions of the Eq. 3.18 in the form of series via a perturbation parameter ε as:

$$\begin{aligned} \bar{a}_1 &= \varepsilon A \cos(\bar{t} - \Phi) + \varepsilon^2 x_1 + \varepsilon^3 x_2 + \cdots \\ \bar{\theta} &= \varepsilon B \cos(\beta \bar{t} - \Psi) + \varepsilon^2 z_1 + \varepsilon^3 z_2 + \cdots \end{aligned} \tag{3.20}$$

They traced system response at different scales of ε and they detected system behaviours at non-resonant and resonant cases, i.e. $\beta \approx \dfrac{1}{2}$ and $\beta \approx 1$ [Struble and Heinbockel, 1963]. They found that during resonant cases, strong energy exchanges between the pendulum mode and higher modes of the beam take place. Carter and Liu [Carter and Liu, 1961] investigated on a system which is depicted in Fig. 3.6. The main system with the mass m_1 is coupled to an oscillator whose mass is m_2. The restoring forcing functions of two systems are $g(x_1)$ and $f(x_2 - x_1)$, respectively which read as:

$$\begin{aligned} g(x_1) &= k_1(x_1 \pm \gamma^2 x_1^3) \\ f(x_2 - x_1) &= k_2\left((x_2 - x_1) \pm \beta^2 (x_2 - x_1)^3\right) \end{aligned} \tag{3.21}$$

The difference between studied systems of Roberson [Roberson, 1952] and Carter and Liu [Carter and Liu, 1961] was only in characteristics of the main system: the one studied by Roberson [Roberson, 1952] was linear while the Carter and Liu [Carter and Liu, 1961] included cubic term in the restoring forcing function of the principal oscillator. With the one term approximation, Carter and Liu [Carter and Liu, 1961] concluded that the combination of a hardening main system and a softening spring of the absorber for the system under sweeping frequency of the external excitation provides very wide suppression width. A detailed investigation on dynamical behaviours of a general two-dof system with weak quadratic nonlinearities carried out by Sethna [Sethna, 1965]. The governing equations in the compact manner are written as:

$$\ddot{\xi}_n + s_n^2 \nu^2 \xi_n = \varepsilon\left(\varepsilon^{-1}\left(s_n^2\nu^2 - \omega_n^2\right)\xi_n - f_n(\xi_1, \xi_2, \dot{\xi}_1, \dot{\xi}_2) - F_n \cos(r\nu t)\right) \tag{3.22}$$

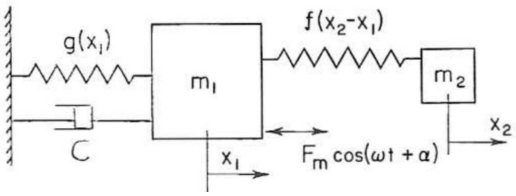

Figure 3.6: Dynamic vibration absorber investigated by Carter and Liu [Carter and Liu, 1961]: a main system with mass m_1 and a nonlinear restoring forcing term g is coupled to an absorber with the cubic nonlinear restoring function as f.

with $0 < \varepsilon \ll 1$ and $n = 1, 2$. After averaging [Bogoliubov and Mitropolsky, 1961, Mitropol'skii, 1965] governing system equations, two global division were made: autonomous and nonautonomous systems, corresponding to $F_n = 0$ and $F_n \neq 0$, respectively. Following cases have been distinguished:

- internal resonance for autonomous systems ($F_n = 0$) and nonautonomous ($F_n \neq 0$) systems: setting $s_2 \approx 2$, or the ratio of linear frequencies to be in the neighbourhood of the integer two.
- external resonance for nonautonomous systems ($F_n \neq 0$): the frequency of the external forcing term to be in the neighbourhood of one of the linear frequencies, i.e. $r \approx 1$ or $r \approx 2$.
- combinations of external and internal resonances for nonautonomous systems ($F_n \neq 0$):
  - the "superharmonic", i.e. $s_2 \approx 2$ and $r \approx 1$. In this case:

$$\begin{matrix} \omega_2 \approx 2\omega_1 \\ \nu \approx \omega_1 \end{matrix} \Rightarrow \omega_2 \approx 2\nu \tag{3.23}$$

  - the "subharmonic", i.e. $s_2 \approx 2$ and $r \approx 2$. In this case:

$$\begin{matrix} \omega_2 \approx 2\omega_1 \\ \nu \approx \omega_2 \end{matrix} \Rightarrow \omega_1 \approx \frac{1}{2}\nu \tag{3.24}$$

Among above mentioned cases, the authors studied in detail following resonance types: i) nonautonomous systems with internal and then external resonance in subharmonic and superharmonic cases; ii) autonomous systems with internal resonance or nonautonomous systems with internal resonance and no external resonance.
They traced an amplitude-modulated responses with modulation frequencies that are much more smaller than the frequency of the excitation.
I believe that the concept and existence (or intentionally creation) of internal and external resonances would be interesting topic for controlling a special mode via creation of subharmonic and superharmonic cases (e.g. see [Mook et al., 1986]).
An autoparametric vibration absorber was studied by Haxton and Barr [Haxton and Barr, 1972]. The absorber consists of a cantilever beam of the length l, first modal damping as c_2 and flexural rigidity EI which carries a concentrated end mass m (see Fig. 3.7). The absorber is coupled to a main system with the mass, damping and rigidity as M, c_1 and k, respectively which is under external excitation as $F(t) = F_0 \sin(2\Omega t)$. If the beam is projected on its first mode, then after ignoring gravitational effects, governing system equations are summarized as [Haxton and Barr, 1972]:

$$\begin{aligned} &\ddot{X} + 2\varepsilon\eta_1\omega_1\dot{X} + \omega_1^2 X - \varepsilon R(\dot{y}^2 - y\ddot{y}) = \omega_1^2 \cos(2\Omega t) \\ &\ddot{y} + 2\varepsilon\eta_2\omega_2\dot{y} + (\omega_2^2 - \varepsilon\ddot{X})y + \varepsilon^2 y(\dot{y}^2 + y\ddot{y}) = 0 \end{aligned} \tag{3.25}$$

with $X_0 = \frac{F_0}{k}$, $X = \frac{X_d}{X_0}$, $y = \frac{y_d}{X_0}$, $\varepsilon = \frac{6X_0}{5l}$, $\omega_1^2 = \frac{k}{M+m}$, $\omega_2^2 = \frac{\lambda}{m}$, $\lambda = \frac{3EI}{l^3}$, $R = \frac{m}{m+M}$, $\varepsilon\eta_1 = \frac{c_1}{2\omega_1(m+M)}$, $\varepsilon\eta_2 = \frac{c_2}{2\omega_2 m}$. They assumed the solution of Eq. 3.25 in the form of series, the same as Struble and Heinbockel [Struble and Heinbockel, 1963] performed for their system under consideration:

$$\begin{aligned} X &= A(t)\cos(\omega_1 t + \phi(t)) + \varepsilon X_1(t) + \varepsilon^2 X_2(t) + \dots \\ y &= B(t)\cos(\omega_2 t + \theta(t)) + \varepsilon y_1(t) + \varepsilon^2 y_2(t) + \dots \end{aligned} \tag{3.26}$$

where $A(t)$, $B(t)$, $\phi(t)$, $\theta(t)$ are slowly varying functions of time t. Variational terms in Eq. 3.25 are referred to $\mathcal{O}(\varepsilon^1)$ order of system of equations. The perturbational equations are those that correspond to higher orders of ε parameter. It has been assumed that $\frac{2\Omega}{\omega_1} \approx 1 + \mathcal{O}(\varepsilon^1)$ and $\omega_1 = 2\omega_2$, i.e. the systems presents combination resonances. First of all, they treated $\mathcal{O}(\varepsilon^1)$ of the system 3.25 imposing that first and second derivatives of slowly variables parameters can be set to zero. Obtained solution are injected back to variation solutions and finally response curve of the system with its stable and unstable zones, have been traced. Theoretical, numerical and experimental results by authors show that the autoparametric absorber is capable of controlling the main systems against vibrations. The comparison has been also carried out between the the control process via a TMD and the autoparametric absorber with the same mass ratio. Obtained results from studied system by Haxton and Barr [Haxton and Barr, 1972] showed that the autoparametric absorber is not favourable towards the TMD. But this comparison was made on a non optimized nonlinear vibration absorber. Meanwhile, the authors emphasise that if the external excitation is composed of multiple angular frequencies such as fundamental one as Ω and its first overtone as 2Ω, then the fundamental component will be absorbed via TMD action of the absorber while the overtone will be activate the autoparametric action of the absorber.

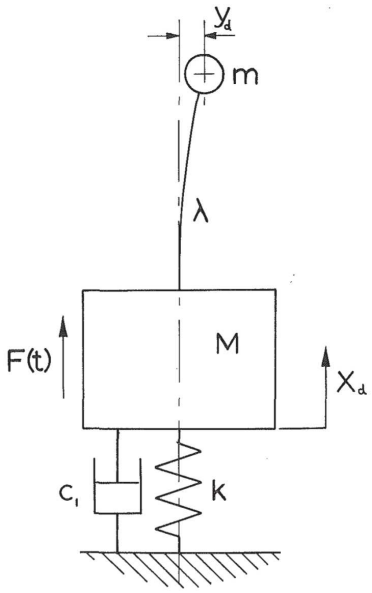

Figure 3.7: The schematic of the considered system by Haxton and Barr [Haxton and Barr, 1972]: an autoparametric absorber system composed of a beam with the flexural rigidity as EI, the point mass m and lateral stiffness as λ is coupled to a main system with the mass M.

The steady-state motion and asymptotic stability of a piece-wise linear oscillator is studied by Masri [Masri, 1972]. The effects of the gravity have been ignored. It has been shown that by proper tuning of parameters of the nonsmooth oscillator, they can be used for controlling the linear oscillator. Yamakawa et al. [Yamakawa et al., 1977] developed a nonlinear absorber which was composed of three permanent circular magnets, arranged to have a common guide going through their centres. This guide keeps the magnets in alignment so that the same poles are opposed to each other. The two magnets at the extremes are fixed (with an adjustable distance) while the middle one floats between two others. Via experimentation they managed to produce two types of nonlinear systems for vertical and horizontal oscillations, with restoring forcing functions as $f(z) = \alpha z - \beta z^2 + \gamma z^3 + \text{H.O.T}$ and $f(z) = \bar{\alpha} z + \bar{\gamma} z^3 + \text{H.O.T}$ for vertical and horizontal systems, respectively. Later on, Kojima and Saito [Kojima and Saito, 1983] implemented the same type of the magnetic nonlinear absorber to the vibration control of a beam. Kojima and Nagaya [Kojima and Nagaya, 1983] developed a torsional absorber which was made up of a circular conducting plate and four cylindrical rare-earth magnets. Their study started with theoretically analysing the magnetic torsional stiffness between two magnets followed by characterisation of magnetic damping experimentally. Their developed torsional restoring forcing function reads as $T(\theta) = \alpha\theta - \beta\theta^3$(softening Duffing-type) where T and θ are torsion and the angle, respectively. Hunt and Nissen [Hunt and Nissen, 1982] developed a nonlinear softening spring via arrays of Belleville washers mounted back to back for vibration control. Then, Nissen et al. [Nissen et al., 1985] optimized such nonlinear absorbers. The bow-type or shallow springs (or shallow buckled beam) has been exploited by Rice and McCraith [Rice and McCraith, 1987] for creation of a nonlinear coupling terms of an absorber. The system could be utilised to present hardening or softening behaviours. A simple back-to-back positioning of bows leads to softening responses as the ones of Hunt and Nissen [Hunt and Nissen, 1982]. The steady state responses of two coupled duffing type oscillators where the one with smaller mass is intended to be the controller is studied by Shaw et al. [Shaw et al., 1989]. They treated system equations with method of multiple scale [Nayfeh, 2000] considering a combination resonance when the operating frequency is approximately mean of two linearised natural frequencies of the system. They discussed about different possible responses of the system highlighting that the system can face quasi periodic responses with very large amplitude which destroys the effectiveness of the absorber. Ema and Marui [Ema and Marui, 1996, Ema and Marui, 2000] developed an impact damper with the application on suppression of vibrations of long, thin cutting tools such as boring tools or drills. They investigated on cases when the main system vibrates on the direction of the gravity or vertical to it. A combination of a TMD and an impact damper has been developed by Collette [Collette, 1998] for passive control of systems under random excitations. A numerical and parametric studies of an impact damper has been carried out by Blazejczyk-Okolewska [Blazejczyk-Okolewska, 2001]. In their studies the mass and the suspension spring of the impact damper are supposed to be smaller than the ones of the main systems. It is shown that the amplitudes of the main system around the first and also the second resonances are much smaller compared to traditional linear absorbers. Vyas and Bajaj [Vyas and Bajaj, 2001] investigated on the dynamical regimes of autoparametric absorbers endowing multiple pendulums inspired from the work of Haston and Bar [Haxton and Barr, 1972]. Instead of coupling a cantilever beam with a tip mass as an autoparametric absorber (see [Haxton and Barr, 1972]), they attached multiple array of pendulums to the main system as the vibration controller. The autoparametric absorbers exploit the energy exchanges between modes and also the saturation phenomena which mainly appear in quadratically coupled oscillators under primary excitation and having 1:2 internal resonances (see [Sethna, 1965]). However, Vyas and Bajaj [Vyas and Bajaj, 2001] showed that the suppression band of their studied absorbers can be augmented by exploiting pendulums with slightly different natural frequencies. Meanwhile, different possible responses of a single autoparametric absorber are discussed by Song et al. [Song et al., 2003] via using a harmonic balance technique and third order expansions of sinus and cosine of the angle of the pendulum.

At the early twenty-one century energy exchanges and the possibility of energy pumping in coupled systems are studied where one of them possessed pure cubic nonlinearity with no linear part. The considered system was two weakly coupled oscillators with linear and pure cubic nonlinearity for their reactions forces [Gendelman, 2001, Gendelman et al., 2001, Vakakis and Gendelman, 2001, Vakakis, 2001]. It has been shown that it is possible to induce a one-way irreversible energy tunnelling between two oscillators [Vakakis and Gendelman, 2001]. The pure nonlinear oscillator is named as nonlinear energy sink (NES). In the following section a brief literature review about the passive nonlinear vibratory control by NES systems to the date is provided.

3.2 Nonlinear passive control of main systems by NES devices

In the Sect. 3.1 a very brief and representative history of nonlinear passive controller systems and their mechanisms which have been developed since 20th century until the early 21th century is provided. In this section we take our attention on the passive control by NES systems which is the main focus of this report. It is seen that via exploiting the nonlinear nature of coupled oscillators, the passive control of primary systems can be improved to large extend with respect to the ones of linear controller systems. Passive vibratory energy transfer through mode localization has been applications in chemical physics, solid state and biological phenomena. Some examples of really extensive works in this domain are: vibratory energy exchanges at the solid-fluid interfaces [Vilallonga and Rabitz, 1986, Micha and Vilallonga, 1986, Vilallonga and Micha, 1987a, Vilallonga and Micha, 1987b, Vilallonga and Rabitz, 1990], energy exchanges in a lattice which consists of coupled Klein-Gordon systems [Akhatov et al., 1995, Khusnutdinova and Pelinovsky, 2003], etc. The vibratory energy exchanges between two nonlinear systems can be also seen that injection of amount of energy to discrete breather(s) of a nonlinear system (donor) which is weakly coupled to another nonlinear system [Aubry et al., 2001, Kopidakis et al., 2001, Maniadis et al., 2004]. Discrete breathers are time periodic and spatially localized solutions of coupled nonlinear oscillator systems [Flach and Willis, 1998, Iooss and James, 2005]. The existence of these intrinsic localized modes has been already spotted in the study of vibrational states of molecules [Scott, 2003]. To my knowledge (ATS), the term targeted energy transfer (TET) and its implementation have been first carried out by Aubry et al. [Aubry et al., 2001] and later on at the same year by [Kopidakis et al., 2001]. The phenomenon has been explained by authors as it follows: any vibratory energy induced to a harmonic oscillator which is weakly coupled to another harmonic oscillator channels back and forth between two oscillators if they are in resonance, i.e. they possess the same linear frequency. When the two oscillators are nonlinear (or anharmonic), their frequencies become amplitude dependent and any possible initial resonance will be broken. In this case, energy transfer will stop unless an almost perfect resonance persists during the whole transfer. In other words, although the frequencies of two oscillators vary during the transfer, but they should stay almost equal. The condition is that a certain detuning function is bounded from above and below. This TET is selective, i.e., it only occurs for an initial energy close to a specific value [Aubry et al., 2001]. The TET has been applied to the problem of ultrafast electron transfer and accounts for the experimentally observed phenomena in bacterial photosynthetic reaction centres [Aubry and Kopidakis, 2005, Memboeuf and Aubry, 2005, Hervé and Aubry, 2006]. The passive control process can be explained via exploiting the modal interactions due to internal and/or autoparametric resonances [Nayfeh and Mook, 1979, Nayfeh and Pai, 1989, Pai and Nayfeh, 1990, Monteil et al., 2014]. These kinds of resonances depend on the the type of nonlinearity of the system: if we suppose that ω_j stands for the natural frequency of the mode number j, then for systems with cubic nonlinearity the modal interactions can be seen if $\omega_m \simeq \omega_n$, $\omega_m \simeq |\pm 2\omega_k \pm \omega_l|$ or $\omega_m \simeq |\omega_n \pm \omega_k \pm \omega_l|$. In systems with quadratic nonlinearities, in additions to above con-

ditions we also can add $\omega_m \simeq 2\omega_n$ or $\omega_m \simeq \pm\omega_k \pm \omega_l$ [Nayfeh and Balachandran, 1989]. As it is shown by Mook et al. [Mook et al., 1986], the existence of internal resonance(s) may reduce the response of the system significantly. Moreover, the vibratory energy can shift periodically between the resonant modes instead of approaching a steady state. A comprehensive theoretical studies about combinational and internal resonances and their effects on the system responses can be found in [Szemplińska-Stupnicka, 1969, Szemplińska-Stupnicka, 1975, Szemplińska-Stupnicka, 1978, Szemplińska-Stupnicka and Bajkowski, 1980]. Globally speaking the TET and internal/combinational resonances are different and they can coincide in some spacial case. A good literature review about the passive control by NES technology using the TET can be found in [Lee et al., 2008, Vakakis et al., 2008].
The TET via exploiting the NES in its original version possessed essential cubic nonlinearity [Vakakis and Gendelman, 2001]. Meanwhile, during the past years other types of nonlinearities, e.g. non-polynomial ones [Gendelman, 2008], have been considered for the aim of TET. Some examples of studied nonpolynomial NES systems are:

- vibro-impact oscillators [Nucera et al., 2007, Lee et al., 2009, Gendelman, 2012, Gendelman and Alloni, 2015, Gourc et al., 2015a, Gourc et al., 2015b];
- piece-wise linear oscillators [Lamarque et al., 2011, Ture Savadkoohi et al., 2012a, Weiss et al., 2016, Hurel et al., 2019];
- oscillators with geometrical and hysteresis nonlinearities [Ture Savadkoohi et al., 2016a];
- oscillators with time-dependent masses [Ture Savadkoohi and Lamarque, 2014b].

Several experimentations for TET by exploiting NES systems have been carried out in mechanical and structural systems via using different nonlinearities. We can categorize these experimental tests according to the type of nonlinearity of the NES as:

- cubic nonlineairties [McFarland et al., 2005, Kerschen et al., 2005, Kerschen et al., 2007, Gourdon et al., 2007, Ture Savadkoohi et al., 2012b, Lamarque et al., 2018];
- vibro-impact systems [Nucera et al., 2008, AL-Shudeifat et al., 2013, Gourc et al., 2015b, Pennisi et al., 2017];
- piece-wise linear systems [Weiss et al., 2018].

After a brief introduction about the passive control by nonlinear absorbers and the TET, in Chapter 4 we will treat in detail the TET between coupled oscillators for passive control of main systems. After presenting a general methodology, some studied cases are presented and discussed.

CHAPTER 4

Targeted energy transfer in mechanical system via pure nonlinear mechanical resonators

Contents

4.1 Introduction

The primary step for passive control of main structural systems or equipments seeks for correct mathematical modelling of such systems describing their real behaviours as much as possible. They can be modelled via differential equations or differential algebraic inclusion. Examples for systems with differential equations are linear systems, smooth nonlinear oscillator and systems presenting hysteresis behaviours leading to nonsmooth differential equations or systems with elasto-plastic responses. Some times systems can not be described via differential equations, such as systems with friction or systems including Saint-Venant elements [Bastien et al., 2013]. In such cases, dynamics of the system should be defined via differential inclusions or differential algebraic inclusion if there exists some constraints in the system. The idea is to control main systems with above mentioned behaviours by one or several NES which can also present smooth or nonsmooth nonlinearities. In this chapter a general methodological package for treating energy exchanges between nonlinear oscillators is presented. Organization of the chapter is as it follows: In Sect. 4.2 passive control of a main systems including a rheology via a NES is studied in a general manner. One of the oscillators is intended to be the main structure/main mode and the second one is a nonlinear energy sink. The considered rheology is represented via a set of internal variables that are governed by either differential inclusions or differential equations or direct algebraic relations between system variables. A step by step methodology is presented to detect system behaviours around a $1:1$ resonance at different time scales. Fast and slow system equations provide its slow invariant manifold and detection of its periodic and modulated responses. The second part of the chapter considers a set of multiple degrees of freedom main systems which are attached to several nonlinear energy sinks housing several rheologies. In Sect. 4.3 the presented methodology of the Sect. 4.2 is extended to cover the general case around a $1:1$ resonances. To clarify explained methodologies in Sect. 4.2 and 4.3 an example is provided in Sect. 4.4 which treats a passive control problem of a linear system via a NES with geometrical nonlinearity and hysteresis responses. A summary of results of some treated systems, consisting of a main linear system and a single nonlinear absorber are presented in Sect. 4.6. The TET between a principal system and a chain of nonlinear oscillators treated via continua approach is discussed in Sect. 4.7. Finally some collaborations in this domain are listed in Sect. 4.8.

4.2 A two degrees of freedom nonlinear system around a $1:1$ resonance

The system is composed of two coupled oscillators: The main one with the mass as 1, the displacement x and internal variables z_j and $\dot{z}_j$ $(j = 1, \ldots, n)$ (representing parameters of a rheology) is under external force $\varepsilon f_0 \sin(\omega T)$. This oscillator is attached to a NES with the displacement y, the mass ε and a cubic or nonsmooth potential function. Governing equations of the system are

summarized as [Ture Savadkoohi et al., 2016b]:

$$\begin{cases} \underbrace{\ddot{x}+\tilde{f}_1(x,\dot{x},z_1,\dots,z_n,\dot{z}_1,\dots,\dot{z}_n)}_{\text{initial system with internal variables } z_j,\dot{z}_j,j=1,\dots,n} + \underbrace{\tilde{f}_2(x,\dot{x},y,\dot{y})}_{\text{coupling}} = \varepsilon f_0 \sin(\omega T) \\ \underbrace{\varepsilon\ddot{y}-\varepsilon f_2(y,\dot{y},x,\dot{x})}_{\text{additional dof (NES)}} = 0 \\ \text{Rheology} \rightarrow z_1,\dots,z_n,\dot{z}_1,\dots,\dot{z}_n(\text{Dimension } n). \text{ Constitutive laws for } z_1,\dots,z_n \\ \text{in neighbourhood of } (0,\dots,0). \end{cases} \tag{4.1}$$

Internal variables z_j and $\dot{z}_j$ ($j=1,\dots,n$) are governed by either differential inclusions, eg. Saint-Venant elements [Bastien et al., 2013], or differential equations, eg. Bouc-Wen models [Bouc, 1971, Ikhouane and Rodellar, 2007], or piece-wise direct algebraic relations between z_j, $\dot{z}_j$, x and $\dot{x}$ (or y and $\dot{y}$) via $\tilde{f}_1(x,\dot{x},z_1,\dots,z_n,\dot{z}_1,\dots,\dot{z}_n)$.
It should be mentioned that

- Equations 4.1 are re-scaled forms of original system equations with respect to the new time domain T.
- The parameter ε which is in fact the mass ratio of the main oscillator and the NES, is very small: $0<\varepsilon\ll 1$.
- We study system behaviour around a $1:1$ resonance. This is carried out by setting $\omega=\omega_0+\sigma\varepsilon$, where ω_0 is the re-scaled linear frequency of the main system, eg. $\omega_0=1$. The detuning parameter σ permits to detect system behaviours around the $1:1$ resonance.

In order to study and to predict behaviours of two oscillators at different scales of time, the system 4.1 is treated in following sections.

4.2.1 Possible change of system coordinates, complexifications and using the Galerkin technique

Some preliminary treatments of system 4.1 are carried out in order to prepare it for the time multi-scale analysis. They are listed here [Ture Savadkoohi et al., 2016b]:

- Linear transformation for x and y coordinates via $\mathbb{A}$ matrix:

$$\begin{pmatrix} v \\ w \end{pmatrix} = \mathbb{A} \begin{pmatrix} x \\ y \end{pmatrix} \tag{4.2}$$

  For instance, transferring the system to the centre of the mass and the relative displacement of two oscillators:

$$\mathbb{A} = \begin{pmatrix} 1 & \varepsilon \\ 1 & -1 \end{pmatrix} \tag{4.3}$$

- Depending on the condition of the system, complex variables of Manevitch (for systems without pre-stress) [Manevitch, 2001] or their extended versions (for pre-stressed systems) [Ture Savadkoohi et al., 2012a, Weiss et al., 2016] are applied ($i^2=-1$):

$$\begin{cases} ib_1+\varphi_1 e^{i\omega T} = \dot{v}+i\omega v \\ ib_2+\varphi_2 e^{i\omega T} = \dot{w}+i\omega w \\ \varphi_{3j} e^{i\omega T} = \dot{z}_j+i\omega z_j \qquad j=1,\dots,n \end{cases} \tag{4.4}$$

It should be mentioned that we can consider higher harmonics such as $(\varphi_{12}e^{2i\omega T} + \varphi_{13}e^{3i\omega T} + \ldots)$, $(\varphi_{22}e^{2i\omega T} + \varphi_{23}e^{3i\omega T} + \ldots)$ and $(\varphi_{3j2}e^{2i\omega T} + \varphi_{3j3}e^{3i\omega T} + \ldots)$.

- We consider different scales of the time, fast time scale (τ_0), slow time scale (τ_1),... connecting to each other by ε parameter:

$$T = \tau_0, \quad \tau_1 = \varepsilon\tau_0, \quad \tau_2 = \varepsilon^2\tau_0, \quad \cdots \tag{4.5}$$

- We use the Galerkin method, i.e. a truncated Fourier series (constant terms and first harmonics). For a general function $\daleth(b_1, b_2, \varphi_1, \varphi_2, \varphi_{31}, \ldots, \varphi_{3n})$ reads:

$$\chi(b_1, b_2, \varphi_1, \varphi_2, \varphi_{31}, \ldots, \varphi_{3n}) = \frac{\omega}{2\pi}\int_0^{\frac{2\pi}{\omega}} \daleth(b_1, b_2, \varphi_1, \varphi_2, \varphi_{31}, \ldots, \varphi_{3n})e^{-li\omega T}dT \tag{4.6}$$

with $l = 0, 1$ for evaluating constant terms and first harmonics of the Fourier series, respectively. For evaluating the integral of the Eq. 4.6, we assume that b_1, b_2, φ_1, φ_2, φ_{31}, ..., φ_{3n} do not depend on fast time scale, i.e. $\tau_0 = T$. This will be either verified during the time multi-scale analysis of the system or we will suppose that after a long transient response, the system reaches to an asymptotic state which is independent to time T (mathematically $\tau_0 \to \infty$).

4.2.2 Detection of system behaviours at different scales of time: fast and slow equations

A multiple scale method [Nayfeh and Mook, 1979] is exploited for detecting system behaviours at different scales of time. After embedding the time T into different scales, i.e. via Eq. 4.5, we would like to study system behaviours at each time scales, which means that we should consider system equations at different orders of ε. If we consider constant terms of Fourier series, i.e. by setting $l = 0$ in Eq. 4.6, then ε^0 and ε^1 orders of system equations provide both constant terms of Eq. 4.4, b_1 and b_2, as a function of pre-stressing terms. In the next sections we will focus on the evolutions of first harmonics of the system at different time scales.

4.2.2.1 Fast equations: ε^0 order of system equations

Let us consider first harmonics of the system via setting $l = 1$ in Eq. 4.6. At fast time scale the system yields to:

$$\frac{\partial\varphi_1}{\partial\tau_0} = 0 \Rightarrow \varphi_1 = \varphi_1(\tau_1, \tau_2, ...) \tag{4.7}$$

$$\frac{\partial\varphi_2}{\partial\tau_0} + \Lambda(\varphi_1, \varphi_2, \varphi_{31}, \varphi_{32}, \ldots, \varphi_{3n}) = 0 \tag{4.8}$$

$$\Upsilon(\varphi_1, \varphi_2, \varphi_{31}, \varphi_{32}, \ldots, \varphi_{3n}) = 0 \tag{4.9}$$

Let us consider Eq. 4.8 at the infinity of fast time scale, i.e. $\dfrac{\partial\varphi_2}{\partial\tau_0} \to 0$:

$$\Lambda(\varphi_1, \varphi_2, \varphi_{31}, \varphi_{32}, \ldots, \varphi_{3n}) = 0 \tag{4.10}$$

Equations 4.9 and 4.10 present an asymptotic equilibrium governed by a manifold called slow invariant manifold (SIM). Equations 4.7, 4.9 and 4.10 show that φ_1,φ_2, φ_{31}, ..., φ_{3n} are constant during the time $\tau_0 = T$, so our assumption for evaluating the constant and first terms of Fourier series in Eq. 4.6 is verified a posteriori. We can distinguish two possible cases for the SIM:

Case 1

Let us assume that Eq. 4.9 provides following explicit relation:

$$\varphi_{3j} = \mathbb{H}_{3j}(\varphi_1, \varphi_2), \quad j = 1, \ldots, n \tag{4.11}$$

so, Eq. 4.10 reads:

$$\Lambda(\varphi_1, \varphi_2, \varphi_{31}, \varphi_{32}, \ldots, \varphi_{3n}) = 0 \iff \tilde{\Lambda}(\varphi_1, \varphi_2) = 0 \tag{4.12}$$

We set $\varphi_j = N_j e^{i\delta_j}$, $j = 1, 2$. There are two possibilities on the relation between φ_1 and φ_2:

I There is an explicit relation between φ_1 and φ_2, i.e.:

$$\varphi_1 = \mathbb{H}(\varphi_2) \tag{4.13}$$

or,

$$\begin{cases} \delta_1 = h_1(\delta_2, N_2) \\ \\ N_1 = h_2(\delta_2, N_2) \end{cases} \iff \begin{pmatrix} \delta_1 \\ N_1 \end{pmatrix} = h(\delta_2, N_2) \tag{4.14}$$

II There is not an explicit relation between φ_1 and φ_2. In this case Eq. 4.12 provides two relations:

$$\tilde{\Lambda}(\varphi_1, \varphi_2) = 0 \iff \widehat{\Lambda}(\delta_2, N_2, \delta_1, N_1) = \begin{pmatrix} 0 \\ 0 \end{pmatrix} \tag{4.15}$$

Functions $\tilde{\Lambda}(\varphi_1, \varphi_2)$ are equations defined in the complex domain and $\widehat{\Lambda}(\delta_2, N_2, \delta_1, N_1)$ correspond to the same equations in the real domain.

Case 2

This case considers a very general form of the SIM supposing that there is not explicit relations between system variables. The general form of the SIM of the system by combining Eqs. 4.9 and 4.10 can be written in the compact form as:

$$\mathscr{S}(\varphi_1, \varphi_2, \varphi_{31}, \varphi_{32}, \ldots, \varphi_{3n}) = 0 \tag{4.16}$$

which is a set of equations in the complex domain. The same equations in the real domain read:

$$\widehat{\mathscr{S}}(\delta_2, N_2, \delta_1, N_1, \delta_{31}, N_{31}, \ldots, N_1, \delta_{3n}, N_{3n}) = 0 \tag{4.17}$$

4.2.2.2 Slow equations: ε^1 order of system equations

We are interested to study the system at slow time scale but around its SIM. This means that in the developments of system equations at ε^1 order, we should consider equations of the SIM which are obtained in Sect.4.2. The core idea is to detect equilibrium and singular points of the system which correspond to periodic regimes and strongly modulated response (SMR) of the system [Starosvetsky and Gendelman, 2008]. We can distinguish different scenarios according to different cases which have been defined in Sect.4.2:

Scenario 1

Let us suppose that the SIM follows assumptions of the **Case 1**:

I There is an explicit relation between φ_1 and φ_2.

$$\frac{\partial \varphi_1}{\partial \tau_1} = \mathscr{H}(\varphi_1, \varphi_2) \iff \begin{pmatrix} \dfrac{\partial \delta_1}{\partial \tau_1} \\ \\ \dfrac{\partial N_1}{\partial \tau_1} \end{pmatrix} = \begin{pmatrix} \mathscr{H}_1(\delta_2, N_2) \\ \\ \mathscr{H}_2(\delta_2, N_2) \end{pmatrix} \tag{4.18}$$

Let us consider evolution of the system along the SIM at τ_1 time scale. We inject Eq. 4.14 in the Eq. 4.18,

$$\nabla_{(\delta_2, N_2)} h \begin{pmatrix} N_2 \dfrac{\partial \delta_2}{\partial \tau_1} \\ \\ \dfrac{\partial N_2}{\partial \tau_1} \end{pmatrix} = \widetilde{\mathscr{H}}(\delta_2, N_2) \tag{4.19}$$

where $\nabla_{(\delta_2, N_2)} h$ denotes the Jacobian matrix of h versus variables δ_2 and N_2 (similar notations are used here after). Equilibrium points of the system are those which provide:

$$\begin{cases} \widetilde{\mathscr{H}}(\delta_2, N_2) = 0 \\ \\ \nabla_{(\delta_2, N_2)} h \text{ be invertible} \end{cases} \tag{4.20}$$

while singular points provide

$$\begin{cases} \widetilde{\mathscr{H}}(\delta_2, N_2) = 0 \\ \\ \nabla_{(\delta_2, N_2)} h \text{ not to be invertible} \end{cases} \tag{4.21}$$

II There is not an explicit relation between φ_1 and φ_2.

$$\frac{\partial \varphi_1}{\partial \tau_1} = \mathscr{F}(\varphi_1, \varphi_2) \iff \begin{pmatrix} \dfrac{\partial \delta_1}{\partial \tau_1} \\ \\ \dfrac{\partial N_1}{\partial \tau_1} \end{pmatrix} = \begin{pmatrix} \mathscr{F}_1(\delta_2, N_2, \delta_1, N_1) \\ \\ \mathscr{F}_2(\delta_2, N_2, \delta_1, N_1) \end{pmatrix} \tag{4.22}$$

Let us consider system modulations along the SIM at τ_1 time scale. Equation 4.15 is derived versus τ_1 time scale:

$$\nabla_{(\delta_2, N_2, \delta_1, N_1)} \widehat{\Lambda} \begin{pmatrix} \dfrac{\partial \delta_2}{\partial \tau_1} \\ \\ \dfrac{\partial N_2}{\partial \tau_1} \\ \\ \dfrac{\partial \delta_1}{\partial \tau_1} \\ \\ \dfrac{\partial N_1}{\partial \tau_1} \end{pmatrix} = \begin{pmatrix} 0 \\ \\ 0 \end{pmatrix} \tag{4.23}$$

The dimension of the matrix $\nabla \widehat{\Lambda}(\delta_2, N_2, \delta_1, N_1)$ is (2×4). In the blocked form it can be re-written as:

$$\nabla_{(\delta_2, N_2, \delta_1, N_1)} \widehat{\Lambda} = \left[\begin{array}{c|c} \nabla_{(\delta_2, N_2)} \widehat{\Lambda} & \nabla_{(\delta_1, N_1)} \widehat{\Lambda} \end{array} \right] \tag{4.24}$$

So, Eq. 4.23 reads:

$$\nabla_{(\delta_2,N_2)}\widehat{\Lambda}\begin{pmatrix}\dfrac{\partial\delta_2}{\partial\tau_1}\\[2ex]\dfrac{\partial N_2}{\partial\tau_1}\end{pmatrix}+\nabla_{(\delta_1,N_1)}\widehat{\Lambda}\begin{pmatrix}\dfrac{\partial\delta_1}{\partial\tau_1}\\[2ex]\dfrac{\partial N_1}{\partial\tau_1}\end{pmatrix}=\begin{pmatrix}0\\[2ex]0\end{pmatrix} \tag{4.25}$$

This equation can be rearranged by considering Eq. 4.22:

$$\nabla_{(\delta_2,N_2)}\widehat{\Lambda}\begin{pmatrix}\dfrac{\partial\delta_2}{\partial\tau_1}\\[2ex]\dfrac{\partial N_2}{\partial\tau_1}\end{pmatrix}=-\nabla_{(\delta_1,N_1)}\widehat{\Lambda}\begin{pmatrix}\mathscr{F}_1(\delta_2,N_2,\delta_1,N_1)\\[2ex]\mathscr{F}_2(\delta_2,N_2,\delta_1,N_1)\end{pmatrix} \tag{4.26}$$

Equations 4.15, 4.22 and 4.26 provide useful information relevant to positions of equilibrium and singular points. Equilibrium points of the system provide:

$$\begin{cases}\widehat{\Lambda}(\delta_2,N_2,\delta_1,N_1)=\begin{pmatrix}0\\0\end{pmatrix}\\[2ex]\mathscr{F}_1(\delta_2,N_2,\delta_1,N_1)=\mathscr{F}_2(\delta_2,N_2,\delta_1,N_1)=0\\[2ex]\nabla_{(\delta_2,N_2)}\widehat{\Lambda}\text{ be invertible}\end{cases} \tag{4.27}$$

Singular points of the system provide:

$$\begin{cases}\widehat{\Lambda}(\delta_2,N_2,\delta_1,N_1)=\begin{pmatrix}0\\0\end{pmatrix}\\[2ex]\mathscr{F}_1(\delta_2,N_2,\delta_1,N_1)=\mathscr{F}_2(\delta_2,N_2,\delta_1,N_1)=0\\[2ex]\nabla_{(\delta_2,N_2)}\widehat{\Lambda}\text{ not to be invertible}\end{cases} \tag{4.28}$$

Scenario 2

Let us consider a very general form of the SIM (see Eq. 4.16) which has been explained in **Case 2** of the Sect. 4.2.

At fast time scale we can write:

$$\begin{pmatrix} \frac{\partial \varphi_1}{\partial \tau_1} \\ \frac{\partial \varphi_{31}}{\partial \tau_1} \\ \vdots \\ \frac{\partial \varphi_{3n}}{\partial \tau_1} \end{pmatrix} = \mathscr{M}(\varphi_1, \varphi_2, \varphi_{31}, \ldots, \varphi_{3n}) \Longleftrightarrow \begin{pmatrix} \frac{\partial \delta_1}{\partial \tau_1} \\ \frac{\partial N_1}{\partial \tau_1} \\ \frac{\partial \delta_{31}}{\partial \tau_1} \\ \frac{\partial N_{31}}{\partial \tau_1} \\ \vdots \\ \frac{\partial \delta_{3n}}{\partial \tau_1} \\ \frac{\partial N_{3n}}{\partial \tau_1} \end{pmatrix} = \mathbb{M} \tag{4.29}$$

with

$$\mathbb{M} = \begin{pmatrix} \mathscr{M}_1(\delta_2, N_2, \delta_1, N_1, \delta_{31}, N_{31}, \ldots, N_1, \delta_{3n}, N_{3n}) \\ \mathscr{M}_2(\delta_2, N_2, \delta_1, N_1, \delta_{31}, N_{31}, \ldots, N_1, \delta_{3n}, N_{3n}) \\ \mathscr{M}_3(\delta_2, N_2, \delta_1, N_1, \delta_{31}, N_{31}, \ldots, N_1, \delta_{3n}, N_{3n}) \\ \vdots \\ \mathscr{M}_{2n+3}(\delta_2, N_2, \delta_1, N_1, \delta_{31}, N_{31}, \ldots, N_1, \delta_{3n}, N_{3n}) \\ \mathscr{M}_{2n+4}(\delta_2, N_2, \delta_1, N_1, \delta_{31}, N_{31}, \ldots, N_1, \delta_{3n}, N_{3n}) \end{pmatrix} \tag{4.30}$$

Equation 4.17 can be derived versus τ_1 time scale as:

$$\nabla_{(\delta_2,N_2,\delta_1,N_1,\delta_{31},N_{31},\ldots,N_1,\delta_{3n},N_{3n})}\widehat{\mathscr{S}}\begin{pmatrix} \frac{\partial\delta_2}{\partial\tau_1} \\ \frac{\partial N_2}{\partial\tau_1} \\ \frac{\partial\delta_1}{\partial\tau_1} \\ \frac{\partial N_1}{\partial\tau_1} \\ \frac{\partial\delta_{31}}{\partial\tau_1} \\ \frac{\partial N_{31}}{\partial\tau_1} \\ \vdots \\ \frac{\partial\delta_{3n}}{\partial\tau_1} \\ \frac{\partial N_{3n}}{\partial\tau_1} \end{pmatrix} = \begin{pmatrix} 0 \\ \vdots \\ 0 \end{pmatrix} \tag{4.31}$$

Dimension of the $\nabla_{(\delta_2,N_2,\delta_1,N_1,\delta_{31},N_{31},\ldots,N_1,\delta_{3n},N_{3n})}\widehat{\mathscr{S}}$ is $(2n+2)\times(2n+4)$. So, Eq. 4.31 provides $(2n+2)$ relations. In the blocked form we can write:

$$\nabla_{(\delta_2,N_2,\delta_1,N_1,\delta_{31},N_{31},\ldots,N_1,\delta_{3n},N_{3n})}\widehat{\mathscr{S}} = \left[\begin{array}{c|c} \nabla_{(\delta_2,N_2)}\widehat{\mathscr{S}} & \nabla_{(\delta_1,N_1,\delta_{31},N_{31},\ldots,N_1,\delta_{3n},N_{3n})}\widehat{\mathscr{S}} \end{array}\right] \tag{4.32}$$

Equation 4.31 reads;

$$\nabla_{(\delta_2,N_2)}\widehat{\mathscr{S}}\begin{pmatrix}\dfrac{\partial\delta_2}{\partial\tau_1}\\ \dfrac{\partial N_2}{\partial\tau_1}\end{pmatrix}+\nabla_{(\delta_1,N_1,\delta_{31},N_{31},\ldots,N_1,\delta_{3n},N_{3n})}\widehat{\mathscr{S}}\begin{pmatrix}\dfrac{\partial\delta_1}{\partial\tau_1}\\ \dfrac{\partial N_1}{\partial\tau_1}\\ \dfrac{\partial\delta_{31}}{\partial\tau_1}\\ \dfrac{\partial N_{31}}{\partial\tau_1}\\ \vdots\\ \dfrac{\partial\delta_{3n}}{\partial\tau_1}\\ \dfrac{\partial N_{3n}}{\partial\tau_1}\end{pmatrix}=\begin{pmatrix}0\\ \vdots\\ 0\end{pmatrix} \tag{4.33}$$

or

$$\nabla_{(\delta_2,N_2)}\widehat{\mathscr{S}}\begin{pmatrix}\dfrac{\partial\delta_2}{\partial\tau_1}\\ \dfrac{\partial N_2}{\partial\tau_1}\end{pmatrix}=-\nabla_{(\delta_1,N_1,\delta_{31},N_{31},\ldots,N_1,\delta_{3n},N_{3n})}\widehat{\mathscr{S}}\mathbb{M} \tag{4.34}$$

Equilibrium and singular points of the system can be traced via Eqs. 4.17, 4.29 and 4.34. Equilibrium points can be detected via

$$\begin{cases}\widehat{\mathscr{S}}(\delta_2,N_2,\delta_1,N_1,\delta_{31},N_{31},\ldots,N_1,\delta_{3n},N_{3n})=0\\ \mathbb{M}=0\\ \nabla_{(\delta_2,N_2)}\widehat{\mathscr{S}}\text{ be invertible}\end{cases} \tag{4.35}$$

Singular points of the system provide:

$$\begin{cases}\widehat{\mathscr{S}}(\delta_2,N_2,\delta_1,N_1,\delta_{31},N_{31},\ldots,N_1,\delta_{3n},N_{3n})=0\\ \mathbb{M}=0\\ \nabla_{(\delta_2,N_2)}\widehat{\mathscr{S}}\text{ not to be invertible}\end{cases} \tag{4.36}$$

4.3 Time multi-scale energy exchanges between a multiple degrees of freedom main oscillator and multiple NES including rheologies

The considered system and all developments in Sect. 4.2 are based on a two-dof system which includes a rheology of the dimension n (see Eq. 4.1). In this section, we consider a system that is composed of n_m-dof main oscillators which are coupled to n_n-dof NES

[Ture Savadkoohi et al., 2016b]. The dimension of the rheology is assumed to be n_r. Let us assume that system equations read:

$$\begin{cases} \ddot{\boldsymbol{Y}}_1+\boldsymbol{\Delta}_1\boldsymbol{Y}_1+\varepsilon\boldsymbol{\Delta}_2\dot{\boldsymbol{Y}}_1+\underbrace{\varepsilon\tilde{\mathfrak{F}}_1(\boldsymbol{Y}_1,\boldsymbol{Y}_2)+\varepsilon\tilde{\mathfrak{F}}_2(\dot{\boldsymbol{Y}}_1,\dot{\boldsymbol{Y}}_2)}_{\varepsilon\tilde{\tilde{\mathfrak{F}}}(\boldsymbol{Y}_1,\boldsymbol{Y}_2,\dot{\boldsymbol{Y}}_1,\dot{\boldsymbol{Y}}_2)}+\mathfrak{E}(\boldsymbol{Y}_1,\boldsymbol{Y}_2,\dot{\boldsymbol{Y}}_3)=\varepsilon\boldsymbol{f}_0 sin(\omega T) \\ \varepsilon\ddot{\boldsymbol{Y}}_2-\varepsilon\tilde{\tilde{\mathfrak{F}}}(\boldsymbol{Y}_1,\boldsymbol{Y}_2,\dot{\boldsymbol{Y}}_1,\dot{\boldsymbol{Y}}_2)=\boldsymbol{0} \\ \dot{\boldsymbol{Y}}_3+\boldsymbol{G}(\boldsymbol{Y}_1,\boldsymbol{Y}_2,\boldsymbol{Y}_3)=\boldsymbol{0} \ \text{ or } \ \left(\dot{\boldsymbol{Y}}_3+\boldsymbol{G}(\boldsymbol{Y}_1,\boldsymbol{Y}_2,\boldsymbol{Y}_3)\right)\ni\boldsymbol{0} \end{cases} \tag{4.37}$$

Where $\boldsymbol{Y}_1$, $\boldsymbol{Y}_2$ and $\boldsymbol{Y}_3$ are vectors of dimensions n_m, n_n and n_r, respectively. $\boldsymbol{f}_0$ is the vector of applied external forcing amplitudes on each dof of the main system (with dimension n_m). Since we would like to study system behaviors around $1:1$ resonances, we assume that:

$$\boldsymbol{\Delta}_1=\omega^2\boldsymbol{I}_d+\varepsilon\boldsymbol{\Sigma} \tag{4.38}$$

where $\boldsymbol{\Sigma}$ is a diagonal matrix of detuning parameters and $\boldsymbol{I}_d$ is the unity matrix. To detect system behaviours at different scales of time, we follow similar steps which have been explained in Sect. 4.2.

4.3.1 Complexifications and using the Galerkin technique

System variables could be submitted to the following linear transformation:

$$\begin{pmatrix} \boldsymbol{V} \\ \boldsymbol{W} \end{pmatrix}=\mathbb{A}\begin{pmatrix} \boldsymbol{Y}_1 \\ \boldsymbol{Y}_2 \end{pmatrix} \tag{4.39}$$

In order to simplify, let us assume that $\mathbb{A}=\boldsymbol{I}_d$. Complex variables of Manevitch [Manevitch, 2001] or their extended versions [Ture Savadkoohi et al., 2012a, Weiss et al., 2016] are applied to system variables:

$$\begin{cases} i\boldsymbol{B}_1+\boldsymbol{\Phi}_1 e^{i\omega T}=\dot{\boldsymbol{V}}+i\omega\boldsymbol{V} \\ i\boldsymbol{B}_2+\boldsymbol{\Phi}_2 e^{i\omega T}=\dot{\boldsymbol{W}}+i\omega\boldsymbol{W} \\ \boldsymbol{\Phi}_3 e^{i\omega T}=\dot{\boldsymbol{Y}}_3+i\omega\boldsymbol{Y}_3 \end{cases} \tag{4.40}$$

The Galerkin technique is endowed for keeping constant and first harmonics of the Fourier series. For any arbitrary function $\boldsymbol{\daleth}(\boldsymbol{B}_1,\boldsymbol{B}_1,\boldsymbol{\Phi}_1,\boldsymbol{\Phi}_2,\boldsymbol{\Phi}_3)$ this task is carried out via:

$$\boldsymbol{\chi}(\boldsymbol{B}_1,\boldsymbol{B}_1,\boldsymbol{\Phi}_1,\boldsymbol{\Phi}_2,\boldsymbol{\Phi}_3)=\frac{\omega}{2\pi}\int_0^{\frac{2\pi}{\omega}}\boldsymbol{\daleth}(\boldsymbol{B}_1,\boldsymbol{B}_1,\boldsymbol{\Phi}_1,\boldsymbol{\Phi}_2,\boldsymbol{\Phi}_3)e^{-li\omega T}dT \tag{4.41}$$

with $l=0,1$. For solving integrals of Eq. 4.41 we use the same assumptions that are explained in Sect. 4.2.1.

4.3.2 Time multi-scale behaviours of the system

If we use $l=0$ in Eq. 4.41, i.e. we keep constant terms of the Fourier series, then vectors $\boldsymbol{B}_1$ and $\boldsymbol{B}_2$ can be revealed by considering system equations at ε^0 and ε^1 orders. Let us concentrate at first harmonics of Fourier series, i.e. we set $l=1$ in Eq. 4.41. The ε^0 order of system equations provide:

$$\frac{\partial\boldsymbol{\Phi}_1}{\partial\tau_0}=0\Rightarrow\boldsymbol{\Phi}_1=\boldsymbol{\Phi}_1(\tau_1,\tau_2,...) \tag{4.42}$$

$$\frac{\partial \mathbf{\Phi}_2}{\partial \tau_0} + \mathbf{\Lambda}(\mathbf{\Phi}_1, \mathbf{\Phi}_2, \mathbf{\Phi}_3) = 0 \tag{4.43}$$

$$\mathbf{\Upsilon}(\mathbf{\Phi}_1, \mathbf{\Phi}_2, \mathbf{\Phi}_3) = 0 \tag{4.44}$$

Equation 4.42 provides n_m relations in the complex domain. When $\tau_0 \to \infty$ ($\frac{\partial \mathbf{\Phi}_2}{\partial \tau_0} = 0$), Eq. 4.43 and 4.44 provide asymptotic responses of the system which is in fact its SIM. In the compact form and as a set of equations in the complex domain, it reads:

$$\mathscr{S}(\mathbf{\Phi}_1, \mathbf{\Phi}_2, \mathbf{\Phi}_3) = \mathbf{0} \tag{4.45}$$

which provides $n_m + n_r$ relations in the complex domain. Equations 4.45 in real domain yield to:

$$\widehat{\mathscr{S}}(\boldsymbol{\delta}_2, \boldsymbol{N}_2, \boldsymbol{\delta}_1, \boldsymbol{N}_1, \boldsymbol{\delta}_3, \boldsymbol{N}_3) = \mathbf{0} \tag{4.46}$$

where $\boldsymbol{\delta}_j$, $\boldsymbol{N}_j$, $j = 1, 2, 3$ are phase and amplitude vectors of $\mathbf{\Phi}_j$, $j = 1, 2, 3$, respectively. Equation 4.46 provides $2(n_m + n_r)$ relations. Detection of slow dynamics of the system demands consideration of system equations at ε^1 order. We can write:

$$\begin{pmatrix} \frac{\partial \mathbf{\Phi}_1}{\partial \tau_1} \\ \\ \frac{\partial \mathbf{\Phi}_3}{\partial \tau_1} \end{pmatrix} = \mathscr{M}(\mathbf{\Phi}_1, \mathbf{\Phi}_2, \mathbf{\Phi}_3) \Longleftrightarrow \begin{pmatrix} \frac{\partial \boldsymbol{\delta}_1}{\partial \tau_1} \\ \\ \frac{\partial \boldsymbol{N}_1}{\partial \tau_1} \\ \\ \frac{\partial \boldsymbol{\delta}_3}{\partial \tau_1} \\ \\ \frac{\partial \boldsymbol{N}_3}{\partial \tau_1} \end{pmatrix} = \mathbb{M} \tag{4.47}$$

Let us find the evolution of the SIM at τ_1 time scale. Equation 4.46 is derived versus τ_1 time scale:

$$\nabla_{(\boldsymbol{\delta}_2, \boldsymbol{N}_2, \boldsymbol{\delta}_1, \boldsymbol{N}_1, \boldsymbol{\delta}_3, \boldsymbol{N}_3)} \widehat{\mathscr{S}} \begin{pmatrix} \frac{\partial \boldsymbol{\delta}_2}{\partial \tau_1} \\ \\ \frac{\partial \boldsymbol{N}_2}{\partial \tau_1} \\ \\ \frac{\partial \boldsymbol{\delta}_1}{\partial \tau_1} \\ \\ \frac{\partial \boldsymbol{N}_1}{\partial \tau_1} \\ \\ \frac{\partial \boldsymbol{\delta}_3}{\partial \tau_1} \\ \\ \frac{\partial \boldsymbol{N}_3}{\partial \tau_1} \end{pmatrix} = \mathbf{0} \tag{4.48}$$

Dimension of $\nabla_{(\boldsymbol{\delta}_2,\boldsymbol{N}_2,\boldsymbol{\delta}_1,\boldsymbol{N}_1,\boldsymbol{\delta}_3,\boldsymbol{N}_3)}\widehat{\mathscr{S}}$ is $2(n_n+n_r)\times 2(n_m+n_n+n_r)$. System of equations 4.48 can be reorganized as:

$$\nabla_{(\boldsymbol{\delta}_2,\boldsymbol{N}_2)}\widehat{\mathscr{S}}\begin{pmatrix}\dfrac{\partial\boldsymbol{\delta}_2}{\partial\tau_1}\\ \dfrac{\partial\boldsymbol{N}_2}{\partial\tau_1}\end{pmatrix}+\nabla_{(\boldsymbol{\delta}_1,\boldsymbol{N}_1,\boldsymbol{\delta}_3,\boldsymbol{N}_3)}\widehat{\mathscr{S}}\begin{pmatrix}\dfrac{\partial\boldsymbol{\delta}_1}{\partial\tau_1}\\ \dfrac{\partial\boldsymbol{N}_1}{\partial\tau_1}\\ \dfrac{\partial\boldsymbol{\delta}_3}{\partial\tau_1}\\ \dfrac{\partial\boldsymbol{N}_3}{\partial\tau_1}\end{pmatrix}=\mathbf{0} \tag{4.49}$$

Dimension of $\nabla_{(\boldsymbol{\delta}_2,\boldsymbol{N}_2)}\widehat{\mathscr{S}}$ is $2(n_n+n_r)\times 2n_n$ while dimension of $\nabla_{(\boldsymbol{\delta}_1,\boldsymbol{N}_1,\boldsymbol{\delta}_3,\boldsymbol{N}_3)}\widehat{\mathscr{S}}$ is $2(n_n+n_r)\times 2(n_m+n_r)$. Equations 4.46, 4.47 and 4.49 provide useful tools for detecting equilibrium and singular pints of the system. Equilibrium points of the system can be traced by:

$$\begin{cases}\widehat{\mathscr{S}}(\boldsymbol{\delta}_2,\boldsymbol{N}_2,\boldsymbol{\delta}_1,\boldsymbol{N}_1,\boldsymbol{\delta}_3,\boldsymbol{N}_3)=\mathbf{0}\\ \&\\ \mathbb{M}=0\\ \&\\ \nabla_{(\boldsymbol{\delta}_2,\boldsymbol{N}_2)}\widehat{\mathscr{S}}\text{ be invertible}\end{cases} \tag{4.50}$$

Singular points of system can be revealed by:

$$\begin{cases}\widehat{\mathscr{S}}(\boldsymbol{\delta}_2,\boldsymbol{N}_2,\boldsymbol{\delta}_1,\boldsymbol{N}_1,\boldsymbol{\delta}_3,\boldsymbol{N}_3)=\mathbf{0}\\ \&\\ \mathbb{M}=0\\ \&\\ \nabla_{(\boldsymbol{\delta}_2,\boldsymbol{N}_2)}\widehat{\mathscr{S}}\text{ not to be invertible}\end{cases} \tag{4.51}$$

In the next section a step by step pedagogical technique for treatment of two coupled oscillators is presented which uses the explained methodology in Sects. 4.2 and 4.3.

4.4 Fast/slow dynamics of two coupled oscillators with hysteresis behaviour

The system under consideration is illustrated in Fig. 4.1 [Ture Savadkoohi et al., 2016a]: It consists of a linear forced oscillator, standing for the main system, that is coupled to a NES which presents geometrical nonlinearity (pure cubic restoring forcing function) and a hysteresis behaviour. Characteristics of the main system are: the mass M, the linear stiffness k_1, damping c, generalized displacement x_1, that is under external periodic force $\Gamma\sin(\Omega t)$. The mass of the NES is very light that is defined as $m=\varepsilon M$ $(0<\varepsilon\ll 1)$, its damping and generalized displacement read as λ and x_2, respectively. Its nonlinear geometrical function reads $F(\alpha)=k_3\alpha^3$ while its hysteresis behaviour is supposed to be of Bouc-Wen type [Bouc, 1971, Laxalde et al., 2006, Ikhouane and Rodellar, 2007], $f(a,k_2,A,\beta,n,\gamma)$, with following characteristics: x_3 is the internal variable of the hysteresis model, k_2 is the initial linear stiffness, a is the ratio of the post-yield (k_p) to initial stiffness i.e. $a=\dfrac{k_p}{k_2}$ and A, β, n and γ are parameters of the Bouc-Wen model that control hysteresis behaviour.

Governing system equations read:

$$\begin{cases} M\ddot{x}_1 + c\dot{x}_1 + k_1x_1 + ak_2(x_1 - x_2) + (1-a)k_2(x_1 - x_3) + \lambda(\dot{x}_1 - \dot{x}_2) + \\ k_3(x_1 - x_2)^3 = \Gamma\sin(\Omega t) \\ m\ddot{x}_2 + \lambda(\dot{x}_2 - \dot{x}_1) + ak_2(x_2 - x_1) + (1-a)k_2(x_3 - x_1) + k_3(x_2 - x_1)^3 = 0 \\ \dot{x}_3 = A\dot{x}_2 - \beta|\dot{x}_2||x_3|^{n-1}x_3 - \gamma\dot{x}_2|x_3|^n \end{cases} \tag{4.52}$$

We would like to rescale the system which is presented in Eq. 4.52. To this end, define new

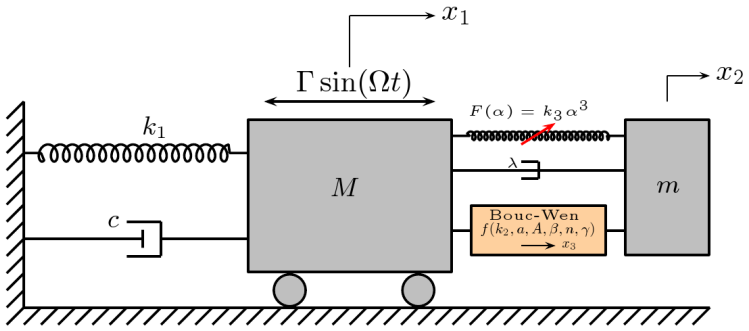

Figure 4.1: Schematic of a linear oscillator and a coupled NES: the NES possesses a cubic geometrical restoring forcing function ($F(\alpha) = k_3\alpha^3$) and presents a Bouc-Wen type hysteresis behaviour ($f(k_2, a, A, \beta, n, \gamma)$).

time domain as: $T = \sqrt{\dfrac{k_1 + k_2}{M}}t = \overline{\theta}t$. The system of (4.52) yields to ($x_1(t)$,$x_2(t)$,$x_3(t)$)$\rightarrow$ ($y_1(T)$,$y_2(T)$,$z(T)$):

$$\begin{cases} \ddot{y}_1 + \varepsilon\xi\dot{y}_1 + \tilde{k}_1y_1 + a\varepsilon\tilde{k}_2(y_1 - y_2) + (1-a)\varepsilon\tilde{k}_2(y_1 - z) + \varepsilon\tilde{\lambda}(\dot{y}_1 - \dot{y}_2) + \\ \varepsilon\tilde{k}_3(y_1 - y_2)^3 = \varepsilon\tilde{f}_0\sin(\omega T) \\ \ddot{y}_2 + \tilde{\lambda}(\dot{y}_2 - \dot{y}_1) + a\tilde{k}_2(y_2 - y_1) + (1-a)\tilde{k}_2(z - y_1) + \tilde{k}_3(y_2 - y_1)^3 = 0 \\ \dot{z} = A\dot{y}_2 - \beta|\dot{y}_2||z|^{n-1}z - \gamma\dot{y}_2|z|^n \end{cases} \tag{4.53}$$

The parameters of the Eq. 4.53 are: $\dfrac{k_2}{k_1 + k_2} = \varepsilon\tilde{k}_2$, $\dfrac{k_1}{k_1 + k_2} = \mathcal{O}(\varepsilon^0) + \mathcal{O}(\varepsilon^1) = \tilde{k}_1 = 1 - \varepsilon\tilde{k}_2$, $k_3 = \varepsilon\tilde{k}_3$, $\dfrac{c}{\sqrt{M(k_1 + k_2)}} = \varepsilon\xi$, $\dfrac{\lambda}{\sqrt{M(k_1 + k_2)}} = \varepsilon\tilde{\lambda}$, $\dfrac{\Gamma}{\sqrt{k_1 + k_2}} = \varepsilon\tilde{f}_0$ and $\omega = \dfrac{\Omega}{\overline{\theta}}$. Let us shift the system to the centre of the mass and relative displacement of two oscillators. Similar to Eq. 4.2, we set:

$$\begin{pmatrix} v(T) \\ w(T) \end{pmatrix} = \begin{pmatrix} 1 & \varepsilon \\ 1 & -1 \end{pmatrix} \begin{pmatrix} y_1(T) \\ y_2(T) \end{pmatrix} \tag{4.54}$$

Equation 4.53 yields to:

$$\begin{cases} \ddot{v} + \varepsilon\xi\dfrac{\dot{v} + \varepsilon\dot{w}}{1+\varepsilon} + \tilde{k}_1\dfrac{v + \varepsilon w}{1+\varepsilon} = \varepsilon\tilde{f}_0\sin(\omega T) \\ \\ \ddot{w} + \varepsilon\xi\dfrac{\dot{v} + \varepsilon\dot{w}}{1+\varepsilon} + \tilde{k}_1\dfrac{v + \varepsilon w}{1+\varepsilon} + a\tilde{k}_2(1+\varepsilon)w + \tilde{\lambda}(1+\varepsilon)\dot{w} \\ +(1-a)\tilde{k}_2(1+\varepsilon)\Big(\dfrac{v + \varepsilon w}{1+\varepsilon} - z\Big) + (1+\varepsilon)\tilde{k}_3w^3 = \varepsilon\tilde{f}_0\sin(\omega T) \\ \\ \dot{z} = A\dfrac{\dot{v} - \dot{w}}{1+\varepsilon} - \beta\Big|\dfrac{\dot{v} - \dot{w}}{1+\varepsilon}\Big||z|^{n-1}z - \gamma\Big(\dfrac{\dot{v} - \dot{w}}{1+\varepsilon}\Big)|z|^n \end{cases} \tag{4.55}$$

Complex variables of Manevitch (for systems without pre-stress) [Manevitch, 2001] which are provided in Eq. 4.4 are injected to system variables. Since there is no any pre-stressing terms in system, we set $b_1 = b_2 = 0$. The first harmonics of system variables are kept as is illustrated in Eq. 4.6 via setting $l = 1$. Following variables and functions are defined:

$$\varphi_j = N_j e^{i\delta_j}, j = 1, 2, 3 \tag{4.56}$$

$$s = \omega T + \delta_3 \Rightarrow ds = \omega dT \tag{4.57}$$

$$N_1 e^{i(\delta_1 - \delta_3)} - N_2 e^{i(\delta_2 - \delta_3)} = P + iQ \quad (P, Q \in \mathbb{R}) \tag{4.58}$$

with

$$\begin{aligned} P &= N_1 \cos(\delta_1 - \delta_3) - N_2 \cos(\delta_2 - \delta_3) \\ Q &= N_1 \sin(\delta_1 - \delta_3) - N_2 \sin(\delta_2 - \delta_3) \end{aligned} \tag{4.59}$$

$$R = \sqrt{P^2 + Q^2} = \sqrt{N_1^2 + N_2^2 - 2N_1 N_2 \cos(\delta_1 - \delta_2)} \tag{4.60}$$

$$\vartheta = \arctan(\frac{Q}{P}) \tag{4.61}$$

$$B = -\frac{\beta}{2\pi(1+\varepsilon)} e^{i\delta_3} (\frac{N_3}{\omega})^n \tag{4.62}$$

$$C = -\frac{\gamma}{1+\varepsilon} \frac{1}{\pi} e^{i\delta_3} |\frac{N_3}{\omega}|^n \tag{4.63}$$

$$J_1 = \int_0^{2\pi} |\cos(\vartheta + s)||\sin(s)|^{n-1} \sin(s)\cos(s) ds \tag{4.64}$$

$$J_2 = \int_0^{2\pi} |\cos(\vartheta + s)||\sin(s)|^{n-1} \sin(s)\sin(s) ds \tag{4.65}$$

$$J_3 = \int_0^{2\pi} \cos(\vartheta + s)|\sin(s)|^n \cos(s) ds \tag{4.66}$$

$$J_4 = \int_0^{2\pi} \cos(\vartheta + s)|\sin(s)|^n \sin(s) ds \tag{4.67}$$

The system (4.55) reads:

$$\begin{cases} \dot{\varphi}_1 - \frac{\omega}{2i}\varphi_1 + \frac{\varepsilon\xi}{2(1+\varepsilon)}(\varphi_1 + \varepsilon\varphi_2) + \frac{\tilde{k}_1}{(1+\varepsilon)(2i\omega)}(\varphi_1 + \varepsilon\varphi_2) = -\frac{i}{2}\tilde{f}_0\varepsilon \\ \dot{\varphi}_2 - \frac{\omega}{2i}\varphi_2 + \frac{\varepsilon\xi}{2(1+\varepsilon)}(\varphi_1 + \varepsilon\varphi_2) + \frac{\tilde{k}_1}{(1+\varepsilon)(2i\omega)}(\varphi_1 + \varepsilon\varphi_2) + \tilde{\lambda}(1+\varepsilon)\frac{\varphi_2}{2} \\ + \frac{a\tilde{k}_2}{2i\omega}(1+\varepsilon)\varphi_2 + (1-a)\frac{\tilde{k}_2}{2i\tilde{\omega}}(\varphi_1 + \varepsilon\varphi_2) - (1-a)\frac{\tilde{k}_2}{2i\omega}(1+\varepsilon)\varphi_3 \\ - \frac{i}{2}(1+\varepsilon)\frac{3\tilde{k}_3}{4\omega^3}|\varphi_2|^2\varphi_2 = -\frac{i}{2}\tilde{f}_0\varepsilon \\ \frac{\varphi_3}{2} = \frac{A}{2(1+\varepsilon)}(\varphi_1 - \varphi_2) + BR(J_1 - iJ_2) + CR(J_3 - iJ_4) \end{cases} \tag{4.68}$$

To treat system equations a time multi-scale method [Nayfeh and Mook, 1979] is endowed around $1:1$ resonance by imposing $\omega = 1 + \sigma\varepsilon$.

4.4.1 Time multiple scale behaviour of the system: general methodology

Different scales of time which are provided in Eq. 4.5 are considered. Let us study system equations at fast time scale, i.e. taking into account ε^0 order of system equations. The goal is to trace periodic and modulated regimes of the system under consideration. At first step, all developments are quite general which follows explained methodology in Sects. 4.2 and 4.3. Then, we will focus on treatments of the Eq. 4.68. The first equation of the system 4.68 at the order of ε^0 is:

$$\frac{\partial \varphi_1}{\partial \tau_0} = 0 \Rightarrow \varphi_1 = \varphi_1(\tau_1, \tau_2, ...) \tag{4.69}$$

The second equation of the system (4.68) at the order of ε^0 in a general representation reads:

$$\frac{\partial \varphi_2}{\partial \tau_0} + \Lambda(\varphi_1, \varphi_2, \varphi_3) = 0 \tag{4.70}$$

where

$$\Lambda(\varphi_1, \varphi_2, \varphi_3) = 0 \tag{4.71}$$

covers fixed points of Eq. 4.70. The last equation of the system 4.68 at the ε^0 order by consideration of the Eq. (4.71) becomes:

$$\Upsilon(\varphi_1, \varphi_2, \varphi_3) = 0 \tag{4.72}$$

Equations 4.71 and 4.72 represent the SIM of the system. Let us suppose that the general form of the SIM (by considering both of Eqs. 4.71 and 4.72) reads the following form (see Eq. 4.16):

$$\mathscr{S}(\varphi_1, \varphi_2, \varphi_{31}, \varphi_{32}, \ldots, \varphi_{3n}) = 0 \tag{4.73}$$

Via shifting to phase and amplitude domains (see Eq. (4.56)), Eq. 4.73 in an explicit manner can be represented as:

$$\begin{cases} N_1 &= h_1(\delta_1, N_1, \delta_2, N_2, \delta_3, N_3) \\ \delta_1 &= h_2(\delta_1, N_1, \delta_2, N_2, \delta_3, N_3) \\ N_3 &= h_3(\delta_1, N_1, \delta_2, N_2, \delta_3, N_3) \\ \delta_3 &= h_4(\delta_1, N_1, \delta_2, N_2, \delta_3, N_3) \end{cases}$$
$$\Leftrightarrow \widehat{\mathscr{S}}(\delta_1, N_1, \delta_2, N_2, \delta_3, N_3) = 0 : \begin{cases} \widehat{\mathscr{S}_1} &= N_1 - h_1 &= 0 \\ \widehat{\mathscr{S}_2} &= \delta_1 - h_2 &= 0 \\ \widehat{\mathscr{S}_3} &= N_3 - h_3 &= 0 \\ \widehat{\mathscr{S}_4} &= \delta_3 - h_4 &= 0 \end{cases} \tag{4.74}$$

Let us study system behaviour at slow time scale τ_1. The first equation of the system (4.68) at the order of ε^1 in a general manner is expressed as:

$$\frac{\partial \varphi_1}{\partial \tau_1} = \mathscr{F}(\varphi_1, \varphi_2, \varphi_3) \tag{4.75}$$

which in the polar domain reads:

$$\begin{cases} \dfrac{\partial N_1}{\partial \tau_1} = \mathscr{F}_1(\delta_1, N_1, \delta_2, N_2, \delta_3, N_3) \\ \dfrac{\partial \delta_1}{\partial \tau_1} = \mathscr{F}_2(\delta_1, N_1, \delta_2, N_2, \delta_3, N_3) \end{cases} \tag{4.76}$$

We are interested to look at system behaviours around the SIM. From Eqs.4.74 and 4.76 we obtain:

$$\begin{pmatrix} 1 & 0 & -\frac{\partial h_1}{\partial N_2} & 0 & 0 & 0 \\ -\frac{\partial h_2}{\partial N_1} & 1 & -\frac{\partial h_2}{\partial N_2} & \frac{\partial h_2}{\partial \delta_2} & 0 & 0 \\ -\frac{\partial h_3}{\partial N_1} & -\frac{\partial h_3}{\partial \delta_1} & -\frac{\partial h_3}{\partial N_2} & -\frac{\partial h_3}{\partial \delta_2} & 1-\frac{\partial h_3}{\partial N_3} & -\frac{\partial h_3}{\partial \delta_3} \\ -\frac{\partial h_4}{\partial N_1} & -\frac{\partial h_4}{\partial \delta_1} & -\frac{\partial h_4}{\partial N_2} & -\frac{\partial h_4}{\partial \delta_2} & -\frac{\partial h_4}{\partial N_3} & 1-\frac{\partial h_4}{\partial \delta_3} \end{pmatrix} \begin{pmatrix} \frac{\partial N_1}{\partial \tau_1} \\ \frac{\partial \delta_1}{\partial \tau_1} \\ \frac{\partial N_2}{\partial \tau_1} \\ \frac{\partial \delta_2}{\partial \tau_1} \\ \frac{\partial N_3}{\partial \tau_1} \\ \frac{\partial \delta_3}{\partial \tau_1} \end{pmatrix} = \begin{pmatrix} 0 \\ 0 \\ 0 \\ 0 \\ 0 \\ 0 \end{pmatrix} \tag{4.77}$$

Reorganization of Eq. 4.77 takes following form:

$$\underbrace{\begin{pmatrix} -\frac{\partial h_1}{\partial N_2} & 0 & 0 & 0 \\ -\frac{\partial h_2}{\partial N_2} & \frac{\partial h_2}{\partial \delta_2} & 0 & 0 \\ -\frac{\partial h_3}{\partial N_2} & -\frac{\partial h_3}{\partial \delta_2} & 1-\frac{\partial h_3}{\partial N_3} & -\frac{\partial h_3}{\partial \delta_3} \\ -\frac{\partial h_4}{\partial N_2} & -\frac{\partial h_4}{\partial \delta_2} & -\frac{\partial h_4}{\partial N_3} & 1-\frac{\partial h_4}{\partial \delta_3} \end{pmatrix}}_{\mathcal{B}} \begin{pmatrix} \frac{\partial N_2}{\partial \tau_1} \\ \frac{\partial \delta_2}{\partial \tau_1} \\ \frac{\partial N_3}{\partial \tau_1} \\ \frac{\partial \delta_3}{\partial \tau_1} \end{pmatrix} = - \begin{pmatrix} 1 & 0 \\ -\frac{\partial h_2}{\partial N_1} & 1 \\ -\frac{\partial h_3}{\partial N_1} & -\frac{\partial h_3}{\partial \delta_1} \\ -\frac{\partial h_4}{\partial N_1} & -\frac{\partial h_4}{\partial \delta_1} \end{pmatrix} \begin{pmatrix} \mathscr{F}_1 \\ \mathscr{F}_2 \end{pmatrix} \tag{4.78}$$

Equilibrium points of the system verify:

$$\begin{cases} \widehat{\mathscr{S}} = 0 \\ \mathscr{F}_1 = \mathscr{F}_2 = 0 \\ \det(\mathcal{B}) \neq 0 \end{cases} \tag{4.79}$$

while its fold singularities check:

$$\begin{cases} \widehat{\mathscr{S}} = 0 \\ \mathscr{F}_1 = \mathscr{F}_2 = 0 \\ \det(\mathcal{B}) = 0 \end{cases} \tag{4.80}$$

with

$$\det(\mathcal{B}) = \frac{\partial h_1}{\partial N_2}\frac{\partial h_2}{\partial \delta_2}\Big((1-\frac{\partial h_3}{\partial N_3})(1-\frac{\partial h_4}{\partial \delta_3}) - \frac{\partial h_3}{\partial \delta_3}\frac{\partial h_4}{\partial N_3}\Big) \tag{4.81}$$

4.4.2 Fast and slow equations of the system under consideration

The general development in previous section are endowed to develop the fast and slow equations of the system 4.68. Moreover, we suppose that

$$(a \to 1) \Rightarrow (1-a) = a_1 \to 0 \tag{4.82}$$

or $(1-a) = \mathcal{O}(\varepsilon)$.

4.4.3 Fast system equations

The ε^0 order of the second equation of the system 4.68 reads:

$$\frac{\partial \varphi_2}{\partial \tau_0} + \frac{i\varphi_2}{2} - \frac{i\varphi_1}{2} + \tilde{\lambda}\frac{\varphi_2}{2} - a\tilde{k}_2\frac{i}{2}\varphi_2 - \frac{i}{2}\frac{3}{4}\tilde{k}_3|\varphi_2|^2\varphi_2 = 0 \tag{4.83}$$

Here, the corresponding Λ function which is clarified in Eq.4.70, is expressed as:

$$\Lambda(\varphi_1, \varphi_2, \varphi_3) = \frac{i\varphi_2}{2} - \frac{i\varphi_1}{2} + \tilde{\lambda}\frac{\varphi_2}{2} - a\tilde{k}_2\frac{i}{2}\varphi_2 - \frac{i}{2}\frac{3}{4}\tilde{k}_3|\varphi_2|^2\varphi_2 \tag{4.84}$$

So, fixed points of the system verify:

$$\varphi_1 = f(\varphi_2, \varphi_2^*) = (1 - i\tilde{\lambda} - a\tilde{k}_2)\varphi_2 - \frac{3}{4}\tilde{k}_3 \overbrace{|\varphi_2|^2}^{=\varphi_2\varphi_2^*} \varphi_2 \tag{4.85}$$

Expressing Eq. 4.85 in polar domain yields to detection of the SIM as:

$$\cos(\delta_1 - \delta_2) = \frac{N_2}{N_1}(1 - a\tilde{k}_2 - \frac{3}{4}\tilde{k}_3 N_2^2) \tag{4.86}$$

$$\sin(\delta_1 - \delta_2) = -\frac{N_2}{N_1}\tilde{\lambda} \tag{4.87}$$

or

$$\delta_1 = \delta_2 - \arctan(\frac{\tilde{\lambda}}{1 - a\tilde{k}_2 - \frac{3}{4}\tilde{k}_3 N_2^2}) \tag{4.88}$$

$$N_1 = N_2\sqrt{(1 - a\tilde{k}_2 - \frac{3}{4}\tilde{k}_3 N_2^2)^2 + \tilde{\lambda}^2} \tag{4.89}$$

The ε^0 order of the the third equation of the system 4.68 reads:

$$\varphi_3 = A(\varphi_1 - \varphi_2) - 2B^\circ R(J_1 - iJ_2) - 2C^\circ R(J_3 - iJ_4) \tag{4.90}$$

The variables B° and C° are ε^0 order of B and C in Eqs.4.62 and 4.63:

$$B^\circ = -\frac{\beta}{2\pi}e^{i\delta_3}N_3^n \tag{4.91}$$

$$C^\circ = -\frac{\gamma}{\pi}e^{i\delta_3}N_3^n \tag{4.92}$$

Via Eq.(4.72) we obtain:

$$\begin{aligned}\Upsilon(\varphi_1, \varphi_2, \varphi_3) &= A\left((1 - \tilde{\lambda}i - a\tilde{k}_2)\varphi_2 - \frac{3}{4}\tilde{k}_3|\varphi_2|^2\varphi_2 - \varphi_2\right) \\ &-2\big(-\frac{\beta}{2\pi}e^{i\delta_3}N_3^n\big)R\,(J_1 - iJ_2) - 2\big(-\frac{\gamma}{\pi}e^{i\delta_3}N_3^n\big)R\,(J_3 - iJ_4) - \varphi_3 = 0\end{aligned} \tag{4.93}$$

Equation 4.93 in polar domain reads:

$$N_3 = A(-\tilde{\lambda}i - a\tilde{k}_2 - \frac{3}{4}\tilde{k}_3 N_2^2)N_2 e^{-i\delta_3} + \left(\frac{\beta}{\pi}(J_1 - iJ_2) + \frac{2\gamma}{\pi}(J_3 - iJ_4)\right)RN_3^n \tag{4.94}$$

4.4.3.1 Stability zones of the SIM

For tracing stable zones of the SIM, we linearise the polar form of the Eq. (4.83) via perturbing N_2 and δ_2 as:

$$\begin{aligned} N_2 &\to N_2 + \Delta N_2 \\ \delta_2 &\to \delta_2 + \Delta\delta_2 \end{aligned} \tag{4.95}$$

Here, we do not perturb corresponding polar variables of φ_1 as it is independent of the time scale τ_0 (see Eq. 4.69). From Eqs. 4.86 and 4.87 we obtain:

$$\begin{pmatrix} \dfrac{\partial(\triangle N_2)}{\partial\tau_0} \\ \\ \dfrac{\partial(\triangle\delta_2)}{\partial\tau_0} \end{pmatrix} = \mathbf{A} \begin{pmatrix} \triangle N_2 \\ \\ \triangle\delta_2 \end{pmatrix} \tag{4.96}$$

with

$$\mathbf{A} = \begin{pmatrix} -\dfrac{\lambda}{2} & \dfrac{1}{2}N_2(1 - a\tilde{k}_2 - \dfrac{3}{4}\tilde{k}_3 N_2^2) \\ -\dfrac{1}{2N_2}(1 - a\tilde{k}_2 - \dfrac{9}{4}\tilde{k}_3 N_2^2) & -\dfrac{\lambda}{2} \end{pmatrix} \tag{4.97}$$

To have an idea about the stable zones, we seek for the characteristic equation of the matrix $\mathbf{A}$; it reads:

$$P(\chi) = \chi^2 + \lambda\chi + \frac{\lambda^2}{4} - A_{12}A_{21} \tag{4.98}$$

Let us set χ_j, $j = 1, 2$ as eigenvalues the $\mathbf{A}$ matrix; From Eq. (4.98) one can say that:

$$\begin{aligned} \chi_1 + \chi_2 &= -\lambda < 0 \\ \chi_1\chi_2 &= \frac{\lambda^2}{4} - A_{12}A_{21} \end{aligned} \tag{4.99}$$

Three distinct cases can be clarified:

- $\dfrac{\lambda^2}{4} - A_{12}A_{21} < 0$
  the zone is unstable.

- $\dfrac{\lambda^2}{4} - A_{12}A_{21} > 0$
  Two eigenvalues can be complex or real. If they are complex, then they will have the same real part equal to $-\dfrac{\lambda}{2} < 0$; so the zone is stable for the linearised system. If eigenvalues are real, then they will be negative; again the zone will be stable for the linearised system.

- $\dfrac{\lambda^2}{4} - A_{12}A_{21} = 0$
  One of the eigenvalues is zero and the other one is $-\lambda < 0$. Here we can not judge about the stability zone of the τ_0-invariant by linearisation.

As a summary, one can confirm that stable zones of the SIM read:

$$\mathcal{S} = \lambda^2 + (1 - a\tilde{k}_2 - \tfrac{3}{4}\tilde{k}_3 N_2^2)(1 - a\tilde{k}_2 - \tfrac{9}{4}\tilde{k}_3 N_2^2) > 0 \tag{4.100}$$

4.4.4 Slow system equations

The $\mathscr{F}$ function in Eq.(4.75) reads:

$$\mathscr{F}(\varphi_1,\varphi_2,\varphi_3)=(-i\sigma-\frac{\xi}{2}-\frac{i}{2}-\frac{i\tilde{k}_2}{2})\varphi_1+\frac{i}{2}\varphi_2-\frac{i}{2}\tilde{f}_0 \tag{4.101}$$

The functions $\mathscr{F}_1$ and $\mathscr{F}_2$ in Eq. 4.76 verify:

$$\begin{cases}\mathscr{F}_1(\delta_1,N_1,\delta_2,N_2,\delta_3,N_3)=-\frac{1}{2}\xi N_1+\frac{1}{2}N_2\sin(\delta_1-\delta_2)-\frac{1}{2}\tilde{f}_0\sin(\delta_1)\\ N_1\mathscr{F}_2(\delta_1,N_1,\delta_2,N_2,\delta_3,N_3)=-(\sigma+\frac{1}{2}+\frac{1}{2}\tilde{k}_2)N_1+\frac{1}{2}N_2\cos(\delta_1-\delta_2)-\frac{1}{2}\tilde{f}_0\cos(\delta_1)\end{cases} \tag{4.102}$$

Now, we have all necessary elements for detecting all possible periodic and modulated regimes as explained in Sect. 4.4.1. In the next section, we consider a Dahl model [Dahl, 1968] as a representative model for a general Bouc-Wen model which has been adapted in Sect. 4.4.

4.4.5 An example of the hysteresis behaviour of the NES: Dahl model

Let us consider an alternative to the Coulomb model for dry friction, which is named as the Dahl model [Dahl, 1968]. The model can be also obtained from general Bouc-Wen hysteresis model via setting $n=1$ and $\gamma=0$ [Ikhouane and Rodellar, 2007]. The SIM of the system, traced from Eq. 4.89, which is valid for any family of Bouc-Wen hysteresis model (under our provided assumptions, e.g. see Eq. 4.82), and its stability borders (see Eq. 4.100), for some given system parameters are presented in Fig. 4.2. Let us detect all terms of the Eq. 4.74: From Eqs. 4.88 and 4.89, we obtain:

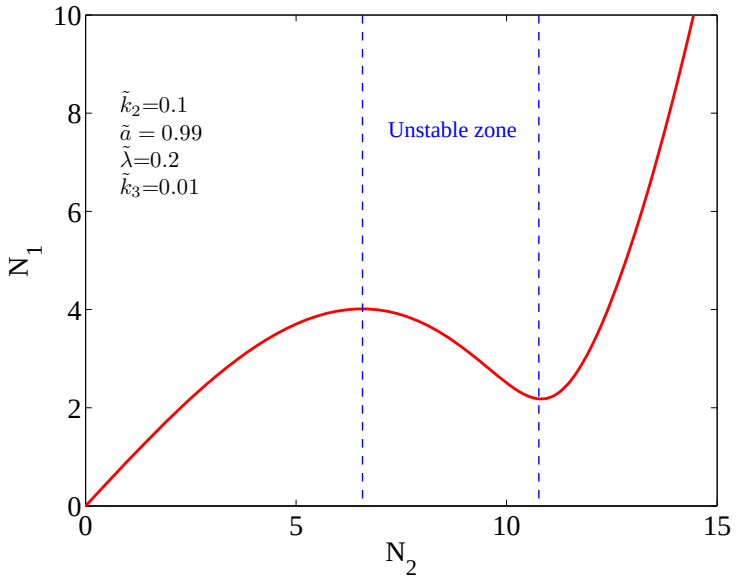

Figure 4.2: The SIM (—) and its stability borders (− − −).

$$\widehat{\mathscr{S}_1}=N_1-h_1=N_2\sqrt{(1-a\tilde{k}_2-\frac{3}{4}\tilde{k}_3N_2^2)^2+\tilde{\lambda}^2}-h_1=0 \tag{4.103}$$

$$\widehat{\mathscr{S}_2} = \delta_1 - h_2 = \delta_2 - \arctan(\frac{\tilde{\lambda}}{1 - a\tilde{k}_2 - \frac{3}{4}\tilde{k}_3 N_2^2}) - h_2 = 0 \tag{4.104}$$

Equation 4.94 becomes:

$$N_3 = A(-\tilde{\lambda}i - a\tilde{k}_2 - \frac{3}{4}\tilde{k}_3 N_2^2)N_2 e^{-i\delta_3} + \frac{2iN_3 e^{-2i\delta_3}\beta\sqrt{N_1^2 + N_2^2 - 2N_1 N_2\cos(\delta_1 - \delta_2)}}{3\pi(N_1 e^{i\delta_2} - N_2 e^{i\delta_1})} \times \left(N_1\left(e^{i(2\delta_1+\delta_2)} - 3e^{i(\delta_2+2\delta_3)}\right) + N_2\left(-e^{i(\delta_1+2\delta_2)} + 3e^{i(\delta_1+2\delta_3)}\right)\right) \tag{4.105}$$

For the pedagogical reason and for having simpler form of equations, we assume that $\beta = 0$. The function $\widehat{\mathscr{S}_3}$ and $\widehat{\mathscr{S}_4}$ can be obtained from Eq. 4.105 as:

$$\widehat{\mathscr{S}_3} = N_3 - h_3 = N_2\sqrt{A^2\left((a\tilde{k}_2 + \frac{3}{4}\tilde{k}_3 N_2^2)^2 + \tilde{\lambda}^2\right)} - h_3 = 0 \tag{4.106}$$

$$\widehat{\mathscr{S}_4} = \delta_3 - h_4 = \arctan(\frac{\tilde{\lambda}}{a\tilde{k}_2 + \frac{3}{4}\tilde{k}_3 N_2^2}) - h_4 = 0 \tag{4.107}$$

meanwhile Eq. (4.81) yields to:

$$\det(\mathcal{B}) = \frac{\tilde{\lambda}^2 + (1 - a\tilde{k}_2 - \frac{3}{4}\tilde{k}_3 N_2^2)(1 - a\tilde{k}_2 - \frac{9}{4}\tilde{k}_3 N_2^2)}{\sqrt{(1 - a\tilde{k}_2 - \frac{3}{4}\tilde{k}_3 N_2^2)^2 + \tilde{\lambda}^2}} \tag{4.108}$$

Figure 4.3 presents the two-dimensional flow of N_2 and N_3 at the infinity of fast time scale (See Eqs. 4.94 and 4.106) for a system equipped with a NES of Dahl type hysteresis behaviour, while the three-dimensional view of the SIM is provided in Fig. 4.4 Let us set $\det(\mathcal{B}) = 0$ which is one

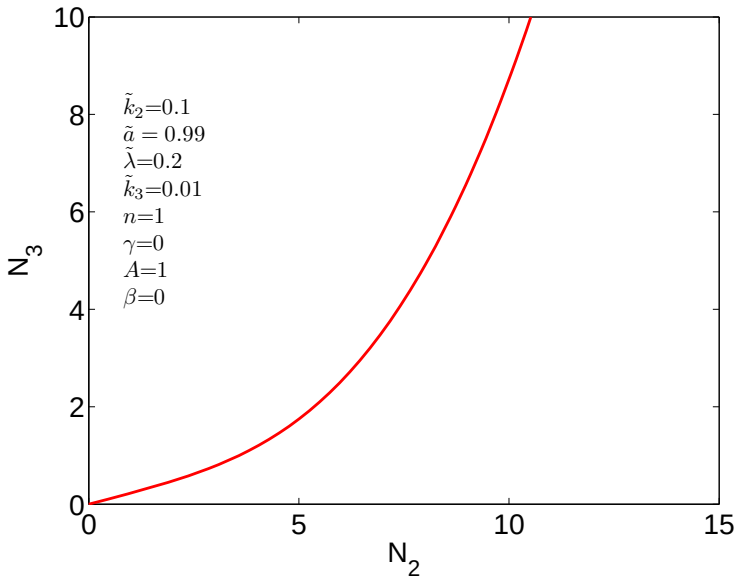

Figure 4.3: N_3 vs. N_1 at the infinity of fast time scale. The hysteresis behaviour of the NES is Dahl type ($n = 1, \gamma = 0$).

of the conditions for existence of fold singularities as presented in Eq. 4.80,

$$\det(\mathcal{B}) = 0 \quad \Leftrightarrow \quad \tilde{\lambda}^2 + (1 - a\tilde{k}_2 - \frac{3}{4}\tilde{k}_3 N_2^2)(1 - a\tilde{k}_2 - \frac{9}{4}\tilde{k}_3 N_2^2) = 0 \tag{4.109}$$

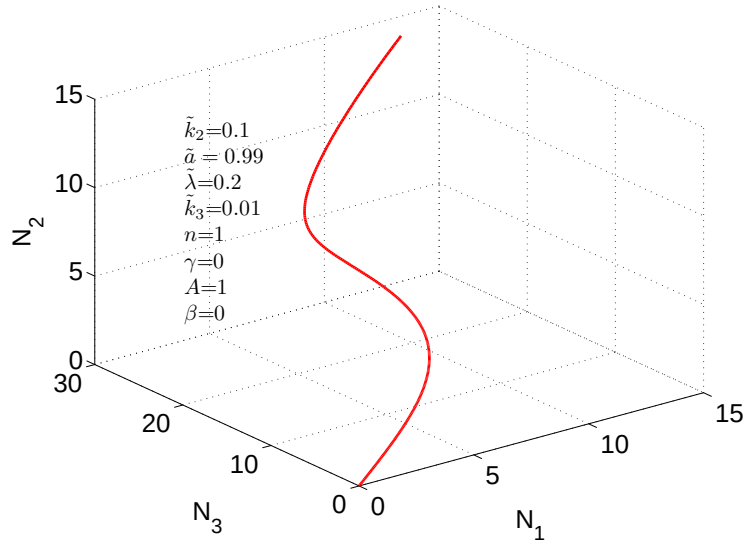

Figure 4.4: 3D flow of the τ_0-invariant. The hysteresis behaviour of the NES is Dahl type ($n = 1, \gamma = 0$).

Comparing the stability borders of the SIM which are clarified in Eq. 4.100 and Eq. 4.109 we can confirm that:

$$\det(\mathcal{B}) = 0 \quad \Leftrightarrow \quad \mathcal{S} = 0 \tag{4.110}$$

Equation 4.110 states that the stability borders of the SIM, Eq. 4.100, house singular points of system as well. These correspond to modulated responses of the system via repeated bifurcations between its stable zones [Starosvetsky and Gendelman, 2008, Lamarque et al., 2011]. Equation 4.109 reveals two lines corresponding to N_2, presented as $N_{2,1}$ and $N_{2,2}$ and named as "fold lines" of the system:

$$N_{2,l} = \frac{2}{3}\sqrt{\frac{2(1-a\tilde{k}_2) \mp \sqrt{1-2a\tilde{k}_2+a^2\tilde{k}_2^2-3\tilde{\lambda}^2}}{\tilde{k}_3}} \quad , \qquad l = 1,2 \tag{4.111}$$

To trace all possible equilibrium and singular points of the system, as explained in Eqs. 4.79 and 4.80, we set $\mathscr{F}_1 = 0$ and $\mathscr{F}_2 = 0$ in Eq. 4.102 and we introduce following variable:

$$r = 1 - a\tilde{k}_2 - \tfrac{3}{4}\tilde{k}_3 N_2^2 \tag{4.112}$$

Via including Eqs. 4.86, 4.87, 4.103 and 4.104 in Eq. 4.102 one can obtain:

$$\tilde{f}_0 \begin{pmatrix} \alpha_{11} & \alpha_{12} \\ \alpha_{21} & \alpha_{22} \end{pmatrix} \begin{pmatrix} \cos(\delta_2) \\ \sin(\delta_2) \end{pmatrix} = N_2 \begin{pmatrix} \varrho_1 \\ \varrho_2 \end{pmatrix} \tag{4.113}$$

with

$$\begin{aligned} \alpha_{11} &= -\text{sgn}(r)\tilde{\lambda} \\ \alpha_{12} &= r \\ \alpha_{21} &= r \\ \alpha_{22} &= \text{sgn}(r)\tilde{\lambda} \end{aligned} \tag{4.114}$$

and

$$\begin{aligned}\varrho_1(N_2) &= -\left(\tilde{\lambda} + \xi(r^2 + \tilde{\lambda}^2)\right) < 0 \\ \varrho_2(N_2) &= r - (1 + \tilde{k}_2 + 2\sigma)(r^2 + \tilde{\lambda}^2)\end{aligned} \tag{4.115}$$

Equation.(4.113) is represented as:

$$\begin{cases} \tilde{f}_0\Big(-\text{sgn}(r)\tilde{\lambda}\cos(\delta_2) + r\sin(\delta_2)\Big) = N_2\varrho_1 \\ \tilde{f}_0\Big(r\cos(\delta_2) + \text{sgn}(r)\tilde{\lambda}\sin(\delta_2)\Big) = N_2\varrho_2 \end{cases} \tag{4.116}$$

or

$$\begin{cases} \dfrac{\tilde{f}_0}{\sqrt{\tilde{\lambda}^2 + r^2}}\Big(-\text{sgn}(r)\tilde{\lambda}\cos(\delta_2) + r\sin(\delta_2)\Big) = \dfrac{N_2\varrho_1}{\sqrt{\tilde{\lambda}^2 + r^2}} \\ \dfrac{\tilde{f}_0}{\sqrt{\tilde{\lambda}^2 + r^2}}\Big(r\cos(\delta_2) + \text{sgn}(r)\tilde{\lambda}\sin(\delta_2)\Big) = \dfrac{N_2\varrho_2}{\sqrt{\tilde{\lambda}^2 + r^2}} \end{cases} \tag{4.117}$$

Let us assume that:

$$\begin{cases} \dfrac{-\text{sgn}(r)\tilde{\lambda}}{\sqrt{\tilde{\lambda}^2 + r^2}} = \cos(\theta) \\ \dfrac{r}{\sqrt{\tilde{\lambda}^2 + r^2}} = \sin(\theta) \end{cases} \tag{4.118}$$

Equation 4.117 yields to:

$$\begin{cases} \tilde{f}_0\cos(\theta - \delta_2) = \dfrac{N_2\varrho_1}{\sqrt{\tilde{\lambda}^2 + r^2}} \\ \tilde{f}_0\sin(\theta - \delta_2) = \dfrac{N_2\varrho_2}{\sqrt{\tilde{\lambda}^2 + r^2}} \end{cases} \tag{4.119}$$

which provides

$$\delta_2 = \theta \pm \arccos\left(\frac{N_2\varrho_1}{\tilde{f}_0\sqrt{\tilde{\lambda}^2 + r^2}}\right) \tag{4.120}$$

$$\tilde{f}_0 = \frac{N_2\sqrt{\varrho_1^2 + \varrho_2^2}}{\sqrt{\tilde{\lambda}^2 + r^2}} \tag{4.121}$$

Equation 4.121 can be represented as:

$$\nu_3 r^3 + \nu_2^2 r^2 + \nu_3 r + \nu_0 = 0 \tag{4.122}$$

with

$$\begin{aligned}
\nu_3 &= \frac{-4}{3\tilde{k}_3}(\xi^2 + (1 + \tilde{k}_2 + 2\sigma)^2) \\
\nu_2 &= \frac{8}{3\tilde{k}_3}(1 + \tilde{k}_2 + 2\sigma) - \frac{4}{3\tilde{k}_3}(-1 + a\tilde{k}_2)(\xi^2 + \Big(1 + \tilde{k}_2 + 2\sigma\Big)^2) \\
\nu_1 &= \frac{-4}{3\tilde{k}_3}(1 + 2\xi\tilde{\lambda}) + \frac{8}{3\tilde{k}_3}(-1 + a\tilde{k}_2)(1 + \tilde{k}_2 + 2\sigma) - \frac{4\tilde{\lambda}^2}{3\tilde{k}_3}(\xi^2 + (1 + \tilde{k}_2 + 2\sigma)^2) \\
\nu_0 &= \frac{-4}{3\tilde{k}_3}(-1 + a\tilde{k}_2)(1 + 2\xi\tilde{\lambda}) - \frac{4\tilde{\lambda}^2}{3\tilde{k}_3}(-1 + a\tilde{k}_2)(\xi^2 + (1 + \tilde{k}_2 + 2\sigma)^2) - \tilde{f}_0^2
\end{aligned} \tag{4.123}$$

To trace solutions of the cubic polynomial which is defined in Eq. 4.122, Cardano's method [Cardano and Witmer, 1968] can be used. Then, by using Eqs. 4.112 and 4.89 all possible characteristics points of the system which house all equilibrium and singular points can be obtained as functions of detuning parameter σ or sweeping frequency $\omega = 1 + \sigma\varepsilon$.
Let us now to detect critical values of external forcing amplitude $\tilde{f}_0$ for leading the system to modulated response. We set the system to posses singularities, i.e. all conditions of Eq. 4.80 are verified. So, we should consider two fold lines of the system, i.e. $N_{2,l}, l = 1, 2$ (see Eq. 4.111), in all developments which are defined in Eqs. 4.113-4.117. Considering Eq.(4.121), necessary forcing conditions for leading the system to modulated responses reads:

$$\tilde{f}_0 \geq \frac{N_{2,l}|\varrho_1(N_{2,l})|}{\sqrt{\tilde{\lambda}^2 + (1 - a\tilde{k}_2 - \frac{3}{4}\tilde{k}_3 N_{2,l}^2)^2}} \quad , \qquad l = 1, 2 \tag{4.124}$$

Moreover, according to Eq. 4.120 each fold line of the system houses "two" phases, namely $\delta_{2,l}, l = 1, 2$.

4.4.5.1 Some numerical examples

Following initial conditions are set for the system 4.53:

$$(y_1, \dot{y}_1, y_2, \dot{y}_2)\Big|_{T=0} = (4.5, 0, 0, 0) \tag{4.125}$$

We assume that $\tilde{k}_2 = 0.1$, $\tilde{a} = 0.99$, $\tilde{\lambda} = 0.2$, $\xi = 0.1$ and $\tilde{k}_3 = 0.01$. Equation 4.53 is numerically integrated by Runge-Kutta method ($ode45$ function of Matlab) for different amplitude and detuning parameter of the external excitation.

External excitation with $\tilde{f}_0 = 4$: Variations of system system amplitudes (N_2 and N_1) with respect to the detuning parameter σ when $\mathscr{F}_1 = 0$ and $\mathscr{F}_2 = 0$ in Eq. 4.102 (leading to 4.113 and 4.122) are shown in Figs. 4.5 and 4.6. It is seen that some zones correspond to multiple states. These responses can be periodic (stable, unstable) which can also be reached at other slow time scales, such as $\tau_2 = \varepsilon^2 T$, $\tau_3 = \varepsilon^3 T$, etc. They can also correspond to modulated regimes [Starosvetsky and Gendelman, 2008] due to existence of fold singularities. Let us study a zone with a single possible behaviour, for instance the zone corresponding to $\sigma = 2$. The two- and three-dimensional view of the SIM accompanied by numerical results are provided in Figs. 4.7 and 4.8, respectively. These figures show that starting from initial conditions, numerical results follow the SIM (but with oscillations). When the system reaches to the stability border of the SIM, it experiences a bifurcation and jump to other stable branch of the SIM. Finally, it is attracted by an equilibrium point which has been already predicted and presented in Figs. 4.5 and 4.6. Histories of N_2 and N_1 which are given in Figs. 4.9 and 4.10 confirm this prediction (see amplitudes for $\sigma = 2$ in Figs. 4.5 and 4.6). This equilibrium point corresponds to a regime presenting low amplitudes of the main system which means that the NES with hysteresis behaviour can control the main system under periodic external excitation under the given forcing amplitude and detuning parameter. Oscillation of the numerical results around the SIM, see Figs. 4.7 and 4.8, are normal as they house all harmonics of the system while the SIM is formulated based on consideration of first harmonics.
As for second example for the system under forcing amplitude $\tilde{f}_0 = 4$, would like to study system behaviours where there will be several possible states for systems. Figures 4.5 and 4.6 show that $\sigma = 0.6$ provides three possible states for the system. Different views of the SIM and corresponding numerical results are depicted in Figs. 4.11 and 4.12. Moreover, time histories of N_2 and N_1 are provided in Figs. 4.13 and 4.14. It is seen that the system faces a pair of bifurcation (direct and

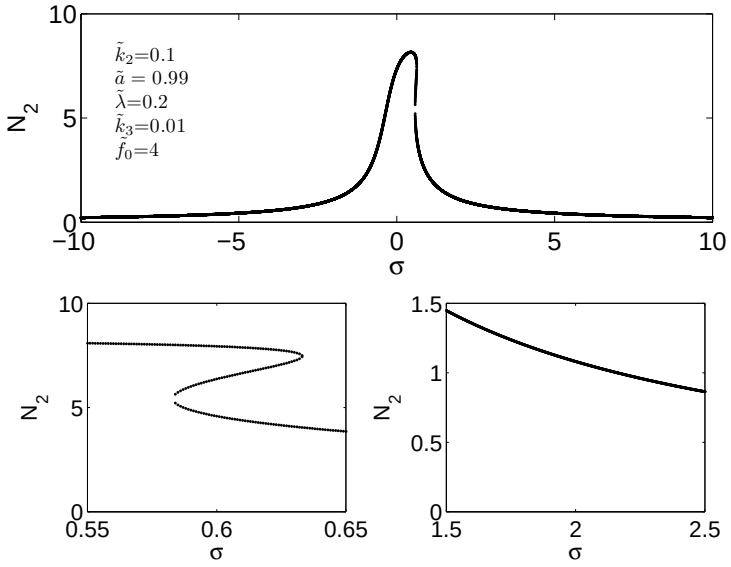

Figure 4.5: Variation of the amplitude of NES with respect to the detuning parameter σ, ($\omega = 1 + \sigma\varepsilon$). The system is under external forcing term $\tilde{f}_0 = 4$. Zones with multiple and unique responses are zoomed.

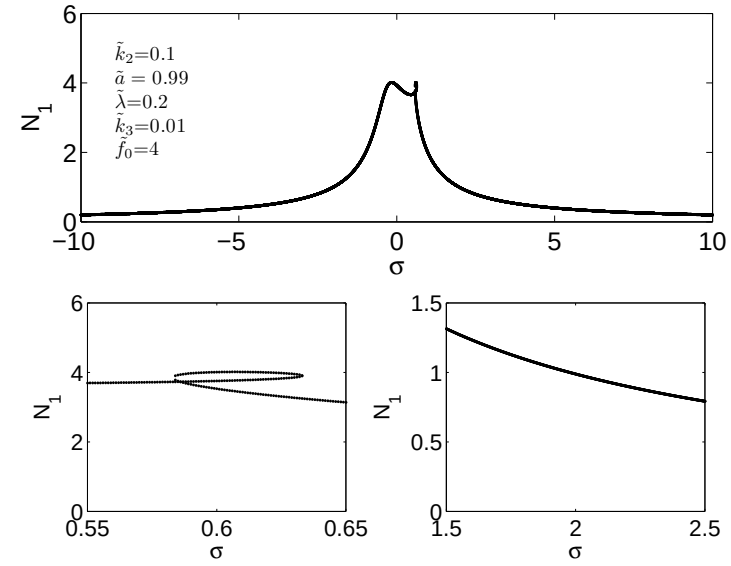

Figure 4.6: Variation of the amplitude of the main oscillator with respect to the detuning parameter σ, ($\omega = 1+\sigma\varepsilon$). The system is under external forcing term $\tilde{f}_0 = 4$. Zones with multiple and unique responses are zoomed.

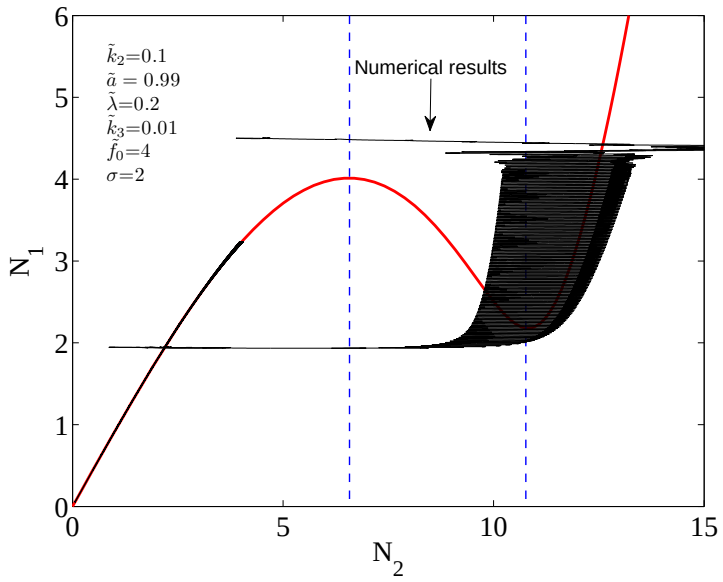

Figure 4.7: Two-dimensional flow of the SIM. Numerical results are collected from direct integration of Eq. 4.53 with $\tilde{f}_0 = 4$ and detuning parameter $\sigma = 2$.

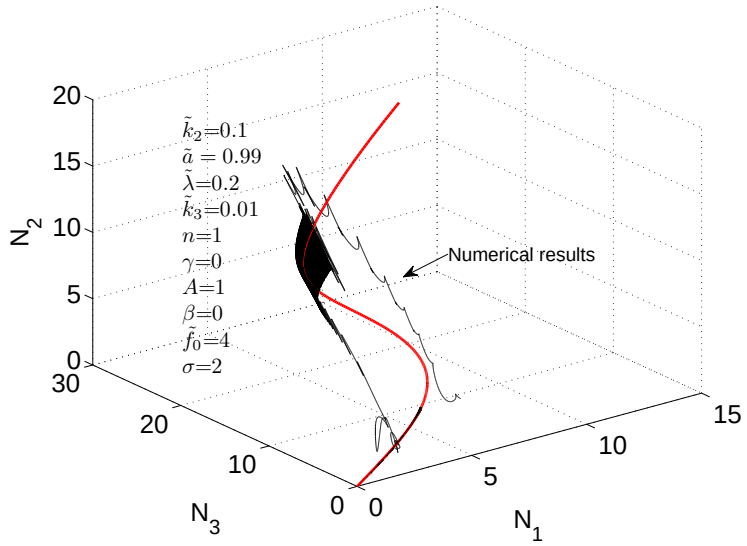

Figure 4.8: Three-dimensional flow of the SIM. Numerical results are collected from direct integration of Eq. 4.53 with $\tilde{f}_0 = 4$ and detuning parameter $\sigma = 2$.

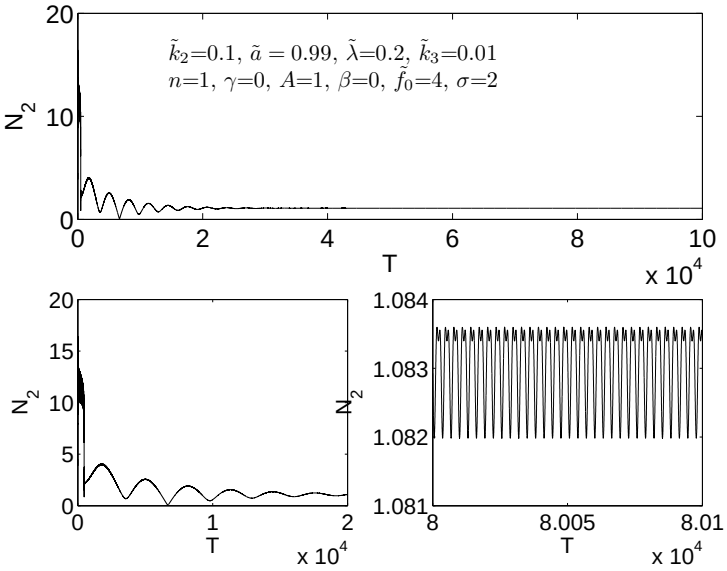

Figure 4.9: Histories of the amplitude N_2 for the system with external forcing amplitude $\tilde{f}_0 = 4$ and detuning parameter $\sigma = 2$. Results are obtained by direct integration of the Eq. (4.53).

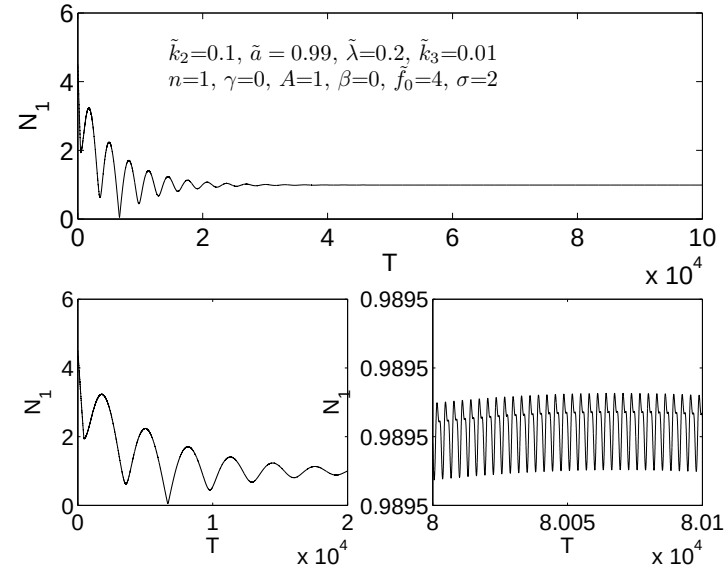

Figure 4.10: Histories of the amplitude N_1 for the system with external forcing amplitude $\tilde{f}_0 = 4$ and detuning parameter $\sigma = 2$. Results are obtained by direct integration of the Eq. (4.53).

inverse) and finally it is attracted by one of three possible equilibrium points, the lowest one here, as it is shown in Figs. 4.5 and 4.6. Other two remaining possible regimes corresponding to $\sigma = 0.6$ can be stable or unstable. They can be reached after a very long time of τ_1 time scale or during other slow time scales such as τ_2 scale. Current response finally correspond to acceptable energy levels of the main structure which is interesting from passive control view point.

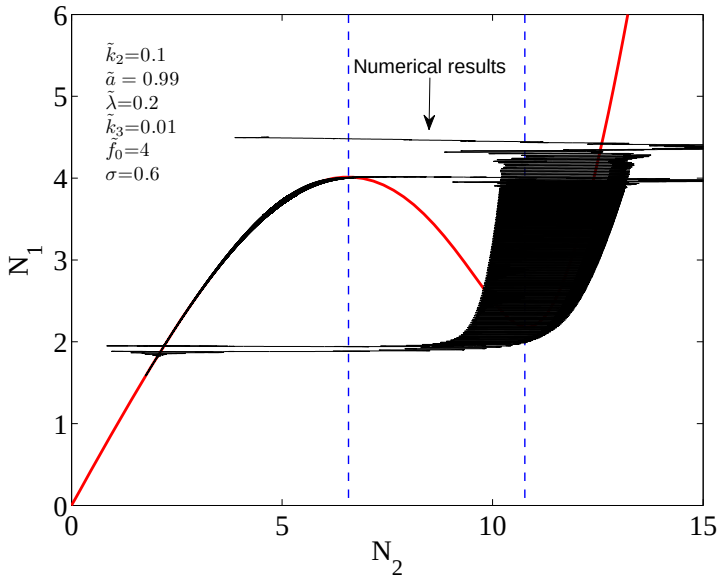

Figure 4.11: Two-dimensional flow of the SIM. Numerical results are collected from direct integration of Eq. 4.53 with $\tilde{f}_0 = 4$ and detuning parameter $\sigma = 0.6$.

External excitation with $\tilde{f}_0 = 6$: All possible scenarios for the system under external excitation with amplitude $\tilde{f}_0 = 6$ with sweeping frequency, i.e. $\omega = 1 + \sigma\varepsilon$ are provided in Figs. 4.15 and 4.16. Let us look at system responses for a σ which corresponds to a zone covered by an isolated branch and possesses three possible responses. We set $\sigma = -1$. The SIM and histories of system amplitudes are illustrated in Figs. 4.17-4.20 indicating that the system faces a modulated response. Figures 4.19 and 4.20 indicate that the system touches the first two possible points (from low to high) corresponding to $\sigma = -1$ in Figs. 4.15 and 4.16.

4.4.5.2 Conclusion of the section

In Sect. 4.4 a step-by-step methodology is endowed which are explained in Sect. 4.2 and 4.3. The aim is to control the main forced structure (or the main mode) by a NES which presents a hysteresis behaviour. Detected SIM and equilibrium and singular points of the system provide necessary design tools for tuning parameters of the nonlinear absorber. In given numerical results, we see that there are possibilities of existence of multiple regimes and also isolated branches for frequency response of the system. For design, all possible ranges of the frequency and forcing amplitudes should be verified in order to be sure the system presents acceptable amplitude intervals during its periodic or modulated regimes.

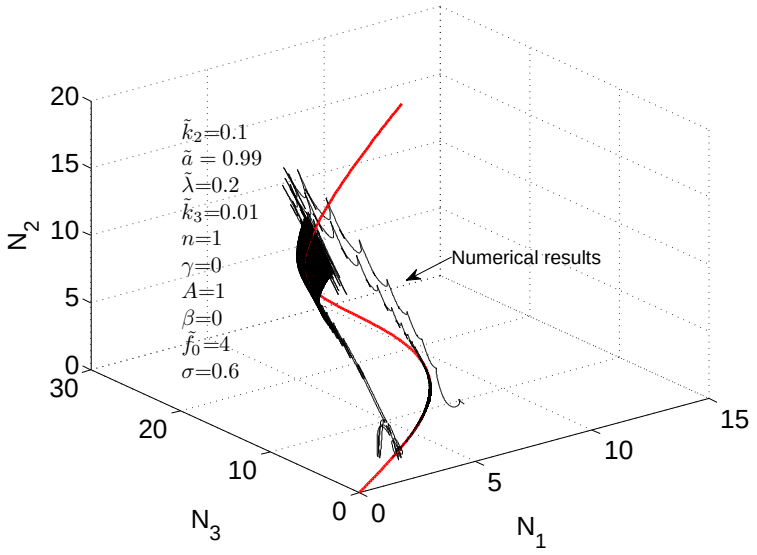

Figure 4.12: Three-dimensional flow of the SIM. Numerical results are collected from direct integration of Eq. 4.53 with $\tilde{f}_0 = 4$ and detuning parameter $\sigma = 0.6$.

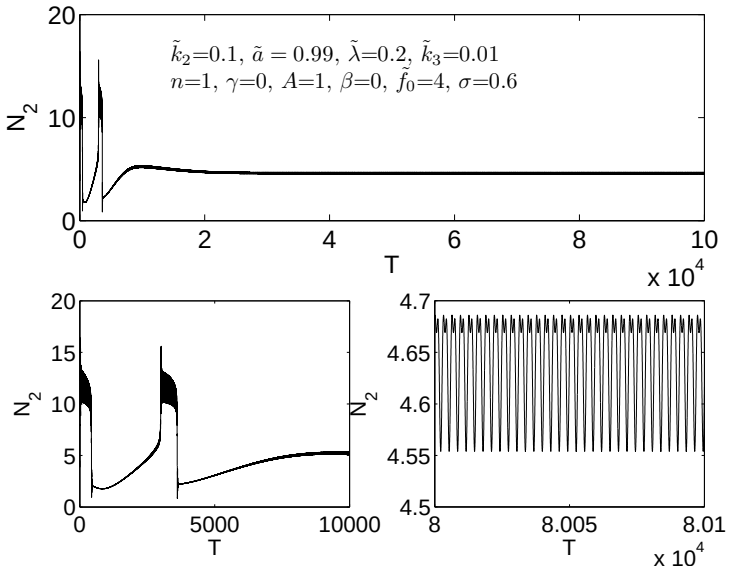

Figure 4.13: Histories of the amplitude N_2 for the system with external forcing amplitude $\tilde{f}_0 = 4$ and detuning parameter $\sigma = 0.6$. Results are obtained by direct integration of the Eq. (4.53).

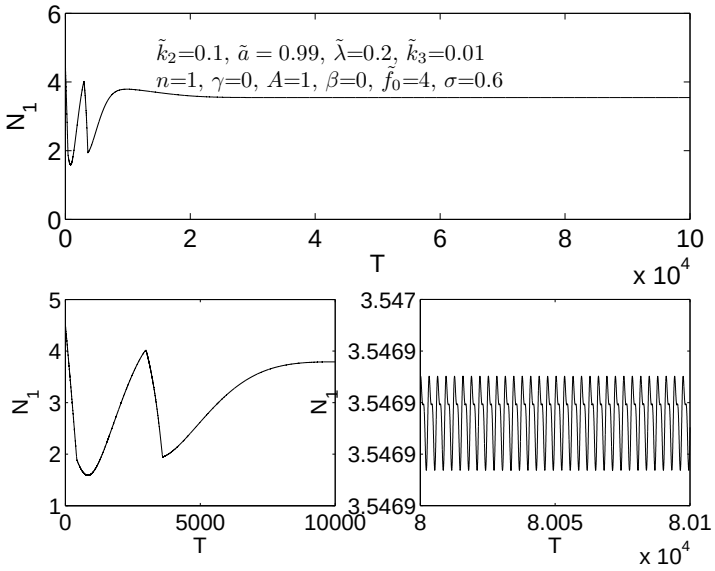

Figure 4.14: Histories of the amplitude N_1 for the system with external forcing amplitude $\tilde{f}_0 = 4$ and detuning parameter $\sigma = 0.6$. Results are obtained by direct integration of the Eq. (4.53).

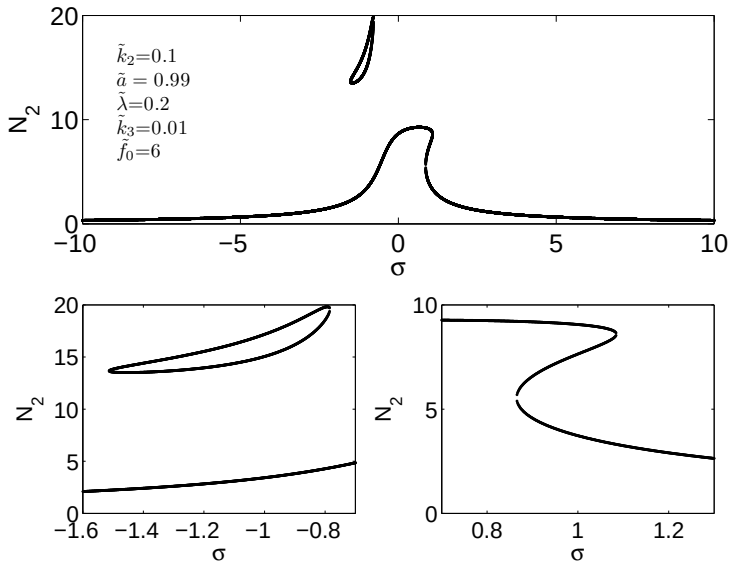

Figure 4.15: Variation of the amplitude of NES with respect to the detuning parameter σ, ($\omega = 1 + \sigma\varepsilon$). The system is under external forcing term $\tilde{f}_0 = 6$. Zones with multiple and unique responses are zoomed.

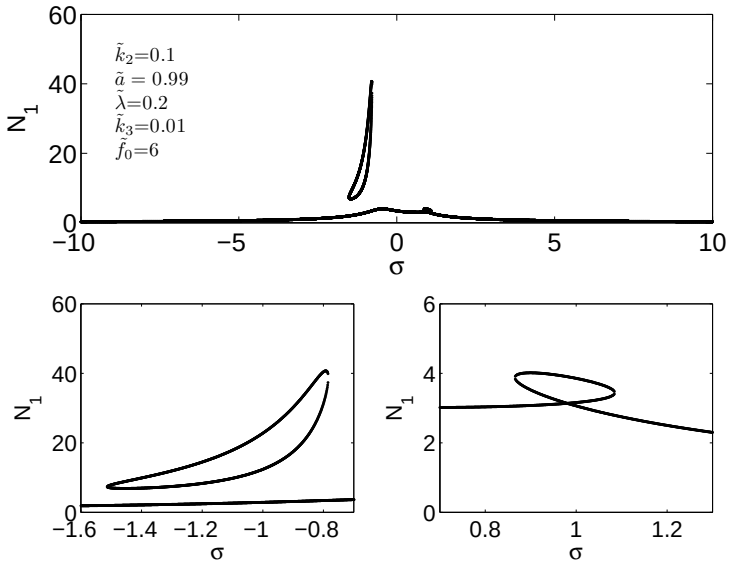

Figure 4.16: Variation of the amplitude of the main oscillator with respect to the detuning parameter σ, ($\omega = 1+\sigma\varepsilon$). The system is under external forcing term $\tilde{f}_0 = 6$. Zones with multiple and unique responses are zoomed.

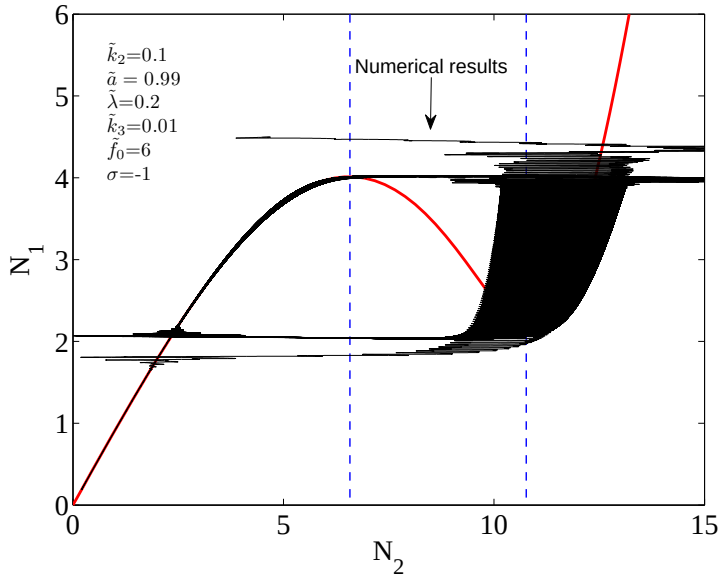

Figure 4.17: Two-dimensional flow of the SIM. Numerical results are collected from direct integration of Eq. 4.53 with $\tilde{f}_0 = 6$ and detuning parameter $\sigma = -1$.

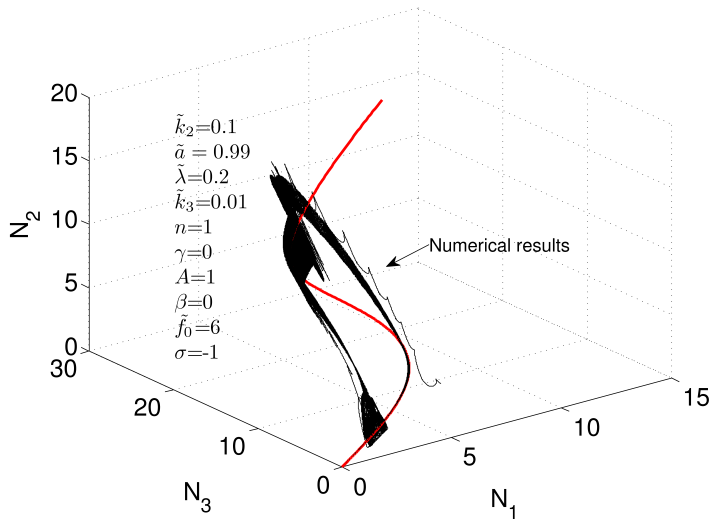

Figure 4.18: Three-dimensional flow of the SIM. Numerical results are collected from direct integration of Eq. 4.53 with $\tilde{f}_0 = 6$ and detuning parameter $\sigma = -1$.

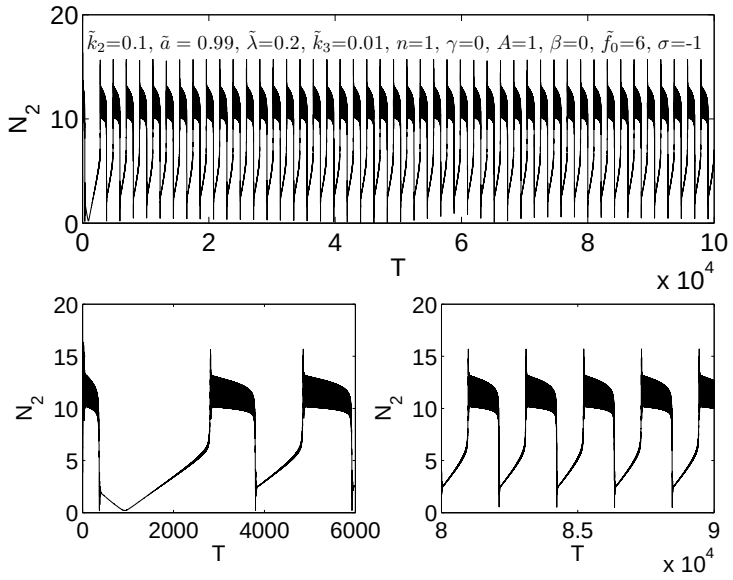

Figure 4.19: Histories of the amplitude N_2 for the system with external forcing amplitude $\tilde{f}_0 = 6$ and detuning parameter $\sigma = -1$. Results are obtained by direct integration of the Eq. (4.53).

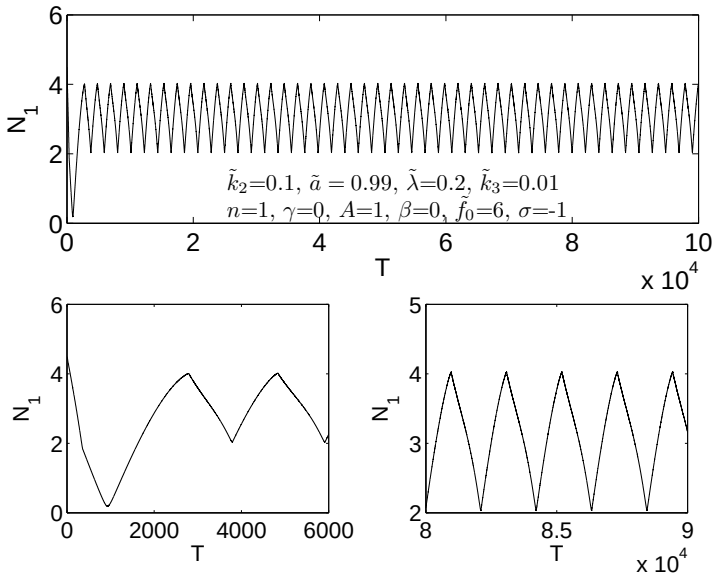

Figure 4.20: Histories of the amplitude N_1 for the system with external forcing amplitude $\tilde{f}_0 = 6$ and detuning parameter $\sigma = -1$. Results are obtained by direct integration of the Eq. (4.53)

4.5 Passive control of systems modelled via differential algebraic inclusion by NES

Let us consider a system in the modal domain which is composed of differential inclusion under an algebraic constraint [Lamarque and Ture Savadkoohi, 2018]:

$$\ddot{\boldsymbol{Y}}(T) + \mathbb{D}\boldsymbol{Y}(T) + \varepsilon\xi_0\dot{\boldsymbol{Y}}(T) + \varepsilon\mathscr{A}_0(\boldsymbol{Y}(T), \dot{\boldsymbol{Y}}(T)) + \varepsilon\mathscr{H}_0(\boldsymbol{Z}(T)) - \varepsilon\boldsymbol{f}_0\sin(\omega t) \ni 0 \tag{4.126}$$

or in a compact manner we can write:

$$\ddot{\boldsymbol{Y}}(T) - \mathscr{F}(\dot{\boldsymbol{Y}}(T), \boldsymbol{Y}(T), T) \ni 0 \tag{4.127}$$

with inclusion of an additional algebraic constraint as:

$$\mathbb{G}(\boldsymbol{Z}(T), \boldsymbol{Y}(T), \dot{\boldsymbol{Y}}(T)) = 0 \tag{4.128}$$

where $0 < \varepsilon \ll 1$ is a small parameter, $\boldsymbol{Y}(T) \in \mathbb{R}^n$, $n \in \mathbb{N}^\star$, $f_0 \in \mathbb{R}^n$, $Z(T) \in \mathbb{R}^m$, $n \geq m \in \mathbb{N}^\star$, $\mathscr{H}_0 : \mathbb{R}^m \to \mathbb{R}^n$ is a smooth function and $\mathscr{A}_0$ is assumed to be a nonsmooth term defined via a maximal monotone operator so that existence and uniqueness questions are solved in the frame of theoretical results are provided by Bastien et al. [Bastien et al., 2013]. Typically $\mathscr{A}_0(\dot{\boldsymbol{Y}}(T), \boldsymbol{Y}(T)) = \mathscr{A}_0(\dot{\boldsymbol{Y}}(T))$, with $\mathscr{A}_0$ maximal monotone graph on $\mathbb{R}^n$. $G : \mathbb{R}^m \times \mathbb{R}^n \times \mathbb{R}^n \to \mathbb{R}^n$ is a smooth (nonlinear) function verifying $\nabla_{\boldsymbol{Z}}\mathbb{G}(\boldsymbol{Z}(T), \boldsymbol{Y}(T), \dot{\boldsymbol{Y}}(T))$ is invertible, and either $\nabla_{\dot{\boldsymbol{Y}}}\mathbb{G}(\boldsymbol{Z}(T), \boldsymbol{Y}(T), \dot{\boldsymbol{Y}}(T)) = 0$ or more generally differentiation of the equation (4.128) lead to the following differential inclusion:

$$\begin{aligned}\Big(&\nabla_{\boldsymbol{Z}}\mathbb{G}(\boldsymbol{Z}(T), \boldsymbol{Y}(T), \dot{\boldsymbol{Y}}(T))\dot{\boldsymbol{Z}}(T) + \nabla_{\boldsymbol{Y}}\mathbb{G}(\boldsymbol{Z}(T), \boldsymbol{Y}(T), \dot{\boldsymbol{Y}}(T))\dot{\boldsymbol{Y}}(T) + \\ &\nabla_{\dot{\boldsymbol{Y}}}\mathbb{G}(\boldsymbol{Z}(T), \boldsymbol{Y}(T), \dot{\boldsymbol{Y}}(T))\mathscr{F}(\dot{\boldsymbol{Y}}(T), \boldsymbol{Y}(T), T)\Big) \ni 0\end{aligned} \tag{4.129}$$

corresponding to a well-posed coupled problem for the nonsmooth terms occurring via $\mathscr{F}$. In order to simplify, we consider here the case $\nabla_{\dot{\boldsymbol{Y}}}\mathbb{G}(\boldsymbol{Z}(T),\boldsymbol{Y}(T),\dot{\boldsymbol{Y}}(T)) = 0$. We assume also $G(\mathbf{0},\mathbf{0},\mathbf{0}) = \mathbf{0}$. The $\mathbb{D}$ is a diagonal matrix with diagonal elements associated to the n frequencies $(\omega_1^2,\omega_2^2,\ldots,\omega_n^2)$ and ∇_U stands for the gradient operator versus the variable U.
For control purpose, we assume that a NES (with a very small mass) is coupled to a targeted mode of the main system, let us assume the mode with the frequency as ω_1. So the differential algebraic equations (4.126)-(4.128) coupled to the NES read:

$$\begin{cases} \ddot{\boldsymbol{Y}}(T) + \mathbb{D}\boldsymbol{Y}(T) + \varepsilon\boldsymbol{\xi}_0\dot{\boldsymbol{Y}}(T) + \varepsilon\mathscr{A}_0(\boldsymbol{Y}(T),\dot{\boldsymbol{Y}}(T)) + \varepsilon\mathscr{H}_0(\boldsymbol{Z}(T)) + \\ \varepsilon\left(\Gamma(y_1 - x) + \lambda(\dot{y}_1 - x)\right)\begin{pmatrix} 1 \\ 0 \\ \vdots \\ 0 \end{pmatrix} - \varepsilon\boldsymbol{f}_0\sin(\omega t) \ni 0 \\ \nabla_{\boldsymbol{Z}}\mathbb{G}(\boldsymbol{Z}(T),\boldsymbol{Y}(T),\dot{\boldsymbol{Y}}(T))\dfrac{\mathrm{d}\boldsymbol{Z}}{\mathrm{d}T}(T) + \nabla_{\boldsymbol{Y}}\mathbb{G}(\boldsymbol{Z}(T),\boldsymbol{Y}(T),\dot{\boldsymbol{Y}}(T))\dfrac{\mathrm{d}\boldsymbol{Y}}{\mathrm{d}T}(T) = 0 \\ \varepsilon\ddot{x}(T) + \varepsilon\lambda(\dot{x}(T) - \dot{y}_1(T)) - \varepsilon\Gamma(y_1 - x) = 0 \end{cases} \tag{4.130}$$

where $\boldsymbol{\xi}_0$ stands for the diagonal matrix of specific damping of the main system while λ and Γ are damping and essential nonlinear restoring forcing function of the NES, e.g. $\Gamma(\mathfrak{Z}) = \gamma\mathfrak{Z}^3$, respectively. The $x(T) \in \mathbb{R}$ and f_0 is a vector of $\mathbb{R}^n$ which stands for amplitudes of external excitations. We assume that the system does not present neither internal, nor combinational nor sub-combination resonances. We assume that the frequency of the external excitation, i.e. ω is varying around the j^{th} frequency of the main system via a detuning parameter σ_j. It reads as:

$$\omega = \omega_j + \sigma_j\varepsilon \tag{4.131}$$

Let us write the second equation of the system 4.130 as:

$$\begin{aligned} \nabla_{\boldsymbol{Z}}\mathbb{G}(\boldsymbol{Z}(T),\boldsymbol{Y}(T),\dot{\boldsymbol{Y}}(T))\frac{\mathrm{d}\boldsymbol{Z}}{\mathrm{d}T}(T) + \nabla_{\boldsymbol{Y}}\mathbb{G}(\boldsymbol{Z}(T),\boldsymbol{Y}(T),\dot{\boldsymbol{Y}}(T))\frac{\mathrm{d}\boldsymbol{Y}}{\mathrm{d}T}(T) = \\ \mathbb{P}(\boldsymbol{Z}(T),\boldsymbol{Y}(T),\dot{\boldsymbol{Y}}(T))\frac{\mathrm{d}\boldsymbol{Z}}{\mathrm{d}T}(T) + \mathbb{Q}(\boldsymbol{Z}(T),\boldsymbol{Y}(T),\dot{\boldsymbol{Y}}(T))\frac{\mathrm{d}\boldsymbol{Y}}{\mathrm{d}T}(T) \end{aligned} \tag{4.132}$$

where $\mathbb{P}$ and $\mathbb{Q}$ are matrices of the dimensions of $m \times m$ and $m \times n$, respectively. We are interested in analytically treatment of the system 4.130 via looking at the modulations of system amplitudes around the principle resonance. To this end, we can directly complexify system variables via complex variables of Manevitch [Manevitch, 2001]. The other method can be changing system coordinates via linear transformation as described in Eq. 4.2 to be implemented in $\boldsymbol{Y}(T)$ and $x(T)$; for instance since in Eq. 4.130 we are interested in studying the interaction between the principle mode with the modal displacement as y_1 and the NES with rescaled displacement in modal domain as x, one can transfer y_1 and x to the centre of the mass of the main principle mode and the ε relevant to the scaled mass of the NES and to the relative displacement as $y_1 - x$. The other coordinates can leave un-transferred. In this study, we choose the first method.

4.5.1 Complexification of system variables

Due to the type of the considered resonance which is given in Eq. 4.131, we assume that the response of the system 4.130 can be represented by modulations of dynamical behaviours around harmonics of the Fourier series governed by the frequency ω. For this, we endow complex variables

Manevitch [Manevitch, 2001]:

$$\left\{\begin{array}{c}\phi_1 e^{i\omega T} = \dot{y}_1(T) + i\omega y_1(T)\\ \vdots\\ \phi_n e^{i\omega T} = \dot{y}_n(T) + i\omega y_n(T)\\ \vdots\\ \phi_{n+2} e^{i\omega T} = \dot{z}_1(T) + i\omega z_1(T)\\ \vdots\\ \phi_{n+m+1} e^{i\omega T} = \dot{z}_m(T) + i\omega z_m(T)\\ \vdots\\ \phi_{n+1} e^{i\omega T} = \dot{x}(T) + i\omega x(T)\end{array}\right. \tag{4.133}$$

so, variables of the Eq. 4.130 can be presented as ($j = 1, \ldots, n$ and $l = 1, \ldots, m$):

$$\left\{\begin{array}{c}\dot{y}_j = \dfrac{1}{2}(\phi_j e^{i\omega T} + \phi_j^\star e^{-i\omega T})\\ \\ y_j = \dfrac{1}{2i\omega}(\phi_j e^{i\omega T} - \phi_j^\star e^{-i\omega T})\\ \\ \dot{z}_l = \dfrac{1}{2}(\phi_{l+n+1} e^{i\omega T} + \phi_{l+n+1}^\star e^{-i\omega T})\\ \\ z_l = \dfrac{1}{2i\omega}(\phi_{l+n+1} e^{i\omega T} - \phi_{l+n+1}^\star e^{-i\omega T})\\ \\ \dot{x} = \dfrac{1}{2}(\phi_{n+1} e^{i\omega t} + \phi_{n+1}^\star e^{-i\omega t})\\ \\ x = \dfrac{1}{2i\omega}(\phi_{n+1} e^{i\omega T} - \phi_{n+1}^\star e^{-i\omega T})\end{array}\right. \tag{4.134}$$

where $.^\star$ stands for the complex conjugate of the variable under consideration.

4.5.2 Time multiple scale behaviour: fast and slow equations

The time T is embedded to different scales as described in Eq. 4.5 and system equations are treated at each time scales. As already highlighted in Sect. 4.2 and 4.3, it is assumed that variables ϕ_{g} and $\phi_{\mathrm{g}}^\star$, $\mathrm{g} = 1, 2, \ldots, n+m+1$, are independent of the fast time scale τ_0. This will be verified during multiple scale analyses of the system or during the studying of system behaviours at fixed points. From Eq. 4.134 we can write:

$$\left\{\begin{array}{ll}\dot{\phi}_j e^{i\omega t} = \ddot{y}_j + \omega^2 y_j, & j = 1, \ldots, n\\ \dot{\phi}_{n+1} e^{i\omega t} = \ddot{x} + \omega^2 x & \\ \dot{\phi}_{l+n+1} e^{i\omega t} = \ddot{z}_l + \omega^2 z_l, & l = 1, \ldots, m\end{array}\right. \tag{4.135}$$

Let us set $\mathscr{T} = \dfrac{2\pi}{\omega}$. For keeping first harmonics of the system, Eq. 4.6 should be used as:

$$\frac{1}{\mathscr{T}}\int_0^{\mathscr{T}} \dot{\phi}_{\mathrm{g}} e^{i\omega\tau_0} e^{-i\omega\tau_0} \mathrm{d}\tau_0 = \frac{1}{\mathscr{T}}\int_0^{\mathscr{T}} \dot{\phi}_{\mathrm{g}}(\tau_1, \tau_2, \ldots) e^{i\omega\tau_0} e^{-i\omega\tau_0} \mathrm{d}\tau_0 = \dot{\phi}_{\mathrm{g}}(\tau_1, \ldots) \tag{4.136}$$

with $\mathfrak{g} = 1, 2, \dots, n+m+1$. For instance for $\mathfrak{g} = 1$ we obtain:

$$\dot{\phi}_1 + (\omega_1^2 - \omega^2)\frac{\phi_1}{2i\omega} + \varepsilon\Bigg(\frac{\xi_{01}}{2}\phi_1 + F_1(\phi_1, \phi_1^\star, \dots, \phi_n, \phi_n^\star) + \mathcal{H}_{01}(\phi_{n+2}, \dots, \phi_{n+m+1}^\star) + \frac{\lambda}{2}(\phi_1 - \phi_{n+1}) + \mathscr{C}(\phi_1, \phi_1^\star, \phi_{n+1}, \phi_{n+1}^\star) - \frac{\boldsymbol{f}_{01}}{2}\Bigg) = 0 \tag{4.137}$$

For $\mathfrak{g} = 2, \dots, n$, we have:

$$\dot{\phi}_\mathfrak{g} + (\omega_\mathfrak{g}^2 - \omega^2)\frac{\phi_\mathfrak{g}}{2i\omega} + \varepsilon\Bigg(\frac{\xi_{0\mathfrak{g}}}{2}\phi_\mathfrak{g} + F_\mathfrak{g}(\phi_1, \phi_1^\star, \dots, \phi_n, \phi_n^\star) + \mathscr{H}_{0\mathfrak{g}}(\phi_{n+2}, \dots, \phi_{n+m+1}^\star) - \frac{\boldsymbol{f}_{0j}}{2}\Bigg) = 0 \tag{4.138}$$

For the equation which represents the dynamics of the coupled NES, i.e. for $\mathfrak{g} = n+1$ we have:

$$\varepsilon\Bigg(\dot{\phi}_{n+1} + i\frac{1}{2\omega}\phi_{n+1} + \frac{\lambda}{2i\omega}(\phi_{n+1} - \phi_1) - \mathscr{C}(\phi_1, \phi_1^\star, \phi_{n+1}, \phi_{n+1}^\star)\Bigg) = 0 \tag{4.139}$$

For $\mathfrak{g} = n+2, \dots, n+m+1$, the algebraic relations are obtained via

$$\frac{1}{\mathscr{T}}\int_0^{\mathscr{T}}\Bigg(\sum_{l=1}^{m}\mathbb{P}_{\mathfrak{g}l}(\boldsymbol{Z}(T), \boldsymbol{Y}(T), \dot{\boldsymbol{Y}}(T))\dot{z}_l(T) + \sum_{l=1}^{n}\mathbb{Q}_{\mathfrak{g}l}(\boldsymbol{Z}(T), \boldsymbol{Y}(T), \dot{\boldsymbol{Y}}(T))\dot{y}_l(t)\Bigg)e^{-i\omega\tau_0}d\tau_0 \tag{4.140}$$

Equation 4.140 in the functional form can be written as:

$$\mathscr{G}_\mathfrak{g}(\phi_1, \dots, \phi_n^\star, \phi_{n+2}, \dots, \phi_{n+m+1}^\star) = 0 \tag{4.141}$$

Functions F_1, $\mathcal{H}_{0\mathfrak{g}}$ and $\mathscr{C}$ in Eqs. 4.137, 4.138, 4.139 are defined as:

$$F_\mathfrak{g}(\phi_1, \phi_1^\star, \dots, \phi_n, \phi_n^\star) = \frac{1}{\mathscr{T}}\int_0^{\mathscr{T}}\mathscr{A}_{0\mathfrak{g}}\big(\tau_0, \boldsymbol{\Phi}(\tau_1, \dots), \boldsymbol{\Phi}^\star(\tau_1, \dots)\big)e^{-i\omega\tau_0}\mathrm{d}\tau_0 \tag{4.142}$$

where $\boldsymbol{\Phi} = (\phi_1, \dots, \phi_n)^t$;

$$\mathscr{C}(\phi_1, \phi_1^\star, \phi_{n+1}, \phi_{n+1}^\star) = \frac{1}{\mathscr{T}}\int_0^{\mathscr{T}}\Gamma(y_1 - x)e^{-i\omega\tau_0}\mathrm{d}\tau_0 \tag{4.143}$$

with

$$y_1 - x = \frac{1}{2i\omega}\Big(\big(\phi_1(\tau_1, \dots) - \phi_{n+1}(\tau_1, \dots)\big)e^{i\omega\tau_0} - \big(\phi_1^\star(\tau_1, \dots) - \phi_{n+1}^\star(\tau_1, \dots)\big)e^{-i\omega\tau_0}\Big) \tag{4.144}$$

and finally

$$\mathcal{H}_{0\mathfrak{g}} = \frac{1}{\mathscr{T}}\int_0^{\mathscr{T}}\mathscr{H}_{0\mathfrak{g}}\big(\phi_{n+2}(\tau_1, \dots)e^{i\omega\tau_0}, \dots, \phi_{n+m+1}^\star(\tau_1, \dots)e^{-i\omega\tau_0}\big)e^{-i\omega\tau_0}d\tau_0 \tag{4.145}$$

In order to study system behaviours at different time scales, we seeks for fast and slow equations which can be traced via selection of equations at different scales of ε. Let us consider ε^0 order of system equations for $\mathfrak{g} = 1, \dots, n$, i.e. for Eqs. 4.137 and 4.138; they read:

$$\begin{aligned}\frac{\partial\phi_1}{\partial\tau_0} + \mathcal{O}(\varepsilon) = 0 \Rightarrow \phi_1 = \phi_1(\tau_1, \tau_2, \dots)\\ \vdots\\ \frac{\partial\phi_n}{\partial\tau_0} + \mathcal{O}(\varepsilon) = 0 \Rightarrow \phi_n = \phi_n(\tau_1, \tau_2, \dots)\end{aligned} \tag{4.146}$$

It should be mentioned that in Eqs. 4.137 and 4.138:

$$(\omega_{\mathfrak{g}}^2-\omega^2)\frac{\phi_{\mathfrak{g}}}{2i\omega}=i\sigma_{\mathfrak{g}}\phi_{\mathfrak{g}}\varepsilon-\frac{i\sigma^2\phi_{\mathfrak{g}}}{2\omega_{\mathfrak{g}}}\varepsilon^2+\mathcal{O}(\varepsilon^3) \tag{4.147}$$

Let us suppose that the ε^0 order of the Eq. 4.141 yields to:

$$\mathscr{G}_{\mathfrak{g}0}(\phi_1,\ldots,\phi_n^\star,\phi_{n+2},\ldots,\phi_{n+m+1}^\star)=0 \tag{4.148}$$

We are interested in passive control of the first mode of the system; to this end we set in Eq.4.131 as $j=1$. Let us investigate more on Eq. 4.139 via simplifying it by removing the the term ε.

$$\frac{\partial\phi_{n+1}}{\partial\tau_0}+\frac{\lambda}{2i\omega_1}(\phi_{n+1}-\phi_1)-\mathscr{C}_0(\phi_1,\phi_1^\star,\phi_{n+1},\phi_{n+1}^\star)=0 \tag{4.149}$$

where $\mathscr{C}_0$ stands for the ε^0 order of the $\mathscr{C}$ and $\omega=\omega_1+\mathcal{O}(\varepsilon)$. We would like to trace the asymptotic response of the system versus fast time scale; we set:

$$\tau_0\longrightarrow+\infty\quad,\quad\frac{\partial\phi_{n+1}}{\partial\tau_0}=0 \tag{4.150}$$

Then, Eq.4.149 reads:

$$\frac{\lambda}{2i\omega_1}(\phi_{n+1}-\phi_1)-\mathscr{C}_0(\phi_1,\phi_1^\star,\phi_{n+1},\phi_{n+1}^\star)=0 \tag{4.151}$$

The $m+1$ relations of Eqs. 4.148 and 4.151 define the SIM. As we have started from $n+m+1$ complex variables ϕ_j, then the evolution of the the dynamical system around the SIM yields to a reduced order of n models. Let us study modulations of the system responses around the SIM. For this, we look at system responses at slow time scale τ_1 which is equivalent to ε^1 order of system of equations for $\phi_{\mathfrak{g}}$, $\mathfrak{g}=1,\ldots,n$. We have:

$$\frac{\partial\phi_1}{\partial\tau_1}+(i\sigma_j+\frac{\xi_{01}}{2})\phi_1+F_1+\mathscr{H}_{01}+\frac{\lambda}{2}(\phi_1-\phi_{n+1})+\mathscr{C}-\frac{\boldsymbol{f}_{01}}{2}=0 \tag{4.152}$$

and

$$\frac{\partial\phi_j}{\partial\tau_1}+(i\sigma_j+\frac{\xi_{0j}}{2})\phi_j+F_j+\mathscr{H}_{0j}-\frac{\boldsymbol{f}_{0j}}{2}=0,\qquad j=2,\ldots,n \tag{4.153}$$

The analysis of systems 4.152 and 4.153 around the SIM leads to detections of equilibrium and singular points of system which correspond to periodic and modulated regimes as explained in Sects. 4.2 and 4.3: The variables $\phi_1,\ldots,\phi_N$ are set as functions of the $\phi_{n+1},\ldots,\phi_{n+m+1}$, then Eqs. 4.152 and 4.153 can expressed as:

$$\mathscr{M}(\phi_{n+1},\ldots,\phi_{n+m+1}^\star)\begin{pmatrix}\frac{\partial\phi_{n+1}}{\partial\tau_1}\\ \vdots\\ \frac{\partial\phi_{m+n+1}}{\partial\tau_1}\\ \frac{\partial\phi_{n+1}^\star}{\partial\tau_1}\\ \vdots\\ \frac{\partial\phi_{m+n+1}^\star}{\partial\tau_1}\end{pmatrix}=S(\phi_{n+1},\ldots,\phi_{n+m+1}^\star) \tag{4.154}$$

4.5.3 An example: passive control of a main system with friction terms coupled to NES

Here, we consider a semi-explicit differential algebraic equation with friction terms which is coupled to a NES with an essentially cubic nonlinearity. The model is governed by a semi-explicit differential algebraic inclusion as:

$$\begin{cases} \ddot{y} + \omega_1^2 y + \varepsilon a_0 \dot{y} + \alpha\rho(\dot{y}) + h(z) + \varepsilon\lambda(\dot{y} - \dot{x}) + \varepsilon\Gamma(y - x) \ni f(T) \\ g(\dot{y}, y, z) = 0 \\ \varepsilon\ddot{x} + \varepsilon\lambda(\dot{x} - \dot{y}) - \varepsilon\Gamma(x - y) = 0 \end{cases} \tag{4.155}$$

The parameters $\omega_1, \lambda, \gamma, \alpha, a_0$ are constants, while ε is small and positive parameter which is generally associated with the mass ratio, i.e. the ratio of the mass of the main system and the mass of the NES. So ε is finite and is not a book-keeping parameter that could tends to 0^+. The graph of "sign" function relevant to definition to the friction term is represented by ρ. The variable z governs the algebraic equation defined by g while h is a function of z. We are interested in capturing the the principal resonance. Moreover, we set: $\Gamma(y - x) = \gamma(y - x)^3, f(T) = \varepsilon f_0 \sin(\omega T), \alpha = \varepsilon\alpha_0, h(z) = \varepsilon h_0(z)$ and $\omega = \omega_1 + \sigma\varepsilon$. We also consider following simple definitions for g and h_0 functions:

$$g(\dot{y}, y, z) = -z + \frac{y^3}{3} \Rightarrow \begin{cases} \dfrac{\partial g}{\partial \dot{y}} = 0 \\ \dfrac{\partial g}{\partial y} = y^2 \\ \dfrac{\partial g}{\partial z} = -1 \end{cases} \tag{4.156}$$

$$h_0(z) = \beta z$$

So, the semi differential algebraic equation of the system 4.155 can be represented as:

$$\begin{cases} \ddot{y} + \omega_1^2 y + \varepsilon(a_0\dot{y} + \alpha_0\rho(\dot{y}) + h_0(z) + \lambda(\dot{y} - \dot{x}) + \gamma(y - x)^3 - f_0\sin(\omega T)) \ni 0 \\ \varepsilon\left(\ddot{x} + \lambda(\dot{x} - \dot{y}) + \gamma(x - y)^3\right) = 0 \\ \dot{z} = y^2\dot{y} \end{cases} \tag{4.157}$$

4.5.3.1 Analytical approximated approach

Following change of variables are carried using Eq. 4.2:

$$\begin{pmatrix} v \\ w \end{pmatrix} = \begin{pmatrix} \dfrac{1}{1+\varepsilon} & \dfrac{\varepsilon}{1+\varepsilon} \\ 1 & -1 \end{pmatrix} \begin{pmatrix} y \\ x \end{pmatrix} \tag{4.158}$$

Following system is obtained,

$$\begin{cases} \ddot{v} + \dfrac{\omega_0^2}{1+\varepsilon}(v + \dfrac{\varepsilon}{1+\varepsilon}w) + \dfrac{\varepsilon}{1+\varepsilon}\big(a_0(\dot{v} + \dfrac{\varepsilon}{1+\varepsilon}\dot{w}) + \alpha_0\rho(\dot{v} + \dfrac{\varepsilon}{1+\varepsilon}\dot{w}) + h_0(z) \\ -f_0\sin(\omega T)\big) \ni 0 \\ \\ \ddot{w} + \omega_0^2(v + \dfrac{\varepsilon}{1+\varepsilon}w) + (1+\varepsilon)(\lambda\dot{w} + \gamma w^3) + \\ \varepsilon\big(a_0(\dot{v} + \dfrac{\varepsilon}{1+\varepsilon}\dot{w}) + \alpha_0\rho(\dot{v} + \dfrac{\varepsilon}{1+\varepsilon}\dot{w}) + h_0(z) - f_0\sin(\omega T)\big) \ni 0 \\ \\ \dot{z} = (v + \dfrac{\varepsilon}{1+\varepsilon}w)^2(\dot{v} + \dfrac{\varepsilon}{1+\varepsilon}\dot{w}) = v^2\dot{v} + \mathcal{O}(\varepsilon) \end{cases} \tag{4.159}$$

Following complex variables of Manevitch (Eq. 4.4) are introduced:

$$\begin{cases} \phi_1 e^{i\omega\tau_0} = \dot{v} + i\omega v \\ \phi_2 e^{i\omega\tau_0} = \dot{w} + i\omega w \\ \phi_3 e^{i\omega\tau_0} = \dot{z} + i\omega z \end{cases} \tag{4.160}$$

To trace fast and slow equations of the system via the multiple scale method [Nayfeh and Mook, 1979] with different scales of time, see Eq. 4.5, A Galerkin method is used. Following system is obtained via keeping first harmonics of the system:

$$\begin{cases} \dot{\phi}_1 + (\frac{\omega_0^2}{1+\varepsilon} - \omega^2)\frac{\phi_1}{2i\omega} + \frac{\omega_0^2}{(1+\varepsilon)^2}\varepsilon\frac{\phi_2}{2i\omega} + \frac{\varepsilon\alpha_0}{1+\varepsilon}F(N_1, N_2, \delta_1, \delta_2) + \frac{\varepsilon}{1+\varepsilon}H_0(\phi_3, \phi_3^\star) - \\ \frac{\varepsilon f_0}{2i(1+\varepsilon)} = 0 \\ \\ \dot{\phi}_2 - \frac{\omega}{2i}\phi_2 + \omega_0^2(\frac{\phi_1}{2i\omega} + \frac{\varepsilon\phi_2}{2i\omega(1+\varepsilon)}) + (1+\varepsilon)\lambda\frac{\phi_2}{2} + \varepsilon a_0(\phi_1 + \frac{\varepsilon\phi_2}{1+\varepsilon}) + \\ +\varepsilon\alpha_0 F(N_1, N_2, \delta_1, \delta_2) + \varepsilon H_0(\phi_3, \phi_3^\star) + (1+\varepsilon)\gamma\frac{3i}{8\omega^3}|\phi_2|^2\phi_2 - \frac{\varepsilon f_0}{2i} = 0 \\ \\ \phi_3 - \frac{1}{4\omega^2}|\phi_1|^2\phi_1 \end{cases} \tag{4.161}$$

where definitions of F and H_0 are provided in Appendix 1. We study system around the 1:1 resonance via setting $\omega = \omega_1 + \sigma\varepsilon$. Organization of Eq. 4.161 versus powers of ε as it follows:

$$\begin{cases} \frac{\partial\phi_1}{\partial\tau_0} + \varepsilon(\frac{\partial\phi_1}{\partial\tau_1} + \frac{i}{2}(\omega_1 + 2\sigma)\phi_1 + \alpha_0 F(N_1, N_2, \delta_1, \delta_2) + H_0(\phi_3, \phi_3^\star) - \frac{f_0}{2i}) + \mathcal{O}(\varepsilon^2) = 0 \\ \\ \frac{\partial\phi_2}{\partial\tau_0} + \frac{i\omega_1}{2}(\phi_2 - \phi_1) + \frac{\lambda}{2}\phi_2 - \frac{3i\gamma}{8\omega_1^3}|\phi_2|^2\phi_2 + \mathcal{O}(\varepsilon) = 0 \\ \\ \phi_3 - \frac{1}{4\omega_1^2}|\phi_1|^2\phi_1 + \mathcal{O}(\varepsilon) = 0 \end{cases} \tag{4.162}$$

Fast equations of the system, i.e. ε^0 orders, provide that $\frac{\partial\phi_1}{\partial\tau_0} = 0$ or $\phi_1 = \phi_1(\tau_1, \tau_2, \dots)$; so our primary assumption in independence of ϕ_1 from time τ_0 is verified. The SIM of the system obtained from its fixed points, i.e. when $\tau_0 \to +\infty$, then $\frac{\partial\phi_1}{\partial\tau_0} = 0$, copies:

$$\phi_1 = \phi_2 - \frac{i\lambda}{\omega_1}\phi_2 - \frac{3\gamma}{4\omega_1^4}|\phi_2|^2\phi_2 \tag{4.163}$$

which indicates that $\phi_2 = \phi_2(\tau_1, \tau_2, \dots)$. This confirms our primary assumption in keeping first harmonics of the system. Let us present variables of the Eq. 4.160 in polar form as:

$$\phi_j = N_j e^{i\delta_j} \quad , N_j, \delta_j \in \mathbb{R} \quad , j = 1, 2, 3 \tag{4.164}$$

The SIM which is provided in Eq. 4.163 reads:

$$\begin{aligned} N_1 &= N_2\sqrt{\frac{\lambda^2}{\omega_1^2} + (1 - \frac{3\gamma}{4\omega_1^4}N_2^2)^2} = H_1(N_2) \\ \delta_1 &= \delta_2 - \arctan\frac{N_2}{N_1}(\frac{\lambda}{\omega_1(1 - \frac{3\gamma}{4\omega_1^4}N_2^2)}) = H_2(\delta_2, N_2) = \delta_2 + H_3(N_2) \end{aligned} \tag{4.165}$$

Equilibrium points of the reduced order model

Let us consider the first slow equation of the system 4.162. It reads,

$$\frac{\partial \phi_1}{\partial \tau_1} = \frac{1}{2i}\big((\omega_1 + 2\sigma)\phi_1 - \omega_1 \phi_2\big) - \alpha_0 F - H_0 + \frac{f_0}{2i} = \text{RHS} \tag{4.166}$$

Equation 4.166 which presents in fact the evolution of ϕ_1 versus slow time scale τ_1, provides the equilibrium points of the system via setting $\dfrac{\partial \phi_1}{\partial \tau_1} = 0$, or RHS $= 0$. In this case two following real equations are obtained:

$$\begin{aligned}
&\frac{\omega_1}{2} N_2 \sin(\delta_1 - \delta_2) + \frac{2\alpha_0 \eta}{\pi} \sin(2\delta_1) + \frac{f_0}{2} \sin(\delta_1) = 0 \\
&\frac{1}{2}(\omega_1 + 2\sigma) N_1 - \frac{\omega_1}{2} N_2 \cos(\delta_1 - \delta_2) + \frac{2\alpha_0 \eta}{\pi} \cos(2\delta_1) - \frac{\beta}{8\omega_1^3} N_1^3 + \frac{f_0}{2} \cos(\delta_1) = 0
\end{aligned} \tag{4.167}$$

with

$$\eta = \mathbf{sgn}(N_1 \cos(\delta_1) + \frac{\varepsilon}{1+\varepsilon} N_2 \cos(\delta_2)) \tag{4.168}$$

where **sgn**$(...)$ stands for the sign function. The equilibrium points are detected via including definitions of the SIM (Eq. 4.165), in the Eq. 4.167 leading to following real relations:

$$\begin{aligned}
&N_1 = H_1(N_2) \\
&\delta_1 = H_2(N_2, \delta_2) = \delta_2 + H_3(N_2) \\
&\cos(\delta_1 - \delta_2) = \frac{N_2}{N_1}(1 - \frac{3\gamma}{4\omega_1^4} N_2^2) \\
&\sin(\delta_1 - \delta_2) = -\frac{N_2}{N_1}\frac{\lambda}{\omega_1} \\
&N_1(\frac{4\alpha_0 \eta}{\pi} \sin(2\delta_1) + f_0 \sin(\delta_1)) = \lambda N_2^2 \\
&N_1(\frac{4\alpha_0 \eta}{\pi} \cos(2\delta_1) + f_0 \cos(\delta_1)) = \omega_1 N_2^2 (1 - \frac{3\gamma}{4\omega_1^4} N_2^2) - (\omega_1 + 2\sigma) N_1^2
\end{aligned} \tag{4.169}$$

From above mentioned equations it is possible to express all variables versus N_2. A single equations can be obtained depending only on N_2. From Eq. 4.169 one can obtain:

$$\sin(3\delta_1) = \pi \frac{\lambda^2 N_2^4 + (\omega_1 N_2^2 (1 - \frac{3\gamma}{4\omega_1^4} N_2^2) - (\omega_1 + 2\sigma) H_1^2)^2 - H_1^2((\frac{4\alpha_0}{\pi})^2 + f_0^2)}{8\alpha_0 \eta f_0 H_1^2} \tag{4.170}$$

which means that one can express $\delta_1 = H_4(N_2)$. Finally, following equations is obtained which depends only N_2 with $\eta = \pm 1$:

$$-\lambda N_2^2 + \frac{4\alpha_0 \eta}{\pi} H_1 \sin(2H_4) + f_0 H_1 \cos(H_4) = 0 \tag{4.171}$$

A verification should be carried out to see if obtained solution for N_2 (and also δ_2, N_1 and δ_2) assuming a value for η is compatible with the Eq. 4.168 or not.

Singular points of the reduced order model

Let us express Eq. 4.166 in the following form:

$$\begin{cases} \dfrac{\partial N_1}{\partial \tau_1} = \Re(\text{RHS}) \\ \\ N_1 \dfrac{\partial \delta_1}{\partial \tau_1} = \Im(\text{RHS}) \end{cases} \tag{4.172}$$

Due to the governing equation of the SIM (see Eq. 4.165), N_1 and δ_1 can be expressed versus N_2 and δ_2. Equation 4.166 can be reorganized as:

$$\begin{pmatrix} \dfrac{\partial H_1}{\partial N_2} & 0 \\ \\ \dfrac{\partial H_2}{\partial N_2} & \dfrac{\partial H_2}{\partial \delta_2} \end{pmatrix} \begin{pmatrix} \dfrac{\partial N_2}{\partial \tau_1} \\ \\ \dfrac{\partial \delta_2}{\partial \tau_1} \end{pmatrix} = \begin{pmatrix} \Re(\text{RHS}) \\ \Im(\text{RHS}) \end{pmatrix} \tag{4.173}$$

Yielding to

$$\begin{pmatrix} \dfrac{\partial H_1}{\partial N_2} & 0 \\ \\ \dfrac{\partial H_2}{\partial N_2} & 1 \end{pmatrix} \begin{pmatrix} \dfrac{\partial N_2}{\partial \tau_1} \\ \\ \dfrac{\partial \delta_2}{\partial \tau_1} \end{pmatrix} = \begin{pmatrix} \Re(\text{RHS}) \\ \Im(\text{RHS}) \end{pmatrix} \tag{4.174}$$

Singular points of the reduced order system are those which verify:

$$\textbf{det} \begin{pmatrix} \dfrac{\partial H_1}{\partial N_2} & 0 \\ \\ \dfrac{\partial H_2}{\partial N_2} & 1 \end{pmatrix} = 0 \tag{4.175}$$

or

$$\frac{\partial H_1}{\partial N_2} = 0 \tag{4.176}$$

Equation 4.176 states that singular points of the system coincide with positions of local maxima of the SIM (see Eq. 4.165).

4.5.3.2 A numerical example: SMR of the system

The system 4.157 is integrated numerically via the implicit Euler scheme with the time step as $\Delta T = 10^{-4}$. System parameters are provided in Table 4.1. Assumed initial conditions for the system are as it follows:

$$(\dot{x}(0), x(0), \dot{y}(0), y(0), z(0)) = (0, 2, 0, 2, \frac{8}{3}) \tag{4.177}$$

Local maxima of the SIM which are also positions of singular points of the system can be obtained via Eq. 4.176. They read as:

$$N_2 = 2.124 \quad , \quad 3.642 \tag{4.178}$$

Supposing that all parameters of the system are fixed, the necessary forcing amplitude for leading the the system to a SMR can be obtained via Eq. 4.171. One should replace N_2 by values which are reported in Eq. (4.178). They copy:

$$f_0 = 0.242 \quad , \quad 4.019 \tag{4.179}$$

Table 4.1: System parameters relevant to Eq. (4.157) (* $h_0(z) = \varepsilon\beta z$)

ε	ω_1	a_0	α_0	$^*\beta$	σ	λ	γ
10^{-3}	1	0.1	0.1	0.1	0.1	0.1	0.1

Let us consider the system under forcing amplitude as $f_0 = 4.019$. Figures 4.21 and 4.22 illustrate time histories of system amplitudes N_j, $j = 1, 2, 3$ and variables x, y and z, respectively. These figures show that the system experiences persisting bifurcations due to existence of singular point on $N_2 = 3.642$. This behaviour can also be seen via confronting obtained numerical results with the SIM (see Eq. 4.165) which is depicted in Fig. 4.23. It should be mentioned that the SIM which is defined in Eq. 4.165 is obtained by keeping only first harmonics of the system while numerical results contain all harmonics of the system. That is why presented numerical results in Fig. 4.23 oscillate around the SIM. The effects of higher harmonics can be seen in Fig. 4.24 where the analytical relations between N_1 and N_3 (see the third equation of the system 4.162) are compared with those obtained from numerical scheme.

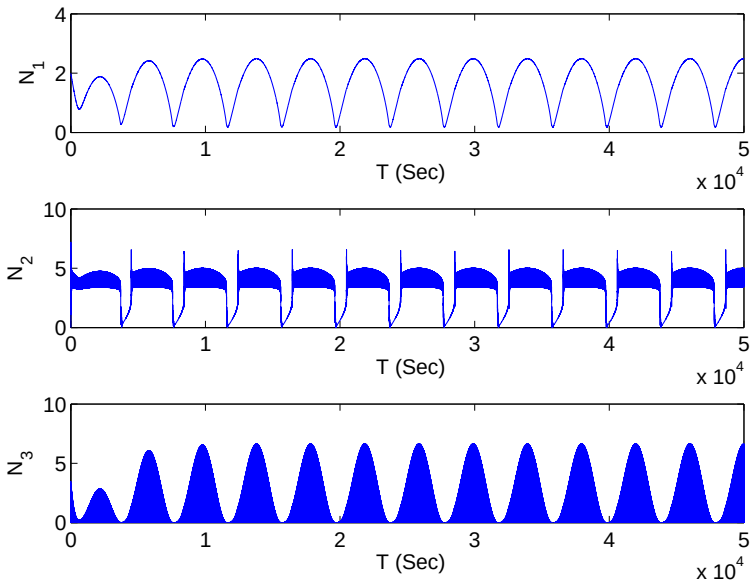

Figure 4.21: Time histories of N_2 and N_1. Results are obtained from numerically integration of the system (4.157) via an implicit Euler scheme with the time step as $\Delta T = 10^{-4}$.

In order to have an idea about the tolerance of the error imposed by the implicit Euler scheme, the time histories of $g(\dot{x}, x, z)$ function, see Eq. 4.155 is depicted in Fig. 4.25. This figure shows that the error stay at the $\mathcal{O}(\Delta T)$ with $\Delta T = 10^{-4}$ which is coherent with the error tolerance of the Euler scheme.

4.6 Some examples of designed nonlinear (smooth or non-smooth) passive controllers for different types of systems

The explained methodologies of Sect. 4.2 and 4.3 are endowed for preparation of design criteria for passive control of wide variety of main systems by different types of NES. Some of considered

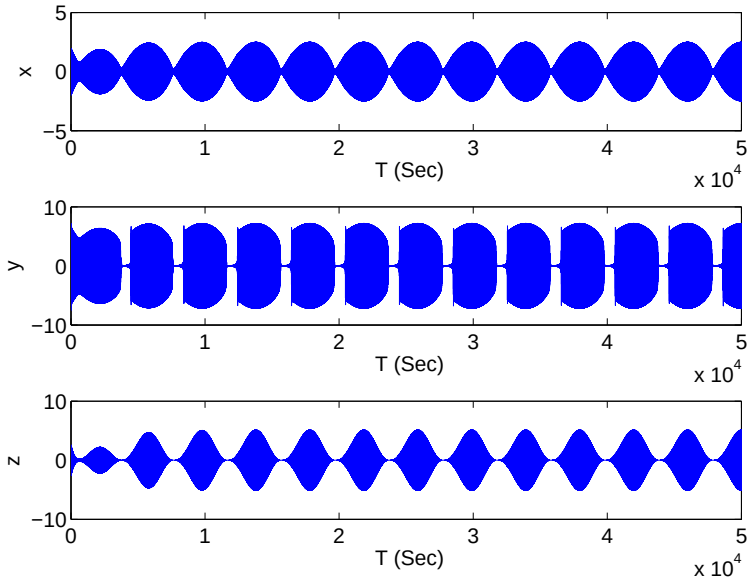

Figure 4.22: Time histories of x, y and z. Results are obtained from numerically integration of the system (4.157) via an implicit Euler scheme with the time step as $\Delta T = 10^{-4}$.

systems are purely academic and some of them are studied to solve the problem of private or public organisations, i.e. industries and the ministry. The treated system with brief applications are summarised in coming section.

4.6.1 Localization of the energy of main linear structures in several NES in parallel

The idea of this work is to distribute the localized energy into a set of parallel NES. This distribution can be according to the demand of the industry due to limitation of the space for positioning a single NES and so to divide the mass of the NES in several ones is parallel in different positions. After treatment of system equations different possible regimes of the system are traced. The developed analytical tools [Vaurigaud, 2011, Vaurigaud et al., 2011b] permit to design two parallel NES which are mounted at the last floor of a prototype four-storey building [Ture Savadkoohi et al., 2012b] as illustrated in Fig. 4.26. The design criteria is to control the first mode of the main structure. Mechanical and physical parameters of each system, in terms of the mass of both systems, length (l) and the rigidity (k) of each spring of the NES are provided in Table 4.2. The structure without coupled NES is subjected to sinusoidal excitation with a sweeping frequency. The frequency response function (FRF) of the system is depicted in Fig. 4.27 while its identified frequencies and damping ratios are collected in Table 4.3. Then two parallel NES are coupled to the main structure and some sinusoidal excitations around the first and second mode are induced. The results are presented in Fig. 4.28. It is seen that two parallel NES reduce the energy of the first mode of the building a lot. As a result, a good passive control is achieved via using two parallel NES.

4.6.2 Targeted energy transfer of linear mechanical systems by a nonsmooth energy sink

For some industrial applications, using a nonsmooth nonlinearity for the NES is more practical. Moreover, if the overall system is initially pre-stressed, such as effects of the gravity, then pure

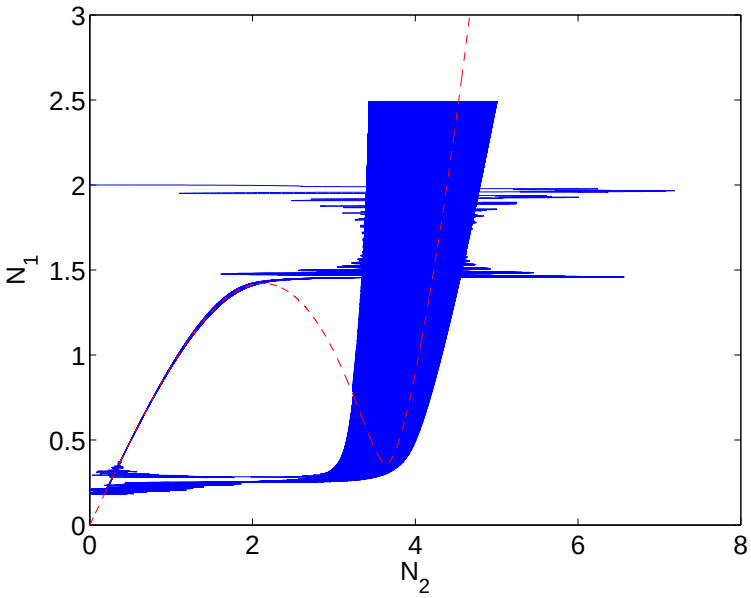

Figure 4.23: The SIM of the system obtained by Eq. (4.165) (red dashed line) and corresponding numerical results (blue solid line) collected from numerically integration of the system (4.157) via an implicit Euler scheme with the time step as $\Delta T = 10^{-4}$.

Table 4.2: Mechanical and physical properties of the system.

Mass (g)			Springs of the NES		
Main Structure	Nes 1	Nes 2	Number	$l\ (m)$	$k\ (N/m)$
2357	30	30	4	5×10^{-2}	480

smooth nonlinearity of NES is broken. That is why in these situations endowing nonsmooth NES is very interesting. My work in this domain started with treating passive control problem of a linear system by a piece-wise linear energy sink [Lamarque et al., 2011, Weiss et al., 2016], then the results are extended to consider a system in the gravitational field [Ture Savadkoohi et al., 2012a, Lamarque et al., 2017]. The initial idea was to control vibration of some mechanical components in the vehicle industry according to a project sponsored by PSA Peugeot, Citroën automobiles. The academic model of the system under consideration is presented in Fig. 4.29. The second oscillator with the mass m and a nonsmooth odd restoring forcing function is intended to be an absorber for

Table 4.3: Identified two first frequencies and damping ratios of the structure.

	Frequency (Hz)	Damping (%)
Mode I	4.44	0.41
Mode II	13.55	0.26

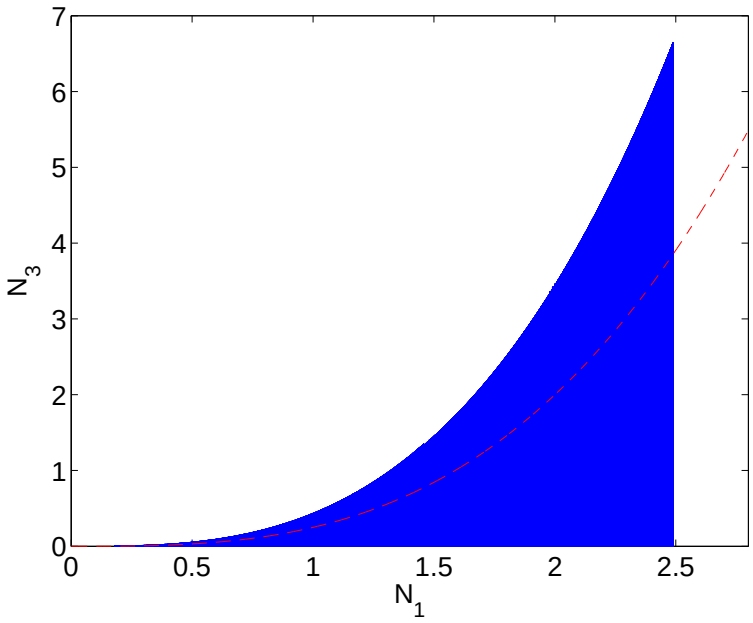

Figure 4.24: Relation between N_3 and N_1: Analytical curve (red dashed line) obtained from third equation of the system 4.162 and numerical one (solid blue line) collected from numerically integration of the system 4.157 via an implicit Euler scheme with the time step as $\Delta T = 10^{-4}$.

the main system with the mass M. Its restoring forcing term reads:

$$F(z) = -\frac{\partial V(z)}{\partial z} = -F(-z) = \begin{cases} 0 & \text{if} \quad -\delta \leq z \leq \delta \\ k_2(z-\delta) & \text{if} \quad z \geq \delta \\ k_2(z+\delta) & \text{if} \quad z \leq -\delta \end{cases} \tag{4.180}$$

Dynamics of the system is summarized as:

$$\begin{cases} M\ddot{y}_1 + k_1 y_1 + F(y_1 - y_2) + \eta(\dot{y}_1 - \dot{y}_2) + Mg = \Gamma \sin(\Omega t) \\ m\ddot{y}_2 + F(y_2 - y_1) + \eta(\dot{y}_2 - \dot{y}_1) + mg = 0 \end{cases} \tag{4.181}$$

With the same manner which is explained in Sect. 4.4, we shift the time domain t to the domain $T = t\sqrt{\frac{k_1}{M}} = t\vartheta$. After introducing $\varepsilon = \frac{m}{M}$, $\gamma = \frac{Mg}{k_1}$, $\varepsilon\lambda = \frac{\eta}{\sqrt{k_1 M}}$, $\frac{1}{k_1}F(z) = \varepsilon\tilde{F}(z)$, $k = \frac{1}{\varepsilon}\frac{k_2}{k_1}$, $\omega = \frac{\Omega}{\vartheta}$ and $\frac{\Gamma}{k_1} = \varepsilon f_0$, the system 4.181 finally takes following form:

$$\begin{cases} \ddot{y}_1 + y_1 + \varepsilon\tilde{F}(y_1 - y_2) + \varepsilon\lambda(\dot{y}_1 - \dot{y}_2) + \gamma = \varepsilon f_0 \sin(\omega T) \\ \varepsilon\ddot{y}_2 + \varepsilon\tilde{F}(y_2 - y_1) + \varepsilon\lambda(\dot{y}_2 - \dot{y}_1) + \varepsilon\gamma = 0 \end{cases} \tag{4.182}$$

where the rescaled restoring forcing function $\tilde{F}$ copies:

$$\tilde{F}(z) = \begin{cases} 0 & \text{if} \quad -\delta \leq z \leq \delta \\ k(z-\delta) & \text{if} \quad z \geq \delta \\ k(z+\delta) & \text{if} \quad z \leq -\delta \end{cases} \tag{4.183}$$

Due to the existence of pre-stressing term γ which is due to the gravity, the system equations should be complexified by extended version of variables of Menevitch which are introduced in Eq. 4.4;

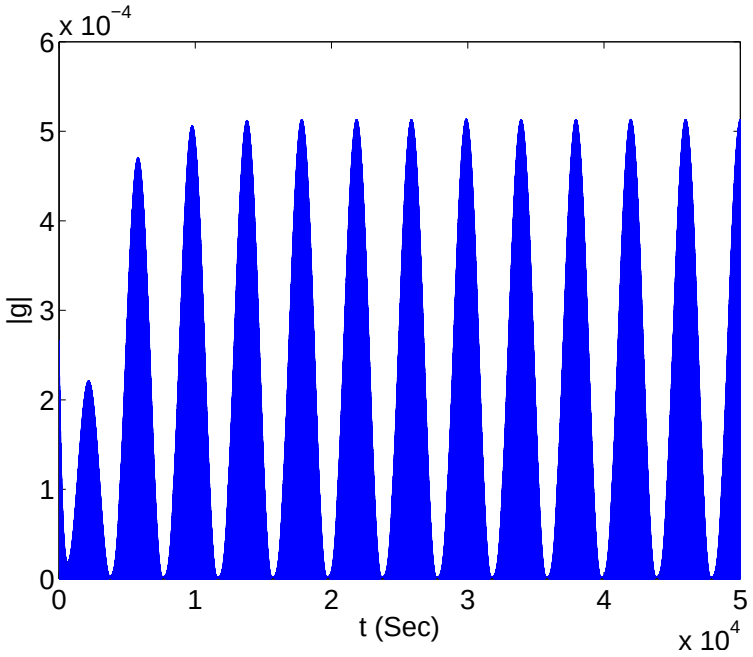

Figure 4.25: The absolute value of the $g(\dot{x}, x, z)$ function, see Eq. 4.155, obtained from an implicit Euler scheme with the time step as $\Delta T = 10^{-4}$.

in fact it keeps constant and firs harmonic terms of the Fourier series. As an example, the SIM of the system and corresponding numerical results are presented in Fig. 4.30. It is see that the system presents a modulated response as a results of possessing fold singularities. This response corresponds to repeated bifurcations of system amplitudes between two fold lines, N_{21} and N_{22}. This behaviour is more evident via looking at their histories which are presented in Fig. 4.31 [Ture Savadkoohi et al., 2012a].
All of studies in this domain aimed to prepare analytical design tools for tuning parameters of nonsmooth NES for controlling main linear or nonlinear main structures [Lamarque et al., 2011, Ture Savadkoohi et al., 2012a, Weiss et al., 2016, Weiss, 2016, Lamarque et al., 2017].

4.6.3 Targeted energy transfer of nonlinear (smooth or nonsmooth) mechanical systems by a energy sink

Some times main structural system presents some kinds of nonlinearities. These behaviours can be due to friction, hysteresis, time variable masses, encased main systems in another system, etc. To this end, several studies are carried to control these kinds of systems via taking into account their nonlinearities. As a summary, the passive control of following nonlinear main systems via NES with smooth or nonsmooth nonlinearities are studied:

- Main system with piece-wise linear behaviour [Lamarque et al., 2012].
- Main system with Dahl-type [Ture Savadkoohi and Lamarque, 2014a] and Bouc-Wen type hysteresis behaviour [Lamarque and Ture Savadkoohi, 2014].
- Main system with time-dependent mass [Lamarque et al., 2014].
- Main system with friction: e.g. using a single [Weiss et al., 2014] or a set of parallel Saint-Venant elements [Lamarque and Ture Savadkoohi, 2015].

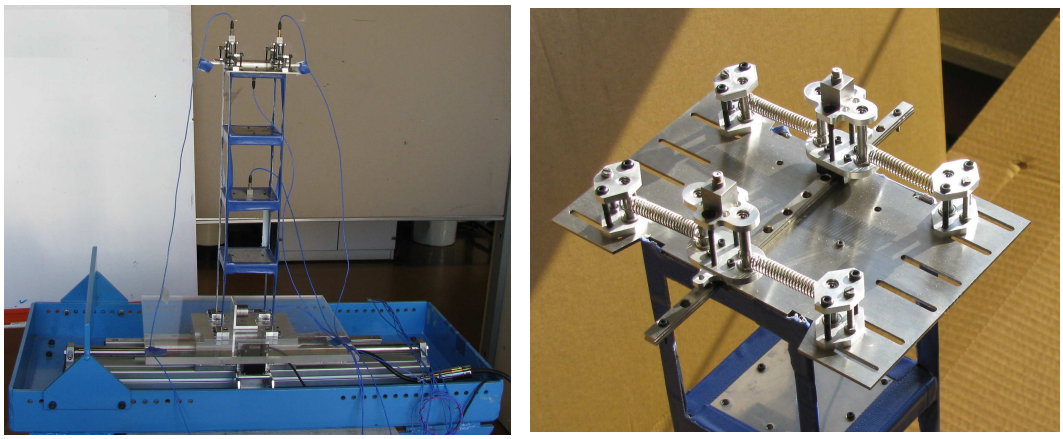

(a) (b)

Figure 4.26: The prototype building equipped with two parallel NES at the last floor: a) The overall view; b) two cubic parallel NES.

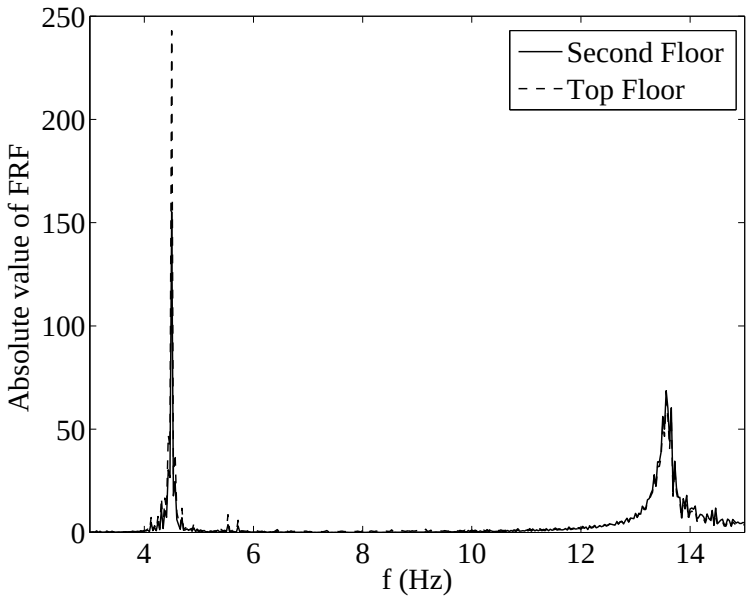

Figure 4.27: The FRF of the prototype structure obtained from accelerometers located at second and the last floors.

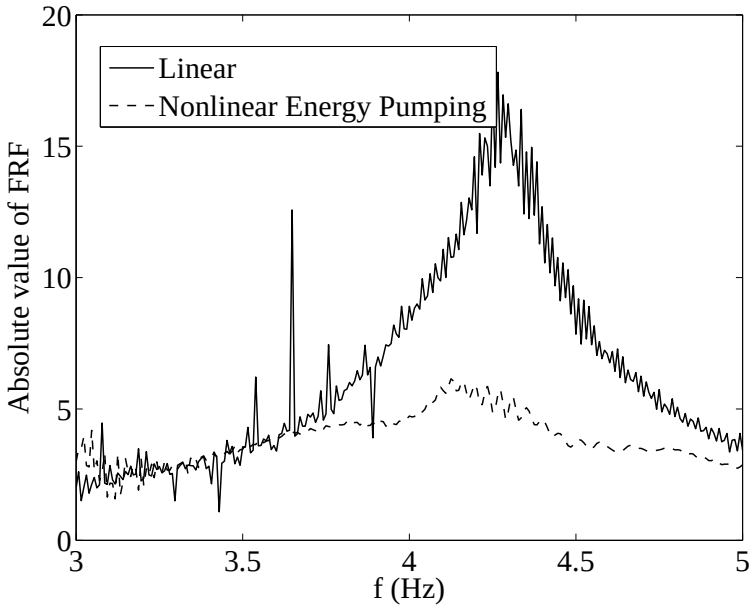

Figure 4.28: The FRF obtained from the accelerometer located at the last floor of the prototype structure.

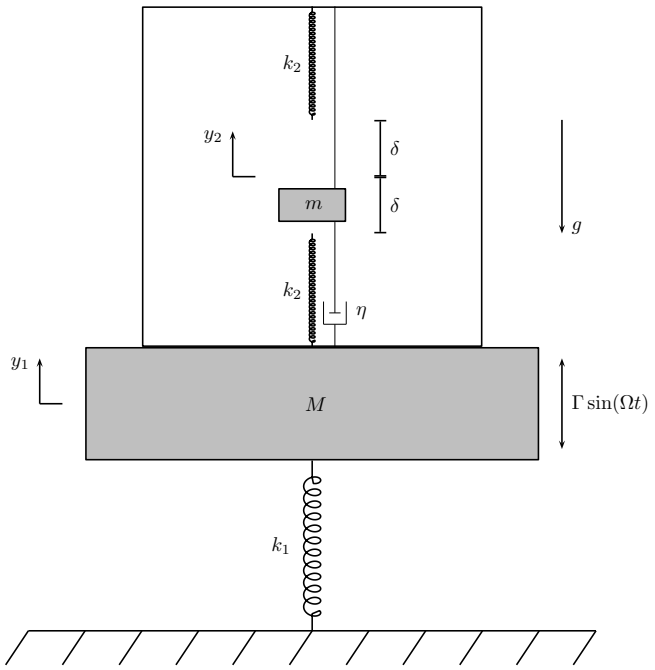

Figure 4.29: The academic model of two coupled oscillators in the gravitational field represented as $\vec{\mathscr{G}} = (0, 0, -g)^T$. The main system is under external force $\Gamma \sin(\Omega T)$.

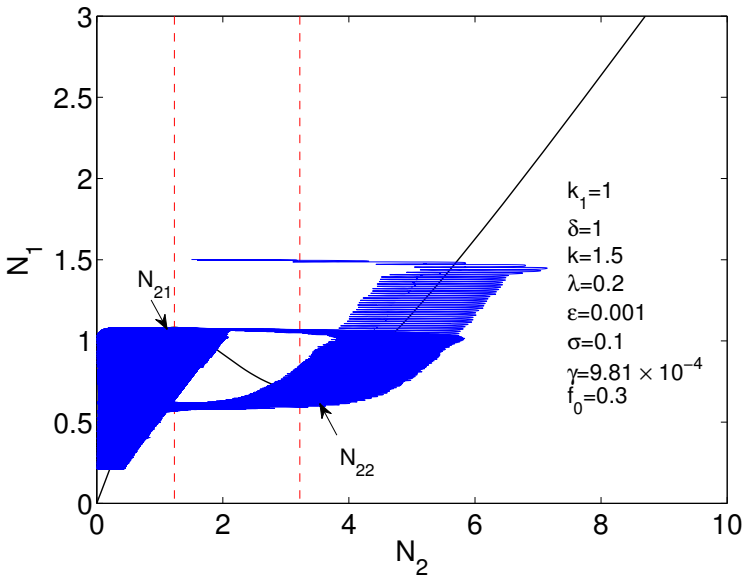

Figure 4.30: The SIM of the system under the gravity.

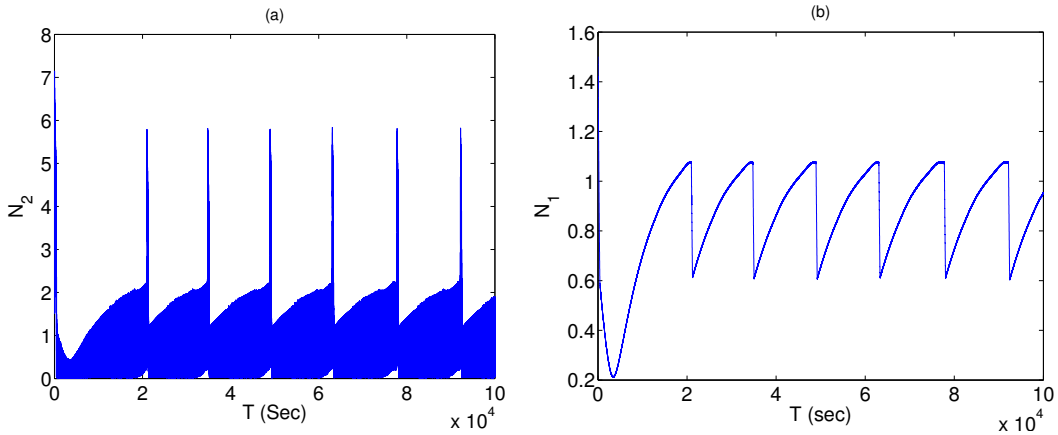

(a) (b)

Figure 4.31: Time histories of system energies obtained from direct integration of the Eq. 4.182.

In the followings a summary of each studied system is presented.

4.6.3.1 Localization of the energy of main systems with nonsmooth behavior in the nonsmooth NES

The main structure has a piece-wise linear behavior: This kind of systems are mainly mechanical equipments which can move between two barriers. The idea is to control this type of systems via a nonsmooth NES. The rescaled form of system equations reads [Lamarque et al., 2012]:

$$\begin{cases} \ddot{x}_1 + \varepsilon\lambda(\dot{x}_1 - \dot{x}_2) + x_1 + F_1(x_1) + \varepsilon F_2(x_1 - x_2) = \varepsilon f_0 \sin(\omega T) \\ \varepsilon\ddot{x}_2 + \varepsilon\lambda(\dot{x}_2 - \dot{x}_1) + \varepsilon F_2(x_2 - x_1) = 0 \end{cases} \tag{4.184}$$

where ε is the mass ration between two oscillators and F_1 and F_2 are nonsmooth restoring forcing functions which copy: it follows:

$$F_1(z) = -\frac{\partial V_1(z)}{\partial z} = -F_1(-z) = \begin{cases} 0 & if \quad -e \leq z \leq e \\ g(z-e) & if \quad z \geq e \\ g(z+e) & if \quad z \leq -e \end{cases} \tag{4.185}$$

$$F_2(z) = -\frac{\partial V_2(z)}{\partial z} = -F_2(-z) = \begin{cases} 0 & if \quad -a \leq z \leq a \\ c(z-a) & if \quad z \geq a \\ c(z+a) & if \quad z \leq -a \end{cases} \tag{4.186}$$

A transformation of system variables via Eq. 4.2 is carried out with the $\mathbb{A}$ as:

$$\mathbb{A} = \begin{pmatrix} 1 & 0 \\ 1 & -1 \end{pmatrix} \tag{4.187}$$

Since there is not any pre-stressing terms in the system, the original form of complex variables of Manevitch is endowed via setting $b_1 = b_2 = 0$ in Eq. 4.4. Then studying of the system at different time scales around a 1:1 resonance reveals the SIM and characteristic points of the system. The SIM copies [Lamarque et al., 2012]:

$$N_2\sqrt{\lambda^2 + \left(-G_2\big(N_2^2\big) + \frac{1}{\omega} + G_1\big(N_1^2\big)\right)^2} = N_1\left(\frac{1}{\omega} + G_1\big(N_1^2\big)\right) \tag{4.188}$$

with

$$G_1\big(|\varphi_1|^2\big) = \begin{cases} 0 & if \quad |\varphi_1| < e \\ \frac{1}{\pi}\Big(2g\arccos\big(\frac{e}{|\varphi_1|}\big) - \frac{2eg\sqrt{|\varphi_1|^2 - e^2}}{|\varphi_1|^2}\Big) & if \quad |\varphi_1| \geq e \end{cases} \tag{4.189}$$

$$G_2\big(|\varphi_2|^2\big) = \begin{cases} 0 & if \quad |\varphi_2| < a \\ \frac{1}{\pi}\Big(2c\arccos\big(\frac{a}{|\varphi_2|}\big) - \frac{2ac\sqrt{|\varphi_2|^2 - a^2}}{|\varphi_2|^2}\Big) & if \quad |\varphi_2| \geq a \end{cases} \tag{4.190}$$

A typical SIM and its stability borders obtained from linear perturbation of system variables is depicted in Fig. 4.32a and included corresponding numerical results are presented in Fig. 4.32b. This figure shows that as much as the ε parameter is smaller, then numerical results follow in a better manner its SIM. In this work the invariant manifold of the system at slow time scale (τ_1) is evaluated

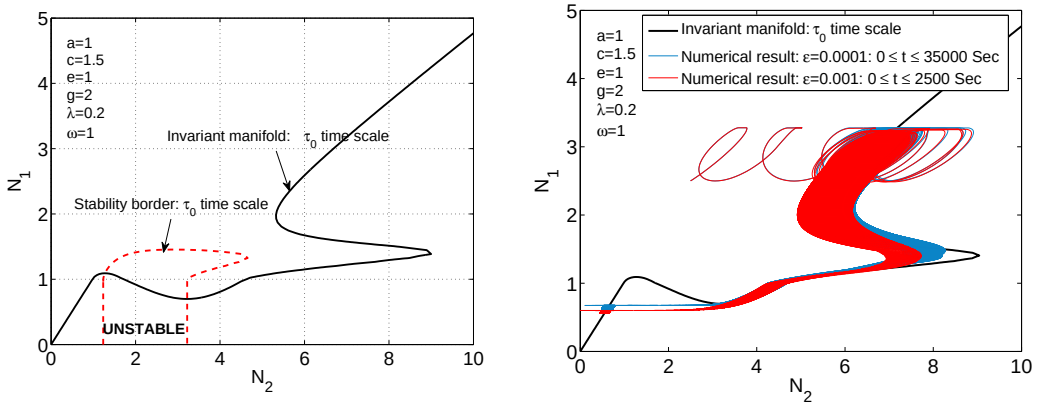

(a) (b)

Figure 4.32: a) The SIM of the described system in Eq. 4.184 and its stability borders; b) The SIM and corresponding numerical results obtained via direct numerical integration of Eq. 4.184 for two different values of mass ratio ε.

as well, which depends to the amplitude of the external excitation [Lamarque et al., 2012]:

$$N_2^2\left[\frac{1}{4}\left(G_2^2(N_2^2)+\lambda^2\right)+\frac{\sigma^2}{\left(G_1^2(N_1^2)+1\right)^2}\times\right.$$
$$\left(\lambda^2+4G_1^2(N_1^2)+1+G_2^2(N_2^2)+4G_1(N_1^2)-4G_1(N_1^2)G_2(N_2^2)-2G_2(N_2^2)\right)+ \quad (4.191)$$
$$\left.\frac{\sigma}{G_1^2(N_1^2)+1}\left(\lambda^2-2G_1(N_1^2)G_2(N_2^2)-G_2(N_2^2)+G_2^2(N_2^2)\right)\right]=\frac{1}{4}f_0^2$$

A typical view of this invariant is illustrated in Fig. 4.33. The intersection of mentioned invariant with the SIM represent characteristic points of the system.

4.6.3.2 Localization of the energy of main systems with hysteresis behaviour in the nonsmooth NES

The aim is to control main structural systems or equipments which present hysteresis behaviours. The rescaled form of system equations is summarized as:

$$\begin{cases}\ddot{x}_1+\varepsilon\zeta\dot{x}_1+x_1+\dfrac{1-a}{a}z+\varepsilon\hat{F}(x_1-x_2)+\varepsilon\lambda(\dot{x}_1-\dot{x}_2)=\varepsilon f_0\sin(\omega T)\\ \varepsilon\ddot{x}_2+\varepsilon\hat{F}(x_2-x_1)+\varepsilon\lambda(\dot{x}_2-\dot{x}_1)=0\\ \dot{z}=A\dot{x}_1-\beta|\dot{x}_1||z|^{n-1}z-\gamma\dot{x}_1|z|^n\end{cases} \quad (4.192)$$

where $\hat{F}$ is the scaled nonsmooth restoring forcing function of the coupled NES which read:

$$\hat{F}(\alpha)=\begin{cases}0 & \text{if} \quad -\delta\le\alpha\le\delta\\ k(\alpha-\delta) & \text{if} \quad \alpha\ge\delta\\ k(\alpha+\delta) & \text{if} \quad \alpha\le-\delta\end{cases} \quad (4.193)$$

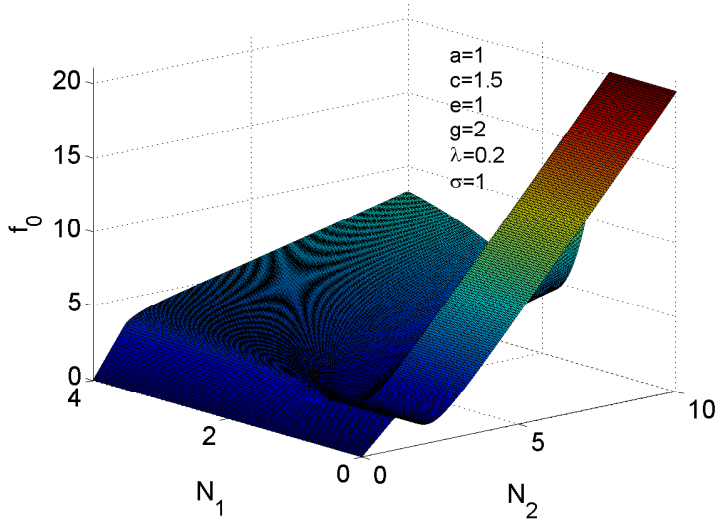

Figure 4.33: The three-dimensional view of the system invariant at τ_1 time scale obtained from Eq. 4.191

The Dahl-type hysteresis modelling of the system is obtained via setting $n = 1$ and $\gamma = 0$ [Dahl, 1968, Ikhouane and Rodellar, 2007]. In order to have a preliminary idea about the behaviour of Dahl-type systems coupled to a NES, let us take a direct numerical integration of the system 4.192 with following initial conditions:

$$(x_1(0), \dot{x}_1(0), x_2(0), \dot{x}_2(0)) = (20, 0, 0, 0) \tag{4.194}$$

and we define η which is in fact the Representative reaction force of the system as:

$$\eta = \varepsilon\zeta\dot{x}_1 + x_1 + \frac{1-a}{a}z + \varepsilon\hat{F}(x_1 - x_2) + \varepsilon\lambda(\dot{x}_1 - \dot{x}_2) \tag{4.195}$$

Figure 4.34a presents the variation of the displacement of the main system with respect to the η while Fig. 4.34b shows phase portraits of the internal variables of the Dahl model, i.e. z. The system is treated via explained methodology in sect. 4.4. The SIM of the system and equilibrium and fold singularities of the system are traced. An example for fold singularities of the system in presented in Fig. 4.35 [Ture Savadkoohi and Lamarque, 2014a]. These points are points which make the matrix $\nabla_{(\delta_2, N_2)}h$ in Eq. 4.20 not to be invertible.

4.6.3.3 Localization of the energy of main systems with time-dependent mass in a nonsmooth NES

The main idea is to control a structure with time-dependent mass. A very simple example of such systems can be rockets, airplanes and vehicles which loose a great amount or some of their masses due to consumption of fuel. Let us consider the model which is provided in Fig. 4.36 [Lamarque et al., 2014]: it represents a main system with the time-dependent mass $\widetilde{M}(t)$, the rigidity and the damping constant as k_1 and C which is coupled to NES with the mass m and damping constant as $\tilde{\lambda}$, respectively. The mass of the NES can move between two springs (with the constant as k_2) in a clearance of 2δ as depicted in Fig. 4.36. To derive governing system equations one should take into account followings [Irschik and Holl, 2004, Pischanskyy and van Horssen, 2012]:

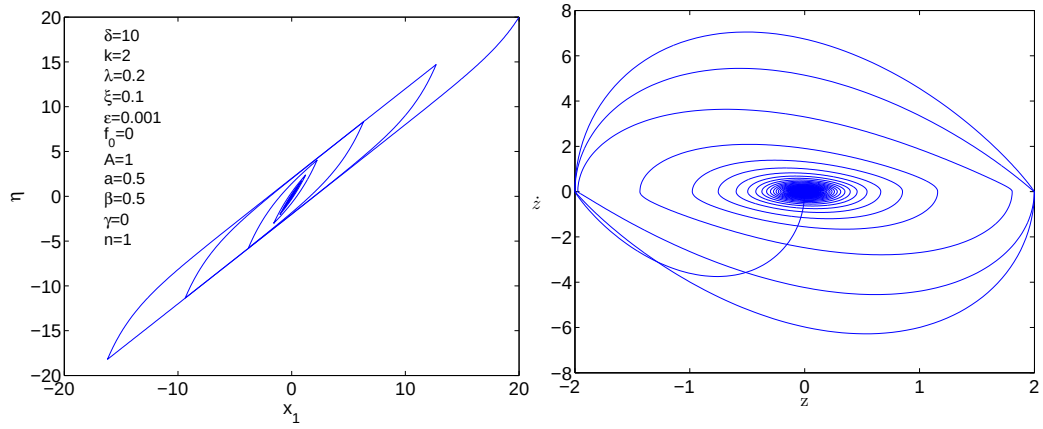

Figure 4.34: a) Displacement of the main system versus representative reaction force of the system, see Eq. 4.195; b) Phase portraits of the internal variable of the Dahl model, z. Results are obtained by direct integration of the system 4.192 with initial condition provided in Eq. 4.194.

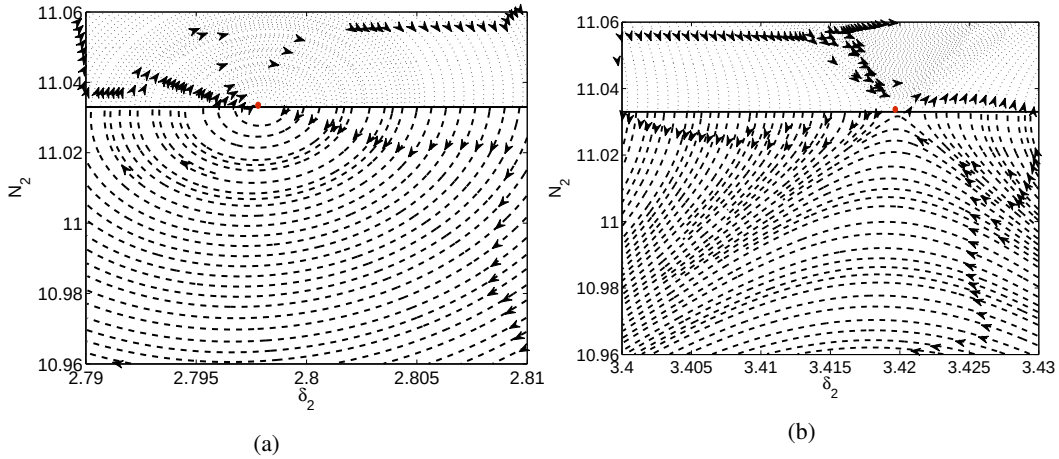

Figure 4.35: Phase portrait of the system under forcing amplitude $f_0 = 50$ on its first fold line. a) The node; b) The saddle point. System parameters read: $\delta = 10$, $k = 2$, $\lambda = 0.2$, $\zeta = 0.1$, $\varepsilon = 10^{-3}$, $A = 1$, $a = 0.99$, $\beta = 0.5$, $\gamma = 0$ and $n = 1$.

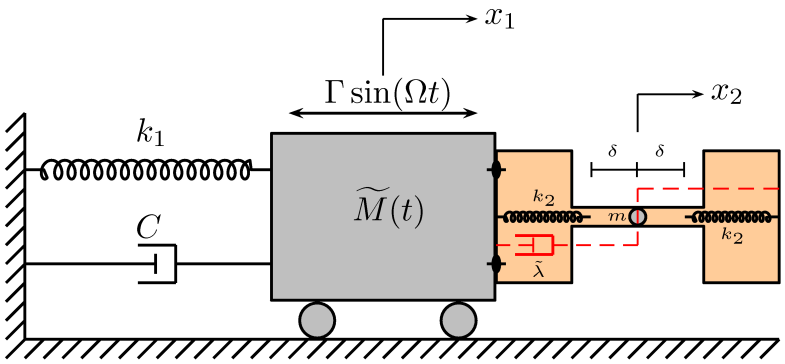

Figure 4.36: A time-dependent main system with the mass $\widetilde{M}(t)$ is coupled to a nonsmooth NES with the mass m.

i) the time derivative of the impulse of the system, i.e. $\dot{\widetilde{M}}(t)\dot{x}_1$; ii) the effects of the velocity at which the mass is "leaving or entering" the heavy mass in x_1-direction. If we represent this velocity by $\mathscr{V}$, then mentioned effect is represented by $\dot{\widetilde{M}}(t)\mathscr{V}$. In this study we assume that $\mathscr{V}$ is negligible and we set $\mathscr{V} = 0$.

$$\begin{cases} \widetilde{M}(t)\ddot{x}_1 + C\dot{x}_1 + k_1 x_1 + \tilde{F}(x_1 - x_2) + \tilde{\lambda}(\dot{x}_1 - \dot{x}_2) + \dot{\widetilde{M}}(t)\dot{x}_1 = \Gamma \sin(\Omega t) \\ m\ddot{x}_2 + \tilde{F}(x_2 - x_1) + \tilde{\lambda}(\dot{x}_2 - \dot{x}_1) = 0 \end{cases} \tag{4.196}$$

Moreover, we assume that the $\widetilde{M}(t)$ obeys following protocol:

$$\widetilde{M}(t) = M_0(1 + \varepsilon M(t)) \tag{4.197}$$

Let us suppose that the ratio of the mass of NES and initial mass of the main system is very small, i.e. $0 < \varepsilon = \dfrac{m}{M_0} << 1$. Moreover, We assume that $(1 + \varepsilon M(t)) \geq 0$ is valid for a time long. We rescale system equations with new time T where $T = t\sqrt{\dfrac{k_1}{M_0}} = t\vartheta$. Equation (4.196) copies $(x_i(t) \to x_i(T))$:

$$\begin{cases} \ddot{x}_1 + (1 + \varepsilon M(T))^{-1}\varepsilon\zeta\dot{x}_1 + (1 + \varepsilon M(T))^{-1}x_1 + (1 + \varepsilon M(T))^{-1}\varepsilon\hat{F}(x_1 - x_2) \\ +(1 + \varepsilon M(T))^{-1}\varepsilon\lambda(\dot{x}_1 - \dot{x}_2) + \varepsilon(1 + \varepsilon M(T))^{-1}\dot{M}(T)\dot{x}_1 = (1 + \varepsilon M(T))^{-1}\varepsilon f_0 \sin(\omega T) \\ \\ \varepsilon\ddot{x}_2 + \varepsilon\lambda(\dot{x}_2 - \dot{x}_1) + \varepsilon\hat{F}(x_2 - x_1) = 0 \end{cases} \tag{4.198}$$

where $\dfrac{C}{\sqrt{M_0 k_1}} = \varepsilon\zeta$, $\dfrac{1}{k_1}\tilde{F} = \varepsilon\hat{F}$, $k = \dfrac{1}{\varepsilon}\dfrac{k_2}{k_1}$, $\dfrac{\tilde{\lambda}}{\sqrt{M_0 k_1}} = \varepsilon\lambda$, $\dfrac{1}{k_1}\Gamma = \varepsilon f_0$ and $\dfrac{\Omega}{\vartheta} = \omega$. We assume that $k = \mathcal{O}(\varepsilon^0)$ and scaled potential of the NES is:

$$\hat{F}(z) = \begin{cases} 0 & \text{if} \quad -\delta \leq z \leq \delta \\ k(z - \delta) & \text{if} \quad z \geq \delta \\ k(z + \delta) & \text{if} \quad z \leq -\delta \end{cases} \tag{4.199}$$

We can present $M(T)$ in the form of Fourier series:

$$M(T) = \sum_{j=-\infty}^{+\infty} m_j e^{i\omega j T} \tag{4.200}$$

so,

$$\dot{M}(T) = \sum_{j=-\infty}^{+\infty} i\omega j m_j e^{i\omega j T} \tag{4.201}$$

We assume that

$$\sum_{j=-\infty}^{+\infty} |m_j| < +\infty \tag{4.202}$$

$$\sum_{j=-\infty}^{+\infty} |\omega j m_j| < +\infty \tag{4.203}$$

We would like to analyse the system around the $1:1$ resonance i.e. $\omega = 1 + \sigma\varepsilon$. The system linearly is transferred to new coordinates as described in Eqs. 4.2 and 4.3 and its first harmonics are kept. Then via the time-multiple scale method the SIM and also all characteristic points are the system are traced [Lamarque et al., 2014], which provide necessary tools for designing appropriate nonsmooth NES for triggering vibratory energy of main system with time-dependent mass. Let us consider a single-dof main system with following governing equation:

$$\begin{aligned}&\ddot{x}_1 + (1+\varepsilon M(T))^{-1}\varepsilon\zeta\dot{x}_1 + (1+\varepsilon M(T))^{-1}x_1 + \varepsilon(1+\varepsilon M(T))^{-1}\dot{M}(T)\dot{x}_1 = \\ &(1+\varepsilon M(T))^{-1}\varepsilon f_0 \sin(\omega T)\end{aligned} \tag{4.204}$$

which is under following initial conditions:

$$(x_1(0), \dot{x}_1(0), x_2(0), \dot{x}_2(0)) = (1.5, 0, 0, 0) \tag{4.205}$$

Let us assume that $M(T) = \gamma\cos(2\omega T)$ which provides a Mathieu-type system of equations [Nayfeh and Mook, 1979]. We set $\gamma = 0.2$ and the detuning parameter $\sigma = 0$ which means that the system faces an exact 1:1 resonance. The system without coupled NES, Eq. 4.204 and with coupled NES, Eq. 4.198 are integrated directly and results are shown in Fig. 4.37. The single-dof system with varying mass and under external excitation at the exact resonance is diverging while the coupled nonsmooth NES controls its diverging behaviour and reduces its displacement in a considerable level.

4.6.3.4 Localization of the energy of main systems with Saint-Venant elements coupled to NES

In this section we treat the passive control of a main system which is nonsmooth containing a set of Saint-Venant elements [Bastien et al., 2013] in parallel. The system is depicted in Fig. 4.38. It is composed of two components: a main oscillator with mass, stiffness and damping as M, k_0 and $\tilde{\lambda}$, which contains a set of parallel Saint-Venant elements with characteristics as $\tilde{k}_j$ (stiffness) and α_j (threshold of the Saint-Venant element) and internal variables u_j, $j = 1, 2, ..., n$. This oscillator is coupled to a NES with the very small mass compared to the mass of the main oscillator, stiffness of the nonlinear restoring forcing function and damping as $m = \varepsilon M$, $\tilde{c}_1$ and $\tilde{\lambda}_1$, respectively. Let us suppose that the restoring forcing function of the NES, F, is general but odd, i.e. $F(-z) = -F(z)$ (e.g. $F(z) = z^3$). The effect of Saint-Venant elements will be in the form of differential inclusions. Governing system equations is summarized as [Lamarque and Ture Savadkoohi, 2015]:

$$\begin{cases} M\dfrac{d^2x}{dt^2} + \tilde{\lambda}\dfrac{dx}{dt} + \tilde{\lambda}_1(\dfrac{dx}{dt} - \dfrac{dy}{dt}) + k_0 x + \displaystyle\sum_{j=1}^{n} \tilde{k}_j u_j + \tilde{c}_1 F(x-y) = f_1(t) \\ m\dfrac{d^2y}{dt^2} + \tilde{\lambda}_1(\dfrac{dy}{dt} - \dfrac{dx}{dt}) + \tilde{c}_1 F(y-x) = 0 \\ \Big(\dfrac{du_j}{dt} + \beta(\dfrac{u_j}{\eta_j})\Big) \ni \dfrac{dx}{dt}, \quad \eta_j = \dfrac{\alpha_j}{\tilde{k}_j}, \quad j = 1, 2, ..., n \end{cases} \tag{4.206}$$

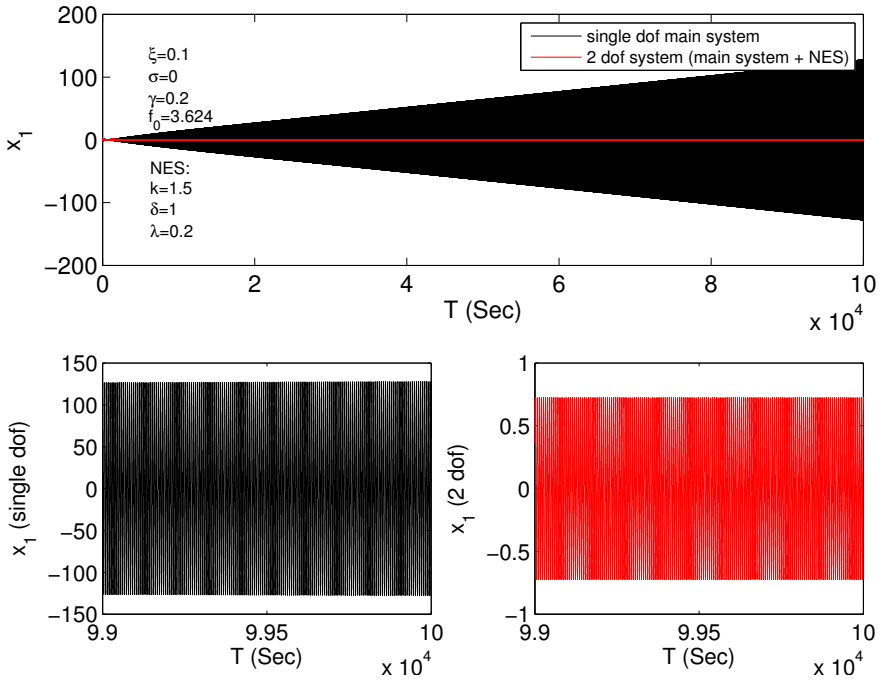

Figure 4.37: Displacement history of the main system with time-dependent mass for two different cases: the main system without and with coupled NES.

The β graph as presented in Fig. 4.39 reads:

$$\beta(x) = \begin{cases} \emptyset & \text{if } x \in \ ]-\infty,-1[\cup]1,+\infty[\\ 0 & \text{if } x \in \ ]-1,1[\\ \mathbb{R}_- & \text{if } x = \ -1 \\ \mathbb{R}_+ & \text{if } x = \ 1 \end{cases} \tag{4.207}$$

We emphasis that differential inclusions of the considered model emerge from basic constitutive equations of the Saint-Venant elements as:

$$k_j u_j \in \alpha_j \mathscr{G}(\frac{dx}{dt} - \frac{du_j}{dt}), \quad j = 1, 2, ..., n \tag{4.208}$$

where $\mathscr{G}$ is the graph of the sign:

$$\mathscr{G}(z) = \begin{cases} -1 & \text{if} \quad z < 0 \\ [-1, 1] & \text{if} \quad z = 0 \\ 1 & \text{if} \quad z > 0 \end{cases} \tag{4.209}$$

Let us introduce new time domain $t^* = t\sqrt{\dfrac{k_0}{M}} = \vartheta t$. So,

$$\tilde{k}_j u_j \in \alpha_j \mathscr{G}\big(\vartheta(\frac{dx}{dt^*} - \frac{du_j}{dt^*})\big) \iff \tilde{k}_j u_j \in \alpha_j \mathscr{G}\big((\frac{dx}{dt^*} - \frac{du_j}{dt^*})\big) \quad , \quad j = 1, 2, ..., n \tag{4.210}$$

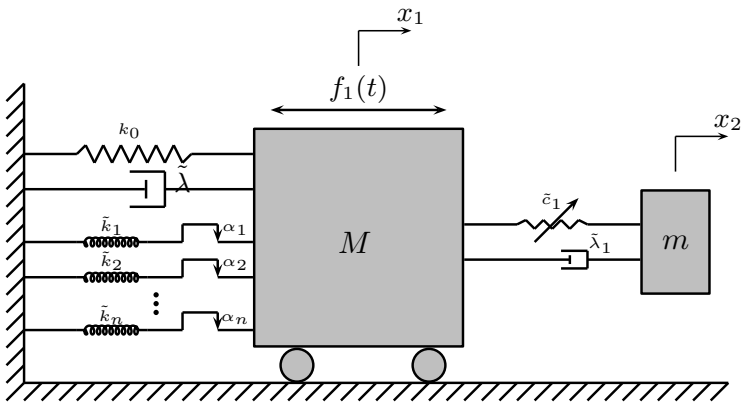

Figure 4.38: A main system with a set of parallel Saint-Venant elements and under external force $f_1(t)$ is coupled to a secondary system with general and odd nonlinear potential function ($m = \varepsilon M$, $0 < \varepsilon \ll 1$).

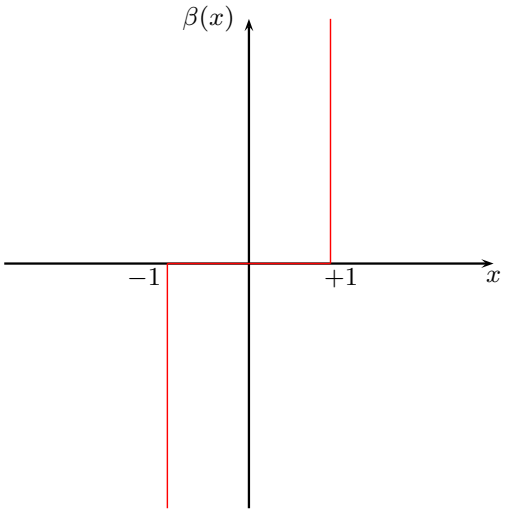

Figure 4.39: The β graph in Saint-Venant element.

Equation 4.206 reads:

$$\begin{cases} \frac{d^2x}{dt^{*2}} + \varepsilon\lambda_0\frac{dx}{dt^*} + \varepsilon\lambda_{10}(\frac{dx}{dt^*} - \frac{dy}{dt^*}) + x + \varepsilon\sum_{j=1}^{n} k_j u_j + \varepsilon c_{10}F(x-y) = \varepsilon f_{10}\sin(\omega t^*) \\ \varepsilon\frac{d^2y}{dt^{*2}} + \varepsilon\lambda_{10}(\frac{dy}{dt^*} - \frac{dx}{dt^*}) + \varepsilon c_{10}F(y-x) = 0 \\ \Big(\frac{du_j}{dt^*} + \beta(\frac{u_j}{\eta_j})\Big) \ni \frac{dx}{dt^*}, \quad \eta_j = \frac{\alpha_j}{\tilde{k}_j}, \quad j = 1,2,...,n \end{cases} \tag{4.211}$$

where $\frac{\tilde{\lambda}\vartheta}{M\vartheta^2} = \varepsilon\lambda_0$, $\frac{\tilde{k}_j}{M\vartheta^2} = \varepsilon k_j$, $\frac{\tilde{c}_1}{M\vartheta^2} = \varepsilon c_{10}$, $\frac{\tilde{\lambda}_1\vartheta}{M\vartheta^2} = \varepsilon\lambda_{10}$, $\frac{f_1(\frac{\tau}{\vartheta})}{M\vartheta^2} = \varepsilon f_{10}\sin(\omega t^*)$. A linear transformation which is explained in Eqs. 4.2 and 4.3 are carried out. The complex variables of Manevitch with considering only the first harmonics is taken, i.e. $b_1 = b_2 = 0$ in Eq. 4.4. A Galerkin technique is endowed via keeping only the first harmonics of the system and truncating higher one, i.e. setting $l = 1$ in Eq. 4.6. System equations read:

$$\omega\dot{\varphi_1} - \frac{\omega}{2i}\varphi_1 + \frac{\varepsilon\lambda_0(\varphi_1+\varepsilon\varphi_2)}{2(1+\varepsilon)} + \frac{\varphi_1+\varepsilon\varphi_2}{2i\omega(1+\varepsilon)} + \varepsilon\frac{\sum_{j=1}^{n} k_j\varphi_{j+2}}{2i\omega} = \varepsilon\frac{f_{10}}{2i}$$

$$\omega\dot{\varphi_2} - \frac{\omega}{2i}\varphi_2 + \frac{\varepsilon\lambda_0(\varphi_1+\varepsilon\varphi_2)}{2(1+\varepsilon)} + \frac{\varphi_1+\varepsilon\varphi_2}{2i\omega(1+\varepsilon)} + \frac{\sum_{j=1}^{n} k_j\varphi_{j+2}}{2\omega i} + (1+\varepsilon)(c_{10}\mathcal{F} + \frac{\lambda_{10}}{2}\varphi_2) = \varepsilon\frac{f_{10}}{2i}$$

$$\varphi_{j+2} = \frac{\varphi_1+\varepsilon\varphi_2}{(1+\varepsilon)\pi}\xi_j\big(\frac{|\varphi_1+\varepsilon\varphi_2|}{(1+\varepsilon)\omega}\big), \quad j = 1,2,...,n \tag{4.212}$$

where

$$\mathcal{F} = \frac{1}{2\pi}\int_0^{2\pi} e^{-iT}F\big(\frac{\varphi_1 e^{iT} - \varphi_2^* e^{-iT}}{2i\omega}\big)\,\mathrm{d}T \tag{4.213}$$

and $\xi_j(z)(\forall z \in \mathbb{R}_+, j = 1,2,...,n)$ reads:

$$\xi_j(z) = \begin{cases} \pi & \text{if } z \leqslant \eta_j \\ \theta + e^{-i\theta}\sin(\theta) - 4e^{-i\frac{\theta}{2}}\sin(\frac{\theta}{2}) - \frac{4\eta_j}{z}e^{-i(\theta+\frac{\pi}{2})} & \text{if } z > \eta_j \end{cases} \tag{4.214}$$

with

$$\theta = \arccos(1 - \frac{2\eta_j}{z}) \tag{4.215}$$

If we set $\omega t^* = T$, then a time multiple scale method is used via considering different scales of T and studying the system at each time scale. The system is studied around a 1:1 resonance via setting $\Omega = 1 + \sigma\varepsilon$. The SIM of the system and all characteristic points is traced [Lamarque and Ture Savadkoohi, 2015]. The system behaviour at slow time scale and invertibility (or not) of the $\nabla_{(\delta_2,N_2)}$ in Eqs. 4.27 and 4.28 imposes that in:

$$\begin{cases} \frac{\partial N_2}{\partial T_1} = \frac{\tilde{f}_1(N_2,\delta_2)}{\tilde{g}(N_2,\delta_2)} \\ N_2\frac{\partial\delta_2}{\partial T_1} = \frac{\tilde{f}_2(N_2,\delta_2)}{\tilde{g}(N_2,\delta_2)} \end{cases} \tag{4.216}$$

equilibrium points are those which provide:

$$\begin{cases} \tilde{f}_1(N_2,\delta_2)=0, \quad \tilde{f}_2(N_2,\delta_2)=0 \\ \\ \tilde{g}(N_2,\delta_2)\neq 0 \end{cases} \tag{4.217}$$

and fold singularities are those which verifies

$$\begin{cases} \tilde{f}_1(N_2,\delta_2)=0, \quad \tilde{f}_2(N_2,\delta_2)=0 \\ \\ \tilde{g}(N_2,\delta_2)=0 \end{cases} \tag{4.218}$$

4.7 Targeted energy transfer from a main linear system to a chain of nonlinear oscillators: continuous approach

The idea is to localize induced energy to a principal system into a chain of nonlinear oscillators with local and global potentials. The section treats the modal behaviours of the overall system via continuous approximation. The passive control process of a principal system coupled to a chain of nonlinear oscillators via discrete approach has been studied by Charlemagne et al. [Charlemagne et al., 2017, Charlemagne, 2018]. They traced periodic and modulated regimes of the system as function of characteristics of the external excitations. In their work, they proved that the response of the chain can be interpreted by the the nonlinear normal mode approach: during the periodic regime, one mode is excited while during modulated responses, the response of the system is dominated by repeated bifurcations between several nonlinear normal modes. A general methodology for continuous approximations and treatment of such systems is introduced which is followed by a given example [Charlemagne, 2018].

4.7.1 Treatments of a general system via continuous approximation: the methodology

Let us consider a linear main system (LMS), with the rescaled mass as 1 and the generalized displacement as v. A nonlinear discrete chain with $L+1$ particles of the mass ε for each $(0<\varepsilon\ll 1)$ with the generalized displacement as u_j, $j=1,\ldots,L+1$ is linearly attached to the LMS. The system equations read [Charlemagne, 2018, Charlemagne et al., 2018]:

$$\begin{cases} \ddot{v}+\underbrace{\omega_0^2 v+\varepsilon\mathscr{G}_1(v,\dot{v})}_{\text{LMS}}+\underbrace{\varepsilon\mathscr{H}_1(v,u_1,\dot{v},\dot{u}_1)}_{\text{LMS-chain coupling}}=\underbrace{\varepsilon f\sin(\omega t)}_{\text{Forcing term}}+\mathcal{O}(\varepsilon^2) \\ \\ \ddot{u}_1-\underbrace{\mathscr{H}_1(v,u_1,\dot{v},\dot{u}_1)}_{\text{LMS-chain coupling}}+\mathscr{H}_2(u_1,u_2,\dot{u}_1,\dot{u}_2)=\mathcal{O}(\varepsilon) \\ \\ \ddot{u}_j+\underbrace{\mathscr{H}_c(u_{j-1},u_j,u_{j+1},\dot{u}_{j-1},\dot{u}_j,\dot{u}_{j+1})}_{\text{Chain}}=\mathcal{O}(\varepsilon) \qquad j=2,\ldots,L \\ \\ \ddot{u}_{L+1}+\mathscr{H}_L(u_L,u_{L+1},\dot{u}_L,\dot{u}_{L+1})=\mathcal{O}(\varepsilon) \end{cases} \tag{4.219}$$

The $\mathscr{G}_1$ stands for a linear operator while $\mathscr{H}_2$, $\mathscr{H}_c$ and $\mathscr{H}_L$ are nonlinear ones. The operator $\mathscr{H}_1$ can be linear or nonlinear. We assume that the frequency of the external excitation is around the frequency of the LMS, i.e. ω_0. To this end, we set $\omega^2=\omega_0^2(1+\sigma\varepsilon)$ with σ being the detuning parameter. For applying the continuous limit to the chain, we consider that number of particles, L,

is very high, i.e. $L \gg 1$. The generalized displacement $u_j(t)$ of the chain can be approximated by the continuous function $u(x,t)$ as:

$$\begin{array}{l} u_j(t) = u(x = j-1, t) \\ x \in [0, L] \end{array} \tag{4.220}$$

with L being the length of the chain. We can perform Taylor expansion as:

$$u_{j\pm1} \approx u(j-1,t) \pm \frac{\partial u}{\partial x}(j-1,t) + \frac{1}{2!}\frac{\partial^2 u}{\partial x^2}(j-1,t) \pm \ldots \pm \frac{1}{n!}\frac{\partial^n u}{\partial x^n}(j-1,t)\ldots \tag{4.221}$$

With above mentioned continuous approximation, Eq. 4.219 is converted to fours systems as it follows: The first equation is relevant to the LMS and the rest constitute a boundary value problem of system of equations. The second and the last equations form the boundary conditions at two extremities of the chain, i.e. the left and the right or at $x = 0$ and $x = L$, while the third equations is a system of partial differential equation which represent the behaviour of the nonlinear chain.
Let us introduce following complex variables of Manevitch [Manevitch, 2001]:

$$\begin{cases} \psi(t)e^{i\omega t} = \dfrac{\partial v(t)}{\partial t} + i\omega v(t) \\ \\ \varphi(x,t)e^{i\omega t} = \dfrac{\partial u(x,t)}{\partial t} + i\omega u(x,t) \end{cases} \tag{4.222}$$

Fast and slow time scales are introduced to the time domain t (see Eq. 4.5) and then a Galerkin's technique is applied as described in Eq. 4.6 via taking into account the same assumptions which are discussed in Sects. 4.2 and 4.3. The system 4.219 reads:

$$\begin{cases} \dfrac{d\psi}{dt} + \dfrac{i}{2}\left(\omega - \dfrac{\omega_0^2}{\omega}\right)\psi + \varepsilon G_1(\psi) + \varepsilon H_1(\psi, \varphi(0)) = \dfrac{\varepsilon f}{2i} + \mathcal{O}(\varepsilon^2) \\ \\ \dfrac{\partial \varphi}{\partial t}(0) + \dfrac{i\omega}{2}\varphi(0) - H_1(\psi, \varphi(0)) + H_2(\varphi(0), \varphi_x(0)) = \mathcal{O}(\varepsilon) \\ \\ \dfrac{\partial \varphi}{\partial t}(x) + \dfrac{i\omega}{2}\varphi(x) + H_c(\varphi(x), \varphi_x(x), \varphi_{xx}(x)) = \mathcal{O}(\varepsilon) \qquad x \in]0, L[\\ \\ \dfrac{\partial \varphi}{\partial t}(L) + \dfrac{i\omega}{2}\varphi(L) + H_L(\varphi(L), \varphi_x(L)) = \mathcal{O}(\varepsilon) \end{cases} \tag{4.223}$$

where the subscript x represents the derivation with respect to the space variable. Then, the fast and slow dynamics should be traced.

The system behaviour at fast time scale We study Eq. 4.223 at ε^0 order: The first equation presents $\dfrac{\partial \psi}{\partial \tau_0} = 0$, which indicates that the amplitudes of oscillations of the LMS will vary slowly as a function of the fast time scale τ_0. The fixed points of the system, $\phi(x)$, are obtained via $\lim\limits_{\tau_0 \to +\infty} \dfrac{\partial \varphi(x)}{\partial \tau_0} = 0$, which lead to tracing the SIM of the system as:

$$\begin{cases} \omega_0\phi(0) + 2i\left[H_1(\psi, \phi(0)) - H_2(\phi(0), \phi_x(0))\right] = 0 \\ \\ \omega_0\phi(x) - 2iH_c(\phi(x), \phi_x(x), \phi_{xx}(x)) = 0 \qquad x \in]0, L[\\ \\ \omega_0\phi(L) - 2iH_L(\phi(L), \phi_x(L)) = 0 \end{cases} \tag{4.224}$$

In the continuous approximation, the described SIM in Eq. 4.224 is an ordinary differential equation with two boundary conditions in $x = 0$ and $x = L$. While the emerged SIM via treatments of the system equations with discrete approaches [Charlemagne et al., 2017, Charlemagne, 2018] forms P complex equations (P stands for the number of nonlinear particles of the chain). The Eq. 4.224 houses all possible monochromatic asymptotic responses. Solving the system 4.224 leads to obtaining the $\phi(x)$ as function of ψ. Variation of the ψ permits to characterize different behaviours of the nonlinear chain. However, for having precise idea about detailed possible destinations of the system under a given excitation, we need to trace system responses at slow time scale.

The system behaviour at slow time scale We would like to see the evolution of the system at slow time scale around the SIM. The first equations of the system 4.223 at ε^1 order reads:

$$\frac{\partial \psi}{\partial \tau_1} + \frac{i\sigma\omega_0}{2}\psi + G_1(\psi) + H_1(\psi, \phi(0)) = \frac{f}{2i} \tag{4.225}$$

Injecting the SIM (see Eq. 4.224) in Eq. 4.225 describes the variation of the envelop of the LMS at slow time scale. Let us suppose that the left boundary condition of the SIM can be summarized as:

$$\psi = F_l(N(0))e^{i\delta(0)} \tag{4.226}$$

where $N(x)$ and $\delta(x)$ are polar variables of $\phi(x)$, i.e. $\phi(x) = N(x)e^{i\delta(x)}$. Combinations of Eqs. 4.225 and 4.226 provides following compact form of system of equations ($N_0 = N(0)$ and $\delta_0 = \delta(0)$):

$$\begin{cases} \dfrac{\partial N_0}{\partial \tau_1} = \dfrac{f_1(N_0, \delta_0)}{g(N_0, \delta_0)} \\ \\ \dfrac{\partial \delta_0}{\partial \tau_1} = \dfrac{f_2(N_0, \delta_0)}{g(N_0, \delta_0)} \end{cases} \tag{4.227}$$

which is in fact a spacial case of the general formulation for a class of coupled nonlinear oscillators which is described in Eq. 4.34. The system 4.227 provides necessary information for tracing equilibrium ($f_1 = f_2 = 0$ & $g \neq 0$) and singular ($f_1 = f_2 = 0$ & $g = 0$) points of the system and so necessary design tools for tuning parameters of the nonlinear chain in order to present the intended responses for a provided external excitation characteristics.

4.7.2 An application: a nonlinear chain with local potentials

As an application of developed methodology which is explained in Sect. 4.7.1, following system is considered: A LMS with the mass, stiffness and damping as M, K and C, respectively, is subjected to an external excitation $F(t)$. The LMS is coupled to a chain of nonlinear oscillators with the mass of $m = \varepsilon M$ for each particle. The interaction between two particles is supposed to be linear representing by a rigidity and damping coefficient as $\tilde{B}$ and Γ, respectively. Each particle interacts locally (with other systems or with the environment) represented by a nonlinear function $\tilde{V}$, see Fig. 4.40. System equations are summarized as:

$$\begin{cases} \ddot{v} + \varepsilon c\dot{v} + \omega_0^2 v + \varepsilon\gamma(\dot{v} - \dot{u}_1) + \varepsilon B(v - u_1) = \varepsilon f \sin(\omega t) \\ \ddot{u}_1 + \gamma(-\dot{v} + 2\dot{u}_1 - \dot{u}_2) + B(-v + 2u_1 - u_2) + Du_1^3 = 0 \\ \qquad\qquad \vdots \\ \ddot{u}_j + \gamma(-\dot{u}_{j-1} + 2\dot{u}_j - \dot{u}_{j+1}) + B(-u_{j-1} + 2u_j - u_{j+1}) + Du_j^3 = 0 \\ j = 2, \ldots, L \\ \qquad\qquad \vdots \\ \ddot{u}_{L+1} + \gamma(\dot{u}_{L+1} - \dot{u}_L) + B(u_{L+1} - u_L) + Du_{L+1}^3 = 0 \end{cases} \tag{4.228}$$

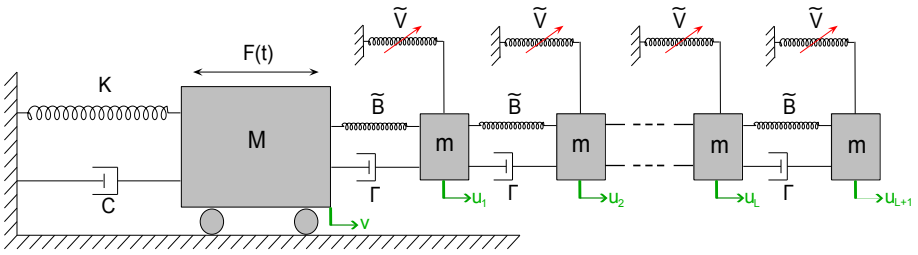

Figure 4.40: The forced LMS coupled to $(L+1)$ nonlinear oscillators with the mass of $m = \varepsilon M$, $0 < \varepsilon \ll 1$ for each particle.

with $\frac{K}{M} = \omega_0^2$, $\frac{\tilde{B}}{M} = \varepsilon B$, $\frac{\tilde{V}(z)}{M} = \varepsilon D z^3$, $\frac{C}{M} = \varepsilon c$, $\frac{\Gamma}{M} = \varepsilon\gamma$, $\frac{F(t)}{M} = \varepsilon f \sin(\omega t)$ and $\omega^2 = \omega_0^2(1+\sigma\varepsilon)$. The described system in Eq. 4.228 is a spacial form of the system which is described in Eq. (4.219). The described methodology is Sect. 4.7.1 is used for treatment of the mentioned system and detection of its dynamical characteristic points.

4.7.2.1 The SIM of the system

Tracing the system equations at ε^0 order leads to detection of the SIM which is provided in general manner in Eq. 4.224. It reads:

$$\begin{cases} \omega_0\phi(0) - \left(i\gamma + \dfrac{B}{\omega_0}\right)\left(-\psi + \phi(0) - \dfrac{\partial\phi}{\partial x}(0)\right) - 2\mathcal{D}|\phi(0)|^2\phi(0) = 0 \\ \omega_0\phi(x) + \left(i\gamma + \dfrac{B}{\omega_0}\right)\dfrac{\partial^2\phi}{\partial x^2}(x) - 2\mathcal{D}|\phi(x)|^2\phi(x) = 0 \qquad x \in]0, L[\\ \omega_0\phi(L) - \left(i\gamma + \dfrac{B}{\omega_0}\right)\dfrac{\partial\phi}{\partial x}(L) - 2\mathcal{D}|\phi(L)|^2\phi(L) = 0 \end{cases} \tag{4.229}$$

with $\mathcal{D} = \frac{3D}{8\omega_0^3}$. Going to the polar domain and separation of real and imaginary parts of second equation of the system 4.229 provides:

$$\omega_0 N + \frac{B}{\omega_0}\left(N_{xx} - N\theta^2\right) - \gamma\left(2N_x\theta + N\theta_x\right) - 2\mathcal{D}N^3 = 0 \tag{4.230}$$

$$\frac{B}{\omega_0}\left(2N_x\theta + N\theta_x\right) + \gamma\left(N_{xx} - N\theta^2\right) = 0 \tag{4.231}$$

with $\theta(x) = \delta_x(x)$. Let us consider that $\gamma = 0$ or we set that rescaled damping of the chain to at the order of ε^2, i.e. $\gamma = \mathcal{O}(\varepsilon^2)$. The integration of Eq. 4.231 leads to:

$$\theta(x) = \frac{\Theta}{N(x)^2} \tag{4.232}$$

where Θ stands for the constant of integration. Concerning Eq. 4.232 we claim that:

- if $\exists x_0, N(x_0) = 0$, then $\theta = \delta_x$ faces a singularity in x_0. This means that independently of Θ, a jump of phase of the chain is expected whenever the amplitude of the chain arrives to zero.

- as $N(x)$ stands for the amplitude of $\phi(x)$, so $N \geq 0$. The solution of equations can lead to negative values for N. In this case, absolute value of the N should be retained and the phase $\delta(x)$ should be supplemented by π at the point where $N(x)$ becomes negative. This adjustment grantees the previous remark as well.

Multiplying Eq. 4.230 by N_x and integrating it, following system is obtained:

$$N_x^2 = -\frac{\Theta^2}{N^2} - \frac{\omega_0^2}{B}N^2 + \frac{\mathcal{D}\omega_0}{B}N^4 + C_1 \tag{4.233}$$

with C_1 is the constant of integration. Constants Θ and C_1 are revealed by endowing the boundary conditions. The last equation of the system 4.229 via consideration of Eqs. 4.232 and 4.233 yields to:

$$\begin{cases} -\omega_0 N(L) + \dfrac{B}{\omega_0}N_x(L) + 2\mathcal{D}N(L)^3 = 0 \\ N(L)\theta(L) = \dfrac{\Theta}{N(L)} = 0 \end{cases} \tag{4.234}$$

From the system 4.234 we conclude that:

- $\Theta = 0$ (check the second equation). This means that the phase $\theta(x)$ is constant through the chain, unless one or several singular points exist in the system when $N(x) = 0$. These points correspond to (artificial) change of the sign of the $N(x)$ and the phase presents a jump of π. This fact clarifies that the admissible behaviours of the nonlinear chain are synchronous periodic oscillations, which are in fact definition of nonlinear normal modes according to Rosenberg [Rosenberg, 1960, Rosenberg, 1962, Rosenberg, 1966].

- The slow evolutions of the last mass of the chain is expressed by the first equations: it is in fact the right boundary condition.

- If $N(L) = 0$, then the first equation implies that $N_x(L) = 0$. In this case Eq. 4.233 demands that $C_1 = 0$.

- If $C_1 = 0$ then from Eq. 4.233 we can conclude that N_x^2 is strictly positive if $N(x) > \sqrt{\dfrac{\omega_0}{\mathcal{D}}}$, which does not lead to $N(L) = 0$. As a result, if $N(L) = 0$, then $\forall x, N(x) = 0$. In this work we focus of the case when $C_1 \neq 0$ which leads to non trivial responses.

Let us consider first equation of Eq. 4.229 via taking into account Eq. 4.232. We obtain ($\psi = N_1 e^{i\delta_1}$):

$$\begin{cases} \left(\dfrac{B}{\omega_0} - \omega_0 + 2\mathcal{D}N(0)^2\right)N(0) - \dfrac{B}{\omega_0}N_x(0) = \dfrac{B}{\omega_0}N_1\cos(\delta_1 - \delta(0)) \\ N_1\sin(\delta_1 - \delta(0)) = 0 \end{cases} \tag{4.235}$$

The second equation of the system 4.235 indicates that the LMS is oscillating in-(or opposite) phase with the first particle of the chain, i.e. $\delta_1 = \delta_0 + k\pi, k = 0, 1, \ldots$. Equation 4.235 leads to:

$$N_1 = \pm\left[\left(1 - \frac{\omega_0^2}{B} + 2\frac{\omega_0\mathcal{D}}{B}N(0)^2\right)N(0) - N_x(0)\right] \tag{4.236}$$

Finally, considering all of above mentioned developments, following equations for the SIM are obtained which should be treated in order to reveal the geometry of the SIM:

$$\begin{cases} N_x^2 = -\dfrac{\omega_0^2}{B}N^2 + \dfrac{\mathcal{D}\omega_0}{B}N^4 + C_1 \\ N_1 = \pm\left[\left(1 - \dfrac{\omega_0^2}{B} + 2\dfrac{\omega_0\mathcal{D}}{B}N(0)^2\right)N(0) - N_x(0)\right] \\ -\omega_0 N(L) + \dfrac{B}{\omega_0}N_x(L) + 2\mathcal{D}N(L)^3 = 0 \end{cases} \tag{4.237}$$

Treatment of the equations of SIM Looking at the first equation of the system 4.237, it is seen that the constant C_1 can change the asymptotic dynamics of the system: if $C_1 > C_{1crit} = \dfrac{\omega_0^3}{4B\mathcal{D}}$, then the polynomial emerging from the ordinary differential equation which expresses N_x^2 does not have any real solutions. Otherwise, the system possesses two real roots X_1 and X_2 which are expressed as ($N_x = 0 \Leftrightarrow N = \sqrt{X_{1,2}}$):

$$X_{1,2} = \frac{\omega_0^2 \pm \sqrt{\omega_0^4 - 4BC_1\mathcal{D}\omega_0}}{2\mathcal{D}\omega_0}, \qquad X_1 < X_2 \tag{4.238}$$

This means that depending on the value of C_1, the asymptotic dynamics of the system can follow three branches. These branches are presented in Fig. 4.41 for some numerical values of system parameters. Let us now consider expression of $N_x(L)$ traced from the ordinary differential equation in the last equation of system 4.237, i.e. the right boundary condition:

$$\frac{B^2}{\omega_0^2}\left(-\frac{\omega_0^2}{B}N(L)^2 + \tilde{\mathcal{D}}N(L)^4 + C_1\right) - (\omega_0 N(L) - 2\mathcal{D}N(L)^3)^2 = 0 \tag{4.239}$$

Due to the symmetry of the phase portraits, see Fig. 4.41, we can concentrate on positive solutions of $N(L)$. This relation has one, two or three real solutions. It has three solutions when:

$$\begin{array}{lll} C_{1crit} < C_1 < C_{1m} & \text{if} & B < 2\omega_0^2 \\ C_{1m} < C_1 < C_{1crit} & \text{if} & B > 2\omega_0^2 \end{array} \tag{4.240}$$

with $C_{1m} = \dfrac{(8\omega_0^2 - B)(B + \omega_0^2)^2}{108B^2\mathcal{D}\omega_0}$. If $B = 2\omega_0^2$, then $C_{1m} = C_{1crit}$ and Eq. (4.239) has one real solution. Numerical solutions of Eq. 4.239 are presented in Fig. 4.42; different line style and colors correspond to the ones illustrated in Fig. 4.41, so one can relate different values of $N(L)$ to the branches 1, 2 or 3. Value of the parameter B is chosen different from Fig. 4.41 for the sake of clarity of Fig. 4.42. For each value of $N(L)$ in Fig. 4.42 , starting from 0 and progressing along the curve, we would like to integrate the first equation of system 4.237, leading to tracing $N(0)$, $N_x(0)$ and also N_1 via the left boundary condition, i.e. the second equation of the system 4.237. This procedure will permit to trace the projection of the SIM in the $(N(L), N_1)$ plane.
Let us concentrate on the branch 1, i.e. the case where $C_1 < C_{1crit}$ and $N(x) < \sqrt{X_1}$. The expression of N_x^2 reads:

$$N_x = \pm\sqrt{\tilde{\mathcal{D}}(X_1 - N^2)(X_2 - N^2)} \tag{4.241}$$

with $\tilde{\mathcal{D}} = \dfrac{\mathcal{D}\omega_0}{B}$. Integrating Eq. (4.241) yields to:

$$N(x) = \sqrt{X_1}\,\mathrm{sn}\left(\sqrt{\frac{C_1}{X_1}}(x - C_2), \frac{X_1}{X_2}\right) \tag{4.242}$$

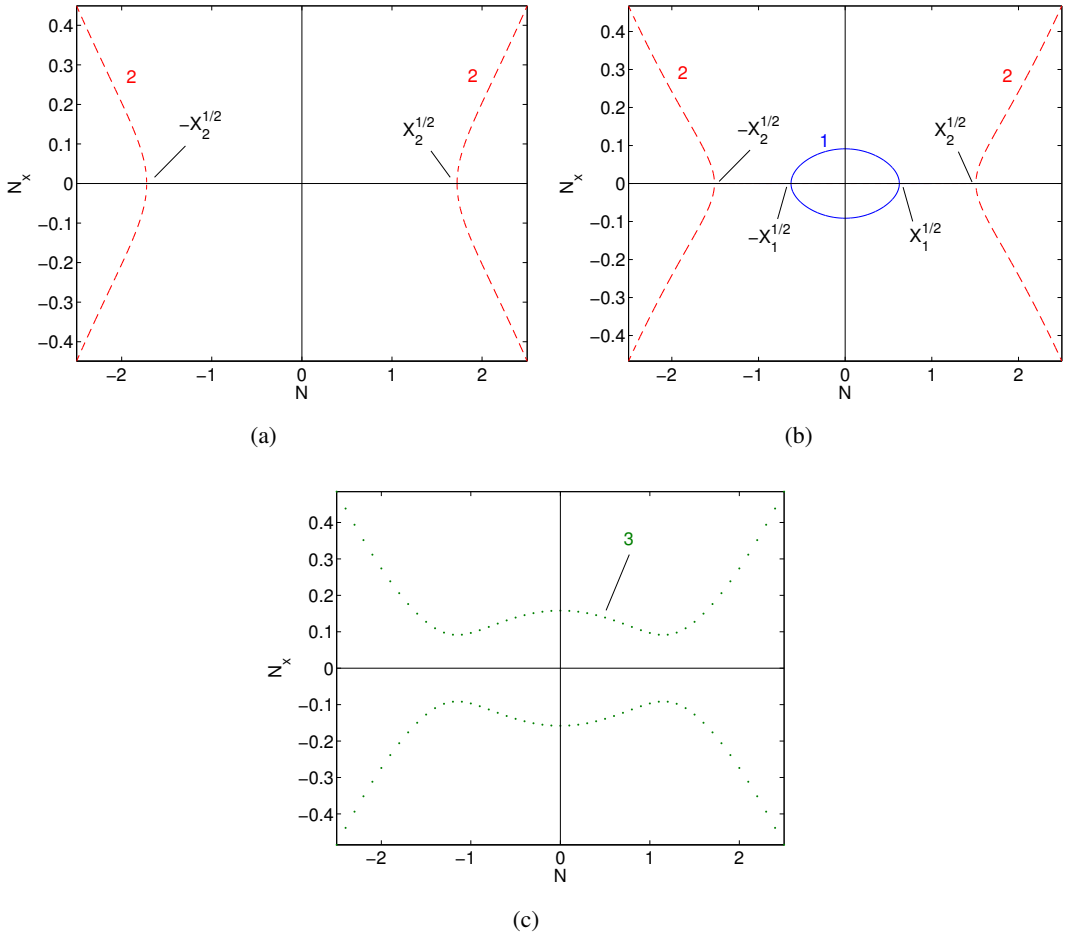

Figure 4.41: Phase portraits obtained from the first equation of system 4.237 for the system parameters as parameters: $\omega_0 = 1$, $B = 40$, $D = 1$ and a) $C_1 = -\frac{1}{2}C_{1crit}$; b) $C_1 = \frac{1}{2}C_{1crit}$; c) $C_1 = \frac{3}{2}C_{1crit}$. Three possible branches are marked as 1, 2 and 3

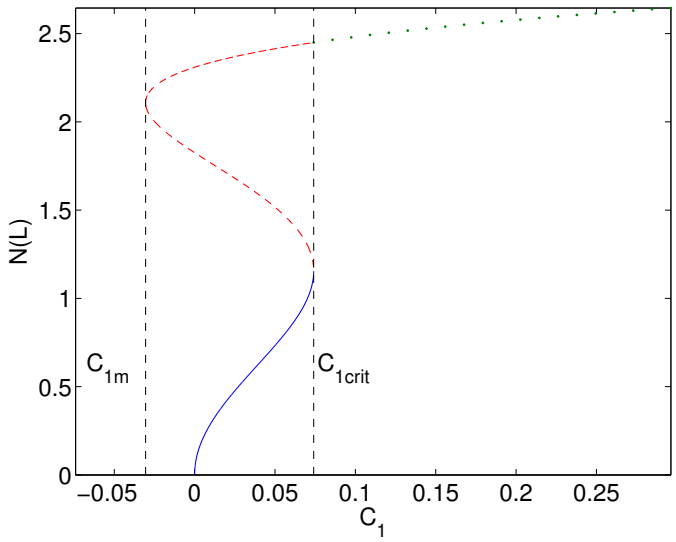

Figure 4.42: Solutions of Eq. 4.239 for system parameters as $\omega_0 = 1$, $B = 9$ and $D = 1$. Line styles correspond to ones illustrated in Fig. 4.41.

where $\mathrm{sn}(X, k^2)$ stands for a Jacobian elliptic function and C_2 is the constant of integration which can be evaluated by the following system:

$$C_2 = L - \sqrt{\frac{X_1}{C_1}} F\left(\arcsin\left(\frac{N(L)}{\sqrt{X_1}}\right), \frac{X_1}{X_2}\right) \tag{4.243}$$

$F(X, k^2)$ is the incomplete elliptic integral of the first kind. Equation (4.242) provides an explicit expression of the modal shapes of the nonlinear normal modes of the nonlinear chain which are able to enter in resonance with the LMS. The part of the SIM resulting from branch 1 is presented in Fig. 4.43 in solid blue line. In order to continue this figure, we should integrate the ordinary differential equation for higher values of $N(L)$ which correspond to branches 2 and 3. However, there is not a closed-form expression of $N(x)$ on those branches. As a result, one needs to numerically integrate the following expression:

$$dx = \pm \frac{dN}{\sqrt{-\frac{\omega_0^2}{B} N^2 + \frac{\mathcal{D}\omega_0}{B} N^4 + C_1}} \tag{4.244}$$

It can be illustrated that this integration yields to detection of a monotonic increasing branch of the SIM shown in Fig. 4.43 (red dotted line).

Equilibrium and singular points The relevant equation describing the LSM at ε^1 order around the SIM reads:

$$\frac{\partial \psi}{\partial \tau_1} + \frac{1}{2}\left(c\psi + i\sigma\omega_0 - \frac{iB}{\omega_0}\right)\psi + \frac{iB}{\omega_0}\phi(0) = \frac{f}{2i} \tag{4.245}$$

Setting $\psi = F_l(N_0)e^{i\delta_0}$, then the left boundary condition of the SIM provides:

$$F_l(N_0) = -N_x(0) + \left(1 - \frac{\omega_0^2}{B} + 2\tilde{\mathcal{D}} N_0^2\right) N_0 \tag{4.246}$$

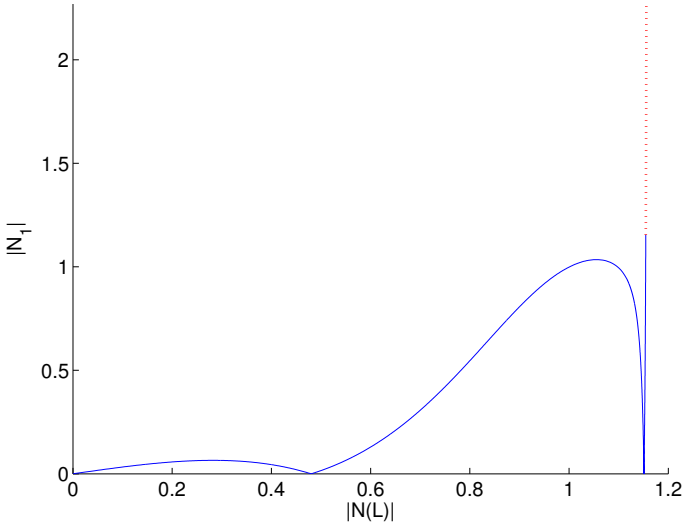

Figure 4.43: An example of SIM for the system with $L = 30$, $\omega_0 = 1$, $B = 40$ and $D = 1$. Types of the lines correspond to ones illustrated in Fig. 4.41.

Considering Eq. (4.246) in Eq. (4.245), following system is obtained:

$$\begin{cases} \dfrac{\partial N_0}{\partial \tau_1} = \dfrac{f_1(N_0, \delta_0)}{g(N_0)} \\ \dfrac{\partial \delta_0}{\partial \tau_1} = \dfrac{f_2(N_0, \delta_0)}{g(N_0)} \end{cases} \tag{4.247}$$

with

$$\begin{aligned} f_1(N_0, \delta_0) &= -\frac{F_l(N_0)}{2}\left[cF_l(N_0) + f\sin(\delta_0)\right] \\ f_2(N_0, \delta_0) &= \frac{1}{2}\frac{\partial F_l(N_0)}{\partial N_0}\left[\left(\frac{B}{\omega_0} - \sigma\omega_0\right)F_l(N_0) - \frac{B}{\omega_0}N_0 - f\cos(\delta_0)\right] \\ g(N_0) &= F_l(N_0)\frac{\partial F_l(N_0)}{\partial N_0} \end{aligned} \tag{4.248}$$

The singular points are revealed via setting $g(N_0) = 0$. These points are located on local extrema of Fig. 4.43. In detail: $F_l(N_0) = 0$ corresponds to minima ($N_1 = 0$) and $\dfrac{\partial F_l(N_0)}{\partial N_0}$ are located on local maxima. Let us set $N_{0,min}^{(k)}$ and $N_{0,max}^{(k)}$, where k stands for the number of local maxima or minima, traced by $F_l(N_{0,min}^{(k)}) = 0$ and $\dfrac{\partial F_l(N_{0,max}^{(k)})}{\partial N_0} = 0$. To obtain fold singularities, the conditions $f_1(N_0, \delta_0) = f_2(N_0, \delta_0) = 0$, should be verified as well, yielding to:

$$\begin{aligned} &\cos(\delta_0) = -\frac{BN_{0,min}^{(k)}}{f\omega_0} \\ &\text{or} \\ &\sin(\delta_0) = -\frac{cF_l(N_{0,max}^{(k)})}{f} \end{aligned} \tag{4.249}$$

Since $|\cos(\delta_0)|$ and $|\sin(\delta_0)|$ are bounded, then it is possible to set critical values of forcing amplitudes which singular points emerge at corresponding values of $N(0)$, i.e. at the local extrema of the SIM [Lamarque et al., 2011]:

$$\begin{aligned} f_{crit,min}^{(k)} &= \left| \frac{BN_{0,min}^{(k)}}{\omega_0} \right| \\ f_{crit,max}^{(k)} &= \left| cF_l(N_{0,max}^{(k)}) \right| \end{aligned} \tag{4.250}$$

The next section provides some numerical examples and application of the considered system in engineering.

4.7.3 Some numerical results

In this section we first validate our analytical developments via comparison with results obtained from direct time integration of system equations; then, application of the considered system in passive control of main structural systems and equipments will be presented.

4.7.3.1 Numerical results versus analytical predictions

Direct time integration of initial discrete system of equations which are presented in Eq. 4.228 are carried out by the Runge-Kutta scheme with following criteria: time step of 0.1, absolute and relative error tolerances of 10^{-12}. Initial conditions are set so that all masses of the system are at rest at time $t = 0$. From traced generalized coordinates via numerical integrations, i.e. $v(t)$ and $u_j(t), j = 1, \ldots, L+1$ we can evaluate ψ and the discrete equivalent of $\varphi(x,t)$, which is a $(L+1)$ dimension vector constituted of the variables as:

$$\varphi_{j+1}(t) = \left(\dot{u}_j(t) + i\omega u_j(t)\right) e^{-i\omega t} = N_{j+1}(t) e^{i\delta_{j+1}(t)} \tag{4.251}$$

Let us consider following system parameters: $L = 30$, $\varepsilon = 0.001$, $\omega_0 = 1$, $B = 100$, $D = 1$, $c = 0.5$, $f = 0.5$, $\sigma = 0$ and a small damping $\gamma = 0.1$ which is only considered in numerical integrations. The SIM and characteristic points of the system are illustrated in Fig. 4.44a. It is seen that the system posses one equilibrium point which is located on the first branch of SIM. The phase portrait around this point is shown in Fig. 4.44b saying that this equilibrium point is stable. The system possesses a singular point which is located on the local maximum of the SIM as $f_{crit,max}^{(1)} = 0.340 < f < f_{crit,min}^{(1)} = 8.370$. These points predict that the system after a transient regime will be attracted by the equilibrium point or it will present a SMR due to the existence of the singular point. Time histories of N_1 are reported in Fig. 4.45a showing that the system is attracted by its equilibrium point. Projecting results on the SIM which is depicted in Fig. 4.45b shows that there is a discrepancy between numerical obtained results (red point) and analytically predicted (blue point) equilibrium point. This discrepancy arises from continuous approximation which is illustrated in Fig. 4.46a where blue triangles presents the prediction of final amplitudes of each oscillator of the chain obtained from the discrete approach presented by Charlemagne et al [Charlemagne et al., 2017, Charlemagne, 2018]. At the same figure the results obtained from numerical integration represented by red crosses are included as well showing that the discrete approach fits well with numerical results. However, the SIM which are obtained from both discrete and continuous approaches are in good agreement, see Fig. 4.46b. Moreover, the developed analytical tools, permits to predict the overall response of the chain during steady-state regimes: the solid blue solid line in Fig. 4.46a reaches zero at $x = 14.4$. This means that during the steady-state regime, two groups of particles of the chain oscillate in opposite phase of each other separated by the middle oscillators, i.e. particles no. 14 and 15, which present near zero amplitudes which can be seen in Fig. 4.47 obtained from numerical results. The discrepancies between obtained results

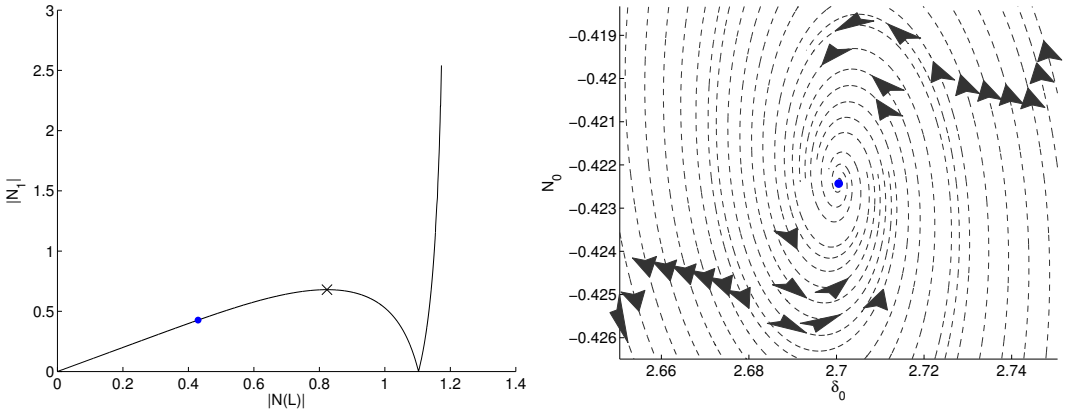

(a) (b)

Figure 4.44: a) The SIM of the system (black line) with equilibrium and singular points (blue point and black cross, respectively) b) Phase portrait around the equilibrium point. System parameters are $L = 30$, $\varepsilon = 0.001$, $\omega_0 = 1$, $B = 100$, $D = 1$, $c = 0.5$, $f = 0.5$ and $\sigma = 0$.

from discrete and continuous approaches decreases as the length of the chain increase. Let us set the length of the chain as $L = 50$ and the amplitude of the external excitation as $f = 2$. Meanwhile, all other system parameters are the same as before. The system possesses five equilibrium points. Figure 4.48 summarizes comparisons between amplitudes of particles of the chain, i.e. N_j or $N(x)$ obtained from continuous and discrete approaches around its equilibrium points. It is seen that both results are in good agreement.

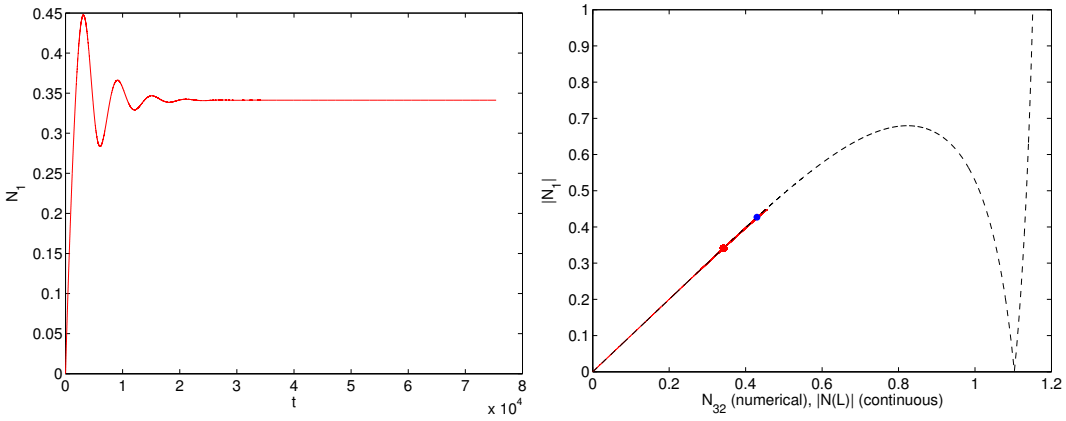

(a) (b)

Figure 4.45: a) N_1 versus time obtained from numerical results b) SIM of the system (dashed black line) and equilibrium point (blue point) with corresponding numerical results (red line). The red point shows the final amplitudes of the system obtained from numerical results. System parameters are $L = 30$, $\varepsilon = 0.001$, $\omega_0 = 1$, $B = 100$, $D = 1$, $c = 0.5$, $f = 0.5$ and $\sigma = 0$.

Let us now change characteristics of the external excitation: we set $f = 4.5$ and $\sigma = 10$. The system possesses three equilibrium pints named as no. 1, 2 and 3 and one singular point which are illustrated on the SIM in Fig. 4.49a. Phase portraits of the system around equilibrium points are provided in Figs. 4.49b-4.49d. It is seen that equilibrium points no. 1 and 2 are unstable while the

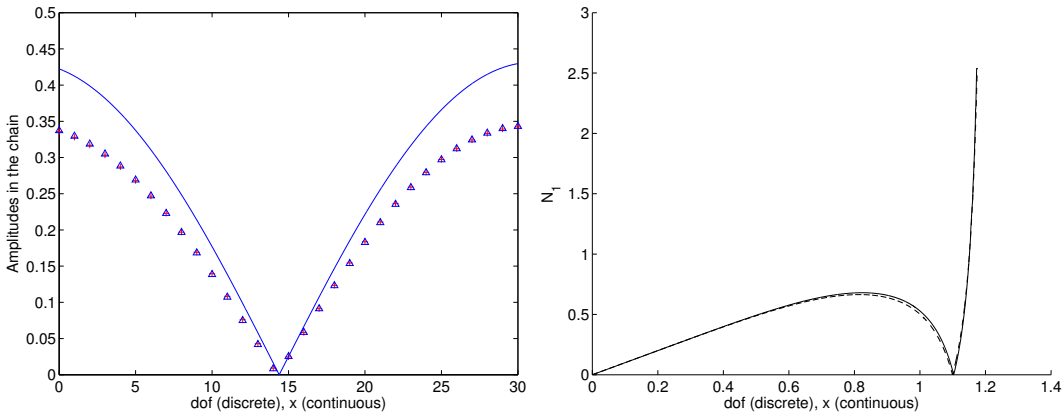

(a) (b)

Figure 4.46: a) Amplitudes of the masses of the chain obtained from discrete (triangles) and continuous (solid line) approaches and numerical results (red crosses)b) The SIM obtained from discrete (dashed line) and continuous (solid line) approaches. System parameters are $L = 30$, $\varepsilon = 0.001$, $\omega_0 = 1$, $B = 100$, $D = 1$, $c = 0.5$, $f = 0.5$ and $\sigma = 0$.

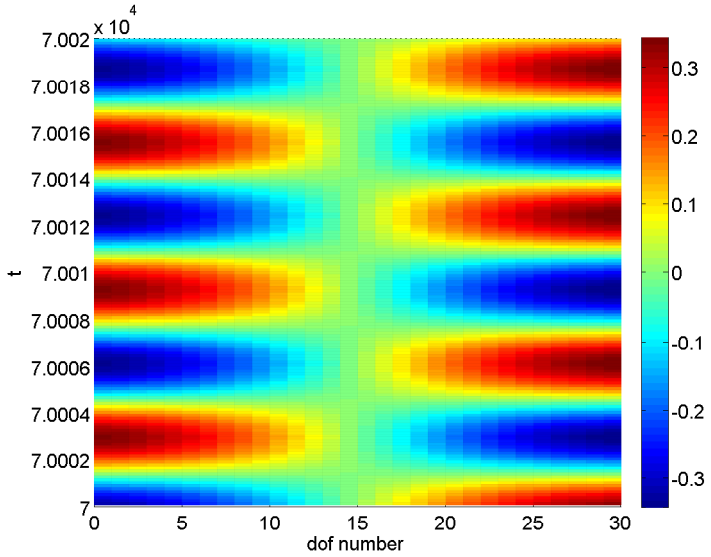

Figure 4.47: Evolution of the physical amplitudes of oscillations of u_j obtained from numerical results at τ_1 time scale. System parameters are $L = 30$, $\varepsilon = 0.001$, $\omega_0 = 1$, $B = 100$, $D = 1$, $c = 0.5$, $f = 0.5$ and $\sigma = 0$.

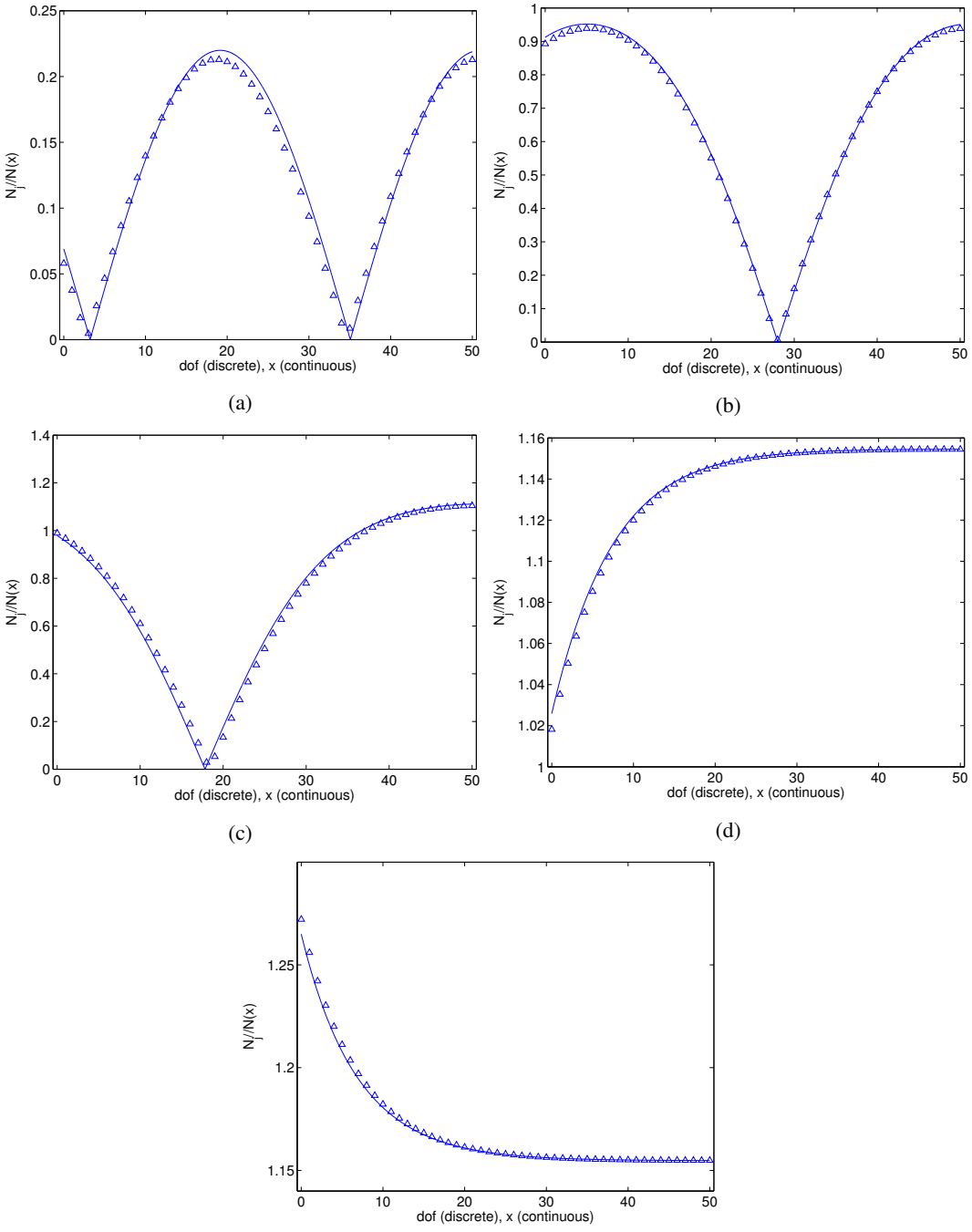

Figure 4.48: Predicted amplitudes of the particles of the nonlinear chain on the five equilibrium points obtained from discrete (triangles) and continuous (solid line) approaches. System parameters are $L = 50$, $\varepsilon = 0.001$, $\omega_0 = 1$, $B = 100$, $D = 1$, $c = 0.5$, $f = 2$ and $\sigma = 0$.

point no. 3 is stable.

Figure 4.50a collects the SIM of the system in terms of N_1 versus N_32 accompanied by results obtained from direct numerical integration of system equations where the damping has been increased to $\gamma = 5$. The figure show that the system presents a SMR. Time histories of mentioned amplitudes are depicted in Figs. 4.50b and 4.50c showing that the system presents persisting bifurcations and cycles between stable branches of the SIM. During these cycles a 1:1 resonance is emerged between two nonlinear normal modes of the chain leading to intense energy exchanges. These bifurcations between two nonlinear modes of the system which are between the lower and higher branches of the SIM are illustrated in Fig. 4.51. This nonstationary behaviour emerging from inter-modal resonance(s) has been also observed and explained within the framework of limiting phase trajectories in different systems such as discrete periodic Klein-Gordon [Smirnov and Manevich, 2011] and Fermi-Pasta-Ulam [Starosvetsky and Manevitch, 2013] chains.

4.7.3.2 Application to passive control

The aim of this section is that the passive control of main structural systems by addition of c chain of nonlinear oscillators is possible. Let us consider $L = 30$, $\varepsilon = 0.001$, $\omega_0 = 1$, $B = 100$, $D = 1$ and $c = 0.5$. Let us investigate a case when the LMS is under external excitation with variable amplitude $f \in [0.1, 10]$ and with exact 1:1 resonance, i.e. $\sigma = 0$. Figure 4.52 summarizes obtained equilibrium and singular points of the system added by the ones for the amplitude N_1 that the LMS would face without coupling the chain. Black solid line denotes the amplitudes that the LMS would face without the chain. It is given by the following relation : $N_1 = \dfrac{f}{\sqrt{c^2 + \sigma^2\omega_0^2}} = 2f$. It is seen that the LMS has lower amplitudes with the chain, especially at relatively high energies. Nonetheless, around $f = 0.6$, an equilibrium point has the same amplitude as the LMS without the chain. Thus, a parametric study needs to be led to enhance the control performance at low energy and to tune optimized parameters of the chain.

4.8 Industrial and inter ministry collaborations in the frame of developed techniques

Several collaborations are carried out in the domain of research and developments with industrial and inter ministry partners for passive control of of civil an mechanical structures. In the followings a brief summary and results of these cooperation are listed.

4.8.1 PSA Peugeot Citroën Automobiles

Several projects have been financed by PSA Peugeot Citroën Automobiles in the frame of the "OpenLab VAT@Lyon" for the ail of passive control of different segments of vehicles as it follows:

- Passive control of nonsmooth system by a nonsmooth absorber [Lamarque et al., 2012]: Some mechanical parts of vehicles globally present linear behaviour but they can move in a clearance showing an additional piece-wise linear response. The aim of the project was to control such nonsmooth systems by addition of another nonsmooth oscillator.

- Passive control of mechanical systems in the gravitational field [Ture Savadkoohi et al., 2012a]: The aim was to control a vertical oscillator taking

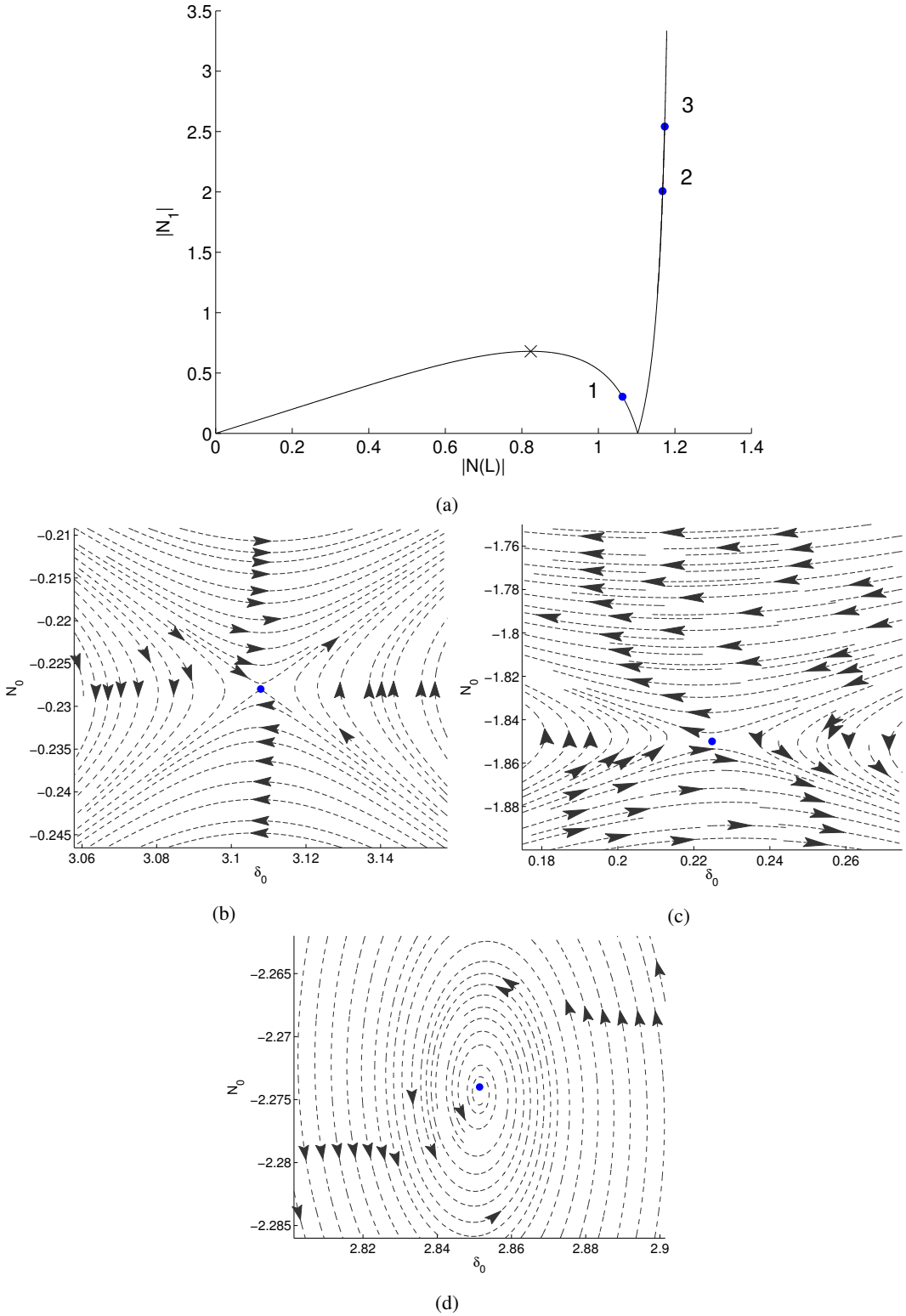

Figure 4.49: a) the SIM of the system (black line) with equilibrium and singular points (blue points and black cross, respectively); b)-d) Phase portraits around equilibrium points no. 1, 2 and 3, respectively. System parameters are $L = 30$, $\varepsilon = 0.001$, $\omega_0 = 1$, $B = 100$, $D = 1$, $c = 0.5$, $f = 4.5$ and $\sigma = 10$

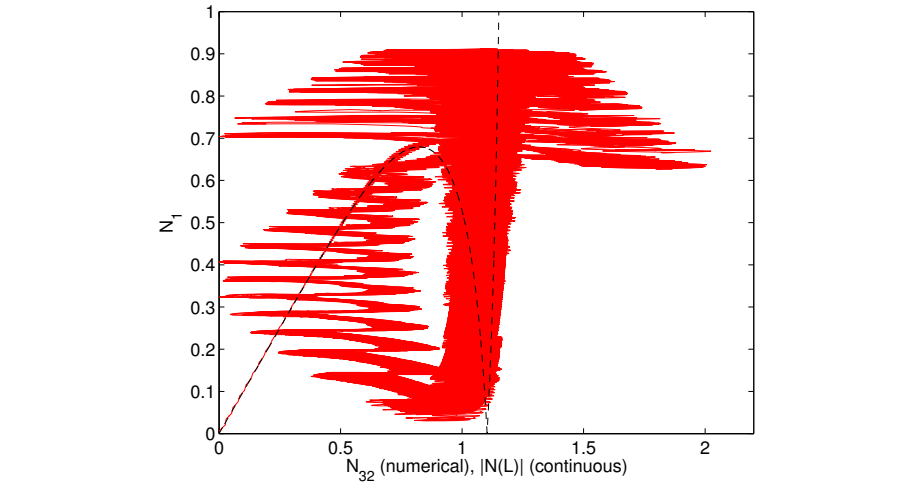

(a)

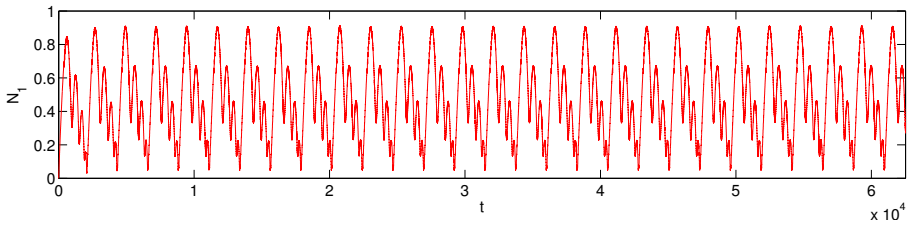

(b)

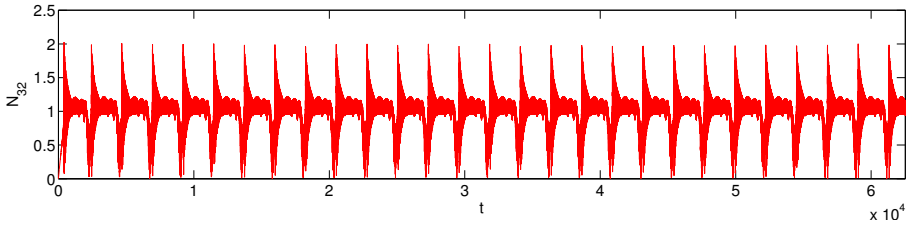

(c)

Figure 4.50: a) The SIM of the system (dashed black line) and corresponding numerical results (red line) c) time histories of N_1 obtained from numerical results; c) Time histories of N_{32} obtained from numerical results. System parameters are $L = 30$, $\varepsilon = 0.001$, $\omega_0 = 1$, $B = 100$, $D = 1$, $c = 0.5$, $f = 4.5$ and $\sigma = 10$.

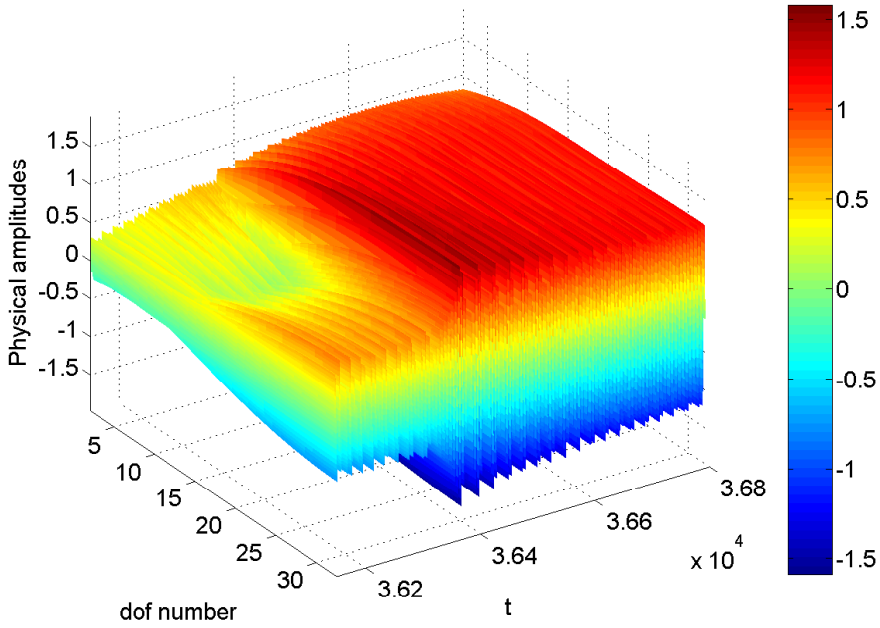

Figure 4.51: Evolution of physical amplitudes of particles of the chain u_j obtained from numerical results at τ_1 time scale. System parameters are $L = 30$, $\varepsilon = 0.001$, $\omega_0 = 1$, $B = 100$, $D = 1$, $c = 0.5$, $f = 4.5$ and $\sigma = 10$.

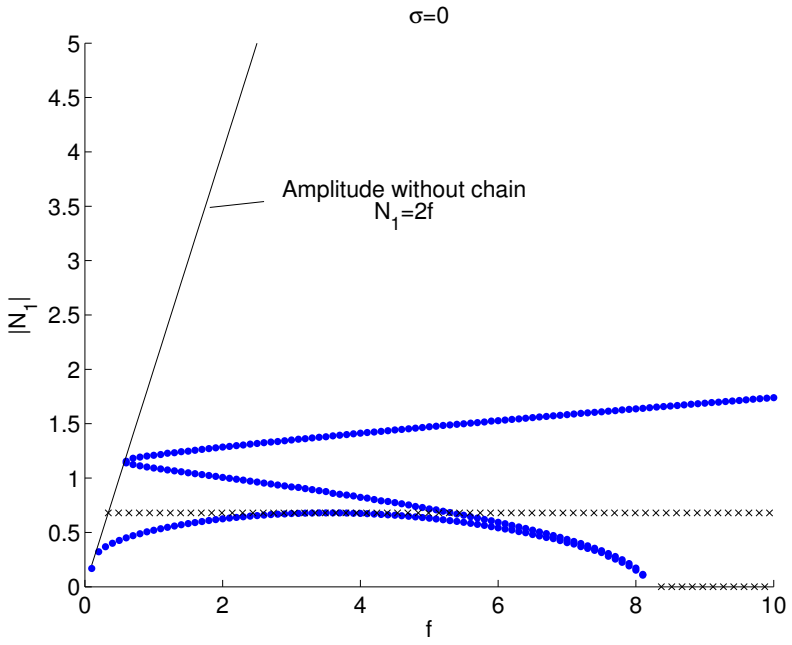

Figure 4.52: Amplitudes of equilibrium and singular points (blue points and black crosses, respectively) of the system in terms of $|N_1|$ when the forcing magnitude $f \in [0.1, 10]$. Black solid line denotes the amplitude the LMS without coupling the chain. System parameters are $L = 30$, $\varepsilon = 0.001$, $\omega_0 = 1$, $B = 100$, $D = 1$, $c = 0.5$ and $\sigma = 0$.

into account the effects of the gravity. The gravity breaks the symmetry and induces pre-stressing in the system and using a polynomial nonlinear absorber in the gravitational field induces additional linear part to the restoring forcing function. For overcoming mentioned obstacles a piece-wise linear vertical absorber is used for passive control of the mechanical segment.

- Passive control of oscillators with time-varying masses [Lamarque et al., 2014]: For some structures the assumption of conservation of the mass is not valid. Two representative examples of such systems are air planes and vehicles as their mass caries due to consumption of the fuel. The goal was to control such systems with nonsmooth absorbers.

4.8.2 Poma

- Passive control of pendulum type systems by TMD has been already articulated by Matsuhisa and Otsu-shi [Matsuhisa and k Otsu-shi, 1994]. The goal of the first collaboration with POMA was to study the passive control of two-dimensional pendular vibration of gondola lifts by a nonlinear absorber [Agrapart, 2016]. Linearised form of governing two-dimensional equations of the pendular movements of the cabin are coupled with the equations of the nonlinear absorber.

- The first step of the collaborations has been extended to preparation of a project in the frame of “Projet la Région Auvergne-Rhône-Alpes" [Lamarque and Ture Savadkoohi, 2017]. The project has been retained is going on. In this project the passive control of linearised form of pendular movements of the cabin in two directions with flexible base, i.e. deformations of the cable, will be studied.

4.8.3 Cerema

The aim of the cooperation was to develop a system for controlling vertical modes of cables of stayed bridges. As the system was in the gravitational field, a special nonsmooth system has been developed and patented [Lamarque et al., 2015] in the frame of the thesis of Weiss [Weiss, 2016].

CHAPTER 5

Targeted energy transfer in acoustics via pure acoustical resonators

Contents

5.1 Introduction

Correct physical modelling of acoustical systems are primary and important steps for designing adapted and robust passive control systems. The linear representation of a system will be sufficiently enough if it experiences small amplitude oscillations. However, the system can present nonlinear responses at high intensities or long propagation distances with low damping [Rossing (Ed.), 2014]. In this chapter, the concept of nonlinear passive control process in the domain of acoustics is presented. At first part of the chapter, a brief description about linear acoustics will be illustrated accompanied by some nonlinear aspects of the acoustics. Then, the main focus of the chapter which is nonlinear passive control in acoustics will be presented. Organization of the chapter is as it follows: an introduction of necessary tools and elements in linear acoustics is provided in Sect. 5.2, while the problem of the passive control (linear and nonlinear) in acoustic is discussed in Sect. 5.3. A detailed literature review about behaviours of Helmholtz resonators in nonlinear regimes is provided in Sect. 5.4. Studying the Helmholtz resonators in extreme nonlinear regimes via analytical/numerical approaches validated by experimental results are presented in Sect. 5.5. Finally, Section 5.6 presents the TET between a main acoustical mode and a Helmholtz resonator in nonlinear regimes.

5.2 A brief description of linear acoustics

Governing systems equations which present small amplitude phenomena, can be represented via linear approximations, that also take into account the principle of superposition, which can be pic-

tured as it follows:

$$\mathscr{L}\left(\sum_{j=1}^{n}\alpha_j\mathscr{F}_j\right)=\alpha_1\mathscr{L}(\mathscr{F}_1)+\alpha_2\mathscr{L}(\mathscr{F}_2)+\dots \tag{5.1}$$

where $\mathscr{F}_j$ are the subjects, $\mathscr{L}(\mathscr{F}_j)$ are the mathematical representation or prediction of the effect of the subjects $\mathscr{F}_j$ and α_j are arbitrary numbers for correct description of the system behaviours. Equations 5.1 states that effects of sum of several subjects is sum of the effects of each subject. Moreover, effects of α_j times of a the subject $\mathscr{F}_j$ will be α_j times of the effect of the $\mathscr{F}_j$. In the followings, a brief descriptions of governing equations of continuum mechanics will be represented and commented upon which are mainly collected from references [Rossing (Ed.), 2014, Royis, 2013]:

Flux: Conservation of mass The flux is the amount of a quantity which passes through a surface per unit time. The flux $\mathcal{Q}$ can be obtained via the vector field flux density, q, in a surface with the normal $\boldsymbol{n}$ as:

$$\mathcal{Q}=\int_{\Sigma}\boldsymbol{q}.\boldsymbol{n}\mathrm{d}\Sigma \tag{5.2}$$

Then, the general conservation law reads as:

$$\frac{\partial\rho(\boldsymbol{x},t)}{\partial t}+\nabla.\boldsymbol{q}=\mathcal{S} \tag{5.3}$$

where ρ is the mass density of the system which globally speaking can be function of space and time and $\mathcal{S}$ stands for the source term. In fluid mechanics, the mass flux reads as $\rho\boldsymbol{v}$ and then Eq. 5.3 presents the conservation of the mass in Eulerian view point as ($\boldsymbol{q}=\rho\boldsymbol{v}$):

$$\frac{\partial\rho(\boldsymbol{x},t)}{\partial t}+\nabla.(\rho\boldsymbol{v})=0 \tag{5.4}$$

where ρ is the mass density of the system which in general can be function of space and time, while $\boldsymbol{v}$ is the Eulerian, i.e. local and instantaneous velocity.

Generalized movement equations The generalized movement equations reads

$$\overrightarrow{\mathrm{div}}(\boldsymbol{\sigma})+\rho\boldsymbol{g}=\rho\frac{\mathrm{D}\boldsymbol{v}}{\mathrm{D}t} \tag{5.5}$$

where $\boldsymbol{\sigma}$ is the Cauchy stress tensor and $\boldsymbol{g}$ stands for the gravitational acceleration vector. The $\dfrac{\mathrm{D}}{\mathrm{D}t}$ states the material derivatives which for an arbitrary tensor field $\boldsymbol{\mathcal{Y}}=\boldsymbol{\mathcal{Y}}(\boldsymbol{x},t)$ copies as:

$$\frac{\mathrm{D}\boldsymbol{\mathcal{Y}}}{\mathrm{D}t}=\frac{\partial\boldsymbol{\mathcal{Y}}}{\partial t}+\boldsymbol{v}.\nabla\boldsymbol{\mathcal{Y}} \tag{5.6}$$

Balance of energy It can be stated that

$$\rho\frac{\mathrm{D}u}{\mathrm{D}t}=\boldsymbol{\sigma}:\nabla\boldsymbol{v}-\nabla.\boldsymbol{q}+\rho\mathcal{S} \tag{5.7}$$

where $u=u(\boldsymbol{x},t)$ is the internal energy per unit mass, $\boldsymbol{q}=\boldsymbol{q}(\boldsymbol{x},t)$ is the flux density vector and $\mathcal{S}$ is the rate at which energy is generated by sources inside the volume per unit mass.

Newtonian fluids Equations 5.5 and 5.7 can be applied to both solid and fluids. For prediction of complete system behaviours, a rheology is needed. Let us consider a special rheology for fluids such as water or air which fall in the category of Newtonian fluids. In Newtonian fluids, the stress tensor due to the movements is proportional to the rate of shear tensor $\boldsymbol{\mathcal{D}}$ as:

$$\boldsymbol{\sigma} = \boldsymbol{\sigma_n} + \mu\boldsymbol{\mathcal{D}} \tag{5.8}$$

where $\boldsymbol{\sigma_n}$ is the stress tensor at rest position or the normal stress, μ is the shear viscosity and

$$\boldsymbol{\mathcal{D}} = \nabla\boldsymbol{v} + \nabla^T\boldsymbol{v} - \frac{2}{3}(\nabla.\boldsymbol{v})\boldsymbol{I} \tag{5.9}$$

where $\boldsymbol{I}$ is the unity matrix.

Some simple concepts in thermodynamics Let us define s as the entropy per unit mass, then the state equation in the simplest form (neglecting other effects such as relaxation) reads as

$$s = s(u, \rho^{-1}) \tag{5.10}$$

or

$$T\mathrm{d}s = \mathrm{d}u + p\mathrm{d}\rho^{-1} \tag{5.11}$$

and for the Newtonian fluids one can write

$$\boldsymbol{\sigma_n} = -p\boldsymbol{I} + \mu_B(\nabla.\boldsymbol{v})\boldsymbol{I} \tag{5.12}$$

where μ_B stands for bulk viscosity. Moreover, if we define κ as the coefficient of the thermal conduction, then the heat flux density vector copies

$$\boldsymbol{q} = -\kappa\nabla T \tag{5.13}$$

Navier-Stokes equations Following equations represent Navier-Stokes equations which in fact are adapted for Newtonian fluids:

$$\rho\frac{\mathrm{D}\boldsymbol{v}}{\mathrm{D}t} = -\nabla p + \nabla(\mu_B\nabla.\boldsymbol{v}) + \nabla.(\mu\boldsymbol{\mathcal{D}}) + \boldsymbol{g}\rho \tag{5.14}$$

$$\rho T\frac{\mathrm{D}s}{\mathrm{D}t} = \frac{1}{2}\mu\boldsymbol{\mathcal{D}} : \boldsymbol{\mathcal{D}} + \mu_B(\nabla.\boldsymbol{v})^2 + \nabla.(\kappa\nabla T) \tag{5.15}$$

Some of thermodynamics coefficients Equation 5.10 indicates that any system variables can be evaluated as function of other variables. For instance, one can states that the pressure p is function of ρ and T or of s and ρ. Here, we list a set of some of such parameters [Rossing (Ed.), 2014]:

- the speed of the sound c:

$$c^2 = (\frac{\partial p}{\partial \rho})_s \tag{5.16}$$

- the bulk modulus B_v:

$$B_V = \rho c^2 \tag{5.17}$$

- the specific heat at constant pressure c_p:

$$c_p = T(\frac{\partial s}{\partial T})_p \tag{5.18}$$

- the specific heat at constant volume c_v:

$$c_v = T(\frac{\partial s}{\partial T})_\rho \tag{5.19}$$

- the coefficient of thermal expansion β:

$$\beta = \rho(\frac{\partial(1/\rho)}{\partial T})_p \tag{5.20}$$

In above mentioned equations, the subscripts in partial derivatives stand for constant term during differentiation. Introduced coefficients are coupled to each other via thermodynamic identity which reads:

$$\gamma = 1 + T\frac{(\beta c)^2}{c_p} \tag{5.21}$$

where $\gamma = \dfrac{c_p}{c_v}$ stands for the specific heat ratio. There are two relations in thermodynamics which are of specific interest in acoustics:

$$\mathrm{d}\rho = \frac{1}{c^2}\mathrm{d}p - \left(\frac{\rho\beta T}{c_p}\right)\mathrm{d}s \tag{5.22}$$

$$\mathrm{d}T = \left(\frac{\beta T}{\rho c_p}\right)\mathrm{d}p + \left(\frac{T}{c_p}\right)\mathrm{d}s \tag{5.23}$$

Thermodynamic coefficients for an ideal gas All types of gases such as air at sufficiently low densities, present (in general) the same type of behaviour which is named as ideal behaviour and the gas is called as ideal gas [de Oliveira, 2013]. The thermodynamic coefficient for an ideal gas read [Rossing (Ed.), 2014]

$$c^2 = \gamma RT = \gamma\frac{P}{\rho} \tag{5.24}$$

$$c_p = \frac{\gamma R}{\gamma - 1} \tag{5.25}$$

$$c_v = \frac{R}{\gamma - 1} \tag{5.26}$$

$$\beta = \frac{1}{T} \tag{5.27}$$

Following parameters can be assigned for air: $R = 278$ J/kg K, $\gamma = 1.4$ which yields to $c_p = 1005$ J/kg K and $c_v = 718$ J/kg K. The sound speed and the density at temperature $T = 293.16$K and pressure $p = 10^5$ Pa, read $c = 343$m/s and $\rho = 1.19$kg/m^3, respectively.

Ideal compressible fluids In an ideal fluid the viscosity μ_B and the coefficient of thermal conduction κ are negligible. In this case the Navier-Stokes equation (see Eq.5.14) reads

$$\rho\frac{\mathrm{D}\boldsymbol{v}}{\mathrm{D}t} = -\nabla p + \boldsymbol{g}\rho \tag{5.28}$$

and Eq. 5.14 yields to isotrope flow conditions as

$$\frac{\mathrm{D}s}{\mathrm{D}t} = 0 \tag{5.29}$$

Considering Eq. 5.22, one can write

$$\frac{\mathrm{D}p}{\mathrm{D}t} = c^2 \frac{\mathrm{D}\rho}{\mathrm{D}t} \tag{5.30}$$

Injecting the equation of the conservation of mass, i.e. Eq. 5.4, in Eq. 5.30 following system is obtained:

$$\frac{\mathrm{D}p}{\mathrm{D}t} + \rho c^2 \nabla . \boldsymbol{v} = 0 \tag{5.31}$$

Here, the bulk modulus read: $B_v = \rho c^2$.

Linearised equations of an ideal fluid A linearisation process can be applied to all of above mentioned equations to reach the governing linear set of equations. As an example let us linearly perturb following variables:

$$\rho \rightarrow \rho_0 + \Delta\rho \tag{5.32}$$

$$\boldsymbol{v} \rightarrow \boldsymbol{v}_0 + \Delta\boldsymbol{v} \tag{5.33}$$

$$p \rightarrow p_0 + \Delta p \tag{5.34}$$

For instance, we inject Eqs. 5.32 and 5.33 in Eq. 5.4. In this case the linearised equations of the conservation of the mass yields to:

$$\frac{\partial \Delta\rho}{\partial t} + \nabla . (\boldsymbol{v}_0 \Delta\rho + \rho_0 \Delta\boldsymbol{v}) = 0 \tag{5.35}$$

Let us linearize governing equations of an ideal compressible fluid in a constant ambient density, i. e. $\rho = \rho_0$ in Eq. 5.32 and neglecting the gravity effects. Linearised forms of Eqs. 5.28 and 5.31 copy:

$$\rho \frac{\partial \Delta\boldsymbol{v}}{\partial t} = -\nabla(\Delta p) \tag{5.36}$$

$$\frac{\partial p}{\partial t} + \rho c^2 \nabla . (\Delta\boldsymbol{v}) = 0 \tag{5.37}$$

Let us take the time derivative of Eq. 5.37 via injection of Eq. 5.36; following spatiotemporal systems is obtained [Rossing (Ed.), 2014]:

$$\nabla . \left(\frac{1}{\rho} \nabla(\Delta p) \right) - \frac{1}{\rho c^2} \frac{\partial^2 (\Delta p)}{\partial t^2} = 0 \tag{5.38}$$

and if $\rho(\boldsymbol{x}, t) = \rho(t)$, then:

$$\nabla^2 (\Delta p) - \frac{1}{c^2} \frac{\partial^2 (\Delta p)}{\partial t^2} = 0 \tag{5.39}$$

which indicates wave equation. Treatment of 1-dimensional wave equation is represented in Annex D.

If the fluctuation of pressure, i.e. Δp, varies with constant angular frequency as:

$$\Delta p = a \cos(\omega t - \Phi) \tag{5.40}$$

then the amplitude a and the phase Φ will be constant. This is the simplest case which one can consider for an acoustic signal. The human ear interacts approximately with frequencies $f \in [20, 20\mathrm{k}]$ Hz. Sound frequencies corresponding to smaller and bigger than the lower and upper limits of this interval are named as infrasonic and ultrasonic, respectively [Rossing (Ed.), 2014].

Classical attenuation of sound: reflection and absorption coefficients at normal incidence

Characteristics impedance Let us define $p_r(x,t) = \mathfrak{A}e^{i(kx+\omega t)}$ and $p_i(x,t) = \mathfrak{B}e^{i(-kx+\omega t)}$ as outgoing and ingoing (reflected and incident pressures), respectively at the surface of the layer $\mathcal{M}$, see Fig. 5.1. So, the total pressure, $p_{\text{total}}(x,t)$ reads as [Allard and Atalla, 2009]:

$$p_{\text{total}}(x,t) = p_i(x,t) + p_r(x,t) \tag{5.41}$$

and considering Eq. 5.36 one can write:

$$v_{\text{total}}(x,t) = v_i(x,t) + v_r(x,t) = \frac{\mathfrak{B}k}{\rho\omega}e^{i(-kx+\omega t)} + \frac{\mathfrak{A}k}{\rho\omega}e^{i(kx+\omega t)} \tag{5.42}$$

The characteristic impedance is the ratio of the pressure in one direction to the velocity of the fluid at the same direction. As an example for the ingoing direction (see Fig. 5.1), we can express:

$$v_{\text{total}}(x,t) = v_i(x,t) + v_r(x,t) = \frac{\mathfrak{B}k}{\rho\omega}e^{i(-kx+\omega t)} + \frac{\mathfrak{A}k}{\rho\omega}e^{i(kx+\omega t)} \tag{5.43}$$

If we consider the ingoing direction of the propagation of the wave, the pressure and the velocity are related with each other as:

$$v_i(x,t) = \frac{1}{Z_c}p_i(x,t) \tag{5.44}$$

with

$$Z_c = \frac{\rho\omega}{k} \tag{5.45}$$

The Z_c is named as characteristics impedance.

Impedance, resistance and reactance Via superposition of two waves (ingoing and outgoing), from Eq. 5.43 one can write:

$$v_{\text{total}}(x,t) = \frac{1}{Z_c}\left(\mathfrak{B}e^{i(-kx+\omega t)} - \mathfrak{A}e^{i(kx+\omega t)}\right) \tag{5.46}$$

The ratio of total pressure and total velocity at the given layer $\mathcal{M}$ with distance x is defined as impedance, formulating as [Allard and Atalla, 2009]:

$$Z(\mathcal{M}) = \frac{p_{\text{total}}(x,t)}{v_{\text{total}}(x,t)} \tag{5.47}$$

The impedance is a complex number. The real part of the impedance is named as specific acoustic resistance of the impedance which should be non negative. Its imaginary part is called as specific acoustic reactance which may be either positive or negative [Rossing (Ed.), 2014].

The reflection coefficient The reflection coefficient R at the surface of the layer is defined as:

$$R(\mathcal{M}) = \frac{p_r(x,t)}{p_i(x,t)} \tag{5.48}$$

The reflection coefficient is a complex number and as the numerator and denominator of the Eq. 5.48 have the same dependency to the time t, then R is independent of the time. If $|R| = 1$, then the ingoing and outgoing waves have the same amplitudes, i.e. the layer is totally reflective and if $R = 0$, then the layer is totally absorptive. The absorption coefficient of the layer $\mathcal{M}$ is defined as [Allard and Atalla, 2009]:

$$\alpha(\mathcal{M}) = 1 - |R(\mathcal{M})|^2 \tag{5.49}$$

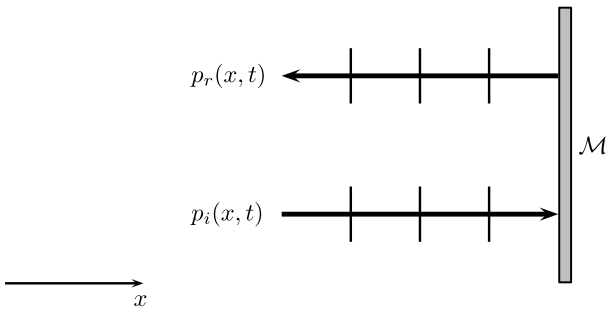

Figure 5.1: Schematic of outgoing ($p_r(x,t)$) and ingoing ($p_r(x,t)$) at the surface of the layer $\mathcal{M}$.

5.3 Passive control in acoustics: from linear to nonlinear: an introduction

Passive noise control in acoustics varies from the large range of systems dividing in linear and nonlinear absorbers. One of the widely used systems for sound attenuation is Helmholtz resonators (HR) [Helmholtz, 1863, Keller and Zauner, 1995]. An idealized form of a HR is depicted in Fig. 5.2. It consists of a cavity with the volume V and its neck with the length l and cross-section A. If the frequency of an acoustical mode is low enough such that the wavelength is much longer than any dimensions of the resonator, then the compressible air in the cavity acts as a spring with the stiffness as [Rossing (Ed.), 2014]

$$k = \frac{\rho c^2 A^2}{V} \tag{5.50}$$

and the air in the neck can be considered as incompressible behaving as a lump mass with with the mass as [Rossing (Ed.), 2014]

$$m = \rho A l' \tag{5.51}$$

where $l' = l + \Delta l$ where Δl stands for the end correction of two ends of the neck. There are

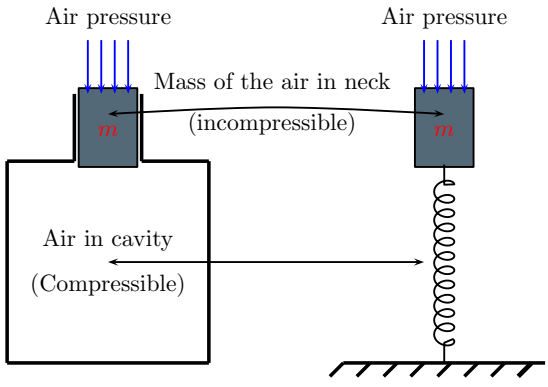

Figure 5.2: An idealized HR and its analogy in mechanics.

some suggestions for the neck correction Δl. For instance, if l can be considered larger than the radius of the neck r_{neck}, then $\Delta l = 0.82 r_{\text{neck}}$ [Rossing (Ed.), 2014]. The depicted analogy between HR and the mechanical system in Fig. 5.2 is in fact the linear theory developed by Helmholtz

[Helmholtz, 1863] which physically assumes that all kinetic energy is concentrated in the moving gas in the neck and in neighbourhood of the neck openings, while the linear restoring forcing term, or the potential energy of the elastic deformation is localized in the gas of the cavity [Borisova et al., 1984]. This mechanical analogy shows that that the HR can be coupled to a targeted acoustical mode of a system for linear noise control in the same manner and logic that TMD [Frahm, 1911] does for mechanical systems. It should be mentioned that the linear analogy between the behaviour of a HR and mechanical mass-spring systems is valid for low pressure conditions. However, at high intensities nonlinear terms enter to the behaviour of the system which can not be neglected. This fact will be pinpointed in following section. In this case, using the HR as a linear solution for passive noise control will have the same main drawback as the TMD, i.e. it will be operational for a very narrow frequency width.
From different nonlinear passive control solutions we can name the work of Cochelin et al. [Cochelin et al., 2006] which exploits the NES technology for control of an acoustical mode via coupling a thin visco-elastic membrane. In detail, the first acoustical mode of the air in the tube is considered as a linear oscillator. The role of the NES as the passive controller system is carried out by this membrane which presents cubic nonlinearity as for its restoring forcing function. The first acoustical mode in tube and the nonlinear oscillator are weakly coupled thanks to the air of the coupling box (see Fig.5.3). Experimental and numerical results of Cochelin et al. [Cochelin et al., 2006] illustrate the transfer of the energy of the low frequency acoustical mode ($\approx$ 100 Hz) to the membrane in an irreversible manner. Developed nonlinear system by Cochelin

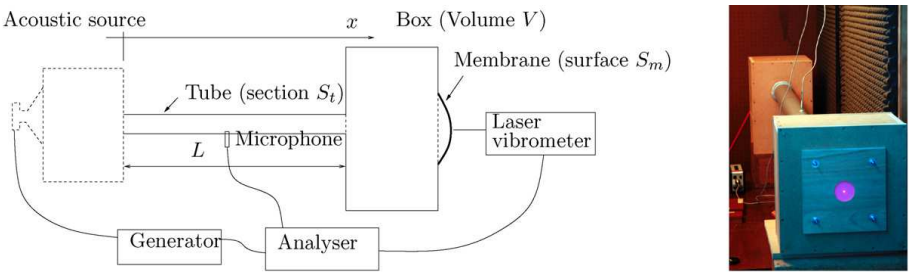

Figure 5.3: The considered system by Cochelin et al. [Cochelin et al., 2006] for creation of the TET by a visco-elastic membrane. The first acoustical mode in tube is weakly coupled to the membrane via the air in the coupling box.

et al.[Cochelin et al., 2006] for passive noise reduction in low frequency domains is a mechanical system. However, we are interested to control noise via targeted energy transfer using a pure nonlinear acoustical system instead of mechanical one.
The aim of this chapter is to detect the behaviours of HR resonators in nonlinear regimes to be used as pure acoustical nonlinear absorbers.

5.4 Nonlinear behaviours of Helmholtz resonators in nonlinear regimes

Observations of nonlinear behaviours/responses in HR have been spotted in 20^{th} century. Nonlinear interactions between resistance of an orifice and particle velocity was observed by Sivian [Sivian, 1935]. They even presented a nonlinear relations between pressure difference on two sides of the orifice and the particle velocity. Bolt et al. [Bolt et al., 1949] reported nonlinear responses in terms of reactance and the velocity. Ingard [Ingard, 1953] investigated on the effects of different geometry of the orifice (circular or rectangular), observing nonlinear effects on the system

responses. They performed further investigation on the effect of viscosity, heat conduction and radiation with emphasising nonlinear effects on the resonance frequency and absorption. They concluded that nonlinear effects influence the response of the system considerably and predicted absorption via linear design methods could provide important errors at high intensities which nonlinear responses become more evident. Ingard and Ising [Ingard and Ising, 1967] investigated on the acoustic nonlinearity of an orifice via measuring the flow velocity in the orifice and variation of the pressure. They spotted that the pressure and the velocity amplitudes interact linearly at low pressure while the same interactions become nonlinear (square-low relation) at large velocity amplitudes. Behaviours of a HR resonator subjected to low-frequency pressures have been studied analytically by Zinn [Zinn, 1970]. They took into account nonlinearities via treating not only first order governing equations but also second order ones. Their developments indicates that the losses in HR can be associated with following two mechanism: i) viscous damping and ii) dissipation of kinetic energy of jets which are periodically created at both extremes of the orifice that is amplitude dependent. They claimed that their developed technique would be valid for a single HR under low frequency pressure excitations. The emphasised that further theoretical developments should be carried out for analysing low to high amplitude behaviours of arrays of HR over winder external excitation frequencies. The fluid mechanical model of HR derived by Hersh and Walker [Hersh and Walker, 1977]: to treat system equations they used a perturbation technique via endowing a small physical parameter (see Eq. 32 in [Hersh and Walker, 1977]) and they distinguished three different cases namely, weak, moderately weak and intense incident sound fields leading to linear, weakly nonlinear and nonlinear regimes. Their analytical studies accompanied by experimental results. They concluded that at high incident sound pressure levels, resistance is independent of the frequency while its is proportional to the square root of the amplitude of the incident sound pressure. Reactance is related to the frequency, geometry of the HR and incident sound pressure in nonlinear manners. Later on, many research works were developed to consider nonlinearities in HR. Borisova et al. [Borisova et al., 1984] developed simple relations via setting some design parameters by taking into account frictional resistance on the neck wall (nonlinear dissipation terms). The effect of nonlinear resorting forcing terms of the HR, (linear and quadratic terms) studied by Boullosa and Orduna-Bustamante [Boullosa and Orduna-Bustamante, 1992] (see Eqs. 12 and 13 in their report). Then, they compared the approximated solutions of the system equation with experimental results. In the classical Helmholtz approximation, phase variations in system elements such as cavity and the throat (or neck) are supposed to be very small. This means that the oscillation process in HR can be seen as periodic conversion of potential energy through pressurized cavity into kinetic energy of moving gas inside the throat and vice versa. However, due to the sound radiation, boundary layer and jet dissipations, some (even small) parts of stored acoustic energy in the resonator, gets destroyed at each cycle which should be compensated by an excitation for remaining at equilibrium (or quasi-equilibrium) state position. To this end, the frequency-dependent control process of HR demands that nonlinear effects due to losses, thermoacoustic boundary layers and higher-order frequency corrections to the Helmholtz approximation to be considered [Keller and Zauner, 1995]. Moreover, Keller and Zauner [Keller and Zauner, 1995] confirmed that (through theoretical studies) for obtaining high attenuation performances via HR, the flow losses should be reduced by rounding both ends of the throat of the HR. Zaikin and Rudenko [Zaikin and Rudenko, 1996] developed a nonlinear model of the HR with movable end wall via taking into account Stokes friction [Stokes, 1845] and the friction of the acoustic boundary layer (see Eqs. 8 and 9 in [Zaikin and Rudenko, 1996]). They took into account the nonlinear correction to the frequency response curves of the HR via inclusion of cubic nonlinearity. Moreover, they performed an investigations on necessary system characteristics for using the HR with movable wall as sound absorber or insulator. The nonlinear absorption process of HR at high amplitude incident waves is studied by Meissner theoretically [Meissner, 1999] and experimentally [Meissner, 2000]. In their study, a HR coupled to the end of a cylindrical tube. When the system faces high amplitudes inci-

dent waves, the instantaneous flew patterns on both of the orifice of the HR are different. During the first half cycle when the flow is guided from the tube to the HR, at the inflow side of the orifice the streamlines converge forming an acoustic near field. At high intensity of incident waves with small ratio between diameters of orifice and the tube, a strong acoustic flow through the orifice is formed which ends with sepration of boundry layer and creation of high velocity axial jet. Moreover, if the edges of the orifice are sharp, the streamlines in the jet converge and create vena contracta, i.e. the point in the streamline where its diameter is minimum and the gas velocity is maximum. The viscus interactions of the created jet and inactive surroundings leads to generation of vortex ring which goes away from the orifice and vanishes into turbulence. During the second half cycle, the flow in the orifice of the HR change its direction vortex ring inside the tube is created [Meissner, 1999]. In the theoretical study of Meissner [Meissner, 1999] the pressure domain has been evaluated separately in the zones with rotational and irrotational fluid motions. They found that the the total pressure drop due to creation of jet and vorticity is proportional to the square of the amplitude of the velocity of the orifice [Meissner, 1999]. Ostrovsky [Ostrovsky, 2004] investigated on the wave interactions in acoustic resonators with hysteresis and also without hysteresis but with quadratic and cubic nonlinearities via perturbation technique. To take into account the nonlinearities, they decomposed the one-dimensional nonlinear wave equation to linear and a nonlinear parts which the latter is a higher order term of the perturbation parameter (see Eq. 2 in [Ostrovsky, 2004]). This decomposition has been carried out thanks to separation of the stress-strain relationship into a linear and nonlinear parts. For treating the nonlinear parts of system equations, they distinguished three different cases as: i) nonhysteretic but quadratic stress-strain relation (see Eq. 7 in [Ostrovsky, 2004]); ii) nonhysteretic but cubic stress-strain relation (see Eq. 11 in [Ostrovsky, 2004]) and finally iii) hysteresis stress-strain relation (see Eqs. 15 and 21 in [Ostrovsky, 2004]). Molotkov [Molotkov, 2008] investigated on the hysteresis behaviour in acoustic medium due to the loading and unloading waves including relaxing nonlinearity, i.e. coming back of the perturbed system to its equilibria, and the viscosity. The main challenge in treatment and integration of the evolution equations (see Eq. 1 in [Molotkov, 2008]) was related to the nonlineairity of the system and also that the evolution equations possessed the unknown pressure which should had been determined by solving the problem. The problem has been treated via several methods such as Stokes small- amplitude approximation and also asymptotic small-distance (small-time) and they revealed dependency of the density on pressure evaluated for different types of media and different hysteresis responses [Molotkov, 2008]. Governing nonlinear equations of a HR, with linear restoring forcing term and nonsmooth term of the loss is treated by Singh and Rienstra [Singh and Rienstra, 2014] (see Eq. 9 in the reference). They did an asymptotic analysis via distinguishing resonant and non-resonant cases concluding that near the resonance cases, nonlinear terms can not be neglected in the overall response of the system. Achilleos et al. [Achilleos et al., 2016] studied the linear wave propagation in a waveguide, with a single HR on its side which present the nonsmooth term pf loss (see Eq. 1 in [Achilleos et al., 2016]) demonstrating nonlinear (softening) behaviour between absorption and frequency for different incident amplitudes (see Fig. 2 in [Achilleos et al., 2016]). In terms of considering nonlinear terms of restoring forcing function of a HR, Yu et al. [Yu et al., 2011] investigated on the nonlinear equations of a HR which includes (apart from linear terms) nonsmooth loss and quadratic and cubic terms of restoring forcing functions. They traced a softening response of such resonators.

In following sections a detailed studies are carried out on HR in nonlinear regimes to be used as an absorber for the TET and control of an acoustical mode. In detail, detection of behaviours of HR in nonlinear regimes via analytical, numerical and experimental studies are presented in Sect. 5.5. The TET between an acoustical mode created in a tube and a HR in nonlinear regimes is discussed in Sect. 5.6.

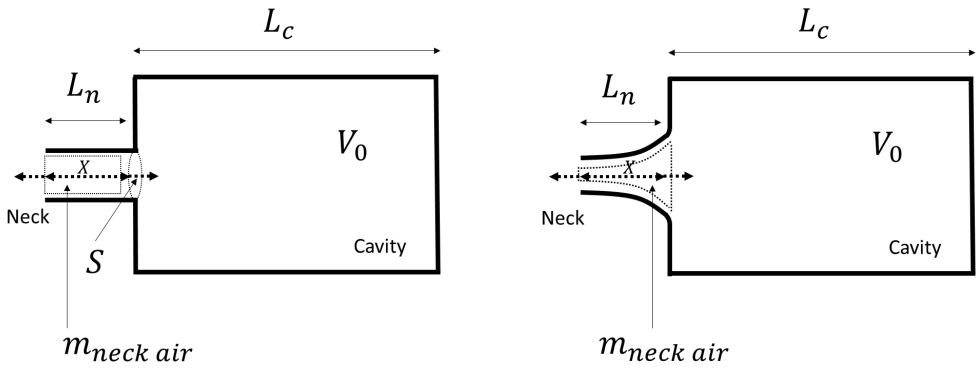

Figure 5.4: Two-dimensional views of two HR with: a) classical neck; b) tailored neck.

5.5 Extreme nonlinear regimes in Helmholtz resonators

In order to prepare analytical tools for detection of nonlinear behaviours of HR and then preparation of design tools, we start we some experiment and then we will validate these results via analytical and numerical obtaining.

5.5.1 Nonlinear behaviours of the HR: preliminary experimental results

Let us consider the academic mode of o HR which is depicted in Fig. 5.4a [Alamo Vargas, 2018, Alamo Vargas et al., 2018]. We suppose that the the air column inside the neck is compressible being responsible for kinetic energy while the the air in the cavity is compressible which is supposed to provide potential energy of the system. Following hypotheses are made over the system behaviours: the transformations inside the acoustic resonator are adiabatic; the length of the neck, L_n, is considered much smaller than length of the cavity, L_c; the mass of the air in the neck, $m_{neck\,air}$, is supposed to be incompressible since the Helmholtz number H_e defined as [Hersh and Walker, 1977, Rienstra and Hirschberg, 2018]:

$$H_e = \frac{fL_n}{c} \tag{5.52}$$

is very small compared to one, i.e. $H_e \ll 1$. The f is the frequency and c the speed of the sound, applied to the segment L_n. Indeed, for the chosen experimental resonator, we obtain $H_e = 0.0072$. The experimental test set-up is depicted in Figs. 5.5 and 5.6. A Kundt tube with a diameter of 4.6 cm is used. A HR is inserted at the end of the tube. A loudspeaker is placed at one side of the tube fed by a B&K® amplifier type 2706. It allows to send noise for a large frequency width. Positions of microphones are clarified in Fig. 5.6: A microphone, $\frac{1}{4}$ inches B&K® type 4178 (embedded to a pre-amplifier B&K® type 2633), is inserted at different positions (M1, M2) of the thin tube and tangential to its wall to measure the sound signals inside the tube without perturbing air displacements. A third position of the microphone (M3) is chosen to be able to measure the sound in the cavity of the resonator. An amplifier B&K® type 2690 treat the signal received by the microphone. The acquisition is carried out by a National Instrument card NI PXI-1031. Characteristics of the tailored HR, with hyperboloid neck, which is illustrated in Fig. 5.4b copy: The cavity length is $L_c = 2.15$ cm. The length of the neck reads $L_n = 9$ mm. The external and internal radius of the neck are $r_{ex} = 2$ mm and $r_{in} = 4$ mm, respectively. A piece of wood is used to create the cavity and the neck geometry of the HR. A rubber layer around the circumference of the piece of wood is used in order to prevent air leakage, see Fig. 5.7. The aim is to obtain

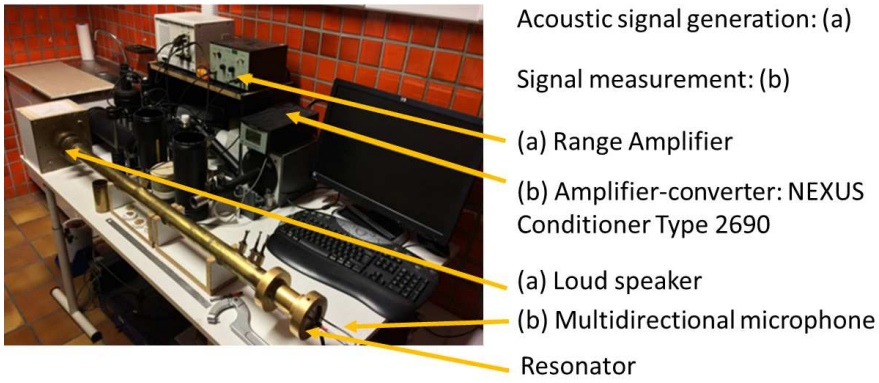

Figure 5.5: Experimental test set-up.

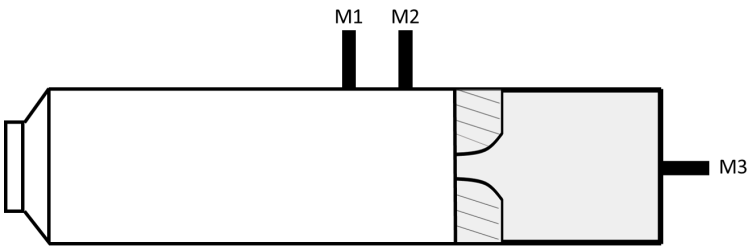

Figure 5.6: Scheme of the Kundt tube with positions of microphone M_1, M_2 and M_3 for measurements of the sound pressure.

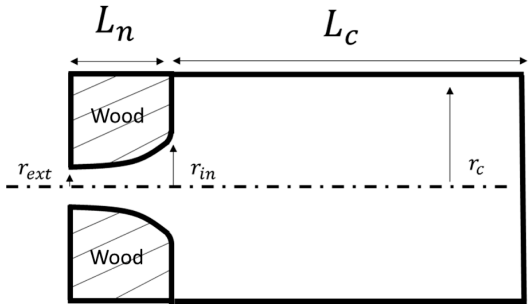

Figure 5.7: The scheme of the HR for the experimental test.

the skeleton curve of the system experimentally. To this end, the frequency is measured when the amplitude of the pressure is maximum. The resonance frequency in linear domain read as $f_0 = 276$ Hz. As for the external excitation, several experimental points for Sound Pressure Level (SPL) with SPL$\in [110, 150]$ dB are chosen. The overall pressure, p_{tot}, is defined as the sum of the atmospheric pressure p_0 and the fluctuation of pressure p' reading as p_{tot}, is $p_{tot} = p_0 + p'$. The ratio $\frac{p'}{p_0}$ calculated for SPL $= 110$ dB and SPL $= 150$ dB are 6.2×10^{-5} and 6.2×10^{-3}, respectively. The results are presented in Fig. 5.8 showing that the system presents hardening behaviour for high intensity pressure levels and slightly softening response for smaller amplitudes. For SPL < 110, there is no frequency shift of the system and so it remains in linear regimes. We only presented results of nonlinear regime in fig. 5.8. These preliminary experimental results provides a motivation to pinpoint governing equations of the HR including nonlinear terms for better understanding its response in nonlinear domains.

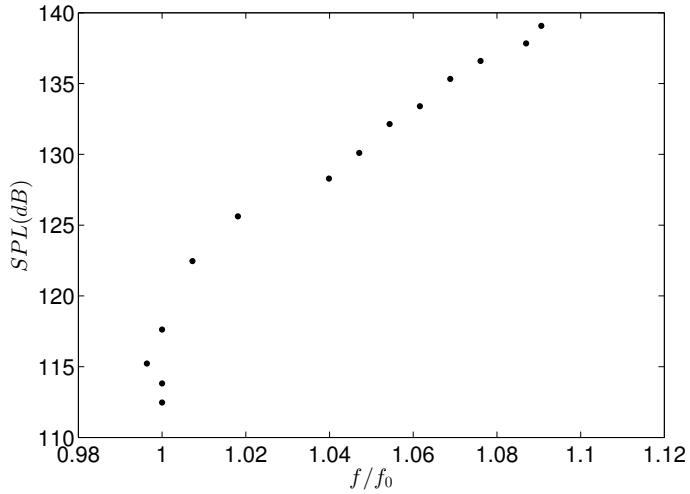

Figure 5.8: Experimental results on the HR with tailored neck. f is frequency of the sinusoidal excitation.

5.5.2 Nonlinear behaviours of the HR: analytical treatments

As it has been clarified already, the potential and kinetic energies of the HR are carried out via the air inside the cavity and the encased mass of the air in the neck, respectively. The friction due to the movement of the air in the neck crates damping [Yu et al., 2011, Singh and Rienstra, 2014]. Generally speaking, several types of damping scenarios exists in a HR: the linear dissipation which originates from thermo-viscous boundary layers and a nonsmooth dissipations which mainly come from vortex shedding [Förner et al., 2015]. Moreover, the geometry of the neck can influence the emerge of the vortex and the dissipation around the neck. In long wave limits, the air in the cavity represents linear and nonlinear restoring forcing functions [Richoux et al., 2007, Yu et al., 2011]. Then, the relation between the displacement of the air in the neck, X and changes the pressure Δp copies [Yu et al., 2011]:

$$\Delta p = -\rho L_e \omega_0^2 \left(X - \frac{(\hat{\gamma}+1)\, S}{2V_0} X^2 + \frac{(\hat{\gamma}+1)\,(\hat{\gamma}+2)\, S^2}{6V_0^2} X^3 \right) \tag{5.53}$$

The ρ is the air density and L_e is the effective length of the neck which reads [Yu et al., 2011]:

$$L_e = L_n + \left(\frac{16r}{3\pi}\right) \tag{5.54}$$

where r is the radius of cylindrical neck, S is the cross section of the neck, V_0 is the volume in the cavity, $\hat{\gamma}$ is the specific heat ratio and ω_0 is the linear resonance frequency of the resonator. Usually the cubic terms of the restoring forcing function are excluded, eg. see [Richoux et al., 2007]. Since are going to study a HR with tailored neck, see Fig. 5.4b, so it will be possible that the vortex and dissipation around the neck are minimized [Förner et al., 2015]. In this case, the HR may present extreme nonlinear responses due to its restoring forcing terms via exploiting more terms of its nonlinearities. To this end, in our study the cubic nonlinearities of the restoring forcing term will be considered [Alamo Vargas, 2018, Alamo Vargas et al., 2018].
The governing equation of the HR under the external pressure variations p' (fluctuation of the pressure around the atmospheric pressure p_0) via considering the momentum equation and conservation of the mass in the real time t^* reads [Alamo Vargas, 2018, Alamo Vargas et al., 2018]:

$$\frac{\mathrm{d}^2X}{\mathrm{d}t^{*2}} + \frac{\xi}{2L_e}\frac{\mathrm{d}X}{\mathrm{d}t^*}\left|\frac{\mathrm{d}X}{\mathrm{d}t^*}\right| + 2\delta^*\frac{\mathrm{d}X}{\mathrm{d}t^*} + \omega_0^2 X\left(1 - \alpha\frac{SX}{V_0} + \beta\left(\frac{SX}{V_0}\right)^2\right) = -\frac{p'}{\rho L_e} \tag{5.55}$$

where

$$\begin{aligned}
\delta^* &= \left(\frac{S}{2\rho L_e}\right)\Re\left(Z_{in} + Z_{vis}\right) \\
\alpha &= \frac{(\hat{\gamma}+1)}{2} \\
\beta &= \frac{(\hat{\gamma}+1)(\hat{\gamma}+2)}{6}
\end{aligned} \tag{5.56}$$

The ξ stands for the total hydraulic-resistance coefficient of the neck. The Z_{in} is the acoustic impedance at inlet of HR, Z_{vis} is the friction acoustic impedance. Let us introduce dimensionless variables as $t = \omega_0 t^*$, $x = \frac{SX}{V_0}$, $\delta = \frac{2\delta^*}{\omega_0}$, $\sigma = \left(\frac{\xi}{2}\right)\left(\frac{V_0}{L_e S}\right)$. We obtain:

$$\frac{\mathrm{d}^2x}{\mathrm{d}t^2} + \sigma\frac{\mathrm{d}x}{\mathrm{d}t}\left|\frac{\mathrm{d}x}{\mathrm{d}t}\right| + \delta\frac{\mathrm{d}x}{\mathrm{d}t} + \left(x - \alpha x^2 + \beta x^3\right) = -p \tag{5.57}$$

where $p = \frac{Sp'}{V_0\omega_0\rho L_e}$. The orders of magnitudes of system parameters play important role in its behaviours. The nonsmooth terms of the dissipation which is represented by the σ parameter, can be neglected in low levels of sound pressure while on high levels this nonlinear damping term is important and is proportional to the ratio of the volume of the cavity and the neck [Yu et al., 2011]. In the very low deriving pressure, the contribution of the nonlinear restoring forcing terms are small compared to the linear damping term. In this case the movement of the air inside the neck can be modelled via a single degree of freedom linear oscillator. For extremely high sound pressure levels, the nonlinear restoring forcing terms dominate the response of the system. So as a summary, depending on system parameters and their order of magnitudes, different dynamical regimes can be faced.
In the following we will identify some of parameters from experimental results.

5.5.2.1 Considered system parameters

As we are considering the air flow, so $\hat{\gamma} = 1.4$. Considering Eq. 5.56, we obtain $\alpha = 1.2$ and $\beta = 1.36$. A very rough approximated method is used for evaluation of damping coefficients:

As shown in Fig. 5.9 a curve is fitted to experimental results. Equation 5.57 is treated via direct integration method for some points of Fig. 5.9 assuming some values for damping coefficients. In Fig. 5.9 and for numerical integrations we suppose that $|p| = \varepsilon^3 F_0$ where with $\varepsilon = 0.1$ is a small parameter. Results of the numerical integrations at steady-state regimes are compared and matched with fitted curve. Identified linear and nonlinear dissipation terms read $\delta = 0.005$ and $\sigma = 0.05$, respectively.

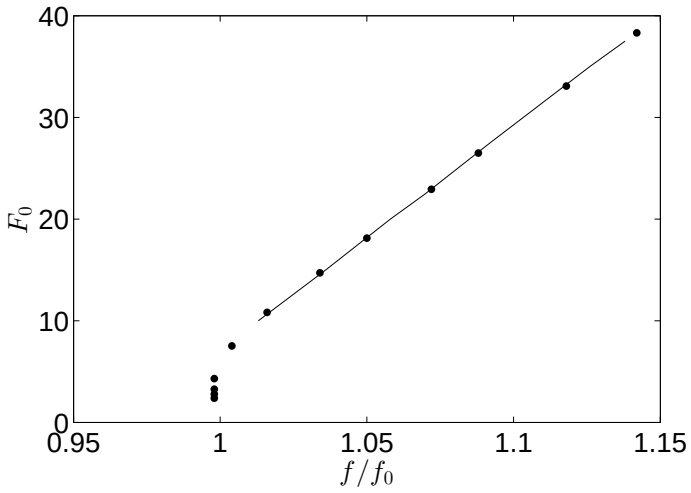

Figure 5.9: Experimental results (•) and the fitted curve (–).

5.5.2.2 Possibility of existence of chaos in the considered system

The described system in Eq.5.57 possesses both quadratic and cubic terms. Such systems can presents chaotic responses [Romeo et al., 2015, Mattei et al., 2016]. Let us suppose that in Eq. 5.57,

$$-p = \zeta F \cos\left(\frac{\omega_f}{\omega_0} t\right) = \zeta F \cos(\Omega t) \tag{5.58}$$

where $\omega_f = 2\pi f$ and f are angular frequency and frequency of the excitation, respectively. Moreover, we set that $\sigma = \zeta\sigma_1$, $\delta = \zeta\delta_1$ where ζ is a small parameter. Equation 5.57 is reorganized as:

$$\begin{cases} \dfrac{\mathrm{d}x}{\mathrm{d}t} = \mathfrak{z} \\ \dfrac{\mathrm{d}\mathfrak{z}}{\mathrm{d}t} = -x + \alpha x^2 - \beta x^3 + \zeta\left(F\cos(\Omega t) - \sigma_1 \mathfrak{z}\,|\mathfrak{z}| - \delta_1 \mathfrak{z}\right) \end{cases} \tag{5.59}$$

It is seen that the Eq. 5.59 is represented in the form of unperturbed and perturbed part coupled to each other via ζ parameter. The unperturbed part of the Eq. 5.59, i.e. the case when $\zeta = 0$, is a Hamiltonian system, i.e.

$$\begin{cases} \dfrac{\partial H}{\partial \mathfrak{z}} = \dfrac{\mathrm{d}x}{\mathrm{d}t} = \mathfrak{z} \\ -\dfrac{\partial H}{\partial x} = \dfrac{\mathrm{d}\mathfrak{z}}{\mathrm{d}t} = -x + \alpha x^2 - \beta x^3 \end{cases} \tag{5.60}$$

where the Hamiltonian functions reads:

$$H(x,\mathfrak{z}) = \frac{1}{2}\mathfrak{z}^2 + \frac{1}{2}x^2 - \frac{1}{3}\alpha x^3 + \frac{1}{4}\beta x^4 \tag{5.61}$$

Let us seek critical points of the Hamiltonian which are in fact fixed points of Hamilton's system 5.60 [Guckenheimer and Holmes, 1983]. Let us set: $\frac{\partial H}{\partial x} = 0$. With provided experimental values for system parameters in our work, i.e., $\hat{\gamma} = 1.4$ for air, so $\alpha = 1.2$ and $\beta = 1.36$, then $\alpha^2 - 4\beta < 0$. This fact clarifies that the system possesses only one fixed point which reads $(0,0)$. It is also seen that:

$$\frac{\mathrm{d}H}{\mathrm{d}t} = \frac{\partial H}{\partial x}\frac{\partial x}{\partial t} + \frac{\partial H}{\partial \mathfrak{z}}\frac{\partial \mathfrak{z}}{\partial t} = \frac{\partial H}{\partial x}\frac{\partial H}{\partial \mathfrak{z}} - \frac{\partial H}{\partial \mathfrak{z}}\frac{\partial H}{\partial x} \equiv 0 \tag{5.62}$$

which means that all level curves $H(x,\mathfrak{z})$ =constant, stand for solution curves for Eq. 5.60. In order to check the possibility of existence of chaos by the Melnikov function [Guckenheimer and Holmes, 1983] one should evaluate the unperturbed homoclinic orbits traced by $H = 0$,

$$\left(\frac{dx}{dt}\right)^2 = -x^2\left(1 - \frac{2}{3}\alpha x + \frac{1}{2}\beta x^2\right) \tag{5.63}$$

Due to parameters α and β of our experimentations, we obtain $\frac{4}{9}\alpha^2 - 2\beta < 0$, meaning that we

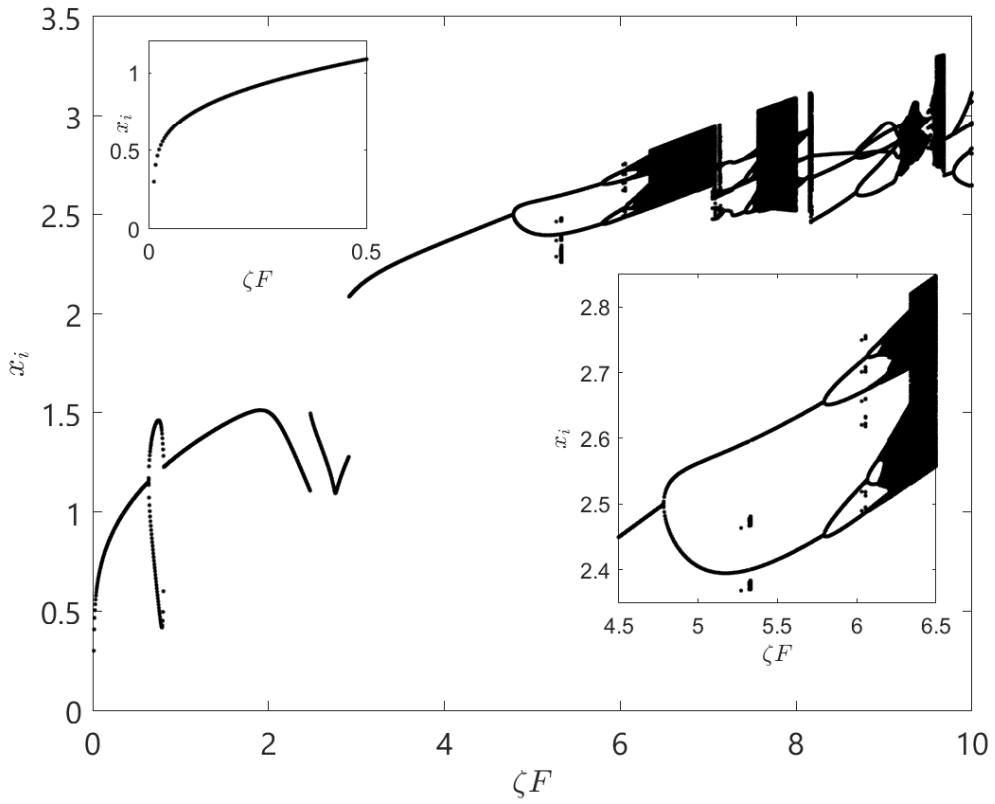

Figure 5.10: Bifurcation diagram obtained from direct integrations of Eq. 5.59 at $\Omega = 1.01$.

can not use Melnikov function for tracing chaos. However, the system can experience chaos without

possessing any homoclinic orbit. In this case numerical techniques should be exploited for tracing chaos. To this end, we endow Poincaré sections and bifurcation diagrams via direct numerical integration of the system 5.59. The Orbit Diagram (or bifurcation diagram) of the Eq. 5.59 at $\Omega = 1.01$ is presented in Fig. 5.10. The stroboscopic sections are selected at each period of external excitation after very long times for different amplitude of excitation ζF. It is seen that selected points at stroboscopic sections, i.e. x_i, and for each external excitations amplitude, i.e. ζF, can count one or several points. It is seen that some forcing amplitudes correspond to a single periodic

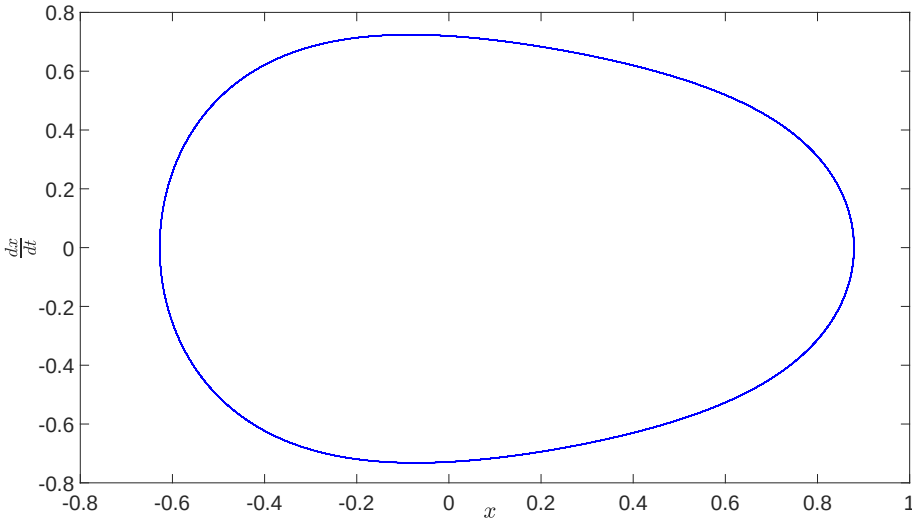

(a)

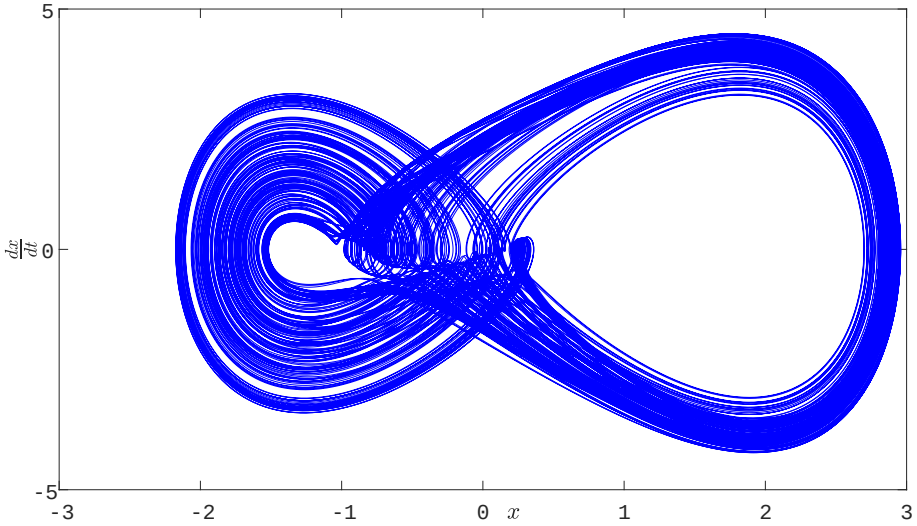

(b)

Figure 5.11: Phase portraits of Eq. 5.59 for the system under two different external excitation amplitudes: a) $\zeta F = 0.2$–Periodic behaviour; b) $\zeta F = 7$–Chaotic behaviour.

solutions, e.g. $\zeta F = 0.2$, while some of the possesses multiple points, for instance $\zeta F = 0.2$, indicating the possibility of existence of chaos in the system. Phase portraits of each case are presented in Fig. 5.11: It is seen that the system under $\zeta F = 0.2$ presents periodic behaviour, see Fig. 5.11a, while the same system under $\zeta F = 7$ presents chaotic response as depicted in Fig. 5.11b. This chaotic response has been confirmed by numerical evaluation of Lyapunov exponent.

Figure 5.10 shows that the possibilities of chaotic responses emerge at very high forcing amplitudes. For a wide variation gaps of Ω and for $\zeta F < 0.5$, only periodic solutions have been spotted. It should be mentioned that for our experimentation, $\zeta F = 0.0383$ corresponds to a 136 dB which is already a very high sound amplitude. That is why for our system under consideration and its applications, reaching to chaotic behaviours is not possible.
In the next section, we will treat the system via multiple scale method which will be compared with numerical and experimental results.

5.5.2.3 Treatment of system equations with the multiple-scale method

Let us study the behaviour of the system which is described in Eq.5.57 with the multiple-scale method [Nayfeh and Mook, 1979]. We assume that the system presents small scaled displacement, so we set $x = \varepsilon y$ with $0 < \varepsilon \ll 1$. Moreover, we set that $\delta = \varepsilon^2 r_2$, $\sigma = \varepsilon r_1$ and $p = \varepsilon^3 F_0 \cos(\Omega t)$. We are interested to trace system behaviours around a $1:1$ resonance. To this end, we set $\Omega = 1 + \varepsilon^2 \mu$ where μ is the detuning parameter. Equation 5.57 reads:

$$\frac{\mathrm{d}^2 y}{\mathrm{d}t^2} + \varepsilon^2 r_1 \frac{\mathrm{d}y}{\mathrm{d}t}\left|\frac{\mathrm{d}y}{\mathrm{d}t}\right| + \varepsilon^2 r_2 \frac{\mathrm{d}y}{\mathrm{d}t} + y - \varepsilon\alpha y^2 + \varepsilon^2 \beta y^3 = \varepsilon^2 F_0 \cos(\Omega t) \tag{5.64}$$

Some preliminary numerical studies To have an overall idea about system behaviours, before applying the multiple scale methods, we take the direct numerical integration of the Eq. 5.64 with the Runge-Kutta method. We set system parameters (experimental ones) as: $\sigma = 0.05$, $\delta = 0.005$, $\alpha = 1.2$, $\beta = 1.36$ with varying forcing amplitudes from with $F_0 = 0.1$ to $F_0 = 12.1$. We collect results after long time enough in order to be sure that we collect data during stationary regimes of the system. Results are illustrated in Fig. 5.12 in terms of $|x|$, see Fig. 5.12. It is seen that for lower amplitudes the resonator presents softening behaviour, i.e. resonance frequency decreases with increasing amplitudes. This behaviour is transferred to the hardening response when the amplitude of excitation increases. The Strouhal number [Blevins, 2006] which is dimensionless parameter, is commonly used as indication of the predominant vortex shedding frequency. This number is defined as [Blevins, 2006]:

$$S_r = 0.198\left(1 - \frac{19.7}{R_e}\right) \tag{5.65}$$

where R_e stands for the Reynolds number which is defined as:

$$R_e = \frac{v L_{car} \rho}{\nu} \tag{5.66}$$

where L_{car} is the characteristic length and ν is the fluid viscosity. The change of the structure of the flow can be associated with the variation of the Strouhal number. These variation are depicted in Fig. 5.12. It can be observed that this value is very close to 0.2. Moreover, we claim that the Strouhal number reaches to its stable value when the forcing term increases, which indicates that vortex shedding effects are limited when forcing terms becomes higher and so the effects of nonlinear restoring forcing function become more evident. Typically in acoustics and for some fixed system parameters, i.e. α, β, either softening or hardening responses are observed. In the presented work, both responses for the same system parameters are observed by varying excitation amplitude thanks to quadratic and cubic nonlinearities of the restoring forcing function which are presented in Eq. 5.53. This behaviour is observed experimentally, see Fig. 5.8 and numerically as illustrated in Fig. 5.12 [Alamo Vargas, 2018, Alamo Vargas et al., 2018]. Generally speaking, the quadratic term creates softening response while the cubic term is responsible of the hardening response. The comparison of experimental results and numerical ones are shown in Fig. 5.13 showing a good agreement between two types of results. However, we should claim that by increasing the forcing

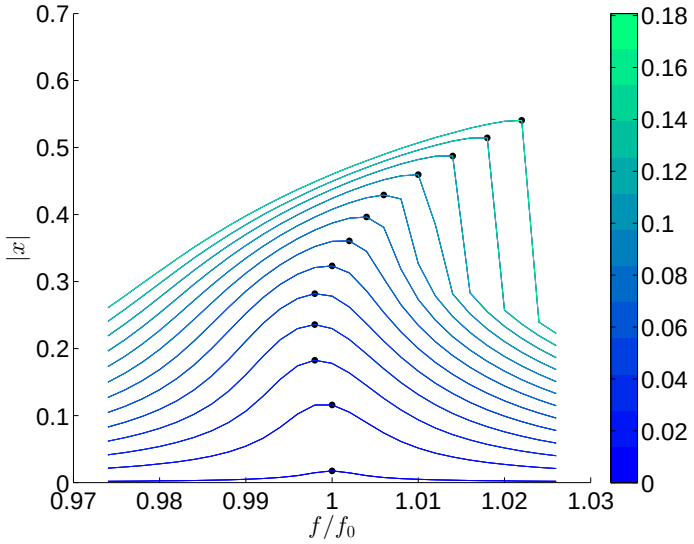

Figure 5.12: Results obtained from direct numerical integration of the Eq. 5.64 (-) and corresponding skeleton curve (•). $|x|$ versus $\Omega = \frac{f}{f_0}$. Variations of Strouhal numbers are provided in the form of the coloured bar at the right hand side of the figure.

terms both results will disperse as different order of developments should be taken into account as for instance is explained in Eq. 5.53. In the followings the system is treated via the multiple scale method for the system with two types of excitations namely, high and very high.

The system under high amplitude excitations Let us express the variable y in Eq. 5.64 as:

$$y = y_0 + \varepsilon y_1 + \varepsilon^2 y_2 + \mathcal{O}\left(\varepsilon^3\right) \tag{5.67}$$

and we define fast and slow time scales as:

Fast Time Scale: $T_0 = \varepsilon^0 t$

Slow Time Scale: $T_1 = \varepsilon^1 t, T_2 = \varepsilon^2 t, \ldots$

Equation 5.64 at different orders of ε reads:

- $\mathcal{O}(\varepsilon^0)$

$$\frac{\partial^2 y_0}{\partial T_0^2} + y_0 = 0 \tag{5.68}$$

- $\mathcal{O}(\varepsilon^1)$

$$2\frac{\partial^2 y_0}{\partial T_0 \partial T_1} + \frac{\partial^2 y_1}{\partial T_0^2} + y_1 - \alpha y_0^2 = 0 \tag{5.69}$$

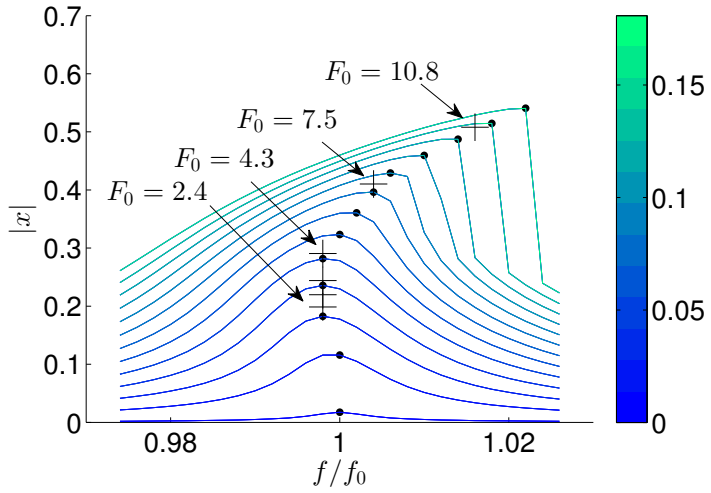

Figure 5.13: Results obtained from direct numerical integration of the Eq. 5.64 (-), corresponding skeleton curve (•) and experimental results collected from low forcing terms, F_0, (+) of the Fig. 5.9. $|x|$ versus $\Omega = \dfrac{f}{f_0}$. Variations of Strouhal numbers are provided in the form of the coloured bar at the right hand side of the figure.

- $\mathcal{O}(\varepsilon^2)$

$$2\frac{\partial^2 y_0}{\partial T_0 \partial T_2} + \frac{\partial^2 y_0}{\partial T_1^2} + 2\frac{\partial^2 y_1}{\partial T_0 \partial T_1} + \frac{\partial^2 y_2}{\partial T_0^2} + r_1 \frac{\partial y_0}{\partial T_0}\left|\frac{\partial y_0}{\partial T_0}\right| + r_2 \frac{\partial y_0}{\partial T_0} + y_2 - 2\alpha y_0 y_1 + \beta y_0^3 = \frac{F_0}{2}\left(e^{i(T_0+\mu T_2)} + e^{-i(T_0+\mu T_2)}\right) \tag{5.70}$$

The solution of Eq. 5.68 reads:

$$y_0 = A\left(T_1, T_2, T_3, ...\right) e^{iT_0} + A^*\left(T_1, T_2, T_3, ...\right) e^{-iT_0} \tag{5.71}$$

After introducing Eq. 5.71 in Eq. 5.69 we have

$$\begin{aligned} A &= A\left(T_2, T_3, ...\right) \\ y_1 &= -\frac{1}{3}\alpha A^2 e^{2iT_0} + 2\alpha A A^* - \frac{1}{3}\alpha A^{*2} e^{-2iT_0} \end{aligned} \tag{5.72}$$

Via defining $A = \hat{y}e^{i\gamma}$, Eq. 5.70 copies

$$\begin{cases} \hat{y}\dfrac{\partial \Delta}{\partial T_2} = -\hat{y}\mu - \dfrac{F_0}{4}\cos\left(\Delta\right) + \hat{y}^3\left(\dfrac{3}{2}\beta - \dfrac{5}{3}\alpha^2\right) \\ \dfrac{\partial \hat{y}}{\partial T_2} = -\dfrac{F_0}{4}\sin\left(\Delta\right) - \dfrac{r_2}{2}\hat{y} - r_1\hat{y}^2\left(\dfrac{8}{3\pi}\right) \end{cases} \tag{5.73}$$

where $\Delta = \gamma - \mu T_2$. Treatment of Eq. 5.73 can be carried out via nonsmooth time transformation method [Pilipchuk, 2010]. A very similar system to Eq. 5.73 is analysed via the mentioned

technique by Ture Savadkoohi et al. [Ture Savadkoohi et al., 2011a] in the domain of mechanics. Here, we are interested in analysing equilibrium points of the system which are obtained via setting $\frac{\partial \Delta}{\partial T_2} = \frac{\partial \hat{y}}{\partial T_2} = 0$. For all experimental system parameters which are provided in Sect. 5.5.2.1, Eq. 5.73 is solved at its equilibrium points. Results obtained from this analytical developments and corresponding numerical ones obtained from direct integration of the Eq. 5.64 are presented in Fig. 5.14. It is seen that analytical predictions are matched with results obtained from direct numerical integration. However, if the amplitude of excitation is increased, the analytical developments depart

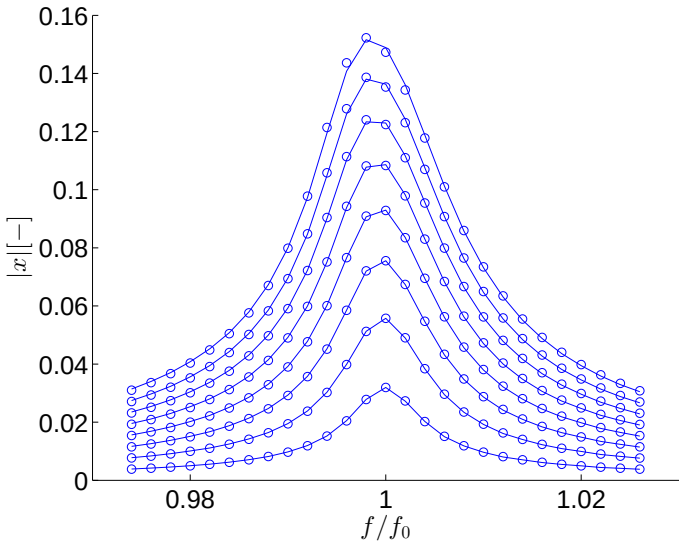

Figure 5.14: Results obtained from Eq. 5.73 at its equilibrium points (o) and those which are obtained from direct numerical integration of Eq. 5.64 (-). The system is under external excitation as $F_0 \in [0.2, 1.6]$ with step of 0.2.

from numerical results, see Fig. 5.15. For instance, see the presented curves for the case of $F_0 = 8$: analytical developments show a softening behaviour for the system while numerical results presents hardening response which is identical to experimental results. This mismatching is due to the fact that with increasing the forcing amplitude we do not respect the basic assumption for our developments leading to Eq. 5.64, i.e. $|p| = \mathcal{O}(\varepsilon^3)$ or $|p| = \varepsilon^3 F_0$ leading to abusing the assumption of $x = \varepsilon y$. In the next paragraph, we will deal with such a case when the amplitude of the excitation copies very high levels.

The system under very high amplitude excitations Let us assume that x stays at the order 1 and we suppose that $y = \mathcal{O}(\frac{1}{\varepsilon})$, leading to $x = y$. Moreover, we set: $r_2 = \dfrac{\hat{r}_2}{\varepsilon}$, $\alpha = \varepsilon^* \alpha_1$, $\beta = \varepsilon^* \beta_1$ and $F_0 = \dfrac{\hat{F}_0}{\varepsilon^2}$. Here, for the case of simplifications, we consider that $\varepsilon^* = \varepsilon$. Equation 5.64 yields to

$$\frac{d^2x}{dt^2} + \varepsilon r_1 \frac{dx}{dt}\left|\frac{dx}{dt}\right| + \varepsilon \hat{r}_2 \frac{dx}{dt} + x - \varepsilon \alpha_1 x^2 + \varepsilon \beta_1 x^3 = \varepsilon \hat{F}_0 \cos(\Omega t) \tag{5.74}$$

The $1:1$ resonance condition is imposed via setting: $\Omega = 1 + \varepsilon\mu$. From Eq. 5.74 it is seen that the quadratic and cubic nonlinearities of the restoring forcing function become at the same order being

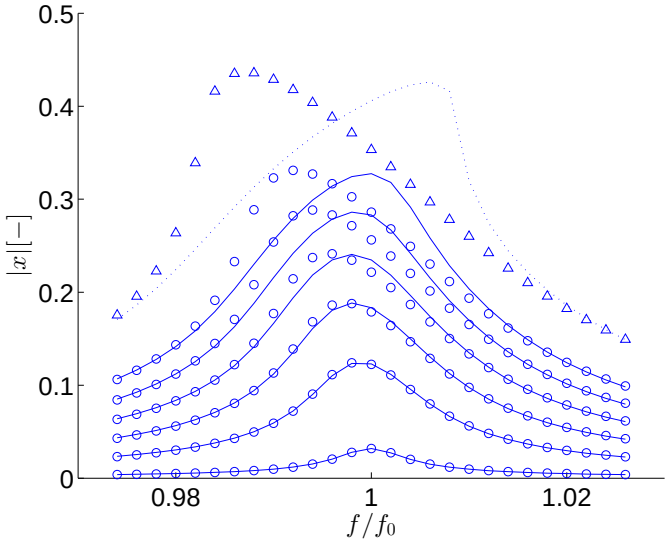

Figure 5.15: Results obtained from Eq. 5.73 at its equilibrium points (o) and those which are obtained from direct numerical integration of Eq. 5.64 (-). The system is under external excitation as $F_0 \in [0.2, 5.2]$ with step of 1. The curve $\triangle$ presents results obtained from analytical developments for the system with $F_0 = 8$, while the dotted curve $(\dots)$ is obtained from numerical integrations.

$\mathcal{O}(\varepsilon)$. Via the multiple scale method we reach finally to:

$$\begin{cases} \hat{x}\dfrac{\partial \Delta}{\partial T_1} = -\dfrac{\hat{F}_0}{4}\cos(\Delta) - \mu\hat{x} + \hat{x}^3\left(\dfrac{3}{2}\beta_1\right) \\ \dfrac{\partial \hat{x}}{\partial T_1} = -\dfrac{\hat{F}_0}{4}\sin(\Delta) - \dfrac{\hat{r_2}}{2}\hat{x} - r_1\hat{x}^2\left(\dfrac{8}{3\pi}\right) \end{cases} \tag{5.75}$$

Equations 5.73 and 5.75 are very similar except the missing coefficient α_1 in Eq. 5.75 representing the quadratic term of the restoring forcing function. Figure 5.16 collects obtained results at the equilibrium points of the Eq. 5.75 and those which are obtained by direct numerical integration of Eq. 5.74 at the stationary regimes for the system under excitations amplitudes $\hat{F}_0 \in [0.03, 0.12]$. It is seen that results match each other. Moreover, this behaviour is coherent with numerical and experimental results which are illustrated in Fig. 5.13.

5.5.2.4 Summary and observations

The HR with the nonlinear restoring forcing function, including linear, quadratic and cubic terms, completed by linear and nonsmooth dissipation terms is considered. Developed analytical techniques, obtained from multiple scale method, are matched with experimental and numerical results showing a good agreements if we respect the order of magnitudes of system parameters such as amplitude of the excitation. Otherwise, different orders should be considered and developed in multiple scale methods. The HR at high levels of excitations presents softening, mainly due to quadratic term of restoring forcing function, and hardening response resulting from cubic term of the restoring forcing function.
The coefficients of the cubic and quadratic terms depend only on the specific heat ratio; so from physical view point, and for a given geometry of HR, these coefficients are fixed and that is why the

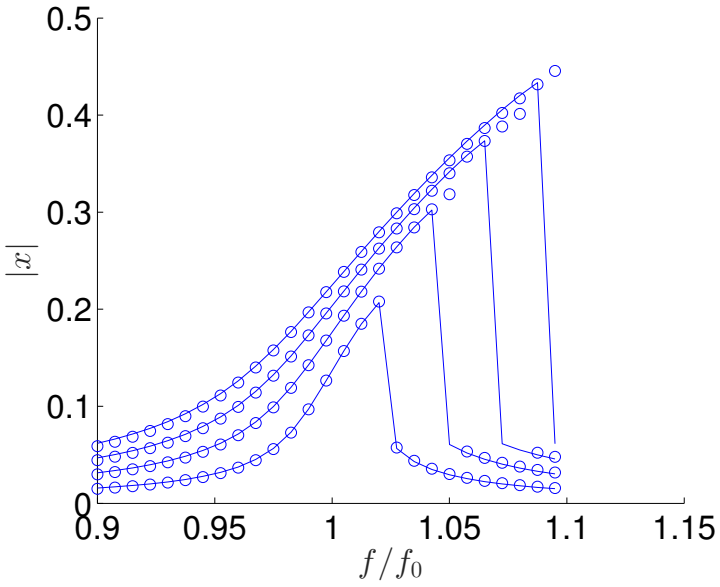

Figure 5.16: Results obtained from Eq. 5.75 at its equilibrium points (o) and those which are obtained from direct numerical integration of Eq. 5.74 (-). The system is under external excitation as $\hat{F}_0 \in [0.03, 0.12]$ with step of 0.03. The parameters of the system are: $\sigma = 0.05$, $\delta = 0.005$, $\beta_1 = 13.6$. The α_1 parameter is ignored in numerical simulations to be consistent with Eq. 5.75.

softening or hardening behaviours depend only on amplitude of excitation. If nonsmooth term of dissipation which is due to the vortex and jet phenomenon is too high, then reaching to hardening response of the system is difficult. In HR with the classical neck, jet phenomenon and vortex are more evident for very high amplitudes and only softening behavior can be observed. The tailored neck lowers the effects of the vortex phenomenon for high amplitudes leading to hardening behaviour. If the geometry of the neck is not fixed, then the ratio of the neck surface to cavity volume must be high to reach to hardening domains.
These developments show that the HR with nonlinear responses at high levels of excitations can be exploited as a pure acoustical resonators to be coupled to acoustical mode(s) for triggering their acoustical energies in a one way and irreversible manner.
The next section, discusses about passive control of an acoustical mode via a HR with nonlinear response in nonlinear regime.

5.6 Nonlinear energy exchanges between an acoustical mode and a Helmholtz resonator with nonlinear behaviours

As introduced in Sect. 5.3, the nonlinear passive control process in acoustics using a mechanical system, i.e. visco-elastic membrane, has been successfully applied by Cochelin et al. [Cochelin et al., 2006] using a simple test set-up. Further studies have been carried out in the recent years in this domain which we list some of them: the targeted energy transfer from an acoustical mode to a nonlinear membrane articulated by Bellet et al. [Bellet et al., 2010]. Their test set-up included a tube with variable length, for creation of an acoustical mode, a coupling box and a visco-elastic membrane representing the nonlinear absorber. During free and forced exci-

tations, the efficient targeted energy transfers have been observed due to the nonlinearity of the membrane leading to controlling the acoustical mode. Later on they enhanced the efficiency of the energy transfer via using several nonlinear membranes in parallel [Bellet et al., 2012]. Mariani et al. [Mariani et al., 2011] replaced the nonlinear membrane by a loudspeaker used as suspended piston, as a nonlinear absorber. They carried out some experimental studies using different types of loudspeakers showing the possibility of the transferring acoustical energy inside the tube to the nonlinear absorber represented by the loudspeaker in low frequency domains. The targeted energy transfer between an acoustic medium inside a parallelepiped cavity and a viscoelastic membrane placed on one of surfaces of the cavity has been investigated by Shao and Cochelin [Shao and Cochelin, 2014] analytically and numerically. After deriving governing system equations, a harmonic balance technique, via using first harmonics, has been used. The expressions of nonlinear normal modes and then periodic responses of the system under external excitations with stability studies are analysed. The study permits to enlighten the energy exchanges between one mode inside the cavity and the membrane on one ot its wall. The study of a nonlinear vibroacsotuc absorber, i.e. a membrane, at low frequency domains namely in $[10, 200]$ Hz and high pressure levels, typically several hundreds of Pascals, has been studied by Chauvin et al. [Chauvin et al., 2018]. According to their test set-up, they showed that the membrane, via exploiting its nonlinear behaviours, cancelled up to 90% of the incoming acoustic waves around an amplitude-dependent frequency.
All of above mentioned studies and realizations, exploit nonlinear behaviours of a mechanical systems, namely viscoelastic membranes. However, we are interested in exploiting nonlinear capacities of pure acoustical resonators for nonlinear passive noise control, similar to the function of classical Helmholtz resonators for linear passive noise control [Helmholtz, 1863]. In Sect. **??** we showed the existence of nonlinear behaviours of the HR in nonlinear domains. In this section a HR with nonlinear behaviour is coupled to an acoustical mode, produced in a tube, for the aim of passive noise control [Alamo Vargas, 2018, Gourdon et al., 2018].

5.6.1 Governing system equations and the general methodology

Let us consider the academic model of a HR with the cylindrical neck which is presented in Fig. 5.17. Detailed governing equation for such resonator in nonlinear domain is presented and discussed in Sect. 5.4. The length of the neck, L_n, is supposed to be very small with respect to the length of the cavity denoted as L_{cav}. The mass of the air inside the neck, m_2, is considered as incompressible, experiencing the displacement U_2. The the radius and the section of the neck are presented by r_2 and S_2, respectively, while L_{cav} and V_{cav} stand for the length and volume of the cavity, respectively. As discussed in Sect. 5.4 and is highlighted by Alamo Vargas et al. [Alamo Vargas, 2018, Alamo Vargas et al., 2018] tailoring the geometry of the neck reduces vortex forcing the system to present more hardening behaviour with the increase of sound pressure amplitudes. In this section, we are interested to couple this HR with nonlinear behaviour to an acoustical mode. To do so, we consider the schematic model of the set-up which is depicted in Fig. 5.18. The acoustical mode can be produced due to endowing a tube with small diameter: p_{ls} reads the pressure in the neighbourhood of the loudspeaker, p_{cb} stands for the pressure in the coupling box, while p_{cav} represents the pressure inside the cavity of the HR. Characteristics of the tube with small diameter is as it follows: r_1, S_1 and L_1 are its radius, cross section and length, respectively, and the mass of the air inside it is m_1 with the displacement U_1. The coupling box has the diameter of r_{cb}, the length as L_{cb} and the volume as V_{cb}. In the following, we will present governing equations of each part of the set-up and then equations of the overall set-up will be derived.
Let us consider the tube with small diameter: We take into account conservation of the mass of a single-dof system in X direction of ideal incompressible air. Equation 5.37, reads:

$$\frac{1}{c_0^2}\frac{\partial p}{\partial t} + \rho \frac{\partial}{\partial X}\left(\frac{\partial U_1}{\partial t}\right) = 0 \tag{5.76}$$

or

$$p = -\rho c_0^2 \frac{\partial U_1}{\partial X} \tag{5.77}$$

where c_0 is the sound speed in the air. Generalized movement equations (or equations of propagations) which is defined in Eq. 5.5, for this case reads:

$$\rho \frac{\partial^2 U_1}{\partial t^2} = -\frac{\partial p}{\partial X} \tag{5.78}$$

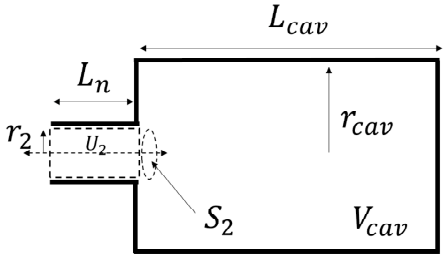

Figure 5.17: Academic model of a HR with cylindrical neck.

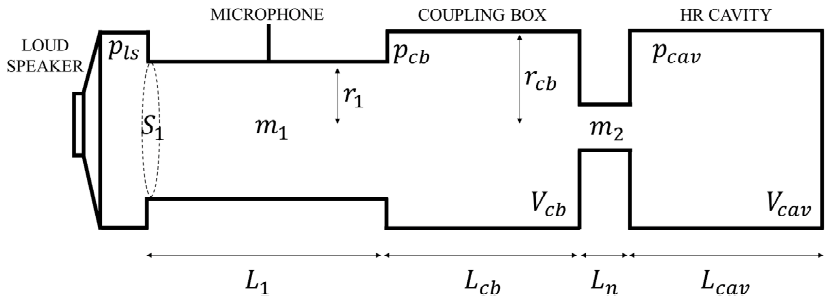

Figure 5.18: Academic model of coupling an acoustical mode to a HR: a tube with small diameter is coupled to the HR via a coupling box.

Injecting Eq. 5.77 in 5.78 and multiplying the system by S_1, we obtain:

$$\rho S_1 \frac{\partial^2 U_1}{\partial t^2} = \rho c_0^2 S_1 \frac{\partial^2 U_1}{\partial X^2} \tag{5.79}$$

We use variational form of the Eq. 5.79 as:

$$\int_0^{L_1} \rho S_1 \frac{\partial^2 U_1}{\partial t^2} \delta U_1 dX = \int_0^{L_1} \rho c_0^2 S_1 \frac{\partial^2 U_1}{\partial X^2} \delta U_1 dX \tag{5.80}$$

which leads to

$$\int_0^{L_1} \rho S_1 \frac{\partial^2 U_1}{\partial t^2} \delta U_1 dX = -\int_0^{L_1} \rho S_1 c_0^2 \frac{\partial U_1}{\partial X} \frac{\partial \delta U_1}{\partial X} dX - p_{cb}(t) S_1 \delta U_1(L_1, t) + p_{ls}(t) S_1 \delta U_1(0, t) \tag{5.81}$$

Let us introduce

$$U_1(X,t) = U_{1a}(t)\left(-\cos\left(\frac{\pi X}{L_1}\right)\right)$$
$$\delta U_1(X,t) = \delta U_{1a}(t)\left(-\cos\left(\frac{\pi X}{L_1}\right)\right) \tag{5.82}$$

and we set $p_{cb} = -\rho c_0^2 \dfrac{\partial U_1(L_1,t)}{\partial X}$ and $p_{ls} = -\rho c_0^2 \dfrac{\partial U_1(0,t)}{\partial X}$. Equations 5.81 yields to:

$$\left(\frac{\rho S_1 L_1}{2}\right)\frac{\mathrm{d}^2 U_1}{\mathrm{d}\,t^2} + \left(\frac{\rho S_1 c_0^2 \pi^2}{2L_1}\right) U_1 = p_{ls}S_1 - p_{cb}S_1 \tag{5.83}$$

In obtaining Eq. 5.83, the nonconservative works of the system are ignored. Normally, they system presents such losses. To take into account the nonconservative works, we consider a damping coefficient c_1 in Eq. 5.83. It reads:

$$m_1\frac{\mathrm{d}^2 U_1}{\mathrm{d}\,t^2} + c_1\frac{\mathrm{d}\,U_1}{\mathrm{d}\,t} + k_1 U_1 = p_{ls}S_1 - p_{cb}S_1 \tag{5.84}$$

with $m_1 = \dfrac{\rho S_1 L_1}{2}$, $k_1 = \dfrac{\rho S_1 c_0^2 \pi^2}{2L_1}$. Equation 5.77 can be used for evaluation of the pressure inside the coupling box, i.e. p_{cb} as a function of the variation of the volume. This pressure is supposed to be constants which reads:

$$p_{cb} = -\rho c_0^2 \frac{\Delta V_{cb}}{V_{cb}} \tag{5.85}$$

After setting $k_b = \dfrac{\rho c_0^2}{V_{cb}}$ it yields to:

$$p_{cb} = -k_b\left(S_2U_2 - S_1U_1\right) \tag{5.86}$$

Let us set the sound source or the loudspeaker as:

$$p_{ls} = F\cos(\omega_f t) \tag{5.87}$$

Then, the equation of the produced acoustical mode inside the tube which is clarified in Eq. 5.84 copies:

$$m_1\frac{\mathrm{d}^2 U_1}{\mathrm{d}\,t^2} + c_1\frac{\mathrm{d}\,U_1}{\mathrm{d}\,t} + k_1U_1 - S_1k_b\left(S_2U_2 - S_1U_1\right) = F\cos(\omega_f t) \tag{5.88}$$

As the HR is coupled to the stub for controlling the produced acoustical mode, we need to provide governing equations of the HR in the considered system. We exploit Eq. 5.55 for the system under consideration:

$$m_2\frac{\mathrm{d}^2 U_2}{\mathrm{d}\,t^2} + \frac{\xi^*}{2L_e}\frac{\mathrm{d}\,U_2}{\mathrm{d}\,t}\left|\frac{\mathrm{d}\,U_2}{\mathrm{d}\,t}\right| + 2\delta^*\frac{\mathrm{d}\,U_2}{\mathrm{d}\,t} = p_{cb}S_2 - p_{cav}S_2 \tag{5.89}$$

with $m_2 = \rho L_e S_2$ where S_2 and L_e copy the cross section of the cylindrical neck and its effective length (taking into account Rayleigh corrections), respectively. The parameter $\xi^* = \xi m_2$ where ξ stands for the coefficient of total hydraulic resistance of the neck of HR. Moreover, $\delta^* = \delta m_2$, while $\delta = \left(\dfrac{S_2}{2\rho L_e}\right)\Re\left(Z_{in} + Z_{vis}\right)$, where Z_{in} is the acoustic impedance at the HR in loudspeaker side and Z_{vis} reads the impedance of the acoustic friction. The $\Re$ stands for the real part of a complex variable. As presented in [Yu et al., 2011] and [Alamo Vargas, 2018, Alamo Vargas et al., 2018] and discussed in detail in Sect. 5.5, we assume that air inside the cavity of the HR represents a

restoring forcing function combining linear, quadratic and cubic effects. Using Eq. 5.53 we can write:

$$p_{cav} = \rho L_e \omega_{hr}^2 \left(U_2 - \frac{(\hat{\gamma}+1)\, S_2}{2V_{cav}} U_2^2 + \frac{(\hat{\gamma}+1)\,(\hat{\gamma}+2)\, S_2^2}{6V_{cav}^2} U_2^3 \right) \tag{5.90}$$

where ω_{hr} is the angular frequency of the HR which is which results from the linear behaviour of the HR. Equation 5.89 becomes:

$$\begin{aligned} &m_2 \frac{d^2U_2}{dt^2} + \frac{\xi^*}{2L_e} \frac{dU_2}{dt} \left| \frac{dU_2}{dt} \right| + 2\delta^* \frac{dU_2}{dt} = \left(\frac{c_0^2 \rho S_2}{V_{cb}} \right) (S_1 U_1 - S_2 U_2) \\ &-\rho L_e \omega_{hr}^2 S_2 \left(U_2 - \frac{S_2}{V_{cav}} \alpha U_2^2 + \frac{S_2^2}{V_{cav}^2} \beta U_2^3 \right) \end{aligned} \tag{5.91}$$

where $\alpha = \dfrac{\hat{\gamma}+1}{2}$ and $\beta = \dfrac{(\hat{\gamma}+1)(\hat{\gamma}+2)}{6}$. Then, governing equations of the system presented in Fig. 5.18 yields to:

$$\begin{cases} m_1 \dfrac{d^2U_1}{dt^2} + c_1 \dfrac{dU_1}{dt} + k_1 U_1 - \dfrac{c_0^2 \rho S_1}{V_{cb}} (S_2 U_2 - S_1 U_1) = F \cos(\omega_f t) \\ \\ m_2 \dfrac{d^2U_2}{dt^2} + \dfrac{\xi^*}{2L_e} \dfrac{dU_2}{dt} \left| \dfrac{dU_2}{dt} \right| + 2\delta^* \dfrac{dU_2}{dt} + \dfrac{c_0^2 \rho S_2}{V_{cb}} (S_2 U_2 - S_1 U_1) \\ +\rho L_e \omega_{hr}^2 S_2 \left(U_2 - \dfrac{S_2}{V_{cav}} \alpha U_2^2 + \dfrac{S_2^2}{V_{cav}^2} \beta U_2^3 \right) = 0 \end{cases} \tag{5.92}$$

Equation 5.92 can be treated with detailed methodologies which are explained in Chapter 4. As illustrated by Gourdon et al. [Gourdon et al., 2018] and Alamo Vargas [Alamo Vargas, 2018] via analytical and experimental developments, the targeted energy transfer from the acoustical modes of the tube to the HR via strongly nonlinear interactions between two oscillators is observed.

CHAPTER 6

Conclusions and perspectives

Contents

6.1 The global conclusions

A contribution in the domain of nonlinear passive control in mechanics and acoustics is presented. The report is structured in three main parts with applications in structural/mechanical engineering and acoustics.

- The Chapter 2 shows the localization of induced cyclic loads on a full scale composite structure on its joints via exploiting the pure nonlinear and hysteresis behaviours.
- The targeted energy transfer in mechanical system is discussed in Chapters 3-4.
- The targeted energy transfer in acoustics is treated in Chapter 5.

It is presented that the localization of the induced energies in structural elements can be carried out via exploitation of their ductile and hysteresis responses. Then, a general methodology is explained for targeted energy transfer and detection of the nature of strong interactions between two classes of coupled nonlinear oscillators. It is seen that according to the parameters of coupled oscillators and also deriving excitations, the system can face periodic or modulated responses. These regimes are reached because of existence of equilibria and singularities of the systems. Several spacial cases are considered and treated according to the explained methodology. We have considered several types of nonlinearities for the coupled light oscillators, namely pure cubic, piece-wise linear and also combination of them with hysteresis. In addition to that we have studied the control process of principal systems with nonlinear behaviours in the form of differential equations or inclusions forming Bouc-Wen type hysteresis models and Saint-Venant elements. Some experimental tests have been performed as well for validating our developed techniques and the proof of concept. In acoustics we showed that the classical Helmholtz resonators in nonlinear regimes and also via tailoring their necks, present nonlinear response. This response is not pure nonlinear due to the existence of the linear part on resorting terms of the resonator. However, we used these properties of Helmholtz resonators for controlling an acoustical mode in a tube via a targeted energy transfer. All of my research works which I have presented in this report, in fact have one common aim: using nonlinearities for the aim of passive control. However, there are some pistes which I would like to continue and to develop for the next five years which are summarized in the next section.

6.2 Perspectives and scientific topics

Confidential

Confidential

Confidential

APPENDIX A

Expressions of F and H_0

The function F is defined as

$$F = \frac{\omega}{2\pi}\int_0^{\frac{2\pi}{\omega}} \rho(\dot{v} + \frac{\varepsilon\dot{w}}{1+\varepsilon})e^{-i\omega\tau_0}\mathrm{d}\tau_0 \tag{A.1}$$

As we have

$$\dot{v} + \frac{\varepsilon\dot{w}}{1+\varepsilon} = \frac{1}{2}(\phi_1 + \frac{\varepsilon}{1+\varepsilon}\phi_2)e^{i\omega\tau_0} + c.c. \tag{A.2}$$

We assume ϕ_1, ϕ_2 are independent of the time scale τ_0. Let us set polar form $\phi_j = N_j \exp(i\delta_j), j = 1, 2$.

$$\dot{v} + \frac{\varepsilon\dot{w}}{1+\varepsilon} = N_1\cos(\omega\tau_0 + \delta_1) + \frac{\varepsilon}{1+\varepsilon}N_2\cos(\omega\tau_0 + \delta_2) \tag{A.3}$$

Then, Eq. A.1 reads

$$F\frac{2i\eta}{\pi}e^{-i\omega t_1^\star} \tag{A.4}$$

where

$$\begin{aligned} &N_1\cos(\omega t_1^\star + \delta_1) + \frac{\varepsilon}{1+\varepsilon}N_2\cos(\omega t_1^\star + \delta_2) = 0 \\ &t_1^\star \in \left[0, \frac{\pi}{\omega}\right] \\ &\eta = \mathrm{sign}(N_1\cos(\delta_1) + \frac{\varepsilon}{1+\varepsilon}N_2\cos(\delta_2)) \end{aligned} \tag{A.5}$$

Finally, following system is obtained

$$\tan(\omega t_1^\star) = \frac{N_1\cos(\delta_1) + \frac{\varepsilon}{1+\varepsilon}N_2\cos(\delta_2)}{N_1\sin(\delta_1) + \frac{\varepsilon}{1+\varepsilon}N_2\sin(\delta_2)} \tag{A.6}$$

which yields to

$$\begin{aligned} F(N_1, N_2, \delta_1, \delta_2) &= \frac{2i}{\pi}\mathrm{sign}(\cos(\delta_1))e^{-i\delta_1}[1 - \varepsilon i\frac{N_2}{N_1}\sin(\delta_1 - \delta_2) + \mathcal{O}(\varepsilon^2)] \\ H_0(\phi_3, \phi_3^\star) &= \frac{\beta\phi_3}{2i\omega_1} = \frac{\beta}{8i\omega_1^3} \mid \phi_1 \mid^2 \phi_1 \end{aligned} \tag{A.7}$$

APPENDIX B

Numerical scheme for differential algebraic inclusion

An implicate Euler numerical scheme [Bastien et al., 2013] which can guarantee the convergence of the approximate solution toward an exact solution (but with, quite small, order 1) is endowed. Let us express the semi-explicit differential algebraic inclusion problem which is given in Eq. 4.157 as the first order differential inclusions as

$$X = \begin{pmatrix} \dot{x} \\ x \\ \dot{y} \\ y \\ z \end{pmatrix} = \begin{pmatrix} x_1 \\ x_2 \\ x_3 \\ x_4 \\ x_5 \end{pmatrix} \tag{B.1}$$

Since we have $\dfrac{\partial g}{\partial x_1} = 0$ and $\dfrac{\partial g}{\partial x_5} = -1$, then we can write:

$$\dot{x}_5 = \frac{\partial g}{\partial x_2}\dot{x}_2 = x_2^2 x_1 \tag{B.2}$$

Finally, governing equations can expressed as:

$$\dot{X} + \mathcal{L}X + G(X,t) + A(X) \ni \mathbf{0} \tag{B.3}$$

where $\mathbf{0} = (0,0,0,0,0)^t$,

$$\mathcal{L} = \begin{pmatrix} \varepsilon(a_0+\lambda) & \omega_1^2 & -\varepsilon\lambda & 0 & 0 \\ -1 & 0 & 0 & 0 & 0 \\ -\lambda & 0 & \lambda & 0 & 0 \\ 0 & 0 & -1 & 0 & 0 \\ 0 & 0 & -1 & 0 & 0 \end{pmatrix} = \begin{pmatrix} L_1 \\ L_2 \\ L_3 \\ L_4 \\ L_5 \end{pmatrix} \tag{B.4}$$

$$G(X,t) = \begin{pmatrix} \varepsilon\left(h_0(x_5) + \gamma(x_2 - x_4)^3 - f_0(t)\right) \\ 0 \\ \gamma(x_4 - x_2)^3 \\ 0 \\ -\dfrac{\partial g}{\partial x_2}x_1 = -x_2^2 x_1 \end{pmatrix} \tag{B.5}$$

and

$$A(X) = \begin{pmatrix} \varepsilon\alpha_0 \\ 0 \\ 0 \\ 0 \\ 0 \end{pmatrix} \tag{B.6}$$

The differential algebraic inclusion problem of the Eq. B.3 with given initial conditions in the phase space of X possesses a unique solution (see [Bastien et al., 2013]). The problem can easily be discretised. We choose a time step $\Delta t > 0$. For any integer n, let us set $t_n = n\Delta t$, $X(t_n) \simeq X_n$, $X(t_{n+1}) \simeq X_{n+1}$. Euler implicit scheme can be built from:

$$\begin{cases} \dfrac{1}{\Delta t}(X_{n+1} - X_n) + \mathcal{L}X_n + G(X_n, t_n) + A(X_{n+1}) = \mathbf{0} \\ \\ X_0 \text{ given} \end{cases} \tag{B.7}$$

The Euler implicit scheme algorithm is provided in Appendix C

APPENDIX C

The Euler implicit scheme algorithm

Let us note

$$X_n = \begin{pmatrix} x_{1n} \\ x_{2n} \\ x_{3n} \\ x_{4n} \\ x_{5n} \end{pmatrix} \tag{C.1}$$

and

$$X_{n+1} = \begin{pmatrix} x_{1n+1} \\ x_{2n+1} \\ x_{3n+1} \\ x_{4n+1} \\ x_{5n} \end{pmatrix} \tag{C.2}$$

Let us suppose that X_0 is given. For $n \geq 0$, we have:

$$aux_n = x_{1n} - \Delta t L_1 X_n - \Delta t \varepsilon \left(h_0(x_{5n}) + \gamma(x_{2n} - x_{4n})^3 - f_0(t_n) \right) \tag{C.3}$$

$$L_1 X_n = \varepsilon(a_0 + \lambda) x_{1n} + \omega_1^2 x_{2n} - \varepsilon\lambda x_{3n} \tag{C.4}$$

$$x_{1n+1} = \begin{cases} 0 & \text{if} \quad \mid aux_n \mid \leq \varepsilon\alpha_0\Delta t \\ aux_n - \varepsilon\alpha_0\Delta t & \text{if} \quad aux_n \geq \varepsilon\alpha_0\Delta t \\ aux_n + \varepsilon\alpha_0\Delta t & \text{if} \quad aux_n \leq -\varepsilon\alpha_0\Delta t \end{cases} \tag{C.5}$$

$$x_{2n+1} = x_{2n} + \Delta t x_{1n} \tag{C.6}$$

$$x_{3n+1} = x_{3n} - \Delta t(L_2 X_n + \gamma(x_{4n} - x_{2n})^3) = x_{3n} - \Delta t(x_{1n} + \gamma(x_{4n} - x_{2n})^3) \tag{C.7}$$

$$x_{4n+1} = x_{4n} + \Delta t x_{3n} \tag{C.8}$$

$$x_{5n+1} = x_{5n} + \Delta t x_{2n}^2 x_{1n} \tag{C.9}$$

APPENDIX D

One-dimensional wave equation

D.1 One-dimensional wave equation

Let us consider following equation which represent mono dimensional wave equations:

$$\frac{\partial^2 \psi}{\partial x^2} = \frac{1}{c^2}\frac{\partial^2 \psi}{\partial t^2} \tag{D.1}$$

In order to fully describe the wave, boundary and initial conditions should be specified. We set boundary conditions as

$$\begin{aligned} \psi(0,t) &= \mathfrak{A}_0(t) \\ \psi(L,t) &= \mathfrak{A}_L(t) \end{aligned} \tag{D.2}$$

and we assume following initial conditions

$$\begin{aligned} \psi(x,0) &= f(x) \\ \frac{\partial \psi}{\partial t}(x,0) &= g(x) \end{aligned} \tag{D.3}$$

To treat Eq. D.1, three methods is presented via using d'Alembert's method, Fourier transform and separation of variables.

D.2 D'Alembert's method

Let us set [D'Alembert, 1750a, D'Alembert, 1750b]

$$\begin{aligned} \xi &\equiv x - ct \\ \eta &\equiv x + ct \end{aligned} \tag{D.4}$$

So,

$$\begin{aligned} \frac{\partial^2 \psi}{\partial x^2} &= \frac{\partial^2 \psi}{\partial \xi^2} + 2\frac{\partial^2 \psi}{\partial \xi \partial \eta} + \frac{\partial^2 \psi}{\partial \eta^2} \\ \frac{1}{c^2}\frac{\partial^2 \psi}{\partial t^2} &= \frac{\partial^2 \psi}{\partial \xi^2} - 2\frac{\partial^2 \psi}{\partial \xi \partial \eta} + \frac{\partial^2 \psi}{\partial \eta^2} \end{aligned} \tag{D.5}$$

Considering Eq. D.5 in Eq. D.1, we obtain

$$\frac{\partial^2 \psi}{\partial \xi \partial \eta} = 0 \tag{D.6}$$

Which leads to following form of solution

$$\psi(\xi,\eta) = f(\eta) + g(\xi) = f(x+ct) + g(x-ct) \tag{D.7}$$

The f and g are any arbitrary functions, representing two waveforms travelling in positive x direction, i.e. g and the negative x direction, i.e. f.

D.3 Fourier transform method

Before applying the Fourier transform [Gasquet and Witomski, 2000] method to treat the Eq. D.1, let us present some preliminary definitions [Weisstein, 2018a]:

- The forward Fourier transform of a function $r(x)$:

$$R(k) = \mathfrak{F}_x\left[r(x)\right](k) = \int_{-\infty}^{+\infty} r(x)e^{-2\pi ikx}\mathrm{d}x \tag{D.8}$$

- The inverse Fourier transform of a function $R(x)$:

$$r(x) = \mathfrak{F}_x^{-1}\left[R(k)\right](k) = \int_{-\infty}^{+\infty} R(k)e^{2\pi ikx}\mathrm{d}x \tag{D.9}$$

- The Fourier transfer of a derivative function $r'(x)$:

$$\mathfrak{F}_x\left[r'(x)\right](k) = \int_{-\infty}^{+\infty} r'(x)e^{-2\pi ikx}\mathrm{d}x \tag{D.10}$$

  To treat Eq. D.10, we use integration by parts:

$$\mathfrak{F}_x\left[r'(x)\right](k) = \left[r(x)e^{-2\pi ikx}\right]_{-\infty}^{+\infty} - \int_{-\infty}^{+\infty} r(x)\left(-2\pi ike^{-2\pi ikx}\right)\mathrm{d}x \tag{D.11}$$

  If we suppose that the function $r(x)$ is bounded, i.e.

$$\lim_{x\to\infty} r(x) = 0 \tag{D.12}$$

  Then

$$\mathfrak{F}_x\left[r'(x)\right](k) = 2\pi ik\int_{-\infty}^{+\infty} r(x)e^{-2\pi ikx}\mathrm{d}x = 2\pi ik\mathfrak{F}_x\left[r(x)\right](k) \tag{D.13}$$

  and with the same manner, it can be proved that the Fourier transfer of the n^{th} derivative function $r^{(n)}(x)$ reads:

$$\mathfrak{F}_x\left[r^{(n)}(x)\right](k) = (2\pi ik)^n\mathfrak{F}_x\left[r(x)\right](k) \tag{D.14}$$

Let us apply the forward Fourier transform to the Eq. D.1 [Weisstein, 2018b]:

$$\int_{-\infty}^{+\infty} \frac{\partial^2\psi(x,t)}{\partial x^2}e^{-2\pi ikx}\mathrm{d}x = \frac{1}{c^2}\int_{-\infty}^{+\infty} \frac{\partial^2\psi}{\partial t^2}e^{-2\pi ikx}\mathrm{d}x \tag{D.15}$$

Considering Eq. D.14, we can set Eq. D.15 as

$$(2\pi ik)^2\,\Psi(k,t) = \frac{1}{c^2}\frac{\partial^2\Psi(k,t)}{\partial t^2} \tag{D.16}$$

where

$$\Psi(k,t) = \mathfrak{F}_x\left[\psi(x,t)\right](k) \tag{D.17}$$

The eigenfunction of the Eq. D.16 can be represented as:

$$\Psi(k,t) = \mathfrak{B}e^{2\pi ikct} + \mathfrak{C}e^{-2\pi ikct} \tag{D.18}$$

Let us take the inverse Fourier transform of the Eq. D.18; it reads

$$\begin{aligned}\psi(x,t) &= \int_{-\infty}^{+\infty} \Psi(k,t)e^{2\pi ikx}\mathrm{d}k \\ &= \int_{-\infty}^{+\infty} \left(\mathfrak{B}(k)e^{2\pi ikct} + \mathfrak{C}(k)e^{-2\pi ikct}\right)e^{2\pi ikx}\mathrm{d}k \\ &= \int_{-\infty}^{+\infty} \left(\mathfrak{B}(k)e^{-2\pi ik(-x-ct)} + \mathfrak{C}(k)e^{-2\pi ik(-x+ct)}\right)\mathrm{d}k \\ &= \psi_1(-x-ct) + \psi_2(-x+ct)\end{aligned} \tag{D.19}$$

with

$$\begin{aligned}\psi_1(\alpha) &= \mathfrak{F}_k\left[\mathfrak{B}(k)\right](\alpha) = \int_{-\infty}^{+\infty} \mathfrak{B}(k)e^{-2\pi ik\alpha}\mathrm{d}k \\ \psi_2(\alpha) &= \mathfrak{F}_k\left[\mathfrak{C}(k)\right](\alpha) = \int_{-\infty}^{+\infty} \mathfrak{C}(k)e^{-2\pi ik\alpha}\mathrm{d}k\end{aligned} \tag{D.20}$$

D.4 Method of separation of variables

Let us separated spatio-temporal variables of the $\psi(x,t)$ as

$$\psi(x,t) = \mathfrak{M}(x)\mathfrak{N}(t) \tag{D.21}$$

Injecting variables of the Eq. D.21 in Eq. D.1 following system can be obtained

$$\frac{1}{\mathfrak{M}(x)}\frac{\partial^2\mathfrak{M}(x)}{\partial x^2} = \frac{1}{c^2}\frac{1}{\mathfrak{N}(t)}\frac{\partial^2\mathfrak{N}(t)}{\partial t^2} = -k^2 \tag{D.22}$$

Equation D.22 represents two well separated differential equations in terms of variables. The solution of the space part reads

$$\mathfrak{M}(x) = C\cos(kx) + D\sin(kx) \tag{D.23}$$

and if we set $-c^2k^2 \equiv -\omega^2$, then the solution of the temporal part of Eq. D.22 yields to

$$\mathfrak{N}(t) = E\cos(\omega t) + F\sin(\omega t) \tag{D.24}$$

Let us suppose that Eq. D.21 describe the behaviour of a string (or a bar element) with following boundary conditions as $\mathfrak{A}_0(t) = \mathfrak{A}_L(t) = 0$ which are detailed in Eq. D.2. after injecting the assumed boundary conditions on Eq. D.23 it is found that

$$\begin{aligned}C &= 0 \\ kL &= m\pi\end{aligned} \tag{D.25}$$

with m being an integer, $m \in \mathbb{N}$. Considering Eq. D.25 in Eq. D.21, following systems is for any integer m obtained

$$\psi_m(x,t) = \left(E_m\cos(\omega t) + F_m\sin(\omega t)\right)D_m\sin(\frac{m\pi x}{L}) \tag{D.26}$$

Let us set $E_mD_m \equiv A_m$ and $F_mD_m \equiv B_m$. The system D.26 reads

$$\psi_m(x,t) = \left(A_m\cos(\omega t) + B_m\sin(\omega t)\right)\sin(\frac{m\pi x}{L}) \tag{D.27}$$

Let us consider a special initial condition as $\frac{\partial\psi}{\partial t}(x,0) = 0$ [Weisstein, 2018b], which provided $B_m = 0$ in Eq. D.27. We have

$$\psi_m(x,t) = A_m\cos(\omega t)\sin(\frac{m\pi x}{L}) \tag{D.28}$$

and the general solution of the system reads

$$\psi(x,t) = \sum_{m=1}^{\infty} A_m \cos(\omega t) \sin(\frac{m\pi x}{L}) \tag{D.29}$$

Let us suppose that a general form for the $\psi(x,0)$ as

$$\psi(x,0) = \sum_{m=1}^{\infty} A_m \sin(\frac{m\pi x}{L}) \tag{D.30}$$

The A_m in Eq. D.29 can be traced via endowing the orthogonality of modes as

$$\int_0^L \sin(\frac{n\pi x}{L}) \sin(\frac{m\pi x}{L}) \mathrm{d}x = \frac{1}{2} L \delta_{nm} \tag{D.31}$$

where δ stands for the Kronecker delta. Let us project the system D.30 on mode m via

$$\int_0^L \psi(x,0) \sin(\frac{m\pi x}{L}) \mathrm{d}x = \int_0^L \sum_{n=1}^{\infty} A_n \sin(\frac{n\pi x}{L}) \sin(\frac{m\pi x}{L}) \mathrm{d}x = \frac{1}{2} L A_m \tag{D.32}$$

So,

$$A_m = \frac{2}{L} \int_0^L \psi(x,0) \sin(\frac{m\pi x}{L}) \mathrm{d}x \tag{D.33}$$

Bibliography

[Achilleos et al., 2016] Achilleos, V., Richoux, O., and Theocharis, G. (2016). Coherent perfect absorption induced by the nonlinearity of a helmholtz resonator. *The Journal of the Acoustical Society of America*, 140(1):94–100. (Cited on page 124.)

[Agrapart, 2016] Agrapart, E. (2016). *Absorbeurs passifs pour contrôler les oscillations d'une cabine de téléphérique*. TFE, ENTPE, Vaulx-en-Velin. (Cited on page 114.)

[Akhatov et al., 1995] Akhatov, I., Baikov, V., and Khusnutdinova, K. (1995). Non-linear dynamics of coupled chains of particles. *Journal of Applied Mathematics and Mechanics*, 59(3):353 – 361. (Cited on page 37.)

[AL-Shudeifat et al., 2013] AL-Shudeifat, M. A., Wierschem, N., Quinn, D. D., Vakakis, A. F., Bergman, L. A., and Spencer, B. F. (2013). Numerical and experimental investigation of a highly effective single-sided vibro-impact non-linear energy sink for shock mitigation. *International Journal of Non-Linear Mechanics*, 52:96 – 109. (Cited on page 38.)

[Alamo Vargas, 2018] Alamo Vargas, V. (2018). *Transfert énergétique irréversible grâce á un résonateur acoustique à comportement non-linéaire*. PhD thesis, Ecole Doctorale Mecanique, Energetique, Genie Civil, Acoustique (MEGA), Université de Lyon, ENTPE, LTDS UMR CNRS 5513. Directors of the thesis: E. Gourdon and A. Ture Savadkoohi. (Cited on pages 125, 128, 132, 138, 140 and 141.)

[Alamo Vargas et al., 2018] Alamo Vargas, V., Gourdon, E., and Ture Savadkoohi, A. (2018). Nonlinear softening and hardening behavior in helmholtz resonators for nonlinear regimes. *Nonlinear Dynamics*, 91(1):217–231. (Cited on pages 125, 128, 132, 138 and 140.)

[Allard and Atalla, 2009] Allard, J. F. and Atalla, N. (2009). *Propagation of sound in porous media*. Wiley,West Sussex, UK. (Cited on page 120.)

[Aubry and Kopidakis, 2005] Aubry, S. and Kopidakis, G. (2005). A nonadiabatic theory for ultrafast catalytic electron transfer: A model for the photosynthetic reaction center. *Journal of biological physics*, 31:375–402. (Cited on page 37.)

[Aubry et al., 2001] Aubry, S., Kopidakis, G., Morgante, A., and Tsironis, G. (2001). Analytic conditions for targeted energy transfer between nonlinear oscillators or discrete breathers. *Physica B: Condensed Matter*, 296(1):222 – 236. Proceedings of the Symposium on Wave Propagation and Electronic Structure in Disordered Systems. (Cited on pages 11 and 37.)

[Badel et al., 2006] Badel, A., Sebald, G., Guyomar, D., Lallart, M., Lefeuvre, E., Richard, C., and Qiu, J. (2006). Piezoelectric vibration control by synchronized switching on adaptive voltage sources: Towards wideband semi-active damping. *The Journal of the Acoustical Society of America*, 119(5):2815–2825. (Not cited)

[Bastien et al., 2013] Bastien, J., Bernardin, F., and Lamarque, C.-H. (2013). *Non Smooth Deterministic or Stochastic Discrete Dynamical Systems: Applications to Models with Friction or Impact*. Wiley, New York. (Cited on pages 40, 41, 71, 93, 151 and 152.)

[Becker et al., 2017] Becker, J., Barbe, M. T., Hartinger, M., Dembek, T. A., Pochmann, J., Wirths, J., Allert, N., Mucke, D., Hermes, A., Meister, I. G., Visser-Vandewalle, V., Grice, M., and Timmermann, L. (2017). The effect of uni- and bilateral thalamic deep brain stimulation on speech

in patients with essential tremor: Acoustics and intelligibility. *Neuromodulation: Technology at the Neural Interface*, 20(3):223–232. (Not cited)

[Bellet et al., 2012] Bellet, R., Cochelin, B., Côte, R., and Mattei, P. (2012). Enhancing the dynamic range of targeted energy transfer in acoustics using several nonlinear membrane absorbers. *Journal of Sound and Vibration*, 331:5657–5668. (Cited on page 138.)

[Bellet et al., 2010] Bellet, R., Cochelin, B., Herzog, P., and Mattei, P. (2010). Experimental study of targeted energy transfer from an acoustic system to a nonlinear membrane absorber. *Journal of Sound and Vibration*, 329:2768–2791. (Cited on page 137.)

[Blazejczyk-Okolewska, 2001] Blazejczyk-Okolewska, B. (2001). Analysis of an impact damper of vibrations. *Chaos, Solitons & Fractals*, 12:1983–1988. (Cited on page 36.)

[Blevins, 2006] Blevins, R. D. (2006). *Flow-Induced Vibration*. Krieger Publishing Company. (Cited on page 132.)

[Bogoliubov and Mitropolsky, 1961] Bogoliubov, N. and Mitropolsky, Y. A. (1961). *Asymptotic Methods in the Theory of Non-Linear Oscillations*. Gordon & Breach. (Cited on pages 30, 31 and 34.)

[Bolt et al., 1949] Bolt, R. H., Labate, S., and Ingard, U. (1949). The acoustic reactance of small circular orifices. *The Journal of the Acoustical Society of America*, 21:94–97. (Cited on page 122.)

[Bonnans et al., 2006] Bonnans, J.-F., Gilbert, J., Lemaréchal, C., and Sagastizábal, C. (2006). *Numerical Optimization: Theoretical and Practical Aspects*. Springer-Verlag. (Cited on page 21.)

[Borisova et al., 1984] Borisova, N. A., Golovin, A. P., Gubarev, A. V., Laptev, S. A., Nekrasov, A. A., and Pechenova, O. I. (1984). Nonlinear forced vibrations in a Helmholtz resonator. *Translated from: Zhurnal Prikladnoi Mekhaniki i Tekhnicheskoi Fiziki. Plenum Publishing Corporation*, 2:82–87. (Cited on pages 122 and 123.)

[Bouc, 1971] Bouc, R. (1971). Modèle mathématique d'hystérésis. *Acustica*, 21:16–25. (Cited on pages 41 and 51.)

[Boullosa and Orduna-Bustamante, 1992] Boullosa, R. R. and Orduna-Bustamante, F. (1992). The reaction force on a Helmholtz resonator driven at high sound pressure amplitudes. *American Journal of Physics*, 60:722–726. (Cited on page 123.)

[Braconi et al., 2008a] Braconi, A., Bursi, O. S., Fabbrocino, G., Salvatore, W., and Tremblay, R. (2008a). Seismic performance of a 3d full-scale high ductility steel-concrete composite moment-resisting structure-part i: design and testing procedure. *Earthquake Engineering and Structural Dynamics*, 37(14):1609–1634. (Cited on pages 2, 11 and 15.)

[Braconi et al., 2008b] Braconi, A., Bursi, O. S., Fabbrocino, G., Salvatore, W., and Tremblay, R. (2008b). Seismic performance of a 3d full-scale high ductility steel-concrete composite moment-resisting structure-part ii: test results and analytical validation. *Earthquake Engineering and Structural Dynamics*, 37(14):1635–1655. (Cited on pages 2, 11 and 15.)

[Bricault et al., 2019] Bricault, C., Pézerat, C., Collet, M., Pyskir, A., Perrard, P., Matten, G., and Romero-García, V. (2019). Multimodal reduction of acoustic radiation of thin plates by using a single piezoelectric patch with a negative capacitance shunt. *Applied Acoustics*, 145:320 – 327. (Not cited)

[Bursi et al., 2004a] Bursi, O. S., Caramelli, S., Fabbrocino, G., Molina, J., Taucer, F., Salvatore, W., and Zandonini, R. (2004a). *3D full scale seismic testing of a steel-concrete composite building at ELSA*. Joint Research Centre, European Community, Italy, Eur Report, EUR 21299 EN. (Cited on pages 11, 13, 14 and 17.)

[Bursi et al., 2004b] Bursi, O. S., Molina, J., Salvatore, W., and Taucer, F. (2004b). *Dynamic characterization of a 3D full scale steel-concrete composite building at ELSA*. Joint Research Centre, European Community, Italy, Eur Report, EUR21206EN. (Cited on page 14.)

[Bursi and Wagg, 2008] Bursi, O. S. and Wagg, D. (2008). *Modern testing techniques for structural systems*. SpringerWienNewYork, International Centre for Mechanical Sciences (CISM), Udine, Italy. (Cited on page 13.)

[Cardano and Witmer, 1968] Cardano, G. and Witmer, T. (1968). *Ars Magna Or The Rules of Algebra*. Dover Books on Advanced Mathematics. Dover. (Cited on page 62.)

[Carter and Liu, 1961] Carter, W. J. and Liu, F. C. (1961). Steady-state behavior of nonlinear dynamic vibration absorber. *Journal of Applied Mechanics*, 67–70(1):433–442. (Cited on pages 33 and 34.)

[Casciati et al., 1998] Casciati, F., Faravelli, L., and Petrini, L. (1998). Energy dissipation in shape memory alloy devices. *Computer-Aided Civil and Infrastructure Engineering*, 13:433–442. (Cited on page 8.)

[Caughey, 1954] Caughey, T. K. (1954). *The existence and stability of periodic motions in forced non-linear oscillations* . PhD Thesis, California Institute of Technology., Pasadena, California. CaltechETD:etd-04072003-115022. (Cited on page 28.)

[CEN. Eurocode 8, 2005] CEN. Eurocode 8 (2005). *design of structures for earthquake resistance. Part 1: general rules, seismic actions and rules for buildings*. EN 1998-1, European Committee for Standardization, Brussels, Belgium. (Cited on pages 14 and 23.)

[Chai et al., 1995] Chai, Y., Romstad, K., and Bird, S. (1995). Energy-based linear damage model for high-intensity seismic loading. *Journal of Structural Engineering*, 121(5):857–864. (Cited on pages 23 and 26.)

[Charlemagne, 2018] Charlemagne, S. (2018). *Dynamique non linéaire d'un assemblage d'oscillateurs: application au contrôle*. PhD thesis, Ecole Doctorale Mecanique, Energetique, Genie Civil, Acoustique (MEGA), Université de Lyon, ENTPE, LTDS UMR CNRS 5513. Directors of the thesis: C.-H. Lamarque and A. Ture Savadkoohi. (Cited on pages 97, 99 and 106.)

[Charlemagne et al., 2017] Charlemagne, S., Lamarque, C.-H., and Ture Savadkoohi, A. (2017). Vibratory control of a linear system by addition of a chain of nonlinear oscillators. *Acta Mechanica*, 228:3111–3133. (Cited on pages 97, 99 and 106.)

[Charlemagne et al., 2018] Charlemagne, S., Ture Savadkoohi, A., and Lamarque, C.-H. (2018). Dynamics of a linear system coupled to a chain of light nonlinear oscillators analyzed through a continuous approximation. *Physica D: Nonlinear Phenomena*, 374–375:10–20. (Cited on page 97.)

[Chauvin et al., 2018] Chauvin, A., Monteil, M., Bellizzi, S., Côte, R., Herzog, P., and Pachebat, M. (2018). Acoustic characterization of a nonlinear vibroacoustic absorber at low frequencies and high sound levels. *Journal of Sound and Vibration*, 416:244–257. (Cited on page 138.)

[Chellini et al., 2008] Chellini, G., De Roeck, G., Nardini, L., and Salvatore, W. (2008). Damage detection of a steel-concrete composite frame by a multilevel approach: Experimental measurements and modal identification. *Earthquake Engineering and Structural Dynamics*, 37(15):1763–1783. (Cited on page 17.)

[Chu et al., 2005] Chu, S. Y., Soong, T. T., and Reinhorn, A. M. (2005). *Active, hybrid, and semi-active structural control: a design and implementation handbook*. Wiley, United Kingdom. (Cited on pages 1 and 2.)

[Cochelin et al., 2006] Cochelin, B., Herzog, P., and Mattei, P.-O. (2006). Experimental evidence of energy pumping in acoustics. *Comptes Rendus Mécanique*, 334:639644. (Cited on pages 11, 122 and 137.)

[Collette, 1998] Collette, F. S. (1998). A combined tuned absorber and pendulum impact damper under random excitation. *Journal of Sound and Vibration*, 216:199–213. (Cited on page 36.)

[Cveticanin et al., 2018] Cveticanin, L., Zukovic, M., and Cveticanin, D. (2018). Influence of nonlinear subunits on the resonance frequency band gaps of acoustic metamaterial. *Nonlinear Dynamics*, 93(3):1341–1351. (Not cited)

[Dahl, 1968] Dahl, P. R. (1968). *A Solid Friction Model*. TOR-158(3107-18), The Aerospace Corporation, El-Segundo, California. (Cited on pages 58 and 90.)

[D'Alembert, 1750a] D'Alembert, J. L. R. (1747, 1750a). Recherches sur la courbe que forme une corde tendue mise en vibration. *Histoire de l'Académie des Sciences et des Belles-Lettres de Berlin*, 3:214–219. (Cited on page 155.)

[D'Alembert, 1750b] D'Alembert, J. L. R. (1747, 1750b). Suite des recherches sur la courbe que forme une corde tendue mise en vibration. *Histoire de l'Académie des Sciences et des Belles-Lettres de Berlin*, 3:220–249. (Cited on page 155.)

[Dao, 2017] Dao, D.-L. (2017). Dispositif non linéaire pour supprimer le tremblement de repos dû á la maladie de Parkinson. Master's thesis, Université de Lyon 1, ENTPE, ECL, ENIS, LTDS UMR CNRS 5513. Director of the Master thesis: A. Ture Savadkoohi. (Not cited)

[de Oliveira, 2013] de Oliveira, M. J. (2013). *Equilibrium thermodynamics*. Springer-Verlag, Berlin Heidelberg. (Cited on page 118.)

[de Silva, 2005] de Silva, C. W. (2005). *Vibration and Shock Handbook*. Taylor & Francis Group, LLC, U.S. (Cited on pages 2, 3 and 4.)

[Den Hartog, 1933] Den Hartog, J. P. (1933). The amplitudes of non-harmonic vibrations. *Journal of the Franklin Institute*, 216(4):459–473. (Cited on page 27.)

[Den Hartog, 1956] Den Hartog, J. P. (1956). *Mechanical Vibrations*. McGraw-Hill Book Company. (Cited on page 27.)

[Döhler et al., 2018] Döhler, M., Hille, F., and Mevel, L. (2018). *Vibration-Based Monitoring of Civil Structures with Subspace-Based Damage Detection*, pages 307–326. Springer International Publishing, Cham. (Cited on page 14.)

[Dorka et al., 2005] Dorka, U., Garcia, A., Severn, R. T., and Bairrao, R. (2005). *Seismic qualification of passive mitigation devices. Cooperative Advancements in Seismic and Dynamic Experiments (CASCADE)*. Laboratorio Nacional de Engenharia Civil, Lisbon. (Cited on page 2.)

[Duffing, 1918] Duffing, G. (1918). *Erzwungene Schwingungen bei veanderlicher Eigenfrequenz und ihre technische Bedeutung*. Braunschweig: Vieweg. (Cited on page 27.)

[Ema and Marui, 1996] Ema, S. and Marui, E. (1996). Damping characteristics of an impact damper and its application. *International Journal of Machine Tools and Manufacture*, 36(3):293–306. (Cited on page 36.)

[Ema and Marui, 2000] Ema, S. and Marui, E. (2000). Suppression of chatter vibration of boring tools using impact dampers. *International Journal of Machine Tools and Manufacture*, 4:1141–1156. (Cited on page 36.)

[Espay et al., 2017] Espay, A. J., Lang, A. E., Erro, R., Merola, A., Fasano, A., Berardelli, A., and Bhatia, K. P. (2017). Essential pitfalls in "essential" tremor. *Movement Disorders*, 32(3):325–331. (Not cited)

[Ewins, 2000] Ewins, D. J. (2000). *Modal testing, theory, practice, and application*. Research Studies Pre. (Cited on pages 14 and 17.)

[Faravelli et al., 2010] Faravelli, L., Fuggini, C., and Ubertini, F. (2010). Toward a hybrid control solution for cable dynamics: theoretical prediction and experimental vamidation. *Structural Control and Health Monitoring*, 17:386–403. (Cited on page 2.)

[Fasano and Deuschl, 2015] Fasano, A. and Deuschl, G. (2015). Therapeutic advances in tremor. *Movement Disorders*, 30(11):1557–1565. (Not cited)

[FIP Industrial, 2016] FIP Industrial (2016). *Anti-seismic devices*. Selvazzano, Italy. (Cited on pages 5, 6, 7, 8, 9, 10 and 11.)

[Flach and Willis, 1998] Flach, S. and Willis, C. (1998). Discrete breathers. *Physics Reports*, 295(5):181 – 264. (Cited on page 37.)

[Flores, 2007] Flores, P. D. (2007). Wikimedia Commons. https://commons.wikimedia.org/wiki/File:Puente_Rosario-Victoria_(panorama)_1.jpg. (Cited on page 10.)

[Förner et al., 2015] Förner, K., Askin Temiz, M., Polifke, W., and Lopez Arteaga, I. (2015). On the non-linear influence of the edge geometry on vortex shedding in the Helmholtz resonators. In *The 22nd International Congress on Sound and Vibration, 12-16 July 2015, Florence, Italy*. (Cited on pages 127 and 128.)

[Frahm, 1911] Frahm, H. (1911). Device for damping vibrations of bodies. US Patent 989,958. (Cited on pages 2, 11, 27 and 122.)

[Friswell and Mottershead, 1995] Friswell, M. I. and Mottershead, J. E. (1995). *Finite element model updating in structural dynamics*. Kluwer Academic Publishers. (Cited on page 14.)

[Gasquet and Witomski, 2000] Gasquet, C. and Witomski, P. (2000). *Analyse de Fourier et applications*. Dunod, Paris. (Cited on page 156.)

[Gendelman, 2012] Gendelman, O. (2012). Analytic treatment of a system with a vibro-impact nonlinear energy sink. *Journal of Sound and Vibration*, 331(21):4599 – 4608. (Cited on page 38.)

[Gendelman and Alloni, 2015] Gendelman, O. and Alloni, A. (2015). Dynamics of forced system with vibro-impact energy sink. *Journal of Sound and Vibration*, 358:301 – 314. (Cited on page 38.)

[Gendelman et al., 2001] Gendelman, O., Manevitch, L., Vakakis, A., and M'Closkey, R. (2001). Energy pumping in nonlinear mechanical oscillators: Part I-dynamics of the underlying hamiltonian systems. *Journal of Applied Mechanics-transactions of The Asme*, 68:34–41. (Cited on page 37.)

[Gendelman, 2001] Gendelman, O. V. (2001). Transition of energy to a nonlinear localized mode in a highly asymmetric system of two oscillators. *Nonlinear Dynamics*, 25(1):237–253. (Cited on pages 11 and 37.)

[Gendelman, 2008] Gendelman, O. V. (2008). Targeted energy transfer in systems with non-polynomial nonlinearity. *Journal of Sound and Vibration*, 315(3):732 – 745. (Cited on page 38.)

[Gendelman and Vakakis, 2000] Gendelman, O. V. and Vakakis, A. F. (2000). Transitions from localization to nonlocalization in strongly nonlinear damped oscillators. *Chaos, Solitons & Fractals*, 11:1535–1542. (Cited on page 11.)

[Gendelman et al., 2010] Gendelman, O. V., Vakakis, A. F., Bergman, L. A., and McFarland, D. M. (2010). Asymptotic analysis of passive nonlinear suppression of aeroelastic instabilities of a rigid wing in subsonic flow. *SIAM Journal on Applied Mathematics*, 70:1655–1677. (Cited on page 11.)

[Gilchrist, 1961] Gilchrist, A. O. (1961). The free oscillations of conservative quasilinear systems with two degrees of freedom. *International Journal of Mechanical Sciences*, 3:286–311. (Cited on pages 30 and 31.)

[Glacet et al., 2019] Glacet, A., Tanguy, A., and Réthoré, J. (2019). Vibrational properties of quasi-periodic beam structures. *Journal of Sound and Vibration*, 442:624 – 644. (Not cited)

[Gourc et al., 2015a] Gourc, E., Michon, G., Seguy, S., and Berlioz, A. (2015a). Targeted energy transfer under harmonic forcing with a vibro-impact nonlinear energy sink: Analytical and experimental developments. *Journal of Vibration and Acoustics*, 137:031008. (Cited on page 38.)

[Gourc et al., 2015b] Gourc, E., Seguy, S., Michon, G., Berlioz, A., and Mann, B. (2015b). Quenching chatter instability in turning process with a vibro-impact nonlinear energy sink. *Journal of Sound and Vibration*, 355:392 – 406. (Cited on page 38.)

[Gourdon et al., 2007] Gourdon, E., Alexander, N., Taylor, C., Lamarque, C., and Pernot, S. (2007). Nonlinear energy pumping under transient forcing with strongly nonlinear coupling: Theoretical and experimental results. *Journal of Sound and Vibration*, 300(3):522 – 551. (Cited on page 38.)

[Gourdon et al., 2018] Gourdon, E., Ture Savadkoohi, A., and Alamo Vargas, V. (2018). Targeted energy transfer from one acoustical mode to an helmholtz resonator with nonlinear behavior. *Journal of Vibration and Acoustics*, 140(6):061005. (Cited on pages 138 and 141.)

[Guckenheimer and Holmes, 1983] Guckenheimer, J. and Holmes, P. (1983). *Nonlinear oscillations, dynamical systems, and bifurcations of vector fields*. Springer-Verlag New York. (Cited on page 130.)

[Guillot, 2021] Guillot, V. (2021). *Conception multi-échelle des structures adaptatifs intégrant des dispositifs non linéaires pour le contrôle et la récupération d'énergie*. PhD thesis, Ecole Doctorale Mecanique, Energetique, Genie Civil, Acoustique (MEGA), Université de Lyon, ENTPE, LTDS UMR CNRS 5513. Undergoing thesis. Directors of the thesis: C.-H. Lamarque and A. Ture Savadkoohi. (Not cited)

[Guillot et al., 2019] Guillot, V., Ture Savadkoohi, A., and Lamarque, C.-H. (2019). Analysis of a reduced-order nonlinear model of a multi-physics beam. *Nonlinear Dynamics*, doi: 10.1007/s11071-019-05054-x. (Not cited)

[Guyomar and Badel, 2006] Guyomar, D. and Badel, A. (2006). Nonlinear semi-passive multimodal vibration damping: an efficient probabilistic approach. *Journal of Sound and Vibration*, 294:249–268. (Cited on page 2.)

[Guyomar et al., 2007] Guyomar, D., Richard, C., and Mohammadi, S. (2007). Semi-passive random vibration control based on statistics. *Journal of Sound and Vibration*, 307:818–833. (Cited on page 2.)

[Hashemi et al., 2004] Hashemi, S. M., Golnaraghi, M. F., and Patla, A. E. (2004). Tuned vibration absorber for suppression of rest tremor in parkinson's disease. *Medical and Biological Engineering and Computing*, 42(1):61–70. (Not cited)

[Haxton and Barr, 1972] Haxton, R. S. and Barr, A. D. S. (1972). The autoparametric vibration absorber. *Journal of Engineering for Industry*, 94:119–125. (Cited on pages 34, 35 and 36.)

[Heller et al., 2009] Heller, L., Foltête, E., and Piranda, J. (2009). Experimental identification of nonlinear dynamic properties of built-up structures. *Journal of Sound and Vibration*, 327(1):183 – 196. (Cited on page 14.)

[Helmholtz, 1863] Helmholtz, H. V. (1863). *Die Lehre von den Tonempfindungen als physiologische Grundlagefur die Theorie der Musik*. Braunschweig, Druck und Verlag von Friedrich Vieweg und Sons. (Cited on pages 121, 122 and 138.)

[Henry and Tobias, 1959] Henry, R. F. and Tobias, S. A. (1959). Instability and steady-state coupled motions in vibration isolating suspensions. *Journal Mechanical Engineering Science*, 1:19–29. (Cited on pages 30 and 32.)

[Henry and Tobias, 1961] Henry, R. F. and Tobias, S. A. (1961). Modes at rest and their stability in coupled non-linear systems. *Journal Mechanical Engineering Science*, 3:163–173. (Cited on pages 30 and 32.)

[Hersh and Walker, 1977] Hersh, A. S. and Walker, B. (1977). *Fluid mechanical model of the Helmholtz resonator*. NASA, Washington, United States, NASA Technical report: NASA-CR-2904. (Cited on pages 123 and 125.)

[Hervé and Aubry, 2006] Hervé, G. and Aubry, S. (2006). Intramolecular signal transmission in regulatory enzymes: Are polarons involved? *Physica D: Nonlinear Phenomena*, 216(1):235 – 245. Nonlinear Physics: Condensed Matter, Dynamical Systems and Biophysics. (Cited on page 37.)

[Hot et al., 2012] Hot, A., Kerschen, G., ete, E. F., and Cogan, S. (2012). Detection and quantification of non-linear structural behavior using principal component analysis. *Mechanical Systems and Signal Processing*, 26:104 – 116. (Cited on page 14.)

[Housner et al., 1997] Housner, G. W., Bergman, L. A., Caughey, T. K., Chassiakos, A. G., Claus, R. O., Masri, S. F., Skelton, R. E., Soong, T. T., spencer, B. F., and Yao, J. T. P. (1997). Structural control: past, present and future. *Journal of Engineering Mechanics*, 123:897–971. (Cited on pages 1 and 2.)

[Huang et al., 2009] Huang, H., Sun, C., and Huang, G. (2009). On the negative effective mass density in acoustic metamaterials. *International Journal of Engineering Science*, 47(4):610 – 617. (Not cited)

[Hunt and Nissen, 1982] Hunt, J. B. and Nissen, J.-C. (1982). The broadband dynamic vibration absorber. *Journal of Sound and Vibration*, 83(4):573–578. (Cited on page 36.)

[Hurel et al., 2019] Hurel, G., Ture Savadkoohi, A., and Lamarque, C.-H. (2019). Passive control of a two degrees-of-freedom pendulum by a non-smooth absorber. *Nonlinear Dynamics*. (Cited on page 38.)

[Ibrahim, 2008] Ibrahim, R. A. (2008). Recent advances in nonlinear passive vibration isolators. *Journal of Sound and Vibration*, 314:371–452. (Cited on pages 2 and 11.)

[IDARC2D, 2002] IDARC2D (2002). *A Computer Program for Seismic Inelastic Structural Analysis*. The American Society of Mechanical Engineers, Department of Civil, Structural and Environment Engineering, University of Buffalo, U.S.A. Version 5.5. (Cited on pages 22 and 26.)

[Ikhouane and Rodellar, 2007] Ikhouane, F. and Rodellar, J. (2007). *Systems with Hysteresis: Analysis, Identification and Control Using the Bouc-Wen Model*. Wiley, West Sussex. (Cited on pages 41, 51, 58 and 90.)

[Ingard, 1953] Ingard, U. (1953). On the theory and design of acoustic resonators. *The Journal of the Acoustical Society of America*, 25(6):1037–1061. (Cited on page 122.)

[Ingard and Ising, 1967] Ingard, U. and Ising, H. (1967). Acoustic nonlinearity of an orifice. *The Journal of the Acoustical Society of America*, 42(6):6–17. (Cited on page 123.)

[Iooss and James, 2005] Iooss, G. and James, G. (2005). Localized waves in nonlinear oscillator chains. *Chaos: An Interdisciplinary Journal of Nonlinear Science*, 15(1):015113. (Cited on page 37.)

[Irschik and Holl, 2004] Irschik, H. and Holl, H. J. (2004). Mechanics of variable-mass systems-part 1: Balance of mass and linear momentum. *Applied Mechanics Reviews*, 57(2):145–160. (Cited on page 90.)

[Jackson et al., 1978] Jackson, K., Joseph, J., and Wyard, S. (1978). A mathematical model of arm swing during human locomotion. *Journal of Biomechanics*, 11(6):277 – 289. (Not cited)

[Keller and Zauner, 1995] Keller, J. J. and Zauner, E. (1995). On the use of helmholtz resonators as sound attenuators. *Zeitschrift für angewandte Mathematik und Physik ZAMP*, 46(3):297–327. (Cited on pages 121 and 123.)

[Kerschen et al., 2007] Kerschen, G., McFarland, D. M., Kowtko, J. J., Lee, Y. S., Bergman, L. A., and Vakakis, A. F. (2007). Experimental demonstration of transient resonance capture in a system of two coupled oscillators with essential stiffness nonlinearity. *Journal of Sound and Vibration*, 299(4):822 – 838. (Cited on page 38.)

[Kerschen et al., 2005] Kerschen, G., Vakakis, A. F., Lee, Y. S., Mcfarland, D. M., Kowtko, J. J., and Bergman, L. A. (2005). Energy transfers in a system of two coupled oscillators with essential nonlinearity: 1:1 resonance manifold and transient bridging orbits. *Nonlinear Dynamics*, 42(3):283–303. (Cited on page 38.)

[Kerschen et al., 2006] Kerschen, G., Worden, K., Vakakis, A. F., and Golinval, J.-C. (2006). Past, present and future of nonlinear system identification in structural dynamics. *Mechanical Systems and Signal Processing*, 20(3):505 – 592. (Cited on page 14.)

[Khusnutdinova and Pelinovsky, 2003] Khusnutdinova, K. and Pelinovsky, D. (2003). On the exchange of energy in coupled Klein-Gordon equations. *Wave Motion*, 38(1):1 – 10. (Cited on page 37.)

[Koh et al., 2003] Koh, C. G., Qiao, G. Q., and Quek, S. T. (2003). Damage identification of structural members: Numerical and experimental studies. *Structural Health Monitoring*, 2:41–55. (Cited on page 14.)

[Kojima and Nagaya, 1983] Kojima, H. and Nagaya, K. (1983). A study on the torsional dynamic vibration absorber consisting of rare-earth magnets. *Bulletin of JSME*, 26(214):611–618. (Cited on page 36.)

[Kojima and Saito, 1983] Kojima, H. and Saito, H. (1983). Forced vibration of a beam with a nonlinear dynamic absorber. *Journal of Sound and Vibration*, 88(4):559–568. (Cited on page 36.)

[Kopidakis et al., 2001] Kopidakis, G., Aubry, S., and Tsironis, G. (2001). Targeted energy transfer through discrete breathers in nonlinear systems. *Physical review letters*, 87:165501. (Cited on pages 11 and 37.)

[Korkmaz, 2011] Korkmaz, S. (2011). A review of active structural control: challenges for engineering informatics. *Computers and Structures*, 89:2113–2132. (Cited on page 1.)

[Lamarque et al., 2011] Lamarque, C.-H., Gendelman, O. V., Ture Savadkoohi, A., and Etcheverria, E. (2011). Targeted energy transfer in mechanical systems by means of non-smooth nonlinear energy sink. *Acta Mechanica*, 221:175–200. (Cited on pages 11, 38, 60, 82, 84 and 106.)

[Lamarque and Ture Savadkoohi, 2014] Lamarque, C.-H. and Ture Savadkoohi, A. (2014). Dynamical behavior of a Bouc-Wen type oscillator coupled to a nonlinear energy sink. *Meccanica*, 49(8):1917–19285. (Cited on page 84.)

[Lamarque and Ture Savadkoohi, 2015] Lamarque, C.-H. and Ture Savadkoohi, A. (2015). Targeted energy transfer between a system with a set of Saint-Venant elements and a nonlinear energy sink. *Continuum Mechanics and Thermodynamics*, 27(4–5):819–833. (Cited on pages 84, 93 and 96.)

[Lamarque and Ture Savadkoohi, 2017] Lamarque, C.-H. and Ture Savadkoohi, A. (2017). Contrôle passif non linéaire d'oscillations pendulaires de sièges ou cabines de dispositifs de transports à câbles. Projet la Région Auvergne-Rhône-Alpes (CALIPSO Project): LTDS UMR CNRS 5513 & POMA. (Cited on page 114.)

[Lamarque and Ture Savadkoohi, 2018] Lamarque, C.-H. and Ture Savadkoohi, A. (2018). *Passive Control of Differential Algebraic Inclusions - General Method and a Simple Example*, pages 269–289. Springer International Publishing, Cham. (Cited on page 71.)

[Lamarque et al., 2018] Lamarque, C.-H., Ture Savadkoohi, A., and Charlemagne, S. (2018). Experimental results on the vibratory energy exchanges between a linear system and a chain of nonlinear oscillators. *Journal of Sound and Vibration*, 437:97–109. (Cited on page 38.)

[Lamarque et al., 2017] Lamarque, C.-H., Ture Savadkoohi, A., Charlemagne, S., and Abdoulhadi, P. (2017). Nonlinear vibratory interactions between a linear and a non-smooth forced oscillator in the gravitational field. *Mechanical Systems and Signal Processing*, 89:131–148. (Cited on pages 82 and 84.)

[Lamarque et al., 2014] Lamarque, C.-H., Ture Savadkoohi, A., and Dimitrijevic, Z. (2014). Dynamics of a linear system with time-dependent mass and a coupled light mass with non-smooth potential. *Meccanica*, 49(1):135–145. (Cited on pages 84, 90, 93 and 114.)

[Lamarque et al., 2012] Lamarque, C.-H., Ture Savadkoohi, A., Etcheverria, E., and Dimitrijevic, Z. (2012). Multi-scale dynamics of two coupled nonsmooth systems. *International Journal of Bifurcation and Chaos*, 22(12):1250295. (Cited on pages 84, 88, 89 and 110.)

[Lamarque et al., 2015] Lamarque, C.-H., Vaurigaud, B., Ture Savadkoohi, A., and Weiss, M. (2015). Dispositif passif non linéaire de contrôle de vibrations d'au moins un câble et installation associée. FR20150060885. (Cited on page 114.)

[Laxalde and Thouverez, 2009] Laxalde, D. and Thouverez, F. (2009). Complex non-linear modal analysis for mechanical systems: Application to turbomachinery bladings with friction interfaces. *Journal of Sound and Vibration*, 322(4):1009 – 1025. (Cited on page 14.)

[Laxalde et al., 2006] Laxalde, D., Thouverez, F., and Sinou, J.-J. (2006). Dynamics of a linear oscillator connected to a small strongly non-linear hysteretic absorber. *International Journal of Non-Linear Mechanics*, 41(8):969 – 978. (Cited on page 51.)

[Lazarov and Jensen, 2007] Lazarov, B. and Jensen, J. (2007). Low-frequency band gaps in chains with attached non-linear oscillators. *International Journal of Non-Linear Mechanics*, 42(10):1186 – 1193. (Not cited)

[Lazarov and Thomsen, 2009] Lazarov, B. and Thomsen, J. (2009). Using high-frequency vibrations and non-linear inclusions to create metamaterials with adjustable effective properties. *International Journal of Non-Linear Mechanics*, 44(1):90 – 97. (Not cited)

[Lee et al., 2009] Lee, Y. S., Nucera, F., Vakakis, A. F., McFarland, D. M., and Bergman, L. A. (2009). Periodic orbits, damped transitions and targeted energy transfers in oscillators with vibro-impact attachments. *Physica D: Nonlinear Phenomena*, 238(18):1868 – 1896. (Cited on page 38.)

[Lee et al., 2008] Lee, Y. S., Vakakis, A. F., Bergman, L. A., McFarland, D. M., Kerschen, G., Nucera, F., Tsakirtzis, S., and Panagopoulos, P. N. (2008). Passive non-linear targeted energy transfer and its applications to vibration absorption: A review. *Proceedings of the Institution of Mechanical Engineers, Part K: Journal of Multi-body Dynamics*, 222(2):77–134. (Cited on page 38.)

[Lhommée et al., 2018] Lhommée, E., Wojtecki, L., Czernecki, V., Witt, K., Maier, F., Tonder, L., Timmermann, L., Hälbig, T. D., Pineau, F., Durif, F., Witjas, T., Pinsker, M., Mehdorn, M., Sixel-Döring, F., Kupsch, A., Krüger, R., Elben, S., Chabardès, S., Thobois, S., Brefel-Courbon, C., Ory-Magne, F., Regis, J.-M., Maltête, D., Sauvaget, A., Rau, J., Schnitzler, A., Schüpbach, M., Schade-Brittinger, C., Deuschl, G., Houeto, J.-L., Krack, P., Negovanska, V., Welter, M.-L., Corvol, J.-C., Agid, Y., Navarro, S., Meier, N., Hartmann, A., Hesekamp, H., Cornu, P., Möller, B., Nebel, A., Raethjen, J., Knudsen, K., Volkmann, J., Falk, D., Paschen, S., Meister, I., Kuhn, J., Donner, K., Kessler, J., Barbe, M., Fink, G., Maarouf, M., Kühn, A., Müller, B., Faust, K., Gruber, D., Schneider, G.-H., Seigneuret, E., Pollak, P., Fraix, V., Kistner, A., Rascol, O., Arbus, C., Danet, L., Chaynes, P., Groiss, S. J., Hartmann, C., Südmeyer, M., Partowinia-Peters, M., Vesper, J., Ledily, S., Damier, P., Raoul, S., Trenkwalder, C., Richter-Dreske, W., Wächter, T., Weiss, D., Eusebio, A., Azulay, J. P., Polo, G., Pinto, S., Levin, J., Dornier, S., Pene, F., Hourton, D., Quintin, M., Hoffart-Jourdain, C., Brocvielle, H., Balthasar, K., Stein, M., Harnisch, S., Reuss, A., Aminossadati, B., Nasemann, C., Oertel, W., Bataille, B., Hellwig, D., Gharabaghi, A., Amtage, F., Mertens, P., Kloss, M., Post, B., and Speelman, H. (2018). Behavioural outcomes of subthalamic stimulation and medical therapy versus medical therapy alone for parkinson's disease with early motor complications (earlystim trial): secondary analysis of an open-label randomised trial. *The Lancet Neurology*, 17(3):223–231. (Not cited)

[Liu et al., 2008] Liu, Y., Matsuhisa, H., and Utsuno, H. (2008). Semi-active vibration isolation system with variable stiffness and damping control. *Journal of Sound and Vibration*, 313:16–28. (Cited on page 2.)

[Liu et al., 2005] Liu, Y., Waters, T. P., and Brennan, M. J. (2005). A comparison of semi-active damping control strategies for vibration isolation of harmonic disturbances. *Journal of Sound and Vibration*, 280:21–39. (Cited on page 2.)

[Ludeke, 1946] Ludeke, C. A. (1946). An experimental investigation of forced vibrations in a mechanical system having a non-linear restoring force. *Journal of Applied Physics*, 17:603. (Cited on page 27.)

[Madsen et al., 2004] Madsen, K., Nielsen, H. B., and Tingleff, O. (2004). Methods for non-linear least squares problems (2nd ed.). (Cited on page 21.)

[Manevitch, 2001] Manevitch, L. I. (2001). The description of localized normal modes in a chain of nonlinear coupled oscillators using complex variables. *Nonlinear Dynamics*, 25:95–109. (Cited on pages 41, 49, 53, 72, 73 and 98.)

[Maniadis et al., 2004] Maniadis, P., Kopidakis, G., and Aubry, S. (2004). Classical and quantum targeted energy transfer between nonlinear oscillators. *Physica D: Nonlinear Phenomena*, 188(3):153 – 177. (Cited on page 37.)

[Mariani et al., 2011] Mariani, R., Bellizzi, S., Cochelin, B., Herzog, P., and Mattei, P. (2011). Toward an adjustable nonlinear low frequency acoustic absorber. *Journal of Sound and Vibration*, 330:5245–5258. (Cited on page 138.)

[Masri, 1972] Masri, S. F. (1972). Forced vibration of a class of non-linear two-degree-of freedom oscillators. *International Journal of Non-Linear Mechanics*, 7:663–674. (Cited on page 36.)

[Matsuhisa and k Otsu-shi, 1994] Matsuhisa, H. and k Otsu-shi, S. (1994). Dynamic vibration absorber for pendulum type structure. E P 0 6 1 8 380 B 1. (Cited on page 114.)

[Mattei et al., 2016] Mattei, P.-O., Iurasov, V., Côte, R., and Pachebat, M. (2016). Le pompage énergétique par absorbeur non-linéaire bi-stable: prédiction de la transition chaotique de l'absorbeur par analyse de Melnikov. In *13e Congrés Français d'Acoustique joint avec le colloque VIbrations, SHocks and NOise (CFA/VISHNO), 11-15 April*, pages 2610–2615. Le Mans, France. (Cited on page 129.)

[McFarland et al., 2005] McFarland, D. M., Bergman, L. A., and Vakakis, A. F. (2005). Experimental study of non-linear energy pumping occurring at a single fast frequency. *International Journal of Non-Linear Mechanics*, 40(6):891–899. (Cited on page 38.)

[McNaney et al., 2003] McNaney, J. M., Imbeni, V., Jung, Y., Papadopoulos, P., and Ritchie, R. O. (2003). An experimental study of the superelastic effect in a shape-memory Nitinol alloy under biaxial loading. *Mechanics of Materials*, 35:969–986. (Cited on page 8.)

[Mead, 1999] Mead, D. J. (1999). *Passive vibration control*. Wiley, West Sussex, England. (Cited on page 1.)

[Meissner, 1999] Meissner, M. (1999). The influence of acoustic nonlinearity on absorption properties of Helmholtz resonators part I. theory. *Archives of Acoustics*, 24(2):179–190. (Cited on pages 123 and 124.)

[Meissner, 2000] Meissner, M. (2000). The influence of acoustic nonlinearity on absorption properties of Helmholtz resonators part II. experiment. *Archives of Acoustics*, 25(2):175–190. (Cited on page 123.)

[Memboeuf and Aubry, 2005] Memboeuf, A. and Aubry, S. (2005). Targeted energy transfer between a rotor and a morse oscillator: A model for selective chemical dissociation. *Physica D: Nonlinear Phenomena*, 207(1):1 – 23. (Cited on page 37.)

[Micha and Vilallonga, 1986] Micha, D. A. and Vilallonga, E. F. (1986). Collisional time-correlation functions for energy transfer: The semiclassical limit. *The Journal of Chemical Physics*, 84(6):3162–3169. (Cited on page 37.)

[Mitropol'skii, 1965] Mitropol'skii, Y. A. (1965). *Problems of the asymptotic theory of nonstationary vibrations*. Jerusalem : Israel Program for Scientific Translations. (Cited on page 34.)

[Mohammadi, 2008] Mohammadi, S. (2008). *Semi-passive vibration control using shunted piezoelectric materials*. PhD Thesis, INSA Lyon, Villeurbanne, France. Génie électrique. Energie et système. N°2008-ISAL-0043. (Cited on page 2.)

[Moheimani and Fleming, 2006] Moheimani, S. O. R. and Fleming, A. J. (2006). *Piezoelectric transducers for vibration control and damping*. Springer, Germany. (Cited on page 2.)

[Molinari et al., 2009] Molinari, M., Ture Savadkoohi, A., Bursi, O. S., Friswell, M. I., and Zonta, D. (2009). Damage identification of a 3D full scale steel-concrete composite structure with partial-strength joints at different pseudo-dynamic load levels. *Earthquake Engineering and Structural Dynamics*, 38:1219–1236. (Cited on page 17.)

[Molotkov, 2008] Molotkov, I. A. (2008). Hysteresis in an acoustic medium with relaxing nonlinearity and viscosity. *Acoustical Physics*, 54(5):626–632. (Cited on page 124.)

[Monteil et al., 2014] Monteil, M., Touzé, C., Thomas, O., and Benacchio, S. (2014). Nonlinear forced vibrations of thin structures with tuned eigenfrequencies: the cases of 1:2:4 and 1:2:2 internal resonances. *Nonlinear Dynamics*, 75(1):175–200. (Cited on page 37.)

[Mook et al., 1986] Mook, D., HaQuang, N., and Plaut, R. (1986). The influence of an internal resonance on non-linear structural vibrations under combination resonance conditions. *Journal of Sound and Vibration*, 104(2):229 – 241. (Cited on pages 34 and 38.)

[Nayfeh and Balachandran, 1989] Nayfeh, A. and Balachandran, B. (1989). Modal interactions in dynamical and structural systems. *Applied Mechanics Reviews*, 42:175–201. (Cited on page 38.)

[Nayfeh, 2000] Nayfeh, A. H. (2000). *Perturbation methods*. John Wiley & Sons. (Cited on page 36.)

[Nayfeh and Mook, 1979] Nayfeh, A. H. and Mook, D. T. (1979). *Nonlinear oscillations*. Wiley, New York. (Cited on pages 37, 42, 53, 77, 93 and 132.)

[Nayfeh and Pai, 1989] Nayfeh, A. H. and Pai, P. F. (1989). Non-linear non-planar parametric responses of an inextensional beam. *International Journal of Non-Linear Mechanics*, 24(2):139 – 158. (Cited on page 37.)

[Nissen et al., 1985] Nissen, J.-C., Popp, K., and Schmalhorst, B. (1985). Optimization of a non-linear dynamic vibration absorber. *Journal of Sound and Vibration*, 99(1):149–154. (Cited on page 36.)

[Nucera et al., 2008] Nucera, F., Iacono, F. L., McFarland, D., Bergman, L., and Vakakis, A. (2008). Application of broadband nonlinear targeted energy transfers for seismic mitigation of a shear frame: Experimental results. *Journal of Sound and Vibration*, 313(1):57 – 76. (Cited on page 38.)

[Nucera et al., 2007] Nucera, F., Vakakis, A. F., McFarland, D. M., Bergman, L. A., and Kerschen, G. (2007). Targeted energy transfers in vibro-impact oscillators for seismic mitigation. *Nonlinear Dynamics*, 50(3):651–677. (Cited on page 38.)

[Ostrovsky, 2004] Ostrovsky, L. A. (2004). Wave interaction in acoustic resonators with and without hysteresis. *Journal of the Acoustical Society of America*, 116(6):3348–3353. (Cited on page 124.)

[Ouisse and Foltête, 2015] Ouisse, M. and Foltête, E. (2015). Model correlation and identification of experimental reduced models in vibroacoustical modal analysis. *Journal of Sound and Vibration*, 342:200 – 217. (Cited on page 14.)

[Pai et al., 1998] Pai, P., Wen, B., Naser, A., and Schulz, M. (1998). Structural vibration control using pzt patches and non-linear phenomena. *Journal of Sound and Vibration*, 215(2):273 – 296. (Not cited)

[Pai and Nayfeh, 1990] Pai, P. F. and Nayfeh, A. H. (1990). Non-linear non-planar oscillations of a cantilever beam under lateral base excitations. *International Journal of Non-Linear Mechanics*, 25(5):455 – 474. (Cited on page 37.)

[Pal et al., 2017] Pal, J., Banerjee, S., Chikermane, S., and Banerji, P. (2017). Estimation of fixity factors of bolted joints in a steel frame structure using a vibration-based health monitoring technique. *International Journal of Steel Structures*, 17(2):593–607. (Cited on page 14.)

[Peng and Pai, 2014] Peng, H. and Pai, P. F. (2014). Acoustic metamaterial plates for elastic wave absorption and structural vibration suppression. *International Journal of Mechanical Sciences*, 89:350 – 361. (Not cited)

[Pennisi et al., 2017] Pennisi, G., Stephan, C., Gourc, E., and Michon, G. (2017). Experimental investigation and analytical description of a vibro-impact nes coupled to a single-degree-of-freedom linear oscillator harmonically forced. *Nonlinear Dynamics*, 88(3):1769–1784. (Cited on page 38.)

[Pilipchuk, 2010] Pilipchuk, V. N. (2010). *Nonlinear Dynamics: Between Linear and Impact Limits*. Springer-Verlag Berlin Heidelberg. (Cited on page 134.)

[Pischanskyy and van Horssen, 2012] Pischanskyy, O. V. and van Horssen, W. T. (2012). On the nonlinear dynamics of a single degree of freedom oscillator with a time-varying mass. *Journal of Sound and Vibration*, 331(8):1887–1897. (Cited on page 90.)

[Powell, 1970] Powell, M. J. D. (1970). A new algorithm for unconstrained optimization. In *Nonlinear Programming*, J. B. Rosen, O. L. Mangasarian, and K. Ritter, editors, pages 31–65. Academic press. (Cited on page 21.)

[Rauscher, 1936] Rauscher, M. (1936). *Steady oscillations of systems with non-linear and unsymmetrical elasticity*. Sc. D. Thesis, Massachusetts Institute of Technology, Cambridge, USA. Aeronautical Engineering Dept. (Cited on page 27.)

[Rice and McCraith, 1987] Rice, H. J. and McCraith, J. R. (1987). Practical non-linear vibration absrober design. *Journal of Sound and Vibration*, 116(3):545–559. (Cited on page 36.)

[Richoux et al., 2007] Richoux, O., Tournat, V., and Le Van Suu, T. (2007). Acoustic wave dispersion in a one-dimensional lattice of nonlinear resonant scatterers. *Physical Review E*, 75:026615. (Cited on pages 127 and 128.)

[Rienstra and Hirschberg, 2018] Rienstra, S. W. and Hirschberg, A. (2018). *An Introduction to Acoustics*. Eindhoven University of Technology. (Cited on page 125.)

[Roberson, 1952] Roberson, R. E. (1952). Synthesis of a nonlinear dynamic vibration absorber. *Journal of Franklin Institute*, 254:205–220. (Cited on pages 2, 27, 28, 29, 30 and 33.)

[Romeo et al., 2015] Romeo, F., Manevitch, L. I., Bergman, L. A., and Vakakis, A. (2015). Transient and chaotic low-energy transfers in a system with bistable nonlinearity. *Chaos*, 25:053109. (Cited on page 129.)

[Roseau, 1987] Roseau, M. (1987). *Vibrations in Mechanical Systems*. Springer-Verlag. (Cited on page 30.)

[Rosenberg, 1960] Rosenberg, R. M. (1960). Normal modes of nonlinear dual-mode systems. *Journal of Applied Mechanics*, 27:263–268. (Cited on page 101.)

[Rosenberg, 1962] Rosenberg, R. M. (1962). The normal modes of nonlinear n-degree-of-freedom systems. *Journal of Applied Mechanics*, 29:7–14. (Cited on page 101.)

[Rosenberg, 1966] Rosenberg, R. M. (1966). On nonlinear vibrations of systems with many degrees of freedom. *Advances in Applied Mechanics*, 9:155–242. (Cited on page 101.)

[Rossing (Ed.), 2014] Rossing (Ed.), T. D. (2014). *Springer Handbook of Acoustics*. Springer-Verlag, New York. (Cited on pages 115, 116, 117, 118, 119, 120 and 121.)

[Royis, 2013] Royis, P. (2013). *Mécanique des Milieux Continus: Cours, Exercices et Problèmes*. Ecole Nationale des Travaux Publics de l'Etat, Vaulx-en-Velin. (Cited on page 116.)

[Samagassi et al., 2019] Samagassi, S., Jacquelin, E., Khamlichi, A., and Sylla, M. (2019). Bayesian sparse regularization for multiple force identification and location in time domain. *Inverse Problems in Science and Engineering*, 27(9):1221–1262. (Cited on page 14.)

[Samagassi et al., 2015] Samagassi, S., Khamlichi, A., Driouach, A., and Jacquelin, E. (2015). Reconstruction of multiple impact forces by wavelet relevance vector machine approach. *Journal of Sound and Vibration*, 359:56 – 67. (Cited on page 14.)

[Scott, 2003] Scott, A. (2003). *Nonlinear Science: Emergence and Dynamics of Coherent Structures*. Oxford Texts in Applied and En. Oxford University Press. (Cited on page 37.)

[Sethna, 1965] Sethna, P. R. (1965). Vibrations of dynamical systems with quadratic nonlinearities. *Journal of Applied Mechanics*, 32(3):576–582. (Cited on pages 33 and 36.)

[Sevin, 1961] Sevin, E. (1961). On the parametric excitation of pendulum-type vibration absorber. *Journal of Applied Mechanics*, 28:330–334. (Cited on pages 31 and 33.)

[Shao and Cochelin, 2014] Shao, J. and Cochelin, B. (2014). Theoretical and numerical study of targeted energy transfer inside an acoustic cavity by a non-linear membrane absorber. *International Journal of Non-Linear Mechanics*, 64:85–92. (Cited on page 138.)

[Shaw et al., 1989] Shaw, J., Shaw, S. W., and Haddow, A. G. (1989). On the response of the non-linear vibration absorber. *International Journal of Non-Linear Mechanics*, 24(4):281–293. (Cited on page 36.)

[Silva et al., 2018] Silva, T. M., Clementino, M. A., Marqui, C. D., and Erturk, A. (2018). An experimentally validated piezoelectric nonlinear energy sink for wideband vibration attenuation. *Journal of Sound and Vibration*, 437:68 – 78. (Not cited)

[Singh and Rienstra, 2014] Singh, D. K. and Rienstra, S. W. (2014). Nonlinear asymptotic impedance model for a helmholtz resonator liner. *Journal of Sound and Vibration*, 333:3536–3549. (Cited on pages 124 and 127.)

[Sivian, 1935] Sivian, L. J. (1935). Acoustic impedance of small orifices. *The Journal of the Acoustical Society of America*, 7:94–101. (Cited on page 122.)

[Smirnov and Manevich, 2011] Smirnov, V. V. and Manevich, L. I. (2011). Limiting phase trajectories and dynamic transitions in nonlinear periodic systems. *Acoustical Physics*, 57(2):271–276. (Cited on page 110.)

[Song et al., 2003] Song, Y., Sato, H., Iwata, Y., and Komatsuzaki, T. (2003). The response of a dynamic vibration absorber system using a parametrically excited pendulum. *Journal of Sound and Vibration*, 259:747–759. (Cited on page 36.)

[Starosvetsky and Gendelman, 2008] Starosvetsky, Y. and Gendelman, O. V. (2008). Strongly modulated response in forced 2dof oscillatory system with essential mass and potential asymmetry. *Physica D: Nonlinear Phenomena*, 237:1719–1733. (Cited on pages 43, 60 and 62.)

[Starosvetsky and Manevitch, 2013] Starosvetsky, Y. and Manevitch, L. (2013). On intense energy exchange and localization in periodic fpu dimer chains. *Physica D: Nonlinear Phenomena*, 264:66 – 79. (Cited on page 110.)

[Stokes, 1845] Stokes, G. G. (1845). On the theories of the internal friction in fluids in motion, and of the equilibrium and motion of elastic solids. *Transactions of the Cambridge Philosophical Society*, 8:287–319. (Cited on page 123.)

[Struble and Heinbockel, 1963] Struble, R. A. and Heinbockel, J. H. (1963). Resonant oscillations of a beam-pendulum system. *Journal of Applied Mechanics*, 30:181–188. (Cited on pages 31, 32, 33 and 35.)

[Sugino et al., 2018] Sugino, C., Ruzzene, M., and Erturk, A. (2018). Merging mechanical and electromechanical bandgaps in locally resonant metamaterials and metastructures. *Journal of the Mechanics and Physics of Solids*, 116:323 – 333. (Not cited)

[Sun et al., 1995] Sun, J. Q., Jolly, M. R., and Norris, M. A. (1995). Passive, adaptive and active tuned vibration absorbers-a survay. *Journal of Mechanical Design*, 117:234–242. (Cited on page 27.)

[Szemplińska-Stupnicka, 1969] Szemplińska-Stupnicka, W. (1969). On the phenomenon of the combination type resonance in non-linear two-degree-of-freedom systems. *International Journal of Non-Linear Mechanics*, 4(4):335 – 359. (Cited on page 38.)

[Szemplińska-Stupnicka, 1975] Szemplińska-Stupnicka, W. (1975). A study of main and secondary resonances in non-linear multi-degree-of-freedom vibrating systems. *International Journal of Non-Linear Mechanics*, 10(6):289 – 304. (Cited on page 38.)

[Szemplińska-Stupnicka, 1978] Szemplińska-Stupnicka, W. (1978). The generalized harmonic balance method for determining the combination resonance in the parametric dynamic systems. *Journal of Sound and Vibration*, 58(3):347 – 361. (Cited on page 38.)

[Szemplińska-Stupnicka and Bajkowski, 1980] Szemplińska-Stupnicka, W. and Bajkowski, J. (1980). Multi-harmonic response in the regions of instability of harmonic solution in multi-degree-of-freedom non-linear systems. *International Journal of Non-Linear Mechanics*, 15(1):1 – 11. (Cited on page 38.)

[Temple, 1928] Temple, G. (1928). The theory of Rayleigh's principle as applied to continuous systems. *Proceedings of the Royal Society of London. Series A, Containing Papers of a Mathematical and Physical Character*, 119(782):276–293. (Cited on page 32.)

[Tirelli and Anthoine, 2013] Tirelli, D. and Anthoine, A. (2013). A method for protecting taut cables from vibrations. European patent application: EP 2 636 795 A1. (Cited on page 11.)

[Tobias, 1959] Tobias, S. A. (1959). Design of small isolator units for the suppression of low-frequency vibration. *Journal of Mechanical Engineering Science*, 1(3):280–292. (Cited on page 28.)

[Ture Savadkoohi, 2008] Ture Savadkoohi, A. (2008). *Inverse modelling of a steel-concrete moment resisting structure subjected to severe cyclic loads and forced vibration tests*. PhD Thesis, University of Trento, Trento, Italy. Structural Engineering-Modelling, Preservation and Control of Materials and Structures. (Cited on pages 13 and 23.)

[Ture Savadkoohi and Lamarque, 2014a] Ture Savadkoohi, A. and Lamarque, C.-H. (2014a). Dynamics of coupled Dahl type and non-smooth systems at different scales of time. *International Journal of Bifurcation and Chaos*, 23(7):1350114. (Cited on pages 84 and 90.)

[Ture Savadkoohi and Lamarque, 2014b] Ture Savadkoohi, A. and Lamarque, C.-H. (2014b). Vibratory energy localization by non-smooth energy sink with time-varying mass. In Awrejcewicz, J., editor, *Applied Non-Linear Dynamical Systems*, pages 429–442, Cham. Springer International Publishing. (Cited on page 38.)

[Ture Savadkoohi et al., 2016a] Ture Savadkoohi, A., Lamarque, C.-H., and Contessa, M. V. (2016a). Trapping vibratory energy of main linear structures by coupling light systems with geometrical and material non-linearities. *International Journal of Non-Linear Mechanics*, 80:3–13. (Cited on pages 38 and 51.)

[Ture Savadkoohi et al., 2012a] Ture Savadkoohi, A., Lamarque, C.-H., and Dimitrijevic, Z. (2012a). Vibratory energy exchange between a linear and a nonsmooth system in the presence of the gravity. *Nonlinear Dynamics*, 70(2):1473–1483. (Cited on pages 38, 41, 49, 82, 84 and 110.)

[Ture Savadkoohi et al., 2011a] Ture Savadkoohi, A., Lamarque, C.-H., and Manevitch, L. I. (2011a). Analysis of the transient behavior in a two dof nonlinear system. *Chaos Solitons & Fractals*, 44(6):450–463. (Cited on page 135.)

[Ture Savadkoohi et al., 2016b] Ture Savadkoohi, A., Lamarque, C.-H., Weiss, M., Vaurigaud, B., and Charlemagne, S. (2016b). Analysis of the 1:1 resonant energy exchanges between coupled oscillators with rheologies. *Nonlinear Dynamics*, 86(3):2145–2159. (Cited on pages 41 and 49.)

[Ture Savadkoohi et al., 2011b] Ture Savadkoohi, A., Molinari, M., Bursi, O. S., and Friswell, M. I. (2011b). Finite element model updating of a semi-rigid moment resisting structure. *Structural Control and Health Monitoring*, 18:149–168. (Cited on pages 17, 23 and 26.)

[Ture Savadkoohi et al., 2012b] Ture Savadkoohi, A., Vaurigaud, B., Lamarque, C.-H., and Pernot, S. (2012b). Targeted energy transfer with parallel nonlinear energy sinks, part II: theory and experiments. *Nonlinear Dynamics*, 67(1):37–46. (Cited on pages 38 and 81.)

[Vakakis, 2001] Vakakis, A. (2001). Inducing passive nonlinear energy sinks in vibrating systems. *Journal of Vibration and Acoustics*, 123:42–48. (Cited on page 37.)

[Vakakis and Gendelman, 2001] Vakakis, A. and Gendelman, O. (2001). Energy pumping in nonlinear mechanical oscillators: Part II-resonance capture. *Journal of Applied Mechanics-transactions of The Asme*, 68. (Cited on pages 37 and 38.)

[Vakakis et al., 2008] Vakakis, A., Gendelman, O., Bergman, L., McFarland, D., Kerschen, G., and Lee, Y. (2008). *Nonlinear Targeted Energy Transfer in Mechanical and Structural Systems, I & II*. Solid Mechanics and Its Applications. Springer Netherlands. (Cited on page 38.)

[Vaurigaud, 2011] Vaurigaud, B. (2011). *contrôle vibratoire passif par assemblage d'absorbeurs nonlinéaire: théorie et expérience*. Thèse de Doctorat, Université de Lyon, ENTPE, Vaulx-en-Velin, France. Ecole Doctorale No 162 MEGA, N d'ordre 2011-ENTP-0001. (Cited on page 81.)

[Vaurigaud et al., 2011a] Vaurigaud, B., Manevitch, L. I., and Lamarque, C.-H. (2011a). Passive control of aeroelastic instability in a long span bridge model prone to coupled flutter using targeted energy transfer. *Journal of sound and vibration*, 330(11):2580–2595. (Cited on page 11.)

[Vaurigaud et al., 2011b] Vaurigaud, B., Ture Savadkoohi, A., and Lamarque, C.-H. (2011b). Targeted energy transfer with parallel nonlinear energy sinks. part I: Design theory and numerical results. *Nonlinear Dynamics*, 4(66):763–780. (Cited on page 81.)

[Vilallonga and Micha, 1987a] Vilallonga, E. and Micha, D. A. (1987a). Collision time-correlation functions in the semiclassical limit. II. vibrational-rotational energy transfer in molecule-molecule collisions. *The Journal of Chemical Physics*, 86(2):750–759. (Cited on page 37.)

[Vilallonga and Micha, 1987b] Vilallonga, E. and Micha, D. A. (1987b). Collisional time-correlation functions in the semiclassical limit. III. application to vibrational-rotational energy transfer in collisions of li+ with n2. *The Journal of Chemical Physics*, 86(2):760–775. (Cited on page 37.)

[Vilallonga and Rabitz, 1986] Vilallonga, E. and Rabitz, H. (1986). Vibrational energy transfer at the gas-solid interface: The role of collective and of localized vibrational modes. *The Journal of Chemical Physics*, 85(4):2300–2314. (Cited on page 37.)

[Vilallonga and Rabitz, 1990] Vilallonga, E. and Rabitz, H. (1990). A hybrid model for vibrational energy transfer at the gas-solid interface: Discrete surface atoms plus a continuous elastic bulk. *The Journal of Chemical Physics*, 92:3957–3976. (Cited on page 37.)

[Vyas and Bajaj, 2001] Vyas, A. and Bajaj, A. (2001). Dynamics of autoparametric vibration absorbers using multiple pendulums. *Journal of Sound and Vibration*, 246:115–135. (Cited on page 36.)

[Wang et al., 2015] Wang, P., Casadei, F., Kang, S. H., and Bertoldi, K. (2015). Locally resonant band gaps in periodic beam lattices by tuning connectivity. *Physical Review B*, 91:020103. (Not cited)

[Weiss, 2016] Weiss, M. (2016). *Conception de capteurs/absorbeurs utilisant la dynamique non linéaire pour la surveillance et le contrôle passif de structures* . Thèse de Doctorat, Université de Lyon, ENTPE, Vaulx-en-Velin, France. Ecole Doctorale No 162 MEGA, N d'ordre NNT : 2016LYSET002. (Cited on pages 84 and 114.)

[Weiss et al., 2016] Weiss, M., Chenia, M., Ture Savadkoohi, A., Lamarque, C.-H., Vaurigaud, B., and Hammouda, A. (2016). Multi-scale energy exchanges between an elasto-plastic oscillator and a light nonsmooth system with external pre-stress. *Nonlinear Dynamics*, 83(1–2):109–135. (Cited on pages 38, 41, 49, 82 and 84.)

[Weiss et al., 2014] Weiss, M., Ture Savadkoohi, A., Gendelman, O. V., and Lamarque, C.-H. (2014). Dynamical behavior of a mechanical system including Saint-Venant component coupled to a nonlinear energy sink. *International Journal of Non-Linear Mechanics*, 63:10–18. (Cited on page 84.)

[Weiss et al., 2018] Weiss, M., Vaurigaud, B., Ture Savadkoohi, A., and Lamarque, C.-H. (2018). Control of vertical oscillations of a cable by a piecewise linear absorber. *Journal of Sound and Vibration*, 435:281 – 300. (Cited on page 38.)

[Weisstein, 2018a] Weisstein, E. W. (2018a). *Fourier Transform*. MathWorld–A Wolfram Web Resource. (Cited on page 156.)

[Weisstein, 2018b] Weisstein, E. W. (2018b). *Wave Equation–1-Dimensional*. MathWorld–A Wolfram Web Resource. (Cited on pages 156 and 157.)

[Witjas et al., 2016] Witjas, T., Carron, R., Boutin, E., Eusebio, A., Azulay, J., and Rï¿½gis, J. (2016). Essential tremor: Update of therapeutic strategies (medical treatment and gamma knife thalamotomy). *Revue Neurologique*, 172(8):408 – 415. Movements disorders. (Not cited)

[Wolfram Research, Inc., 2007] Wolfram Research, Inc. (2007). *Mathematica*. Champaign, Illinois, version 6.0 edition. (Cited on page 22.)

[Wong et al., 1995] Wong, C. W., Mak, W. H., and Ko, J. M. (1995). System and parametric identification of flexible connections in steel framed structures. *Engineering Structures*, 17(8):581–595. (Cited on page 14.)

[Wu and Li, 2006] Wu, J. R. and Li, Q. S. (2006). Structural parameter identification and damage detection for a steel structure using a two-stage finite element model updating method. *Journal of Constructional Steel Research*, 62:231–239. (Cited on page 14.)

[Yamakawa et al., 1977] Yamakawa, I., Takeda, S., and Kojima, H. (1977). Behavior of a new type dynamic vibration absorber. *Bulletin of JSME*, 20(146):947–954. (Cited on page 36.)

[Yi et al., 2017] Yi, K., Collet, M., Chesne, S., and Monteil, M. (2017). Enhancement of elastic wave energy harvesting using adaptive piezo-lens. *Mechanical Systems and Signal Processing*, 93:255 – 266. (Not cited)

[Yu et al., 2011] Yu, G. K., Zhang, Y. D., and Sheng, Y. (2011). Nonlinear amplitude-frequency response of a Helmholtz resonator. *Journal of Vibration and Acoustics*, 133:024502. (Cited on pages 124, 127, 128 and 140.)

[Zaikin and Rudenko, 1996] Zaikin, A. A. and Rudenko, O. V. (1996). A nonlinear model of the Helmholtz resonator with a movable wall. *Acoustical Physics*, 42(3):329–333. (Cited on page 123.)

[Zhou et al., 2014] Zhou, B., Thouverez, F., and Lenoir, D. (2014). Essentially nonlinear piezoelectric shunt circuits applied to mistuned bladed disks. *Journal of Sound and Vibration*, 333(9):2520 – 2542. (Not cited)

[Zinn, 1970] Zinn, B. T. (1970). A theoretical study of non-linear damping by Helmholtz resonators. *Journal of Sound and Vibration*, 13(3):347–356. (Cited on page 123.)

Contribution to the study of passive control by nonlinear interactions in mechanics and acoustic

Abstract: Mechanical and structural systems vulnerabilities against induced vibrations by nature and/or machines create a control problem which seeks for novel design processes for their protection. The control process covers large categories spreading from active to passive controls; meanwhile, the control process can be linear or nonlinear. Passive control soloution exploits the potential(s) of main systems (to be controlled) and/or the potential(s) of coupled oscillators. Potential(s) of systems can present linear or nonlinear behaviours, e.g. hysteresis and/or geometrical nonlinearities. This report deals with passive control of structural systems by endowing nonlinear behaviours of systems themselves or the ones of coupled light oscillators.

The report is divided globally into two main parts: The first global part of this report deals with passive control of civil engineering structures by endowing ductile and hysteresis behaviours of the joints. Results are obtained in the framework of an European research projects, namely the "ECOLEADER HPR-CT-1999-00059" project, Cyclic and PsD testing of a 3D steel-concrete composite frame. The second global part of the report treats the nonlinear targeted energy transfer in mechanical and acoustical systems via exploiting the nonlinear behaviours of coupled oscillators. Results in the domain of mechanical engineering are obtained from an ANR research project namely, "ADYNO ANR-07-BLAN-0193" and several research projects which have been sponsored by PSA Peugeot Citroën Automobiles. The works on the targeted energy transfer in acoustics are treated in the framework of "ANR METAUDIBLE" (ANR-13-BS09-003) and "LABEX CELYA" (ANR-10-LABX-0060) of the Université de Lyon within the program "Investissement d'Avenir" (ANR-11-IDEX-0007).

Keywords: Passive control, nonlinear dynamics, hysteresis, nonlinear energy sink, nonlinear targeted energy transfer